Operational strategies for longer durability of HT-PEM fuel cells operating on reformed methanol

Thomas, Sobi

Publication date:
2017

Document Version
Publisher's PDF, also known as Version of record

OPERATIONAL STRATEGIES FOR LONGER DURABILITY OF HT-PEM FUEL CELLS OPERATING ON REFORMED METHANOL

BY
SOBI THOMAS

DISSERTATION SUBMITTED 2017

AALBORG UNIVERSITY
DENMARK

Operational strategies for longer durability of HT-PEM fuel cells operating on reformed methanol

Ph.D. Dissertation

Sobi Thomas

Dissertation submitted December, 2017

Dissertation submitted:	December 22, 2017
PhD supervisors:	Prof. Søren Knudsen Kær Aalborg University
	Assoc. Prof. Samuel Simon Araya Aalborg University
PhD committee:	Associate Professor Erik Schaltz (chairman) Aalborg University
	Professor Jens Oluf Jensen DTU
	Professor Werner Lehnert Aachen University
PhD Series:	Faculty of Engineering and Science, Aalborg University
Department:	Department of Energy Technology

ISSN (online): 2446-1636
ISBN (online): 978-87-7210-119-4

Published by:
Aalborg University Press
Langagervej 2
DK – 9220 Aalborg Ø
Phone: +45 99407140
aauf@forlag.aau.dk
forlag.aau.dk

Printed in Denmark by Rosendahls, 2018

Thesis Details

Thesis Title:	Operational strategies for longer durability of HT-PEM fuel cells operating on reformed methanol
Ph.D. Student:	Sobi Thomas
Supervisors:	Prof. Søren Knudsen Kær, Aalborg University
	Assoc. Prof. Samuel Simon Araya, Aalborg University

The main body of this thesis consist of the following papers.

[A] **Sobi Thomas**, Jakob Rabjerg Vang, Samuel Simon Araya, Søren Knudsen Kær, "Experimental study to distinguish the effects of methanol slip and water vapour on a high temperature PEM fuel cell at different operating conditions," *Applied Energy*, vol. 192, pp. 422–436, 2017.

[B] **Sobi Thomas**, Samuel Simon Araya, Jakob Rabjerg Vang, Søren Knudsen Kær, "Investigating different break-in procedures for reformed methanol high temperature proton exchange fuel cells",*International Journal of Hydrogen Energy*, December 2017, Status: Under Review.

[C] Jonathan Halter, **Sobi Thomas**, Søren Knudsen Kær, Thomas Justus Schmidt, Felix Büchi, "The Influence of Phosphoric Acid Migration on the Performance of High Temperature Polymer Electrolyte Fuel Cells,", Submitted to *Electrochimica Acta*, August 2017, Status: Under review.

[D] **Sobi Thomas**, Samuel Simon Araya, Thomas Steenberg, Steffen Henrik Frensch, Søren Knudsen Kær, "Mapping phosphoric acid migration with differently doped PBI membrane in an HT-PEM fuel cell,", Submitted to *Journal of Power sources*, December 2017, Status: Under review

[E] **Sobi Thomas**, Christian Jeppesen, Thomas Steenberg, Samuel Simon Araya, Jakob Rabjerg Vang, Søren Knudsen Kær,, " New load cycling

strategy for enhanced durability of high temperature proton exchange membrane fuel cell,", *International Journal of Hydrogen Energy*, vol. 42, no. 44, pp. 27230-27240, 2017.

In addition to the main papers, the following conferences were also attended:

- "Investigating the effect of water vapour and residual methanol on the anode of high temperature PEM fuel cell ", The 6th European Fuel Cell Conference- Piero Lunghi, EFC 17th December 2015, Oral Presentation.
- "Investigating different break-in procedures on an HTPEM fuel cell" ASME- Power and Energy Conference, June 27, 2017, Oral Presentation.

This dissertation has been submitted for assessment in partial fulfilment of the PhD degree. The thesis is based on the submitted or published scientific papers which are listed above. Parts of the papers are used directly or indirectly in the extended summary of the thesis. As part of the assessment, co-author statements have been made available to the assessment committee and are also available at the Faculty.

The following papers were published during the PhD period, however are not part of the papers included for discussion in this dissertation

[1] Samuel Simon Araya, , Fan Zhou, Vincenzo Liso, Simon Lennart Sahlin, Jakob Rabjerg Vang, Sobi Thomas, Xin Gao, Christian Jeppesen, Søren Knudsen Kær, "A comprehensive review of PBI-based high temperature PEM fuel cells," *International Journal of Hydrogen Energy*, vol. 41, no. 46, pp. 21310–21344, 2016.

[2] Sobi Thomas, Alex Bates, Sam Park, A.K. Sahu, Sang C. Lee, Byung Rak Son, Joo Gon Kim, Dong-Ha Lee, "An experimental and simulation study of novel channel designs for open-cathode high-temperature polymer electrolyte membrane fuel cells," *Applied Energy*, vol. 165, pp. 765–776, 2016.

Abstract

Fuel cells are expected to play a key role in meeting the energy goals of many countries including Denmark. However, to be a feasible option for the large-scale adoption, the lifetime of fuel cell system needs to be improved and the cost of production needs to be brought down at the same time. To meet these requirements different paths need to be investigated. There is a lot of focus on reducing the cost of materials used in fuel cell systems and on improving the reliability and the durability. Another approach is to develop a proper operational strategy, which would ensure reduced production cost and better durability, thereby ensuring a large-scale availability of fuel cell systems.

In this dissertation, different operational strategies are investigated to improve the durability as well as reduce the production cost by proposing easier activation of high temperature polymer electrolyte membrane fuel cell (HT-PEMFC). The study focuses on reformed methanol high temperature PEM fuel cell.

Among many, one of the issues associated with the reformed methanol fuel cells are the residual or unconverted methanol vapour and partially converted carbon monoxide (CO) which might enter the fuel cell during operation and cause degradation of the fuel cell. The composition of these residuals are dependant on the reformer temperature, where lower temperature results in a higher methanol slip, while a higher temperature results in higher CO slip[1]. A lower temperature operation would ensure lower parasitic losses (reduced power consumption by the burner fan) [1]. Therefore, the effect of different compositions of methanol vapour in the anode compartment of a single HT-PEMFC fuel cell system are analyzed. The results suggest integration of methanol reformer operating at lower temperature (200 °C) with an HT-PEMFC stack has no or minimal effect on the performance with methanol percentages of less than 3 %. The water present as an output from the reformer also mitigates the methanol effect on the cell.

In another work, the break-in was carried out with 2 % methanol in the

feed and compared to a cell whose break-in was carried out with pure hydrogen. The results show minimal effect in performance during break-in. However, the long term operation shows faster degradation compared to the cell operated with reformed fuel after a break-in with pure hydrogen. Therefore, it can be said that it is not possible with the present strategy as discussed in the dissertation to avoid break-in with pure hydrogen.

Another major problem associated with HT-PEMFC is the acid migration towards the anode gas diffusion layer (GDL) and/or flow channels from the membrane. The acid migration may result from different operating conditions, such as high current density operation, acid doping level,temperature, product water, gas flow rates. Thus, test was carried out to determine how the hydrogen mass transport is affected by migration of acid towards the anode at high current density and the different time constants for the acid flooding and de-flooding were calculated. The time constant for acid flooding and de-flooding under the applied experimental conditions were 8 and 4 min respectively.

The experiments were extended for lower acid doping levels of the membrane and the results obtained were quite different as the acid flooding (high current density operation) and de-flooding (low current density operation) as mentioned in the previous experiment seems to be reversed. At high current density the hydrogen mass transport resistance decreased and increased at low current density. This suggests that a doping level of 10-12 molecules of H_3PO_4 per PBI repeat unit is optimal to avoid flooding of GDL and flow-field at high current densities. The acid migration is assumed to be reaching the catalyst layer and the three phase boundary becomes more accessible for the reactants at high current density. This could be related to capillary pressure not being high enough to force the acid to the GDL pores. The time constants for the present test with doping levels of 11, 8.3 and 7 molecules of H_3PO_4 per PBI repeat unit were 2.8, 5.7, 9.5 min and 3.1, 3.3, 5.6 min for 0.2 and 0.8 $A\,cm^{-2}$ operations, respectively. However, the long duration tests are required to understand the long term implications.

The next step was to develop an operational strategy to avoid acid migration induced degradation on HT-PEMFCs. This could be achieved by operating the cell under load cycling profile. The results show that the degradation after 2000 h was lower at 36 $\mu V\,h^{-1}$ for a time constant of 2 min at low current density (0.2 $A\,cm^{-2}$) compared to 57 $\mu V\,h^{-1}$ for constant current density (0.55 $A\,cm^{-2}$) under the same operating conditions.

Dansk Resumé

Brændselsceller forventes at spille en central rolle i opfyldelsen af energimålene for mange lande, herunder Danmark. For at det skal blive muligt er det imidlertid nødvendigt at levetiden for brændselscellesystemer forbedres samtidigt med prisen reduceres. For at imødekom-me disse krav skal forskellige muligheder undersøges. Der er meget fokus på at reducere omkostningerne ved de materialer der anvendes i brændselscellesystemer og på at forbedre pålideligheden og holdbarheden. En anden tilgang er at udvikle en styrings- og reguleringsstrategi, der kan sikre reducerede produktionsomkostninger og bedre holdbarhed og derved sikre en bedre konkurrence evne af brændselscellesystemer.

I denne afhandling undersøges forskellige operationelle strategier for at forbedre holdbarheden samt reducere produktionsomkostninger ved at foreslå lettere aktivering af høj-temperatur polymer elektrolytmembran brændselsceller (HT-PEMFC). Denne afhandling fokuserer på et reformeret methanol høj temperatur PEM-brændselscelle system.

Langt de fleste problemer, forbundet med reformeret methanol brændselsceller, er den resterende eller ukonverterede methanoldamp og den delvis producerede carbonmonoxid (CO), som kan komme ind i brændselscellen under drift. Sammensætningen af disse rester er afhængig af reformerings temperaturen, hvor lavere temperatur resulterer i en højere methanol-slip, mens højere temperatur resulterer i højere CO-slip [1]. En lavere temperatur vil også sikre lavere parasitisk tab (reduceret strømforbrug ved brænder blæseren) [1]. Derfor analyseres virkningen af forskellige sammensætninger af methanol reformeringen i anoden på en enkelt HT-PEMFC brændselscelle. Resultaterne tyder på at integration af methanol reformer med lav drifts temperatur (200 °C) med en HT-PEMFC stak ingen eller minimal effekt har på ydeevnen med methanol procentdele mindre end 3 %. Vandet der er tilstede fra reformeren mindsker også metanoleffekten på cellen.

I et andet arbejde blev aktiveringen af cellen udført med 2 % methanoldamp

tilsat brinten og sammenlignet med en celle, hvis aktivering blev udført med ren hydrogen. Resultaterne viser en minimal indflydelse på break-in effekten. Den langsigtede kørsel viser imidlertid hurtigere degradering i forhold til cellen, der drives med reformeret brændstof efter en aktivering med rent hydrogen. Det kan derfor siges, at det ikke er muligt med den nuværende strategi, som diskuteret i afhandlingen, for at undgå aktivering med rent hydrogen.

Et andet større problem, forbundet med HT-PEMFC, er syrevandring fra membranen til anode gasdiffusionslaget (GDL) og/eller flow kanalerne. Syrevandringen kan skyldes forskellige driftsbetingelser, så som høj strømdensitet, syre dopingniveau, temperatur, produkt vand eller gasstrø mningshastigheder. Således blev test udført for at bestemme, hvordan hydrogenmassetransporten påvirkes af vandringen af syre mod anoden ved høj strømdensitet, og de forskellige tidskonstanter for syre flooding og de-flooding blev beregnet. Tidskonstanten for syre flooding og de-flooding under de anvendte forsøgsbetingelser var henholdsvis 8 og 4 minutter.

Eksperimenterne blev udvidet til lavere syre dopningsniveauer af membranen, og de opnåede resultater var ret anderledes. Tidskonstanterne for syreoversvømmelsen (høj strømtæthed) og de-flooding (lav strømtæthed) var omvendt. Ved høj strømtæthed faldt hydrogen massetransport modstanden og blevet øget ved lav strømtæthed. Dette antyder, at dopingniveauet af (10-12 molecules af H_3PO_4 pr PBI gentage) er optimalt for at undgå flooding af GDL og flowkanalerne ved høje strømdensitet. Syremigrationen antages at nå katalysatorlaget, og trefasegrænsen bliver mere tilgængeligt for reaktanterne ved høj strømtæthed. Dette kunne være relateret til kapillartrykket, der ikke var højt nok til at tvinge syren til GDL-porerne. Tidskonstanterne for den nuværende test med dopningsniveauer på 11, 8,3 og 7 molecules af H_3PO_4 pr PBI gentage var 2,8, 5,7, 9,5 minut og 3,1, 3,3, 5,6 minut for strømdensitet 0,2 og 0,8 $\mathrm{A\,cm^{-2}}$. Imidlertid kræves der længerevarende tests for at forstå de sene implikationer.

Det næste skridt var at udvikle en operationel strategi for at undgå degradering af cellen som følge af syretransport ud af membranen på HT-PEMFCs. Dette kunne opnås ved at operere cellen under en speciel belastningscyklus. Resultaterne viser, at nedbrydningen efter 2000 timer var lavere nemlig 36 $\mu\mathrm{V\,h^{-1}}$ for en tidskonstant på 2 minutter ved lav strømdensitet (0,2 $\mathrm{A\,cm^{-2}}$) efterfulgt af 2,8 minutter ved høj strømdensitet (0,8 $\mathrm{A\,cm^{-2}}$) sammenlignet med 57 $\mu\mathrm{V\,h^{-1}}$for konstant strømtæthed (0,55 $\mathrm{A\,cm^{-2}}$) under de samme driftsforhold.

Contents

Preface

The work presented in this dissertation was carried out at the Department of Energy Technology, Aalborg University, Denmark. The work was carried out in the frame of 4M Centre project to promote commercialization of HT-PEMFC, which was funded by the Innovation Fund Denmark. The work was carried out in close collaboration with Danish Power Systems and Serenergy.

First of all, I would like to extend my deepest gratitude towards my supervisor Professor Søren Knudsen Kær for his immense patience and guidance throughout my PhD work. I would like to wholeheartedly thank him for providing me the freedom to pursue the path of my interest, to give an honest opinion about my ideas and to keep a check on my path. I am also very grateful to my co-supervisor Assoc. Prof. Samuel Simon Araya for constantly guiding and helping me to move forward with my PhD. I always had the opportunity and freedom to have long and intense discussions on experiment design and analysis of data for which I am very thankful.

I am also thankful to Prof. Thomas J. Schmidt, who provided me with the opportunity to work in his group at PSI, Switzerland. I would also like to thank Dr. Felix N Büchi for extending his technical guidance during my stay and also Jonathan Halter for the intense discussions and practical support at PSI.

I would like to thank my colleagues Jakob, Christian, Steffen, Simon, Saher, Fan, and Debanand for the interesting discussions both technical and non-technical. Also, special thanks to Jan, Frank and Walter for helping me in the laboratory.

I would like to specially extend my gratitude to each and every one at SerEnergy and Danish Power Systems for good discussions and providing MEAs for the experiments.

Finally, I would like to thank my friends and family for being there for me during my ups and downs and extending their support whenever I needed.

Sobi Thomas
Aalborg University, December 22, 2017

Chapter 1

Introduction

> "We must not, in trying to think about how we can make a big difference, ignore the small daily differences we can make which, over time, add up to big differences that we often cannot foresee."
>
> *Marian Wright Edelman*

One of the most important global issue today is the growing greenhouse gas emissions, which is resulting in an increase in the global temperature. The adverse effects associated with greenhouse gas emissions are their ability to absorb infrared radiations which in turn increases the mean temperature of the planet [2]. The predictions as shown by the studies from the Inter governmental panel on climate change 2014 [3] can be seen in Fig. 1.1. The mean temperature rise considering the worst case scenario could reach 4-6 °C by 2100.

These predictions of temperature change are of great concern as that could lead to a shift in the eco-system and make it hard for different species to exist and also scarcity of food could be expected. The World health Organisation (WHO) suggests a great impact of temperature change on the health related issues [4]. In Fig. 1.2 shows the impact of temperature change on the eco-system and the responses being taken to address the issues and its effects. The Paris agreement [5], which was signed by 175 countries, aims to hold the global warming below 2 °C compared to pre-industrial levels and continue to work to achieve a global rise in temperature to 1.5 °C above pre-industrial levels.

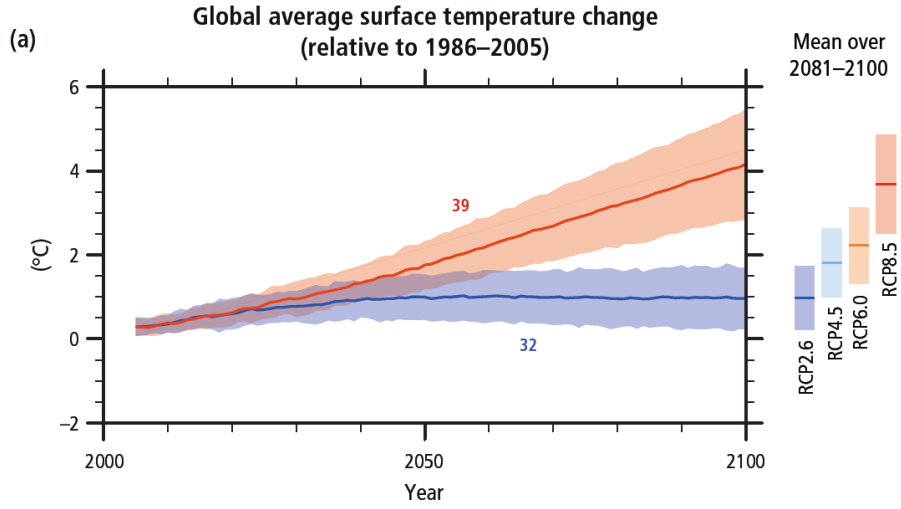

Fig. 1.1: Voltage profile under different anode gas composition and current density at 160 °C, Source: IPCC [3].

According to the united nation (UN) synthesis report 2017, 70 % of the greenhouse gas emissions are contributed by the fossil fuels and cement production [7]. Thus, it is of great importance to look for alternative fuel which could reduce the overall greenhouse emission rates. Different renewable energies are being investigated to achieve the goals set by different countries.

In accordance to the initiative taken in March, 2012 Denmark aims to achieve self-reliance on renewable energy by 2050 [8]. To this effect, the intermediate target for 2020 is to achieve more than 35 % renewable energy integration, around 50 % electricity consumption provided by wind energy and reduction in greenhouse gas emission by 34 % compared to that of 1990. A report by Clean Technica [9], showed that the total electricity consumption in Denmark on 22^{nd} February '17 was provided by wind energy alone. A total of 70 GW h was generated from onshore wind and 27 GW h was supported from off-shore wind turbines.

The Danish government along with different universities is trying to develop 'Smart Energy System' in Denmark [10]. The initiative is to develop a strategy to balance the energy produced and the energy consumed. In Denmark, the main renewable sources of energies are wind, solar and biomass [10]. The wind and solar have a fluctuating nature, which requires a storage system to capture excess energy when generated and supply when the demand is higher than the electricity produced. An attractive option is producing hydrogen by water electrolysis and then using the hydrogen in a fuel cell to balance the grid or to mix with captured CO_2 from different plants and

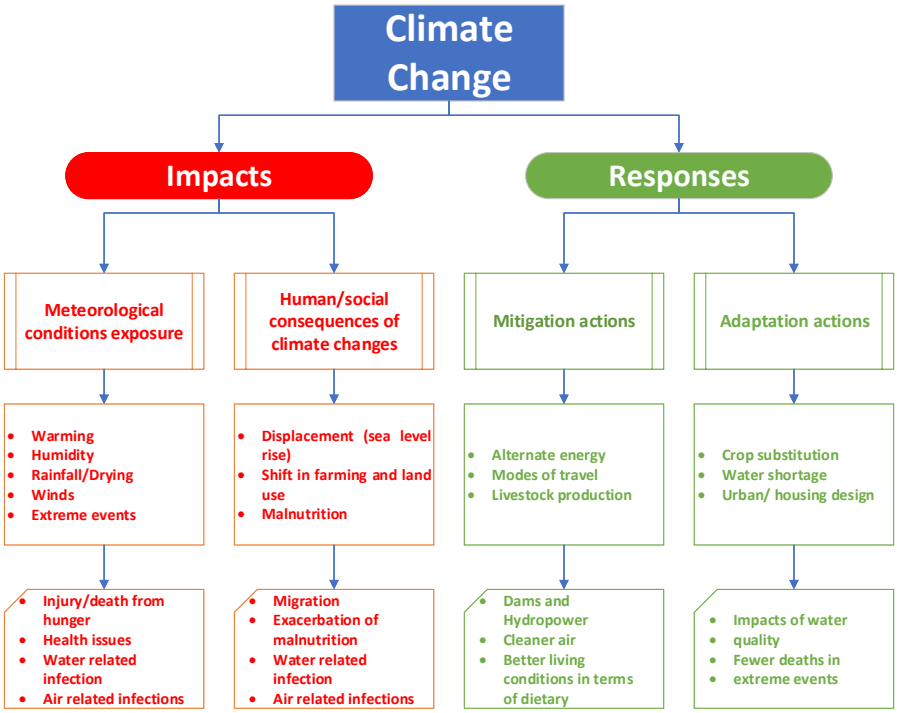

Fig. 1.2: The impacts of climate change and the responses taken to address the problem. Adapted from [6]

produce synthetic fuels like methanol [11–13]. Fuel cells have advantage in terms of reduced greenhouse gas emissions and higher efficiency compared to internal combustion engines [14]. However, the cost of production is still high and their durability needs to improve to make them a viable option.

1.1 Fuel cell classifications

A fuel cell is an electrochemical device which directly converts chemical energy to electrical energy. The most common types of fuel cells are shown in the Table 1.1 with their operating temperature and the kind of ion that are transferred through the electrolyte for completing the reaction.

Among the different kinds of fuel cells, polymer electrolyte membrane fuel cells are the most widely used. They are further classified based on the fuel and the operating temperature as follows; Low temperature PEM (LT-PEMFC), high temperature PEM (HT-PEMFC) and direct methanol fuel cells (DMFC). The first two types are operated generally with gaseous fuel

Fuel cell types	Operating temp [°C]	Ion transfer
Polymer electrolyte membrane fuel cell	0-200 °C	H^+ or OH^{1-}
Molten Carbonate fuel cell	650 °C	CO_3^{2-}
Solid oxide fuel cells	500-100 °C	O^{2-}
Phosphoric acid fuel cell	200 °C	H^+

Table 1.1: Different fuel cell types, operating temperature and ion transfer

(hydrogen and hydrogen rich gas mixtures), the third one operates on liquid fuel (methanol).

The different components of a single fuel cell unit are shown in Fig. 1.3. It consist of two end plates for providing the required strength and compression for the cell. It is followed by current collector plates for connecting to the electrical load. The flow-fields are used to supply the reactants. One of the most important part is the MEA where all the electrochemical reactions takes place. The gaskets are used to provide a leak-tight setup. The tie-rods are used to keep the components in a fuel cell tightened and to provide uniform compression.

1.2 Working principle

In a PEM fuel cell, hydrogen rich fuel is supplied to the anode and oxygen rich air is supplied to the cathode. The electrochemical reactions that take place in a fuel cell are shown in Eqn. 1.1 and 1.2:

$$\textbf{Anode} : 2\,H_2 \longrightarrow 4\,H^+ + 4\,e^- \tag{1.1}$$

$$\textbf{Cathode} : O_2 + 4\,e^- + 4\,H^+ \longrightarrow 2\,H_2O + \text{heat} \tag{1.2}$$

The hydrogen gets oxidized in the anode compartment at the active platinum sites as shown in the reaction, Eqn. 1.1 and the protons are transferred to the cathode by the proton conducting membrane and the electrons are not conducted by the membrane. Thus, the electrons travel through an external circuitry to reach the cathode. This flow of electrons through the external circuit is the electrical output from the fuel cell. At the cathode, oxygen gets reduced by combining with the proton and electrons and generate product water and heat as as shown in reaction, Eqn. 1.2.

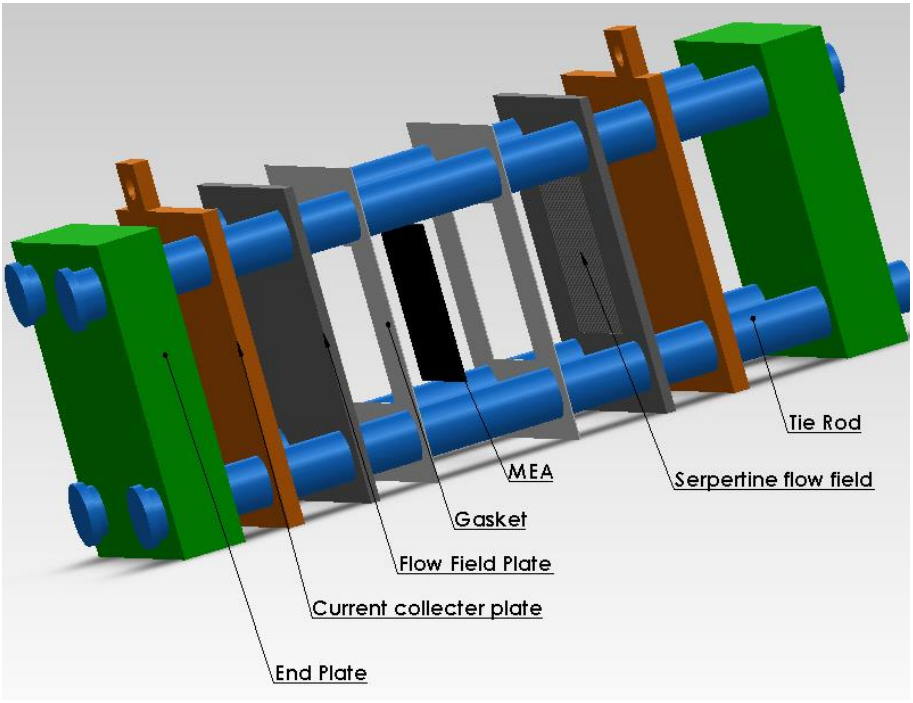

Fig. 1.3: An exploded view of single cell HT-PEMFC

1.3 Methanol economy and reformed methanol fuel cell (RMFC)

1.3.1 Methanol as a fuel

An advantage of thinking towards methanol economy is based on the fact that they could be produced by captured CO_2 and hydrogen. The large industries like cement, iron and steel are some of the major contributors of CO_2 emission [15, 16]. Thus, if CO_2 generated from these plants are captured and mixed with hydrogen a liquid fuel can be generated. Methanol is also environmental friendly as it mixes with water and gets converted to harmless product. Therefore, no contamination of water or soil is resulted from the un-reacted methanol coming out of fuel cell [17].

In recent years several efforts on methanol economy are under-way with companies such as Carbon Recycling International, Mitsui Chemicals Inc (Japan), SABIC (Saudi Arabia) etc., producing CH_3OH by capturing CO_2 from flue gases and power plants (geothermal). Olah et al. [19], first proposed the idea of methanol economy and highlighted its advantages. He proposed

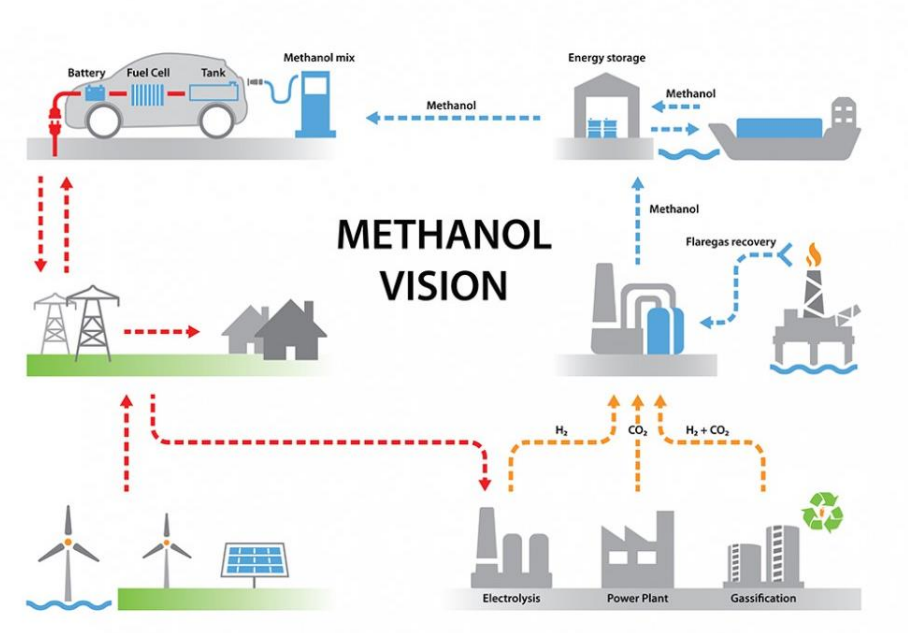

Fig. 1.4: A schematic of vision for developing a methanol economy. Source: Serenergy A/S (http://serenergy.com/) [18]

the capture of carbon dioxide and together with water and hydrogen from an electrolyser or chloro-alkali plant may be used to produce methanol as shown in equation, Eqn. 1.3. Moreover, methanol economy is easier to develop, with minimal modifications in the existing infrastructure, as it is already in use for blending with gasoline [20, 21]. Fig. 1.4, illustrates the methanol vision for a future renewable energy society. The CO_2 from power plants is mixed with H_2 generated using renewable power and electrolyser combination. The mix is then converted to CH_3OH by chemical processes. The flare gases which are rich in CO_2 and H_2 is also being investigated to be added to the mix for generating CH_3OH. The produced fuel may be used in a fuel cell to facilitate as a range-extender in electric vehicles [18].

$$CO_2 + 3\,H_2 \longrightarrow CH_3OH + H_2O \tag{1.3}$$

A report published in the journal of Energy Security suggests methanol can facilitate the monetization of wind and solar energy [22]. The cost involved in the transportation of liquid fuel compared to direct electric current transmission is an order of magnitude lower. Methanol as a fuel has higher energy density at standard temperature and pressure compared to hydrogen

and is easier to transport. The cost of methanol production from CO_2 and H_2 is prominently dominated by the hydrogen production by water electrolysis.

The advantages of using reformed methanol fuel are ease of fuel transportation and higher energy density compared to hydrogen at standard temperature and pressure. Volumetric density of methanol is 4.4 $kW\,h\,L^{-1}$ which is almost 6 times that of hydrogen when the higher heating values are used for the calculations [23].

1.3.2 RMFC operation

The methanol fuel produced by the above mentioned methods are supplied to a reformed methanol fuel cell (RMFC) which has a built-in reformer to convert methanol to hydrogen rich gas, which is then fed to a HT-PEMFC. The higher operating temperature of HT-PEMFC facilitates the use of reformed methanol with higher CO slip [24–26] and less complex humidification system [27]. High temperature PEMFC is an attractive option for both stationary and automotive applications due to its higher tolerance to carbon monoxide [28, 29] and sulphur [30], easier heat rejection [27], and improved reaction kinetics [31]. In applications like back-up power, where the size is not a constraint, HT-PEM fuel cells are widely being investigated [32, 33]. The advantage of HT-PEMFC is the possibility to operate as combined heat and power (CHP) unit because of higher operating temperature which leads to useful heat emissions [17, 34]. HT-PEMFC has also shown the potential to be a part of electric vehicles to facilitate as a range extender [35, 36].

A schematic of HT-PEMFC coupled with a methanol reformer is shown in Fig. 1.5. The fuel used is a mixture of water and methanol in a ratio of 60/40 which corresponds to 1.5 steam to carbon ratio [37, 38]. This fuel is then passed through the evaporator into the reformer which converts it using steam reforming to hydrogen rich gas as shown by the reaction in Eqn. 1.4.

$$CH_3OH + H_2O \rightarrow 2\,H_2 + CO_2 \qquad \Delta H^o = 49.2\,\frac{kJ}{mol} \tag{1.4}$$

The catalytic burner supplies the heat required for the endothermic steam reforming process and the reforming takes place at about 180 to 300 °C. The operation of reformer at these temperatures also facilitates the reaction shown in Eqn. 1.5. This is again a endothermic reaction as seen from the heat requirement shown in the equation.

$$CH_3OH \rightarrow 2\,H_2 + CO \qquad \Delta H^o = 128\,\frac{kJ}{mol} \tag{1.5}$$

The CO produced is partially converted to CO_2 as shown by the reaction in Eqn. 1.6. The excess CO and un-reacted CH_3OH along with H_2 goes into the HT-PEMFC, which has a higher tolerance to CO as mentioned above. The

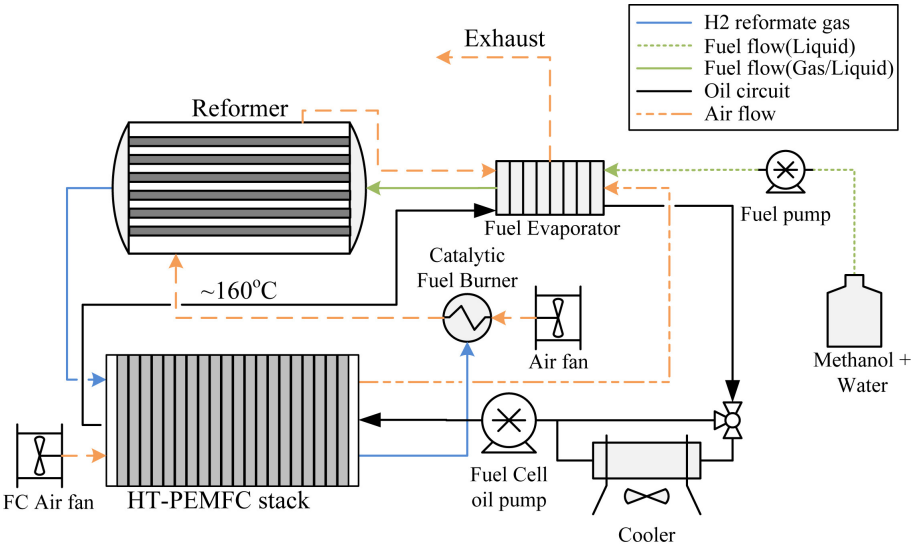

Fig. 1.5: A schematic of reformer coupled HT-PEM fuel cells [1].

amount of CO and CH_3OH is a function of reformer temperature, fuel flow [1, 39]. The effect of CH_3OH slip on the performance and durability was studied in this thesis and is explained in Chapter 3.

$$CO + H_2O \rightarrow H_2 + CO_2 \qquad \Delta H^0 = -41.1 \frac{kJ}{mol} \tag{1.6}$$

1.4 Motivation and research goals

The challenges for making widespread integration of fuel cells in the Danish energy market were identified by the Danish partnership for hydrogen and fuel cells as follows [40]:

- Durability
- Cost
- Performance

The main targets of the Danish roadmap for HT-PEMFC are to achieve a cost of 800€/kW @ 100,000 kW/yr for power modules and 500€/kW @ 500 kW/yr for stacks, by 2020, with lifetime targets of 15,000 h and 20,000 h, respectively [40].

The US Department of Energy (DOE) target for 2020 is to reduce the cost of hydrogen fuel cell, for transport sector to 40 $/kW with 65 % peak-efficiency and a durability of 5000 h, for micro CHP system operating on

natural gas to 1500 $/kW with an electrical efficiency of 45 % and durability of 60000 h [41]. The cost targets seems to be in close proximity when estimated for large scale production (≈53 $/kW was estimated in 2016, assuming 500,000 units/yr production) and the average lab-scaled fuel cell durability as reported by DOE reached ≈3500 h [41].

The research on reducing the system cost and increasing the durability is still on-going. The focus is mostly on the material side to make it cheaper and more durable. However, the focus is shifting towards system optimization as well. For example, a RMFC developer Serenergy has reported a system efficiency of 42 % for its reformed methanol HT-PEMFC intended for mobility, and 45 % for the stationary power and up to 57 % system efficiency for distributed power generators with integrated reformer [18, 42].

In the present project, the importance is given to make fuel cell systems operate more efficiently, thereby reduce the cost and improve durability. Therefore, the main objectives of this dissertation can be summarized as follows:

1. better understanding of reformed methanol high temperature PEM fuel cell operation
2. better understanding of PA redistribution in an HT-PEM fuel cell
3. the development of an operational strategy based on the knowledge gained to improve durability and reduce cost

To achieve these objectives, the following studies were carried out:

- Reformed methanol fuel was simulated with different methanol slips (3 & 5 %) on the anode fuel and the degradation rates were calculated
- Different break-in methods for HT-PEMFC were investigated to speed up the break-in process
- To understand the acid migration and distribution a relationship between acid migration and current density was deduced
- In another study the acid migration as a function of current density and acid doping in the membrane was studied
- Finally, a load cycling strategy is proposed based on different time constant iterations

Chapter 2

State of the art

As discussed in the previous chapter, there are different fuel cells which are being investigated for the widespread implementation in the real world. Among them, polymer electrolyte membrane fuel cells are the most advanced in terms of high power density, low weight and volume [43]. In a PEM fuel cell, the membrane is solid electrolyte composed of a polymer backbone. In low temperature PEM fuel cells, the membrane is composed of nafion while in a high temperature PEM fuel cells it is polybenzimidazole (PBI). In this thesis, the focus is on HT-PEM fuel cells with PBI as the membrane backbone. The polymer PBI is widely used in HT-PEM fuel cell because PBI has a high heat resistance (glass transition temperature of 430 °C), high chemical and mechanical stability, low gas permeability, good electrical insulation and ability to take up high quantity of PA doping, which makes it a good proton conductor [44].

The PBI membrane is doped with phosphoric acid, which acts as the proton conductor in this type of fuel cells. The operating temperature of HT-PEMFC is 160- 180 °C [27]. The advantage of operating at higher temperature are higher CO tolerance [28, 29, 45], less prone to sulphur poisoning [30], easier heat rejection [27], the reaction kinetics on both sides are improved, more importantly the sluggish cathode reaction rate improves [31, 46], water management is not complex as in LT-PEMFC [47, 48]. However, to harness the advantages of HT-PEMFC some hurdles still need to be overcome. One such problem, investigated in the current project is operation with reformed methanol that results in some un-reacted methanol, which enters the anode compartment. The study also investigated how to directly integrate a HT-PEMFC with a methanol reformer with no hydrogen break-in or lowering the time of break-in process using hydrogen.

This chapter will highlight the current state of the art and advancements

in HT-PEM fuel cells with reformed fuel. The characterization of HT-PEM fuel cell and the techniques applied in the present project will also be explained. The focus will be on operation of HT-PEMFC with reformed methanol and also on the understanding of acid migration and distribution. The project outcome focuses on achieving a proper operational strategy for wet reformate based HT-PEMFC with longer durability and reduced cost.

2.1 Fuel cell operating on reformed methanol

In this section, a detailed survey of reformed methanol fuel cells operations is reported and the associated problems discussed. The hydrogen rich gas produced by steam reforming, partial oxidation or auto-thermal reforming has some impurity coming out as by product, which when entering a fuel cell may lead to catalyst poisoning in LT-PEM fuel cells while it has minimal effect on HT-PEM fuel cells as reported by Korsgaard et al. [49].

Romero-Pascual and Soler [50] modelled a HT-PEMFC-based 1 kW combined heat and power (CHP) system with methanol reformer. They presented an efficiency of 24 % when considering the electrical output and a combined efficiency utilizing the heat generated of over 87 %. The CO percentage was considered to be below 30000 ppm. Andreasen et al. [51], developed a cascade control strategy for HT-PEM fuel cell system integrated with a methanol reformer. The focus was on controlling the reformer temperature to ensure high grade quality reformer output with minimal CO and CH_3OH slip under dynamic operation of the system. In another work, different fuel composition simulating a natural gas reformer was investigated and the results in terms of the effect of CO_2, CO and H_2O was presented [52]. The analysis into the cause of degradation showed presence of CO_2 in the fuel increases mass transport resistance while with the presence of CO, catalyst poisoning takes place and as a result reaction kinetics was affected. They reported a positive effect of water in the fuel stream as it improves proton conductivity, enhances anode charge transfer as a result of PA migration along with water towards cathode, and also could convert CO to CO_2 through reverse water gas shift reaction as shown in Eqn. 2.1. The presence of water in the anode chamber was reported beneficial in other works as well [52, 53]. The high temperature operation and presence of water assisted in reducing the effect of CO poisoning in HT-PEM fuel cells [54, 55].

$$CO + H_2O \rightarrow H_2 + CO_2 \tag{2.1}$$

Jiao et al. [56] simulated different flow field designs with CO in the fuel. The performance was evaluated as a function of CO in the fuel and channel design. The inter-digitated and serpentine designs provides more access for the gases to reach the catalyst layer and at the same time CO poisoning

increased due to the easier access to the catalyst sites. On the other hand, parallel design facilitated less access to the catalyst and thereby resulted in lower CO poisoning.

A study of start-stop cycle with increased CO on the anode was shown to reduce the CO_2 at the cathode outlet, which suggest presence of CO mitigates some of the carbon corrosion happening on the cathode during start-stop. They reported a partial pressure of 10 % CO in reformed fuel would improve the fuel cell lifetime operating with intermediate start/stop cycles [57]. The same author in another work [58] investigated the temperature, gas flow rate, water and CO partial pressure effects on carbon corrosion. They carried out 100 start/stop cycles with two MEAs one with 10 % CO and other with 10 % N2 respectively and comparisons show the positive effect of CO in the fuel for HT-PEMFC operating with start/stop cycles.

Chen and Lai [59] did analysis on the effect of temperature and humidity on the fuel cell performance and its associated resistances. Their study concludes minimal effect of humidity on the performance while the membrane resistance changes with humidity. Performance and resistance comparison under different current densities and humidity level was carried out. The charge transfer resistance at low current density decreased with increase in humidity while it showed opposite trend at higher current density [59].

The water transport phenomenon and its effect on HT-PEM fuel cell performance was investigated by Zhang et al. [47]. Two operational modes namely, open-through mode and dead-end mode were investigated to understand the movement of generated water from the cathode to anode. They concluded that the high affinity of phosphoric acid towards water enhances the phosphoric acid mobility, which decreases membrane resistance and thereby a better proton conductivity is obtained.

Chippar et al. [60] developed a new water transport model for PBI membranes and investigated the effect of varying relative humidity (RH) on the cathode. A decrease in performance was observed in spite of an improvement on the proton conductivity. They assumed the effect as a result of loss in phosphoric acid or dilution of oxidant supply [60]. Different studies on how the temperature affects HT-PEMFC have been carried out and the results suggest a better reaction kinetic but lower membrane conductivity due to dehydration of membrane and lower oxygen diffusion at elevated temperature and low RH conditions [61]. Zhang et al. [62] investigated the effect of water management in an HT-PEMFC. The test was carried out to determine the best purging strategy to keep the water content on the anode optimal. A higher water vapour pressure on the anode helps in improving the performance but excess of water results in flooding as observed in LT-PEMFC. The water transport from the cathode to anode was reported to be a function of current density and stoichiometry. The permeability of water with PBI membrane as determined by Bezmalinović et al. [63] was 2.4×10^{-3} at

160 °C.

Some studies on the effect of methanol and water vapour mixture feed to HT-PEMFC anode have also been reported [64, 65]. Araya et al. [64] investigated the methanol effect by introducing different concentration of methanol and water vapour mixture on the anode feed. The degradation under high methanol concentration (8 % by volume) is reported severe (around -3.4 $mV\,h^{-1}$ with increasing trend) while at 3 % the degradation is reversed by cell voltage recovery. The investigation also concluded the reversibility of some degradation effects due to methanol when switched to pure hydrogen. In another work, the effect of temperature and methanol slip on HT-PEMFC was studied under 100 % to 90 % reforming conversion conditions [65]. A degradation rate of -55 $\mu V/h$ was recorded with 90% converted reformed gas composition over a period of 100 h at an operating temperature of 160 °C. Different degradation tests on an HT-PEM fuel cells were carried out in [66]. The test with simulated reformed methanol (H_2, H_2O and CH_3OH) was carried out under start/stop cycle (12 h each). Based on IV curve and EIS analysis the cause of degradation with CH_3OH was reported to be because of decreased ORR kinetics and mass transport resistance increment [66].

2.2 Acid migration and re-distribution in high temperature PEMFC

Another issue hindering the durability of HT-PEM fuel cell is the acid loss and the proton conductivity in an HT-PEMFC is facilitated by the presence of phosphoric acid in the membrane. The membrane for HT-PEMFC is developed by doping PBI matrix with PA and the doping is much higher compared to two PA molecules, which each PBI repetitive unit may be bonded when doped with PA. These free acid molecules are mobile inside the cell and tend to redistribute and move out of the cell. Over time the membrane proton conductivity reduce as a result of acid loss. The acid re-distribution in the cell has been associated with different phenomena, such as water generated or supplied, current density, temperature, gas flow rates etc., [67, 68].

The potential of PA-doped PBI membrane was first suggested by Wainright [69] for use in high temperature fuel cells. They developed a membrane by immersing PBI membrane in phosphoric acid for more than 16 h. The membrane was then tested for direct methanol fuel cell application with low methanol permeability and proton conductivity higher than nafion based membrane at temperatures above 130 °C and low humidity level. Phosphoric acid doped PBI membrane for fuel cell application development process as reported in literature [69–71] are broadly classified in three ways:

- A solution of PBI polymer in NaOH/ethanol is used to cast a membrane in N_2 environment and then washed with water to get a pH of 7, then doped with PA
- A solution of 3-5 % PBI in N,N−dimethylacetamide(DMAc) and 1-2 % LiCl is used for casting, then DMAc evaporated and LiCl washed away using water, doping by immersion in PA
- Direct casting from a solution of PBI and H_3PO_4 in a suitable solvent , most commonly used trifluroacetic acid (TFA)

The doping levels in the first two case is determined by measuring the weight difference of membrane before and after immersion in the acid and reported doping levels are around 9-12 molecules of H_3PO_4 per PBI repeat unit [72]. The last method result in a doping level up to 70 molecules of H_3PO_4 per PBI repeat unit [24].

The proton conductivity in HT-PEM fuel cell is a highly debated topic. The proton conductivity of PA-doped PBI membrane was reported to be influenced by the relative humidity (RH), temperature and doping level, viscosity and many other parameters [70, 73]. The proton conduction is suggested to takes places mostly by Grotthus like mechanism, where the hydrogen bond rearrangement contributes to the intermolecular transfer of protons [74, 75]. However, in the presence of water in the system, some vehicular mechanism was also suggested [76, 77]. The study reveals the presence of two strong and one weak distorted hydrogen bond in phosphoric acid. The weak bond helps in the solvent reorientation which helps in the transfer mechanism. Chin and Chang [73] showed that at high acid concentration the major contributor of proton conduction is inter-molecular interaction of proton with acid or water molecules [73]. There are also others supporting the claim of Grotthuss being the dominant mechanism for PA conductivity in the presence of water [34, 78, 79]. It is suggested from literature that the contribution of Grotthus like mechanism is $\approx$98 % and diffusion of charged species is $\approx$2 % [79, 80].

Therefore, we know that PA-doped PBI has high proton conductivity. However, a proper distribution of PA in fuel cell is required for obtaining good performance. Kwon et al. [81] compared the performance and active surface area of cathode electrode in an HT-PEM fuel cell with different PA content and platinum loading on the cathode electrode. The PA doping and catalyst loading on the anode was maintained constant. The results suggest an optimum level of PA on the cathode significantly improves the active surface area as well as the fuel cell performance. A decrease in catalyst loading is also reported with proper levels of PA in the cathode. In another study Wannek et al. [82] demonstrated that the method of impregnating PA into the MEA does not influence the performance of the fuel cell. The parameter affecting performance of PA based HT-PEMFC is the distribution and

concentration of phosphoric acid. Neutron imaging method was reported to quantify the acid migration towards anode [83]. They report presence of acid in the GDL and also flow channels. The quantification of acid was based on in-plane and through-plane measurements under different relative humidity with a non-operational cell.

In a study by Jeong et al. [84], the degradation of an HT-PEM fuel cell was investigated as a function of acid leaching. The reason for degrading performance was linked to increase in charge transfer resistance and electrochemical surface area decrease. The loss of acid at high current density was reported to be the highest and mainly the cathode side PA loss affected the performance significantly [84]. Lang et al. [85] investigated PA loss by experiments combined with numerical simulations. The test was carried out for 4600 h, first 680 start-stop cycles were performed followed by constant current operation for another 1400 h and a short 90 h water stress test. They reported short test with humidified gas resulted in a high PA loss which was evident from the ohmic resistance increase in the polarization and EIS data.

Bezmalinović et al. [63] investigated the transport of water in an HT-PEMFC and found that water vapour partial pressure on the anode was always higher than cathode side, even with dry hydrogen supply. They confirmed that water transport from the cathode to anode is a function of current density and cathode stoichiometry. The water transport coefficient was reported to be a function of relative humidity within the cell. The effect of water transport and its influence on the performance of HT-PEMFC was investigated in [47]. It was reported around 31.7 % of water generated by chemical reaction was transported from the cathode to anode at 0.2 $A\,cm^{-2}$ while Galbiati et al. [86] reported 18 %. The differences were attributed to different anode stoichiometric ratio in the two experiments. Thus, it could be concluded based on the two work that water transport from the cathode to anode is strongly influenced by the stoichiometric ratio of anode and cathode. A higher stoichiometry on the anode increased the water transport from cathode to anode and higher cathode gas flow rate decreased the water transport [86]. The interaction of water with PA was reported to be the cause of water transport from the cathode to the anode. The gas permeability under different temperature (130-170 °C) was shown to be negligible [87]. The authors state this to be the reason to propose that water permeability takes place as a result of water solubility in the electrolyte as shown in Eqn. 2.2. However, the gas permeability of PBI are reported differently in literature. He et al. [88] reported gas permeability for high PA-doped PBI membrane and showed it to be a function of temperature. The values of permeability values reported in [88] are comparable to the ones reported in [69].

$$H_3PO_4 + H_2O \rightarrow H_2PO_4^- + H_3O^+ \tag{2.2}$$

Further, Oono et al. [89] reported negligible changes in the cross-over due to acid concentration change from 65 % to 78 %. They reported an optimal PA of 10 mg to avoid flooding the 20 µm catalyst. Wippermann et al. [90], showed the effect of hydration and dehydration of PA on the cell resistance as a function of time. The membrane investigated was AB-PBI doped with PA. The water uptake by the PA was faster compared to removal of water by diffusion from the three-phase boundary. This results in a better proton conductivity because of increase in proton acceptors and donors following Eqn. 2.2. Reimer et al. [91] investigated the water transport phenomena in HT-PEM fuel cells and validated the earlier claims of water transport from the cathode to anode. They also reported a small diffusion of hydrogen and oxygen through the membrane by dissolving in the electrolyte and combining on the other side and resulting a small addition of water in the cell. The crossover enhancement at high current density was attributed to swelling of membrane by absorbing water which in turn increases the pore sizes [91].

A high concentration of PA is required for better proton conductivity within the membrane while the presence of liquid PA on the gas diffusion electrode leads to gas transport problems and adsorption of phosphate ions on the catalyst [82]. A study on the doping time and temperature on the performance of HT-PEMFC revealed that the distribution of PA highly influences the fuel cell performance [92]. A temperature range between 80 °C-140 °C was chosen and the doping time between 1 to 6 h. A temperature higher than 120 °C resulted in dissolution of the polymer which affects the durability of membrane in the fuel cell.

Also, a prolonged doping time leads to dissolution. It was concluded that the performance of phosphoric acid based HT-PEM fuel cell, strongly depends on the PA distribution within the cell. The optimum acid concentration on the cathode was investigated to enhance the performance of HT-PEMFC. Different MEAs with varying platinum loading (1.1 to 3 $mg\,cm^{-2}$) on the cathode and different acid impregnated cathode electrode (20 to 243 $\mu mol\,cm^{-2}$) was tested for performance and electrochemical surface area (ECSA) [81]. They concluded that the optimal acid distribution on the cathode would enhance the performance while excess may lead to reduced electrochemical surface area (ECSA). Chevalier et al. [93] studied the transport of acid leading to leaching and thereby performance loss. They used pore-network model to study the effect of micro porous layer (MPL) on the acid redistribution to the gas diffusion electrode. They suggested a mitigation strategy to prevent acid washout by designing a proper MPL structure (shape, size and crack location in the MPL).

However, only few studies focus on the in-situ characterization of PA distribution under fuel cell operation. Maier et al. [94] carried out a study using synchrotron X-ray radiography of an operating cell to understand the acid distribution as a function of current density. They reported an in-

crease (≈20%) in the thickness of the membrane on applying a current of 140 mA cm^{-2} directly from OCV. However, on further increment of current no visible changes in the thickness was observed. The argument was that acid hydration is a fast process compared to dehydration. The acid concentration and distribution as a function of three operating parameter, temperature, media utilization and humidification was investigated using synchrotron X-ray imaging.They observed a change of 1.5 to 3 % change in the PA concentration under different current density operation. Humidification and temperature change did not show drastic changes in the acid distribution [95].

The PA distribution was reported to be non-uniform, especially under higher load operation (350 and 600 mA cm^{-2}). The authors attributed this to non-uniform current generated across the MEA plain due to varying resistances resulting from doping and pore filled with acid. They reported higher acid under the flow channel compare to rib [96]. The cause of cell degradation was investigated under accelerated degradation test using experiments and modelling the polarization curve. They reported the degradation was mostly related to acid loss by a combination of two phenomena occurring at higher current densities. The first was related to non-uniform temperature distribution at the catalyst layer causing change in the acid viscosity that leads to enhanced PA mobility. The second reported issue was higher water generated, which drags the acid to GDL and flow-field thereby causing loss of PA [68]. Eberhardt et al. [97], investigated the lifetime of an HT-PEMFC as a function of acid loss. The acid was collected at the outlet of anode and cathode by operating the cell under accelerated conditions of 190 °C and high flow rates on the anode and cathode. They reported that for an initial acid loading of 36 molecules of H_3PO_4 per PBI repeat unit, the ohmic resistance was not affected significantly up to a loss of 40 % acid, which corresponded to an operation time of 1200 h.

Another interesting aspect reported in the literature is the acid migration towards the anode as a function of current density and doping level. Eberhardt et al. [98] used X-ray tomographic microscopy (XTM) for imaging PA distribution under different load conditions. The migration of PA from the cathode to anode gas diffusion layer (GDL) and flow field was reported. The acid was reported to be migrating to the anode GDL at high current density, while on reducing the current density a back diffusion of PA from the GDL and flow field to the membrane was reported [98]. The same group investigated acid migration as a function of doping level and current density [99]. The MEAs used in their study had doping levels between 23 molecules of H_3PO_4 per PBI repeat unit and 36 molecules of H_3PO_4 per PBI repeat unit. They suggest that acid doping level strongly influence the acid migration but is not linked to the MEA preparation method (pre-doped or post doped). The acid migration was as reported in [98] strongly influenced by current density. Becker et al. [100] developed a method to quantify the acid

migration from the cathode to anode at high current density. They employed micro-electrodes to a PA-doped PBI membrane and measured the ohmic resistance change as a function of operating parameters. The anode side and cathode side resistance changes from OCV to three different current densities (0.2, 0.5 and 0.8 $A\,cm^{-2}$) were investigated. A decrease in the anode side resistance and increase at corresponding cathode side was reported. The cathode resistance change with increase in current density was double that of the anode at high current densities (0.5 $A\,cm^{-2}$ and 0.8 $A\,cm^{-2}$).

A detailed study to improve the lifetime of HT-PEM fuel cell by reducing the PA loss from the cell under varying operating condition needs to be explored. A study on different rest time (i.e., low current density operation) will be experimentally explored to determine the effect and deduce a proper operational strategy.

2.3 Characterization methods

2.3.1 Limiting current

The method involves the determination of the maximum current which the cell is able to draw at a particular hydrogen concentration on the fuel. A mapping of different fuel concentration and limiting current is determined experimentally as discussed in Paper 3. The transport resistance (R_T) is related to the limiting current i_{lim} as follows

$$R_T = \frac{4 \times F \times x_{H_2}^{dry-in}}{i_{lim}} \times \frac{p - p_w}{R \times T} \tag{2.3}$$

where F is the Faraday constant, x_{H_2} is the dry hydrogen inlet mole fraction, p is the total gas pressure, p_w is water vapour pressure, R is universal gas constant, and T is the cell temperature. All the parameter are inputs to the cell except the limiting current, which is determined by reducing the voltage in steps till the current does not increase any more with the decrease in voltage. Limiting current is a known method used to investigate the mass transport in the gas diffusion layer on the cathode. Limiting current method was applied to understand the oxygen diffusion through porous electrode with PA electrolyte [101]. Baker et al. [102] used limiting current method to measure the oxygen transport resistance in PEM fuel cells. The contribution of individual components (diffusion medium, flow channel, pressure dependent and pressure independent component) to oxygen transport resistance was determined. In a recent work, limiting current method using hydrogen pumping mode was investigated to determine the mass transport issues arising due to reduction in expensive precious catalyst [103].

Thus, it is evident that limiting current is a suitable method to determine the mass transport resistance and to separate individual components contributing to the total resistance. Thus in PaperC, limiting current method is analyzed to deduce the hydrogen transport resistance as a function of PA migration towards the anode. To the best of our knowledge, this is the first time, the limiting current method was used in HT-PEMFC to investigate hydrogen transport resistance (Paper C) instead of oxygen transport resistance as reported in literature.

2.3.2 Electrochemical Impedance Spectroscopy

Electrochemical impedance spectroscopy (EIS) is a very common method with electrochemical devices to determine the impedance of the system. The advantage of EIS is its ability to determine the impedance without drastically changing the operating conditions of the system [104]. An impedance measurement maybe carried out in potentiostatic mode, i.e., applying a voltage and measuring current response or galvanostatic mode, i.e., applying a current and measuring the voltage response. The two modes of measurement lead to the same result as shown by Yuan et al. [105]. However, as shown in Fig. 2.1 the IV curve has a very small slope in the region of operation (linear region in the curve) and a small change in voltage could lead to a large change in current and thereby making the system unstable. Thus, galvanostatic mode is the common method employed in EIS measurements for fuel cells.

In PEM fuel cells EIS is widely used for characterizing an MEA [106, 107], to determine transport losses [108, 109], as a diagnostic tool [105, 110, 111] and performance characterization with different gas mixes [53, 112]. It is widely used to characterize single fuel cell performance as well as on stack levels [113, 114]. Some studies on spatially resolved impedance have been carried out to understand the variation in resistance across a specified plane [115, 116].

The schematic of an EIS measurement is shown in Fig. 2.1. When carrying out EIS measurement, there are few considerations to be taken into account. Firstly, the frequency selected for the sweep should cover the range between high and low frequency to reach asymptotic limits (imaginary impedance approaches zero) and secondly, the linearity of the system is maintained by selecting the excitation signal amplitude such that the operating point stays quasi-linear [117]. An excitation of known amplitude as shown in Eqn. 2.4 is applied and the response in terms of amplitude and phase is measured as shown in Eqn. 2.5.

$$\begin{aligned} V(t) &= V_0 sin(\omega t) \\ or, I(t) &= I_0 sin(\omega t) \end{aligned} \tag{2.4}$$

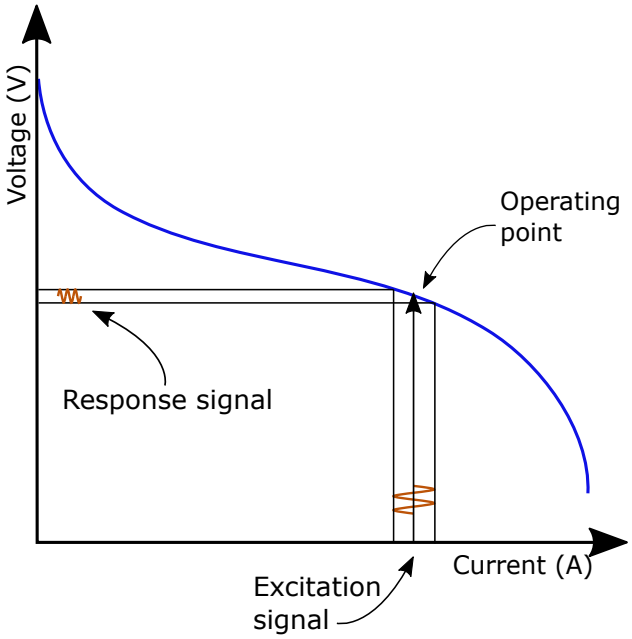

Fig. 2.1: Electrochemical Impedance measurement technique

$$\begin{aligned} I(t) &= I_0 sin(\omega t + \theta) \\ or, V(t) &= V_0 sin(\omega t + \theta) \end{aligned} \tag{2.5}$$

The ratio of alternating voltage to current gives the impedance as shown in Eqn. 2.6. The impedance is recorded by sweeping over a range of frequencies (i.e., usually between 100 mHz to 10 kHz) to isolate various impedance's.

$$Z = \frac{V_0 e^{j(wt-\theta)}}{I_0 e^{-jwt}} = \frac{V_0 e^{-j\theta}}{I_0} = Z_0(cos\theta - jsin\theta) \tag{2.6}$$

where θ is the phase difference between the input and the output signal and is zero for purely resistive component. However, in case of fuel cell, the impedance is not a pure resistance. It is a combination of resistors, capacitors and inductance. Hence, the value of θ at certain frequencies are non-zero. Accordingly, the time domain signal and response signal result in a complex relationship. To simplify the problem Fourier transform is applied and the signal is converted to frequency domain and the impedance is calculated as shown in Eqn. 2.6.

The literature study suggests a number of approaches, namely fitting methods (like non-linear least square method, deconvolution etc.) and mod-

elling approaches (equivalent circuit model, distribution of relaxation time (DRT) etc.) for analyzing EIS spectra. The equivalent circuit models are the most widely used approach with fuel cells but prior knowledge about the possible phenomena within the cell is required [118]. In this PhD project, equivalent circuit model (EQM) was employed to understand the different phenomenon behind the EIS recorded under different conditions.

2.3.2.1 Equivalent circuit model

Equivalent circuit modelling is used for extracting information of processes inside an electrochemical cell. A combination of resistances capacitances and inductance is used to represent an impedance spectrum as shown in Fig. 2.2 . The Nyquist plot representation of impedance data is shown in the figure with real part on the horizontal-axis and imaginary part on the vertical-axis.

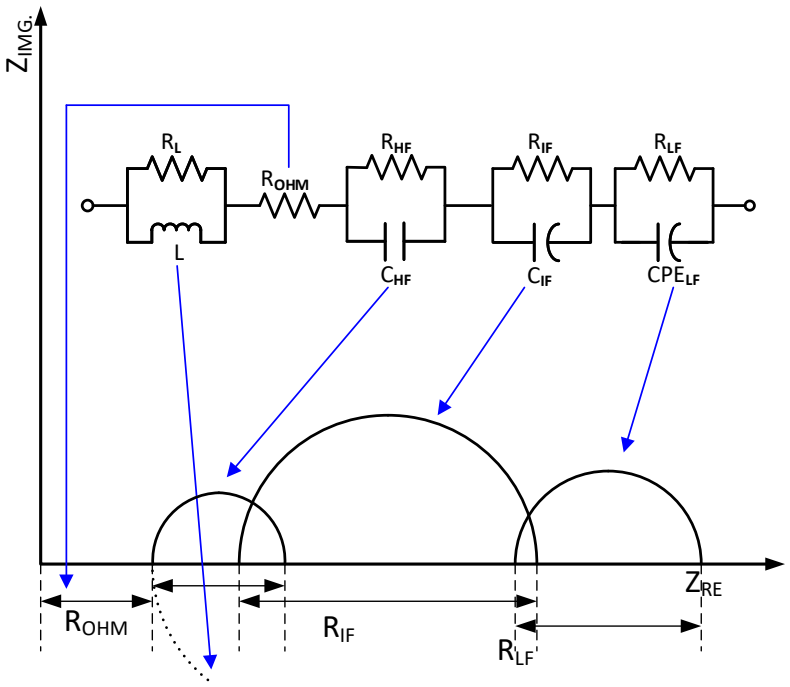

Fig. 2.2: Schematic of Equivalent circuit model and its corresponding Nyquist plot.

The inductance part of the spectrum are mainly contributed by the wiring and connectors used to apply and measure signal and is widely accepted as not being contributed by the fuel cell itself [46, 119, 120]. The series resistance shown as R_{OHM} in Fig. 2.2 is the intersection of spectrum with the real axis in the Nyquist plot. This is pure resistive component of the fuel cell

dominated by the membrane resistance to proton conductivity and also contributed by the contact resistance of different fuel cell components [54, 72]. The RC loops are associated to different process based on the frequency at which they appear in the spectrum. The high frequency resistance (R_{HF}) is not clearly distinguishable for all the MEAs and if distinctly seen are associated with the catalyst conductivity limitation [105, 121] or anode activation process [59, 122]. The intermediate frequency resistances (R_{IF}) is primarily associated to cathode losses. However, sometimes it is also associated with the diffusion losses [53]. The low frequency resistance (R_{LF}) has been attributed to mass transport issues. Again, the mass transport is a subjective term and the cause of mass transport may vary. According to some sources the cause is diffusion process taking place in the gas diffusion layer and/or catalyst layer become dominant [59, 123]. Some sources attributed it to gas channel dynamics [124–126].

In this project, two different equivalent circuit models are used. In Paper A , three RC loops are used to fit the results while in Paper B and Paper E, two RC loops are used. The fitting was carried out using MATLAB function Zfit [127].

Chapter 3

HTPEM operation with reformed fuel

3.1 HT-PEMFC durability with methanol slip

An HT-PEMFC, when operating on reformed methanol, the fuel handling and transport is easier compared to hydrogen as fuel. However, there are still some hurdles associated with a methanol reformer, such as its sensitivity to the operating temperature. Sahlin et al. [1], investigated the methanol slip and CO content at the outlet of the reformer as a function of coolant inlet temperature and fuel inlet flow. The results indicate a high CH_3OH slip at lower temperature and higher fuel flow. While the CO content shows opposite tendency, i.e, higher CO at higher coolant temperature and lower fuel flow rate. Thus, it becomes of great importance to understand which is more of a problem for the durability of an RMFC. Several studies have investigated the effect of CO poisoning on the durability of HT-PEMFC [128–130]. However, studies of the effect of CH_3OH vapour on the durability of HT-PEM fuel cell are very few in the literature and here we try to separate the CH_3OH and H_2O effect. Thus, to investigate the effect, different percentages of methanol were injected on the anode and the voltage and EIS were recorded over time. The MEAs used were supplied by Danish Power Systems (DPS).

The setup used for testing different methanol percentages is shown in Fig. 3.1. It is a home-made test station with different gases (H_2, CO_2 and CO) and vapours (CH_3OH and water) mixing facility. The test station is also capable of performing electrochemical impedance spectroscopy (EIS) and IV curves. The setup is equipped with an evaporator to vaporise the methanol and water injected into the system. The objective was to understand the

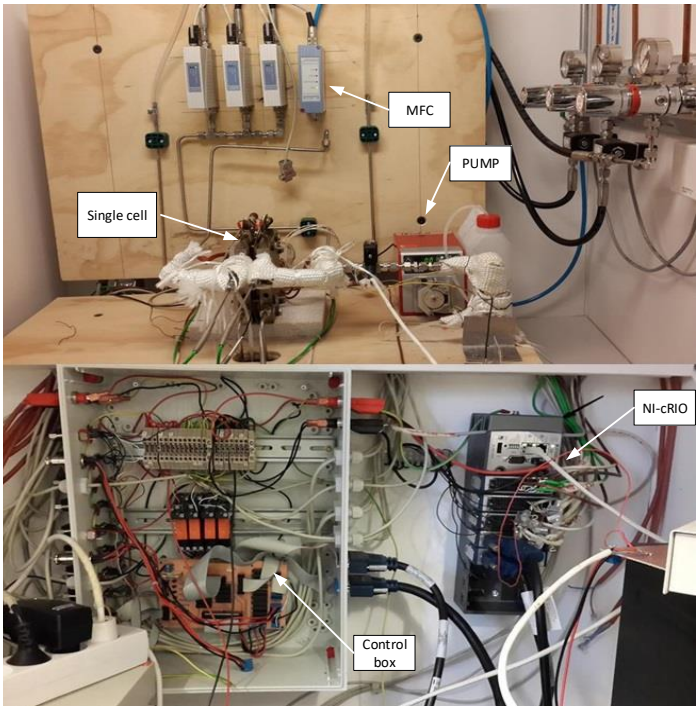

Fig. 3.1: Setup for reformate test

effect of different methanol concentrations and water vapour separately. The percentages of methanol slip, chosen based on previous experience and input from Serenergy reformer, were very low to be supplied by the pump for a single cell with an active area of 45 cm^2. Thus, to distinguish the effects of methanol and water the test was designed for operation with water alone followed by a mixture of water and methanol. The initial test was carried out with a mixture of 1 % methanol and 15 % water vapour and two current densities (0.2 A cm^{-2} and 0.6 A cm^{-2}). The temperature for the test was kept constant at 160 °C. The voltage profile for the test is shown in Fig. 3.2.

Based on the results from the first test, a second test was designed with 3 % and 5 % methanol, while the water vapour was fixed at 15 %. In Paper A, the test was extended for three current densities (0.2 A cm^{-2}, 0.4 A cm^{-2} and 0.6 A cm^{-2}) and two temperatures (160 °C and 180 °C). The fuel compositions used for the test in paper A is shown in Table 3.1.

The test results show minimal degradation effect with methanol (3 and 5

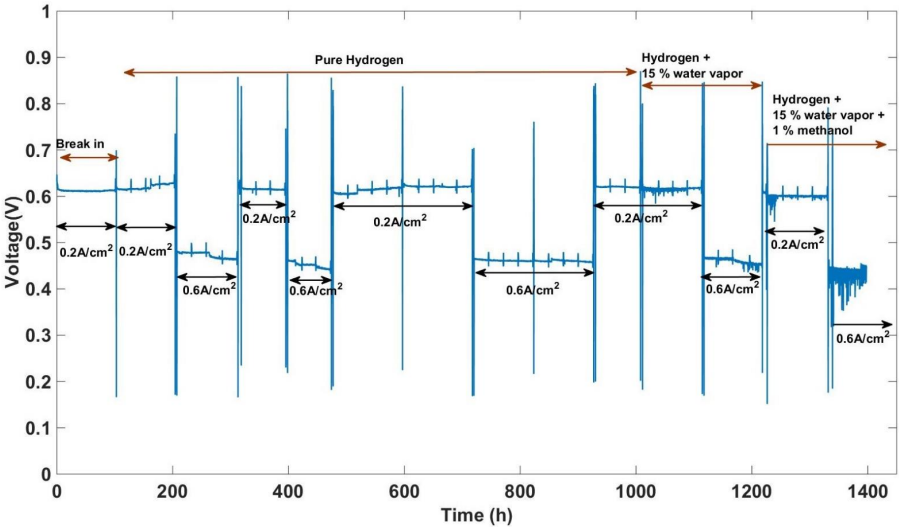

Fig. 3.2: The voltage profile over time with different anode fuel composition [131]

Exp. No.	x_{H_2}/x_{total}	x_{H_2O}/x_{H_2}	x_{H_2O}/x_{total}	x_{CH_3OH}/x_{H_2}	x_{CH_3OH}/x_{total}	Temp. [°C]
1	100.0	00.0	00.0	0.0	0.0	160
2	87.0	15.0	13.0	0.0	0.0	160
3	84.8	15.0	12.7	3.0	2.5	160
4	83.4	15.0	12.5	5.0	4.2	160
5	100.0	00.0	00.0	0.0	0.0	180
6	87.0	15.0	13.0	0.0	0.0	180
7	84.8	15.0	12.7	3.0	2.5	180
8	83.3	15.0	12.5	5.0	4.2	180

Table 3.1: The various fuel compositions on the anode during each test sequence. The values are % with respect to the H_2 flow and the total flow respectively.

%) and water vapour (15 %) mixture. The EIS data suggests that some degradations observed with 5 % CH_3OH is reversible in the presence of H_2O. The results were compared to understand the resistance changes in the presence of water vapour and methanol separately at 160 °C and 180 °C. The total degradation recorded over a period of 1915 h was -44 $\mu V\,h^{-1}$ and on comparing the degradation at 160 °C and 180 °C separately, the values were similar at -39 and -37 $\mu V\,h^{-1}$, over a period of 1106 h and 800 h, respectively. This suggests operating temperature has minimal effect on HT-PEMFC degradation

when operated with reformed methanol in the investigated range of temperatures. The hydration and dehydration phenomena is more pronounced at 180 °C operation when dry hydrogen is replaced with wet hydrogen having 15 % H_2O vapour. The investigation of methanol and water suggests that the presence of water mitigates some degradation effects in the presence of methanol. The presence of methanol may lead to the following reaction as shown in Eqn. 3.1 or form esters with PA as reported in [132]. The ester formation would lead to reduced H_3PO_4 available for the proton conductivity. However, the presence of H_2O improves the mobility of H_3PO_4 and thereby the proton conductivity. Thus, the overall proton conductivity is not compromised.

$$CH_3OH \rightarrow CO + 4\,H^+ + 4\,e^- \tag{3.1}$$

The CO generated could poison the catalyst to some extent. However, in the presence of water the following reaction shown by Eqn. 3.2 is highly possible as also reported in [54, 55]. The converted CO_2 has only dilution effect and can be easily removed from the cell.

$$\begin{aligned} H_2O &\rightarrow H^+ + OH^- \\ CO + OH^- &\rightarrow CO_2 + H^+ + e^- \end{aligned} \tag{3.2}$$

Thus, it was concluded that direct integration of reformed methanol with no intermediate purification system is viable with HT-PEM fuel cells. A CH_3OH slip of $< 3\%$ does not affect the performance as the water in the reformed fuel mitigates some of the effects of methanol slip.This could serve as an important finding to decide the operating temperature which would be optimal for the reformer with lower CO.

3.2 Different break-in procedures

Among the different goals stated in the previous chapter, one was to develop a strategy to reduce the cost of RMFCs. One way is to reduce the production cost of fuel cell stacks. In this context, break-in is a major cost factor. HT-PEM fuel cell systems are required to be conditioned before integrating with the reformer to attain maximum output power. In the industry, this is a costly process that involves two major drawbacks:

- Time consuming process with a minimum of 100 h break-in period
- Pure hydrogen gas supply is required to carry out the break-in of each stack, while the normal operation fuel is reformed methanol

Thus, to address this cost factor different break-in processes were investigated to speed up the break-in process. First, break-in was done for different duration in order to understand whether the break-in process could be eliminated. Secondly, break-in with reformed fuel instead of pure hydrogen was investigated. The analysis was done to estimate the durability and compare the performance. The MEAs used were supplied by Serenergy and are similar to BASF MEAs.

The break-in time was divide into three: No break-in (0 h), Intermediate break-in (30 & 50 h) and normal break-in (100 h). The cells were cycled between 0.2 A cm^{-2} and 0.6 A cm^{-2} after the respective break-in times. The cycling is carried out based on two assumptions:

- Break-in involves the redistribution of PA uniformly across the MEA
- PA migration and diffusion is a function of current density

The voltage over time for cells with different break-in time is shown in Fig. 3.3. The comparison shows minimal difference in the voltage inventory over time for all the cells and it is confirmed by two sets of tests (Test 1 and Test 2). Test 2 was a repetition of test 1 with only one change in the intermediate break-in time. The intermediate time for test 1 was 30 h and it was 50 h for test 2.

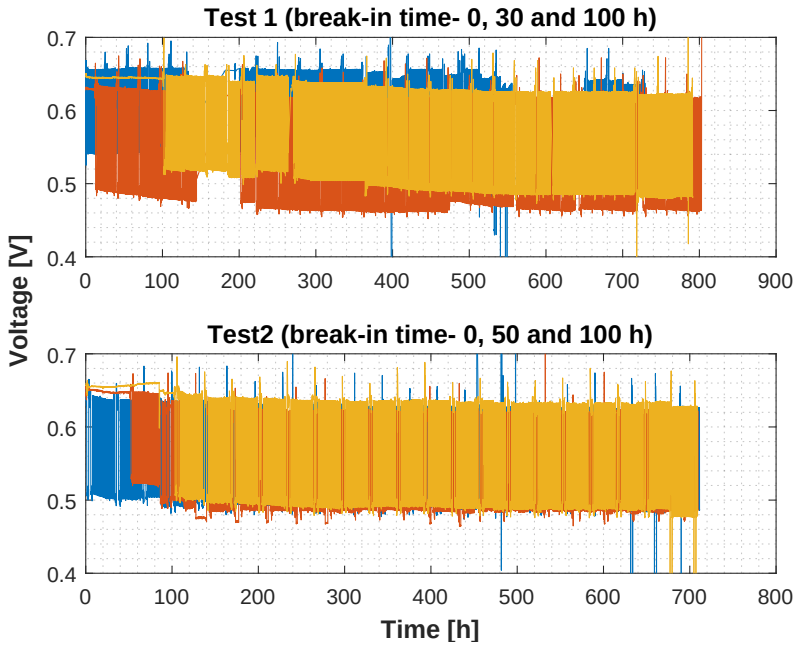

Fig. 3.3: Voltage comparison with different break-in time, Source: Paper B.

Table 3.2: Test description with break-in time and corresponding degradation at 0.2 A cm^{-2} and 0.6 A cm^{-2}.

Test 1 with 0 h, 30 h and 100 h				
Cell name	**Break-in time**	**@ 0.2** A cm^{-2}	**@ 0.6** A cm^{-2}	**Operation time**
-	[h]	[µV h^{-1}]	[µV h^{-1}]	[h]
Cell 1	0	-26	-39	730
Cell 2	30	-13	-40	803
Cell 3	100	-31	-52	791
Test 2 with 0 h, 50 h and 100 h break-in				
Cell 4	0	-33	-30	711
Cell 5	50	-42	-53	710
Cell 6	100	-44	-42	710

The test time and corresponding degradation rates at 0.2 A cm^{-2} and 0.6 A cm^{-2} were calculated and is shown in Table 3.2. The different degradation rates suggest that the break-in time does not affect the performance and the long term durability. This could be related to load cycling results redistribution of acid and is not related to constant current operation. Similar, degradation's were also reported in other studies under load cycling operation [133–135]. The cause of degradation under load cycling was reported to be related to hydration and dehydration of PA. One improves the proton conductivity while the other degrades.

To understand the different break-in operational strategy the EIS recorded over time was analyzed. The EIS data was fitted with an equivalent circuit model and the different resistances calculated. A significant variation among the different MEAs was a problem to carry out comparisons. Therefore, the resistances were compared based on the inventory over time and not the absolute numbers.

The calculated ohmic resistances are shown in Fig. 3.4. A close look into the ohmic resistance suggests that the cell 3 and cell 6 have similar trend. An increase is seen in the beginning and then around ≈300 h the become less steeper. The no break-in cells 1 and 4 and intermediate break-in cells 2 and 5 do not show similarities in the change of resistance over time.

The analysis suggests that the performance in the present study is not affected by the different break-in times. However, the uniformity of cell ohmic resistance is ensured by the normal break-in process. Further, investigation with minimal variations in the MEA is required to suggest the optimal break-in procedure.

The test 3 was carried out with reformed fuel having the following fuel composition, H_2- 64.7 %, H_2O- 12 %, CO_2- 21.3 %, CH_3OH- 2 %. The test

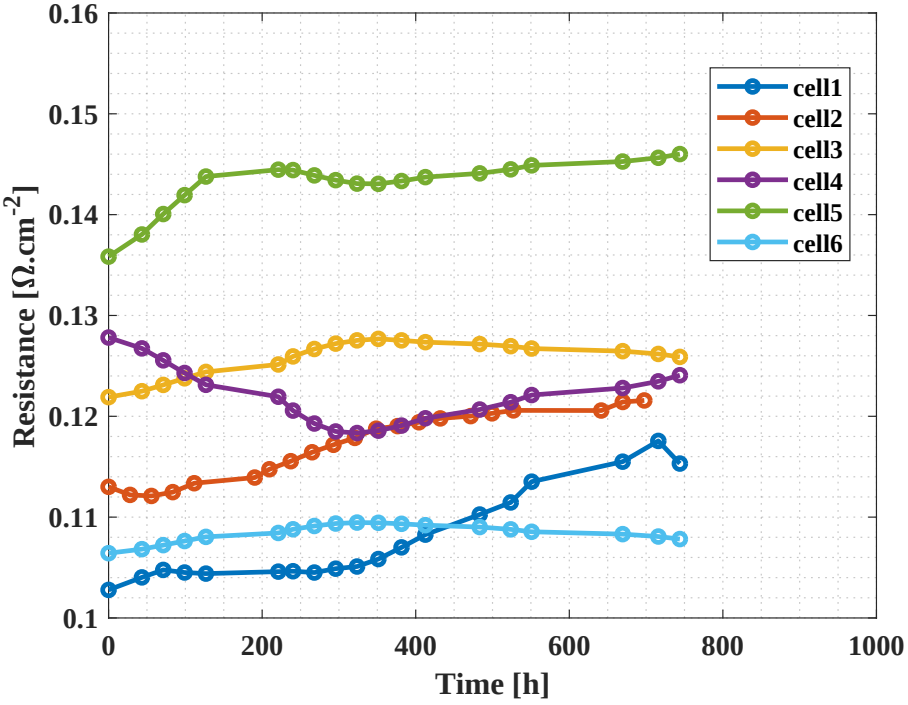

Fig. 3.4: Comparison of fitted ohmic resistance over time for different break-in times, Source: Paper B.

was performed based on Sahlin et al. [1] work that reported a low CO less than 0.5 % when the methanol slip is 2 %. As discussed in Paper A and also by others [64], HT-PEMFC performance is not significantly affected with a methanol slip of 3 %.

Thus, two cells were tested, Cell 1 with pure hydrogen break-in followed by reformed fuel and Cell 2 break-in was using reformed methanol composition as mentioned before. The voltage inventory over time shows a faster degrading cell when break-in was carried out using reformed fuel, Fig. 3.5. The different sections of the voltage inventory were analyzed to understand the cause.

In Table 3.3, the voltage inventory at different sections of the voltage profile is shown. The first section is the break-in process, where we see a positive effect on voltage with pure hydrogen as reported also in the literature. However, the break-in with methanol in the fuel resulted in a decrease in voltage by 30 mV over 100 h. The degradation is attributed to some acid loss due to the water in the feed. This was further confirmed from EIS data recorded before and after the break-in as reported in Paper B. The interesting transi-

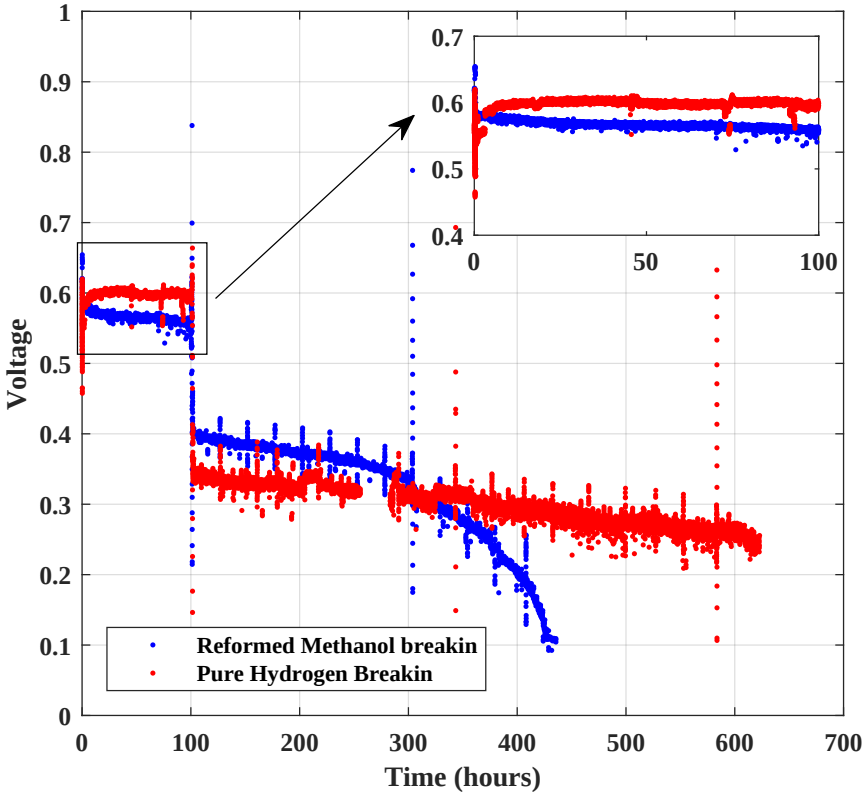

Fig. 3.5: Voltage comparison of break-in with reformed fuel and break-in with pure hydrogen operation, Source: Paper B.

tion was observed when the current density was changed from 0.2 A cm^{-2} to 0.6 A cm^{-2}, the voltage change with current density was lower for the cell 2 compared to Cell 1. This was attributed to sudden change in the fuel composition in Cell 1 from pure hydrogen to reformed fuel. The degradation was much higher for Cell 2 compared to Cell 1 as seen in Table 3.3.

To understand the cause of higher degradation in Cell 2, the EIS recorded over time was analyzed using equivalent circuit modelling and a significant change in the low frequency resistance and ohmic resistance is seen in Fig.3.6. The ohmic resistance as explained in Chapter 2 is related to the membrane resistance and low frequency resistance is a attributed to mass transport issues.

Thus, it is evident that reformed fuel operation enhances the acid loss from the membrane which reduces the proton conductivity. The acid which gets lost over time is assumed to be covering the GDL pore and some are trapped in the flow channel, which enhances the mass transport issues. The

Table 3.3: The voltage changes and degradation rate calculated from the voltage profile

Cell No.	Voltage change during break-in [mV]	Voltage drop on current change [mV]	Degradation @0.6A cm^{-2} [$\mu V\,h^{-1}$]
Cell 1	+60	15	158
Cell 2	-30	26	897

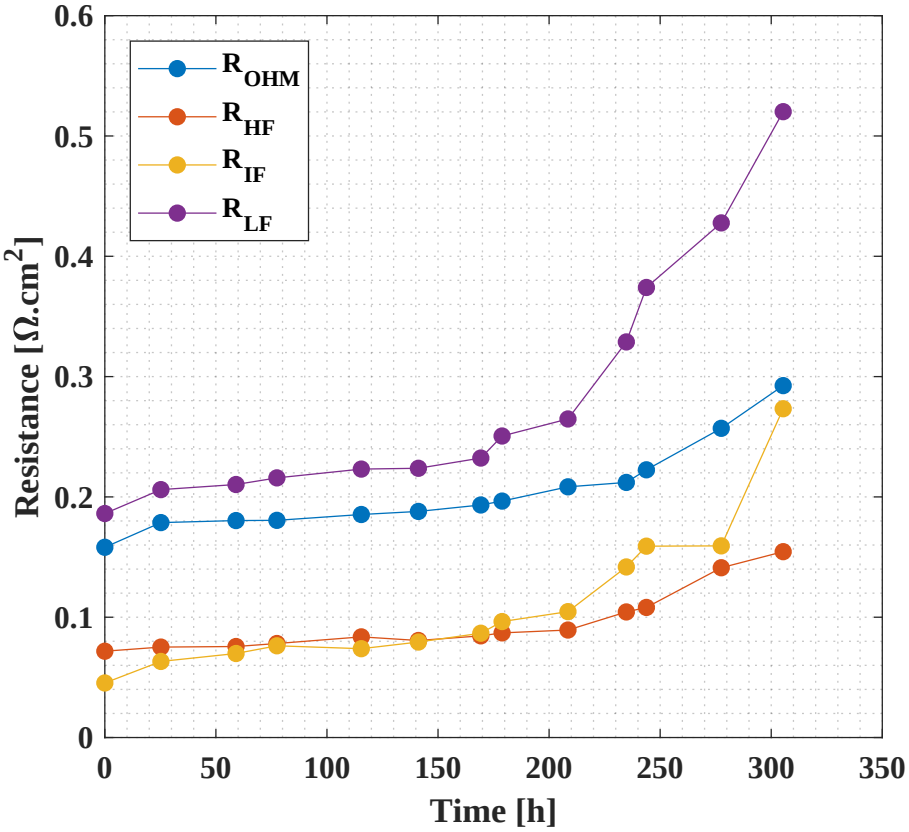

Fig. 3.6: Comparison of different resistances for cells operated on reformed fuel during break-in, Source: Paper B

tests suggests that break-in times do not affect the performance and degradation significantly provided the cells are cycled between 0.2 A cm^{-2} and 0.6 A cm^{-2}. However, the uniform change in resistance could be possible only after normal break-in. The break-in with reformed fuel is not suitable for longer durability. Thus, it is suggested to avoid supplying H_2O into the cell till the acid redistribution is ensured.

3.3 Summary

The different tests carried out to understand the effect of methanol on the performance and durability of HT-PEM fuel cell gave some insight on how to design and operate the system to achieve longer durability. The results suggest the possibility of operating an HT-PEMFC integrated with a methanol reformer with minimal loss in performance when the methanol slip is below 3 %. The test was carried out for ≈2000 h with a total degradation of 44 $\mu V\,h^{-1}$. The test was performed at different current density (0.2, 0.4 and 0.6 $A\,cm^{-2}$) and two temperatures (160 and 180 °C). The positive effect of water in the feed was more significant at 180 °C, and the fact that the degradation is similar for 160 and 180 °C operation suggests the possibility of operating at higher temperatures, which enhances the reaction kinetics. However, the analysis on the catalyst degradation over time at 180 °C needs to be further analyzed. Some reports have suggested higher degradation at 180 °C due to catalyst degradation [136]. Our results based on EIS analysis show no or minimal changes in the charge transfer resistances. This could also be due to the tests being for short period of time at each operating point, 400 h at each current densities and temperatures.

The aim of reducing the break-in time does not seem to be a good idea as it leads to non-uniform resistance changes over time. The cycling of cell with break-in needs to be further investigated as the tests on two cells (same procedure) do not show any uniform trend in the voltage inventory. The performance was found to be not affect much provided the other cells are operated by cycling the current between 0.2 and 0.6 $A\,cm^{-2}$. The ohmic resistance change with normal break-in behaves in a similar fashion. However, the non-uniformity of MEAs needs to be minimized to draw a conclusive outcome.

The reformed fuel with 2 % CH_3OH and 12 % H_2O is also not a good idea as it leads to a faster membrane degradation. The possible reason as discussed is related to the presence of H_2O that reduces the acid viscosity and possibly results in the flooding of the GDL and flow field, which increases the membrane resistance and also the mass transport issues become highly dominant. This leads to faster cell degradation compared to a cell operated with reformed fuel after a proper break-in with pure hydrogen.

Chapter 4

Phosphoric acid migration and diffusion

4.1 Acid migration

One of the most significant losses in high temperature polymer electrolyte membrane fuel cell is loss of acid during operation which degrades the membrane. The performance of the fuel cell decreases as a result of the acid loss from the membrane. As explained in the previous chapters, phosphoric acid is the proton conductor in HT-PEM fuel cells. Thus, it is important to understand the factors influencing the redistribution of PA. In Paper C and Paper D, the acid migration towards anode under the influence of current density and acid concentration is studied and its impact on the hydrogen mass transport deduced. The long term loss of acid is not accounted for in these studies. In Paper C, the tests were carried out with BASF Celtec®, which has a high doping level (33-36 molecules of H_3PO_4 per PBI repeat unit). On the other hand, the tests in paper D were done on MEAs from Danish Power system (Dapozol®) with much lower doping levels (10-12 molecules of H_3PO_4 per PBI repeat unit).

4.2 Acid migration as a function of current density

In Paper C, two different methods were investigated to estimate the hydrogen transport resistance:

1. Anodic limiting current method
2. Electrochemical Impedance spectroscopy (slow and fast)

The scheme used is shown in Fig. 4.1. In Fig. 4.1 (a), the cell is operated for 80-100 h at 0.2 A cm^{-2} for break-in. Then the current density is changed to 0.8 A cm^{-2} to force acid redistribution. After 24 h operation limiting current was measured using the method explained in Chapter 2 and the process was repeated for 0.2 A cm^{-2} and three different sets recorded. In Fig. 4.1 (b), the test was carried out using EIS technique. After 24 h operation at 0.2 A cm^{-2}, the load was switched to 0.8 A cm^{-2} and allowed to stabilize for 2 min(T_2), the EIS measurements were recorded continuously for 1 h. The step was repeated for low current density. In Fig. 4.1, Fast EIS method was employed by reducing the frequency scan to on 1 Hz and measuring at 0.8 A cm^{-2}. The measurement was continued for 60 min then the current density was changed to 0.2 A cm^{-2} for 2min (T_3) and again changed back to 0.8 A cm^{-2} and measurement continued. This was to record the kinetics during the first 2 min at low current density.

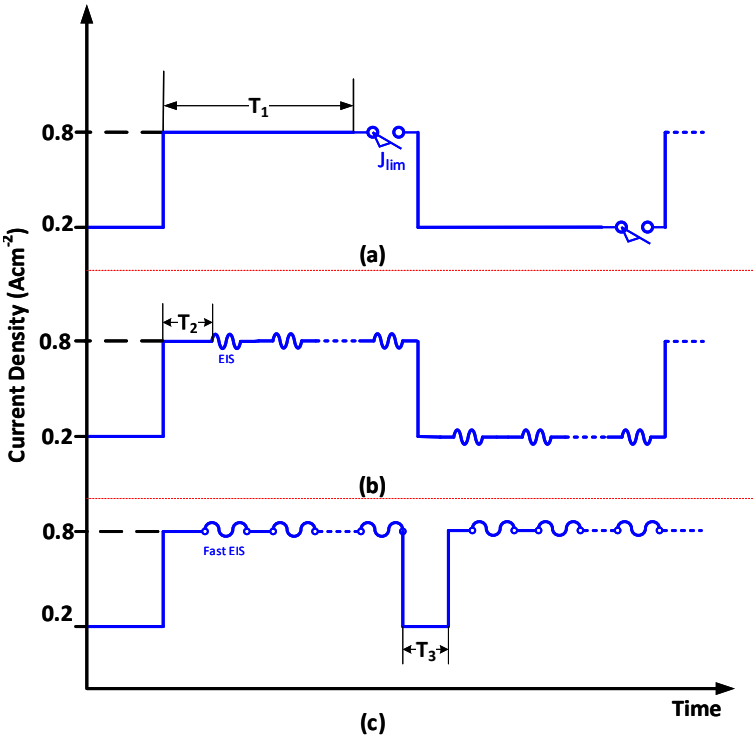

Fig. 4.1: The experimental scheme for acid migration as a function of current density (Source: Paper C)

4.2.1 Anodic limiting current

In Fig. 4.1(a), the limiting current experiment protocol is shown. The break-in for the cell is carried out at 0.2 A cm^{-2} for 100 h.

The MEA for the test was prepared at home using a BASF Celtec® membrane. The acid loading for the membrane was 34-36 molecules of H_3PO_4 per PBI repeat unit. The cell was operated at 0.2 A cm^{-2} and 0.8 A cm^{-2} for 24 hours each before the limiting current measurements were carried out. The voltage for carrying out the limiting current measurements at different hydrogen concentrations were carried out by applying a voltage of 0.2 V. The results are shown in Fig. 4.2 and we see there is no change in the limiting current at high and low current densities. The probable reason as explained in paper C is that the measurement time is too long to capture the flooding dynamics. The first change of concentration from 100 % H_2 to 1 % H_2 and 99 % N_2 takes around 15 min to be uniformly distributed in the cell channel and the current to be stable at that concentration. The subsequent steps were fast enough and achieved within 2 min. Thus it was concluded that limiting current is not able to detect the flooding and deflooding kinetics.

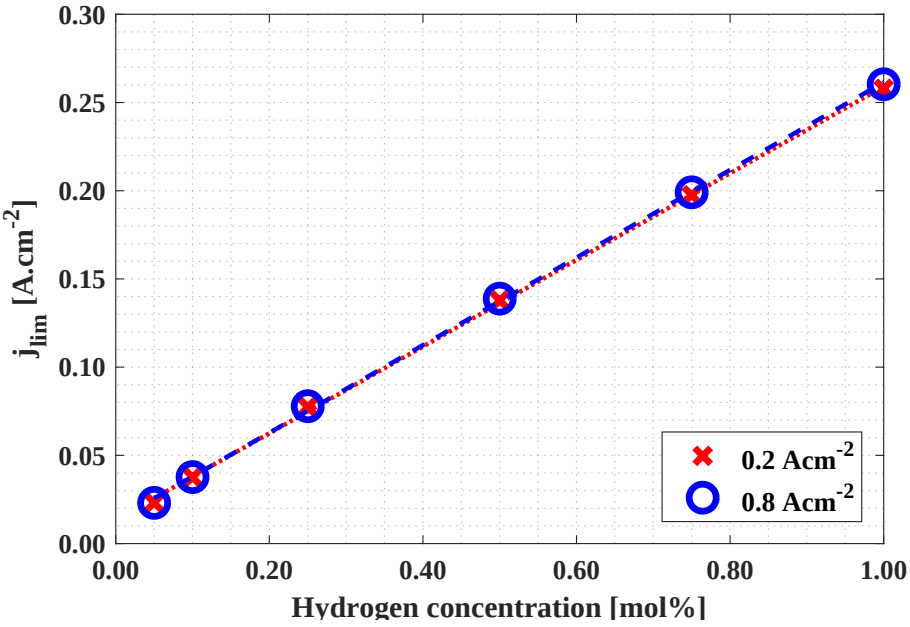

Fig. 4.2: The anodic limiting current as a function of hydrogen concentration. Source: Paper C)

4.2.2 Electrochemical Impedance Spectroscopy

Since limiting current failed to measure the acid migration phenomenon, EIS method was investigated. The EIS measurements were carried out in two different ways:

1. Normal EIS measurement with 5 points per decade and frequency between 100 kHz and 100 mHz was able to capture flooding kinetics
2. Fast EIS measurement with 1 single low frequency (1 Hz) measurement, in which deflooding kinetics were captured

In Fig. 4.3, the time constants for the flooding and de-flooding kinetics is shown. Based on a linear fit the time constant for flooding was calculated as 8.1$\pm$0.1 and for de-flooding 4.8$\pm$0.9 min. These time constants were calculated from the mean of three separate measurements. This shows that flooding is a faster process compared to de-flooding which was also observed by Eberhardt et al. [98].

4.3 Acid migration as a function of acid doping and current density

Based on the results from Paper C, an experiment was designed to quantify the hydrogen transport resistance as a function of acid doping in the membrane and current density. Thus, three different MEAs doped with 85%, 75% and 65% concentrated PA were tested to determine whether acid doping level plays a role in the flooding and de-flooding of GDL and thereby on the hydrogen mass transport. The doping level for the three MEAs were 11, 8.3 and 7 molecules of H_3PO_4 per PBI repeat unit, respectively, which is much less compared to the MEAs used for the test in the previous section (33-36 molecules of H_3PO_4 per PBI repetitive unit). The method used for the characterization work was fast EIS recording at 1 Hz frequency over time. The test was carried out with oxygen on the cathode and 5 % H_2 and 95 % N_2 on the anode. The low concentration of hydrogen on the anode was used to visualise the enhanced mass transport resistance on the anode. The assumption is that with reformed fuel operation at some areas in the cell will have very low concentration. However, it is debatable whether the concentration will be as low as 5 %.

The impedance with a single frequency was measured and the time constants were calculated using an exponential equation for fitting the data. Interestingly, with lower doping levels the trend differs. The flooding case or high current density (0.8 A cm^{-2}) operation results in a decreasing mass transport resistance, while the de-flooding case or low current density (0.2

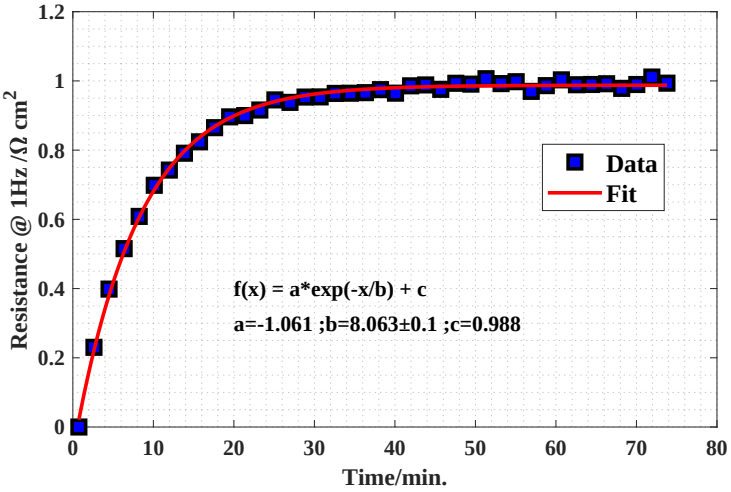

(a) Acid flooding kinetics

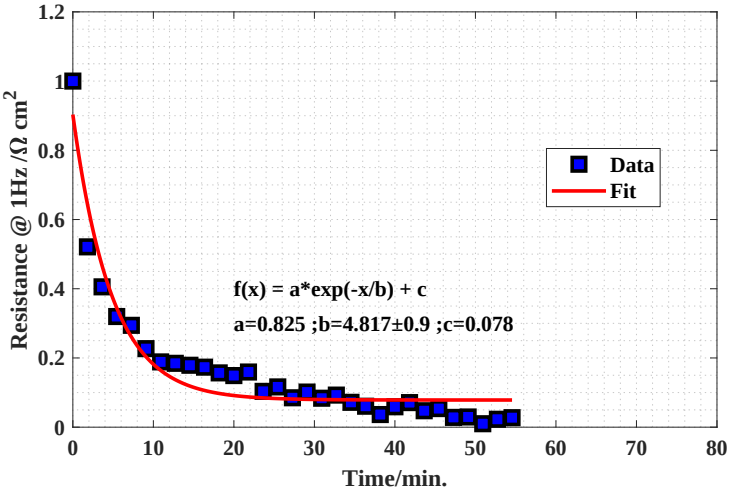

(b) Acid deflooding kinetics

Fig. 4.3: Kinetics of flooding and de-flooding at high and low current density, Source: Paper C

A cm^{-2}) operation results in an increase in the mass transport resistance, which can be seen in Fig. 4.4. The time constants were calculated by fitting the real part of the impedance with Eqn. 4.1, where 'b' gives the time constant.

$$f(x) = a \times \exp(\frac{-x}{b}) + c \tag{4.1}$$

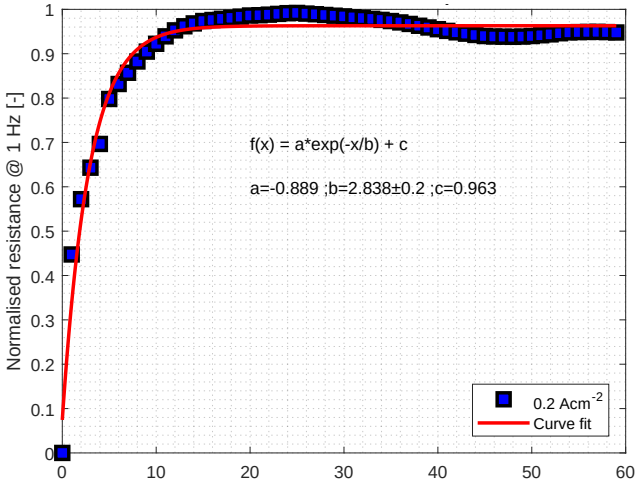

(a) Acid kinetics at low current density (0.2 A cm^{-2}

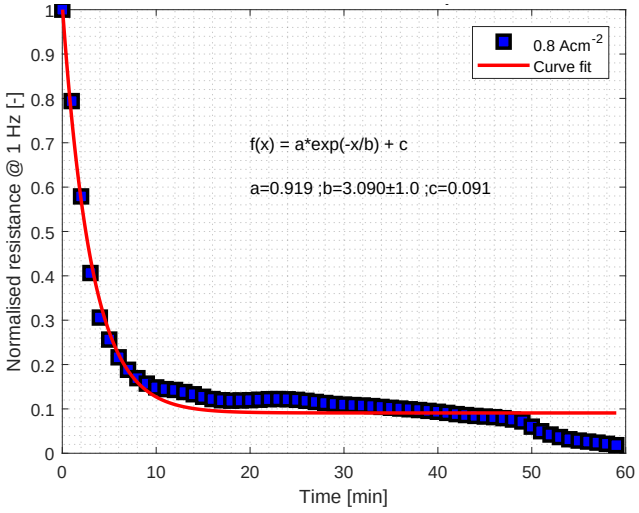

(b) Acid kinetics at high current density (0.8 A cm^{-2})

Fig. 4.4: Kinetics of flooding and de-flooding at high and low current density, Source: Paper D.

The real part of the resistance was normalised to 1 by deducing the maxima and minima from the data. The normalised low frequency (1 Hz) is shown in Fig. 4.4. This trend is repeated for the lower doping levels as well.

The time constant as seen the Table 4.1 clearly indicates a relation to the doping level. As the doping level decreases it takes a longer time for the resistance to become stable. The decrease in low frequency (1 Hz) resistance at

Table 4.1: Time constant for resistance to become stable at 0.2 A cm^{-2} and 0.8 A cm^{-2}, Source: Paper D

Acid doping	Time constant (0.2 A cm^{-2})	Time constant (0.8 A cm^{-2})
[molecules of H_3PO_4 per PBI repeat unit]	[min]	[min]
11	2.8±0.2	3.1±0.2
8.3	5.7±0.5	3.3±0.5
7	9.5±0.8	5.6±0.5

high current density and increase at low current density could be explained based on the water generated at each current density. The water generated dilutes the PA due to strong affinity of PA towards water. This makes the acid redistribution more dominant. However,the low doping level probably prevents the acid from reaching the anode GDL, and therefore, from hindering the mass transport. The change in mass transport resistance could be related to acid reaching the catalyst at high current density and creating three phase boundary easily accessible to the reactants. Then, at low current density the acid could be moving back to the membrane and reversing the effect. Another, explanation could be related to the solubility of O_2 in PA. Due to more acid available, as a result of higher water generation which combines with PA, the O_2 transport to the reaction sites become easier and the cathode side improvement is seen in the resistance. However, the transport resistance improvement at high current density suggest that the loss of acid may not be a problem in the case of low doped MEAs. This is because the chances of acid reaching the GDL and thereby getting removed decreases with decreasing number of free PA molecules. But from the present test it is clear that the acid is not reaching the anode GDL else a low concentration of H_2 would face a mass transport issue. Further investigation of the high frequency intercept which is attributed to membrane resistance was done. The ohmic resistance change over time at 0.2A cm^{-2} and 0.8A cm^{-2} is shown in Fig. 4.5. A similar changes in the high frequency resistance suggests that the low frequency resistance changes shown above in Fig. 4.4 are influenced by the high frequency resistance shown in Fig. 4.5. Thus, it could be said that the acid flooding of GDL is not an issue in low doped MEAs <12 molecules of H_3PO_4 per PBI repeat unit. The change in current only leads to a small change in the membrane resistance which could be explained based on hydration and dehydration of the membrane.

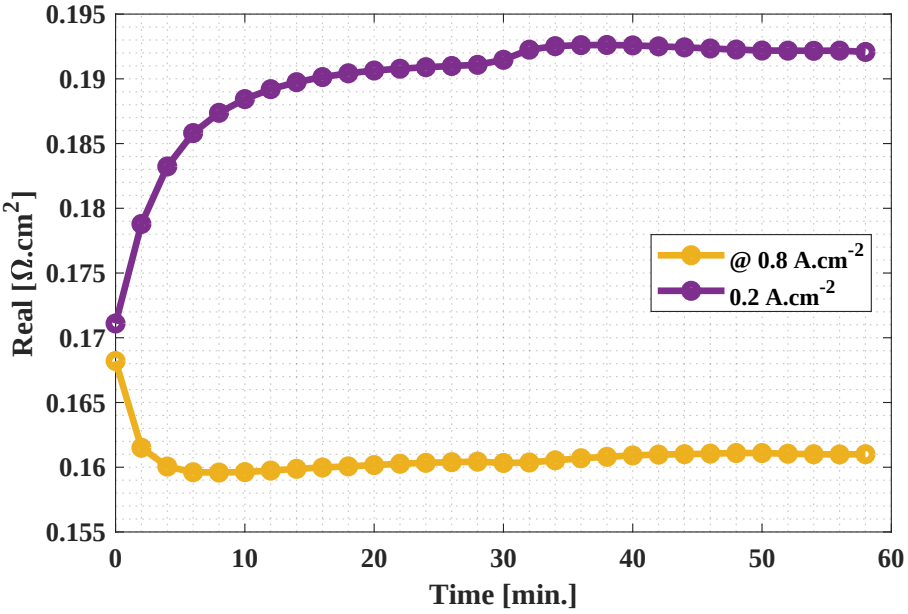

Fig. 4.5: The series or ohmic resistance at 0.2A cm^{-2} and 0.8A cm^{-2}, Source: Paper D

4.4 Summary

The tests to understand the acid migration and redistribution was carried out. The first test focused on understanding the hydrogen mass transport issues arising due to acid migration towards anode as a function of current density. The second test was to understand the same using different PA doping level. The results are interesting to design a HT-PEM fuel cell operational strategy. The first test suggests that acid migrated towards the anode GDL and back as a function of current density. At high current density the hydrogen mass transport increased for ≈8 min before stabilising. While at low current density the resistance decreases for ≈4 min before stabilising. This suggest that flooding and de-flooding are not happening at the same speed and as a result some acid may be lost due to this phenomena and as a result affect the durability.

The second test with low doped MEAs suggest that mass transport resistance decreases at high current density and increases at low current density. The time constants were also seen to be a function of the doping. The results from test 2 suggest that changing current density to 0.8 A cm^{-2} does not force the acid to the GDL as mass transport resistance improves. Therefore, it could be concluded that at high doping levels the loss of acid is an issue when operating at high current density. However, it is not a problem when

the doping level is low $\approx$10. This leads to the conclusion that even if there is some loss of acid from the high doped MEAs, after a certain loss it would not have the same rate of acid loss with high current density operation. Another possibility is if the acid migration is also a function of the MEA preparation process. But, that is beyond the scope of this thesis and would be a useful investigation to be made in the future.

Chapter 5

Mitigation strategy to avoid phosphoric acid loss

In this chapter, the discussion is based on Paper E, in which we propose a mitigation strategy to tackle the acid loss in HT-PEM fuel cells. The work is based on the assumption that the acid migration and diffusion is a function of current density. At high current density (>0.5 $A\,cm^{-2}$) the acid migrates towards anode and at low current density (<0.3 $A\,cm^{-2}$) back diffusion of acid takes place.

The focus was to develop a mitigation strategy for acid loss which leads to HT-PEM fuel cell degrading in performance. The proton conductor in HT-PEMFC being PA is of great importance to make sure it stays with the MEA. The acid in a HT-PEMFC MEA is quite mobile and the redistribution of acid is contributed mainly by the migration and diffusion processes. The acid movement is strongly influenced by the current density (explained in chapter 4, section 1), acid concentration (explained in Chapter 4, section 2) and also temperature. Thus, to develop a mitigation strategy which would relax the cell in order for the acid to remain within the cell, current density function was investigated. The MEAs used were from DPS with a doping level of ≈11 molecules of H_3PO_4 per PBI repeat unit.

5.1 Load cycling with different relaxation time

The relaxation time as defined in Paper E, is the time of cell operation at low current density (0.2 $A\,cm^{-2}$). The experimental conditions and the corresponding degradation calculated is shown in Table 5.1. The last row in the table is cell 5 with 2 min of relaxation time and it shows the minimal degra-

dation at different current densities also when compared to cell 1 operating at constant current density of 0.55 A cm^{-2}. The different degradation rates calculated for same MEA show a positive as well as negative effect of load cycling. The load cycling with a relaxation time <1 min was found to degrade much faster compared to the others having a relaxation time >1 min and the one operating at constant current density. Furthermore, comparing constant current density operating cell to load cycling cells the degradation for constant current density operation is higher. Thus, it is evident that load cycling is able to enhance the operational lifetime of an HT-PEMFC with PA doped PBI membranes.

An operation of 2000 h with a degradation of 36 µV h^{-1} when extrapolated to 5000 h results in a voltage of 0.35 V at 0.55 A cm^{-2} for cell 5. The constant current operation (Cell1) would result a voltage of 0.23 V. These numbers are just indicative and not a certain number since its hard for fuel cell performance to be extrapolated over time. Thus, it would require for a long term operation to support these claims.

Table 5.1: The time at different current densities, experimental duration and corresponding degradations calculated at different current densities, Source: adapted from Paper E

MEA.	**Time @ 0.2**A cm^{-1}	**Time @ 0.8**A cm^{-1}	**Test duration**	**@0.2** A cm^{-2}	**@0.8** A cm^{-2}	**@0.55** A cm^{-2}
(No.)	(s)	(s)	(h)	(µV h^{-1})	(µV h^{-1})	(µV h^{-1})
1	-	-	2000	-	-	57
2	15	21	775	195	434	460
3	30	42	1600	44	157	109
4	60	84	2000	26	93	52
5	**120**	**168**	**2000**	**16**	**55**	**36**

5.1.1 Impedance and Performance analysis

To further account for the differences in degradation, EIS data recorded every 25 h were fitted to an equivalent circuit model with series resistance and two parallel RC elements. The fitted resistances were used to calculate the changes in resistance over time after the break-in as shown in Table 5.2. Based on the explanation in chapter 2, the series resistance is associated with membrane resistance to proton conductivity, the intermediate frequency resistance is associated with a combination of cathode and anode kinetic limitations, while the low frequency is attributed to mass transport issue arising at the cathode and sometimes also the anode.

The comparison of % changes in different resistances, show that the low

Table 5.2: Changes in different resistances after the completion of tests, Source: adapted from Paper E.

MEA	Series		Intermediate		Low	
no.	($\Omega\,cm^2\,min^{-1}$)	Change [%]	($\Omega\,cm^2\,min^{-1}$)	Change [%]	($\Omega\,cm^2\,min^{-1}$)	Change [%]
1	**0.30**	**8.9**	**0.25**	**7.3**	**0.07**	**1.9**
2	0.165	19.1	1.57	18.2	2.97	34.5
3	0.51	12.5	0.40	9.8	0.28	6.9
4	0.22	6.4	0.24	7.0	0.12	3.6
5	**0.13**	**3.7**	**0.18**	**5.3**	**0.04**	**1.1**

frequency, intermediate frequency and series resistances for all the cells except cell 2 show small changes. The series resistance is directly related to PA in the membrane, which is the proton conductor. The series resistance changes more than double for cell 1 operating on constant current density compared to cell 5 which was load cycling with a time constant of 2 h, which confirms load cycling helps in keeping the distribution of PA close to the three phase boundary more uniform. This keeps the cell performance higher compared to steady state operation. The intermediate resistance changes indicate that diffusion limitations remain low when the cell is load cycled with a 2 min relaxation time. The low frequency resistance is mostly dominated by the mass transport issues. Two major driving forces which could cause the change in mass transport is gas channel dynamics and catalyst active site blockages [54, 112]. In the present case, no poisonous gases like CO is present and the flow rates are high. Thus, the possibility could be acid covering some of the catalyst sites which leads to higher mass transport resistance.

The power and efficiency comparison of different cells over time is shown in Fig. 5.1. The power generated shown in Fig. 5.1(a) and the efficiency, as can be seen in Fig. 5.1(b) is not compromised due to load cycling. The power generated and the efficiency of cell 1 and cell 5 are similar, while for cell 2 as expected due to the degradation rates, they are the lowest. The efficiency was calculated based on the lower heating value of H_2 using equation 5.1 and Eqn. 5.2

$$P_{H_2O} = \dot{V}_{H_2} \times \rho_{H_2} \times LHV_{H_2} \tag{5.1}$$

where $\dot{V}_{H_2}$ is the flow rate of hydrogen in $L\,min^{-1}$ and LHV_{H_2} is the lower heating value of hydrogen. The density of hydrogen is denoted by ρ_{H_2}.

$$Efficiency = \frac{Output\ power\ (P_1)}{Input\ power\ (P_{H_2O}) \times 100}\% \tag{5.2}$$

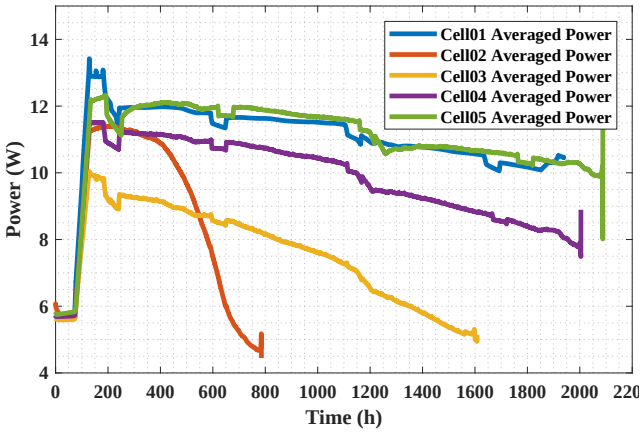

(a) Comparison of power generated over time

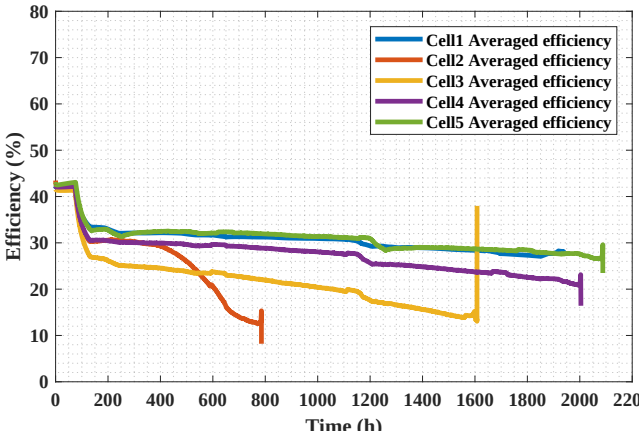

(b) Efficiency comparison over time

Fig. 5.1: Performance comparison in terms of power generated and electrical efficiency, Source: Paper E.

5.2 Summary

The analysis of results from Paper E, clearly shows a positive influence of load cycling on the degradation. The lowest degradation is for Cell 5 with a low current density operation of 2 min and high current density operation of 2.8 min. The resistance changes further support the claim that the degradation is lower due to improved distribution of acid and less acid getting evaporated or flushed out from the cell. The comparison of performance suggests load cycling does not lead to a loss in performance or efficiency.

Chapter 6

Final Remark

This chapter will highlight the results obtained during the three years of my PhD and the application of these results to develop a cost effective and durable reformed methanol fuel cell systems.

6.1 Conclusions

A detailed literature study shows that the research focus on HT-PEMFC systems over the last few years has been very active. The two major problems of fuel impurity and acid dynamics are still an open challenge in the field of HT-PEMFCs.

The project focuses on high temperature polymer electrolyte membrane fuel cells coupled with methanol reformer (RMFC). An experimental approach was taken to develop a better understanding of the HT-PEM fuel cells. The focus was on improving the lifetime and reduce the cost of production of these systems. The project was divided into three major questions:

1. How feasible is it to operate HT-PEMFC with reformed fuel (CH_3OH reformer)?
2. What are the implication of acid migration and redistribution in HT-PEMFC operating under different operating conditions?
3. Which operational strategies would ensure a longer durability and reduced cost?

The focus of this dissertation was based on different characterization methods to gain better knowledge about the system and thereby suggest optimal operational strategies. The study was carried out on single cell level

to reduce the complexities involved in a stack. Different approaches were investigated to understand the degradation of HT-PEMFC with simulated reformer output. The focus was restricted to CH_3OH slip in the anode fuel stream. The acid dynamics was studied to understand the optimal operational approach to reduce the acid loss (if any) due to different operational parameters such as current density and doping level.

Two well established methods, IV curve and electrochemical impedance spectroscopy (EIS) were used to gain more understanding about the system. The EIS data analysis was carried out using equivalent circuit models. A third approach based on limiting current method was also investigated in one part of the work to understand acid dynamics. However, the method was found not suitable for detecting the fast acid dynamics.

The results obtained with simulated reformed fuel (CH_3OH, H_2O and H_2), suggest the operation of RMFC with 3% CH_3OH does not affect the performance and the durability. However, the attempt to reduce production cost by fast break-in strategy was not successful as there were significant differences among the tested MEAs and secondly, reformate break-in reduced the durability markedly. Thus, from the present studies it seems break-in is a vital process to ensure longer durability for RMFCs.

The acid migration from the cathode to anode at high current density (0.8 $A\,cm^{-2}$) is a problem when the doping levels ($\approx$ 33-36 moleculesof H_3PO_4 per PBI repeat unit) are high. The high doping level leads to migration of acid to the gas diffusion layer (GDL), bipolar plate and the catalyst and thereby, hinders the transport of hydrogen to the active catalyst sites. Hence, the performance could be affected as a result and also the durability will be affected. The presence of acid in the GDL pores and bipolar plates are easier to be removed from the cell by the gas and/or evaporation. However, a lower doping level behaves differently.

The acid migration related hydrogen mass transport limitation is not evident at high current density (0.8 $A\,cm^{-2}$). Moreover, the results suggest that the hydrogen mass transport improves with a lower doping level ($\approx$ 11-12 molecules of H_3PO_4 per PBI repeat unit). The assumption is that the water generated decreases the viscosity of PA and thereby, PA has a higher tendency to migrated towards other components within the cell. However, the PA vapour pressure is lower compared to highly doped MEAs due to which the acid is only moving to the catalyst and thereby creating more easily accessible three phase active sites. The acid quantity being less results in no flooding of catalyst.

Based on the results with differently doped MEAs, it was deduced that acid redistribution takes place when the cell is operated under current cycling. Thus, to ensure the acid redistribution does not lead to acid loss, load cycling profile with different relaxation time was investigated. The relaxation time here is the operation of cell at 0.2 $A\,cm^{-2}$.

The load cycling test with 2 min at low current density and 2.8 min at high current density, resulted in the least degradation. This is in line with the time constants of 3 min calculated for Dapazol MEAs which have a doping level of $\approx$ 11-12 molecules of H_3PO_4 per PBI repeat unit. Thus, it could be assumed that the current loading helps in the redistribution of acid to the catalyst layer at high current density and back to the membrane at low current density. This back and forth movement of acid could be the reason for decreased degradation compared to constant current density operation.

6.2 Main Contributions

- A test with CH_3OH slip on the anode was investigated and a safe operating CH_3OH slip of $<$3 % was found.
- Break-in time could be reduced, provided HT-PEMFC operates with pure H_2 and mode of operation is load cycling.
- Break-in with reformed fuel was found not suitable for long term durability of HT-PEMFC.
- Anodic mass transport is affected by the acid redistribution taking place as a function of current density and doping level.
- Limiting current method to investigate the fast acid kinetic was found not suitable
- When doping level is high >30 molecules of H_3PO_4 per PBI repeat unit, acid flooding of anode GDL was found.
- When doping level is low <11 molecules of H_3PO_4 per PBI repeat unit, acid flooding of anode GDL was not found.
- Current cycling of HT-PEMFC was found to be beneficial in improving the durability.

6.3 Future prospective approaches

Distribution of relaxation time (DRT), a method used to analysis EIS data, was investigated to deduce a better understanding and to do away with the assumptions involved in equivalent circuit model fits. Fuel cells being a complex systems, the separation of different time constant during operation was found not feasible at this point.However, it has some advantages which needs to be understood further.

Electrochemical impedance spectroscopy is a very useful tool to investigate different phenomena on an operating cell. However, it is time consuming and requires sophisticated equipment to carry out. Thus, it could be modified to make it faster and easier to map the cell issues with a frequency which will be interesting in the diagnostics of HT-PEMFC. One such method, which was investigated during the PhD for understanding acid migration was Total Harmonic Distortion Analysis (THDA). Though, the preliminary test did not fetch interesting outcomes, it would be interesting to investigate further and deduce a relationship.

Break-in is a complex process and it seems very interesting to pursue further to develop a better understanding which could be used to develop a faster method to break-in an HT-PEMFC.

Furthermore, the acid doping plays a major role when the cell is operated at different current densities. Thus, to further investigate whether an acid doping level between ≈33-36 and ≈10-12 is beneficial to improve the transport resistance at high current density, MEAs with different doping levels should be further characterized.

References

[1] Simon Lennart Sahlin et al. *Characterization and Modeling of a Methanol Reforming Fuel Cell System*. Aalborg Universitetsforlag. (Ph.d.-serien for Det Teknisk-Naturvidenskabelige Fakultet, Aalborg Universitet), 2016. ISBN 978-87-7112-466-8. doi: 10.5278/vbn.phd.engsci.00059.

[2] Mausami Desai and Reid P. Harvey. Inventory of U.S. Greenhouse Gas Emissions and Sinks: 1990-2015. *Federal Register*, 82(30):10767, 2017. ISSN 00976326. doi: EPA430-R-13-001.

[3] IPCC. A report of the intergovernmental panel on climate change 2014. Technical report, Intergovernmental panel on climate change, 2014.

[4] Jonathan A. Patz, Diarmid Campbell-Lendrum, Tracey Holloway, and Jonathan A. Foley. Impact of regional climate change on human health. *Nature*, 438(7066):310–317, 2005. ISSN 0028-0836. doi: 10.1038/nature04188. URL http://www.nature.com/doifinder/10.1038/nature04188.

[5] The Parties, Being Parties, United Nations, Framework Convention, Climate Change, Durban Platform, Enhanced Action, and Mother Earth. Paris Agreement. Technical report, Uninted Nations, 2015.

[6] ME Assessment. Synthesis report. Technical Report November, University of Copenhagen, 2007. URL http://scholar.google.com/scholar?hl=en{&}btnG=Search{&}q=intitle:Synthesis+Report{#}2.

[7] United Nations Environment Programme (UNEP). The Emissions Gap Report 2017: A UN Environment Synthesis Report. Technical report, United Nation (UN), 2017. URL http://www.unep.org/pdf/2012gapreport.pdf.

[8] ENS. Accelerating green energy towards 2020. Technical Report March, Danish Ministry for Climate, Energy and Building, 2012. URL https://ens.dk/sites/ens.dk/files/EnergiKlimapolitik/accelerating{_}green{_}energy{_}towards{_}2020.pdf.

[9] Joshua S Hill. Denmark Generated Enough Wind Energy To Power All Its Electricity Needs On Wednesday, 2017. URL https://cleantechnica.com/2017/02/24/denmark-generated-enough-wind-energy-power-power-needs-wednesday/.

[10] The Partnership Smart Energy Networks. Vision for Smart Energy in Denmark. Technical report, The Danish Smart Energy Research, Development and Demonstration, 2015. URL

http://www.smartenergynetworks.dk/uploads/3/9/5/5/39555879/vision{_}for{_}smart{_}energy{_}in{_}denmark.pdf.

[11] M. Becherif, H. S. Ramadan, K. Cabaret, F. Picard, N. Simoncini, and O. Bethoux. Hydrogen Energy Storage: New Techno-Economic Emergence Solution Analysis. *Energy Procedia*, 74(0):371–380, 2015. ISSN 18766102. doi: 10.1016/j.egypro.2015.07.629. URL http://dx.doi.org/10.1016/j.egypro.2015.07.629.

[12] John Andrews and Bahman Shabani. Re-envisioning the role of hydrogen in a sustainable energy economy. *International Journal of Hydrogen Energy*, 37(2):1184–1203, 2012. ISSN 03603199. doi: 10.1016/j.ijhydene.2011.09.137. URL http://dx.doi.org/10.1016/j.ijhydene.2011.09.137.

[13] S. Pacala. Stabilization Wedges: Solving the Climate Problem for the Next 50 Years with Current Technologies. *Science*, 305(5686):968–972, 2004. ISSN 0036-8075. doi: 10.1126/science.1100103. URL http://www.sciencemag.org/cgi/doi/10.1126/science.1100103.

[14] Bruno G. Pollet, Iain Staffell, and Jin Lei Shang. Current status of hybrid, battery and fuel cell electric vehicles: From electrochemistry to market prospects. *Electrochimica Acta*, 84:235–249, 2012. ISSN 00134686. doi: 10.1016/j.electacta.2012.03.172. URL http://dx.doi.org/10.1016/j.electacta.2012.03.172.

[15] Konstantinos Vatopoulos and Evangelos Tzimas. Assessment of CO 2 capture technologies in cement manufacturing process. *Journal of Cleaner Production*, 32:251–261, 2012. ISSN 09596526. doi: 10.1016/j.jclepro.2012.03.013. URL http://dx.doi.org/10.1016/j.jclepro.2012.03.013.

[16] Nicolás Pardo and José Antonio Moya. Prospective scenarios on energy efficiency and CO2 emissions in the European Iron & Steel industry. *Energy*, 54:113–128, 2013. ISSN 03605442. doi: 10.1016/j.energy.2013.03.015. URL http://dx.doi.org/10.1016/j.energy.2013.03.015.

[17] Marge Ryan. Methanol and Fuel Cells. *Fuel Cells Bulletin*, 2012(May): 1–6, 2012. URL http://www.fuelcelltoday.com/media/1637842/12-05-23{_}methanol{_}and{_}fuel{_}cells.pdf.

[18] Serenergy. http://www.serenergy.com. *Serenergy fuel cell applications*, jun 2015. URL http://www.serenergy.com.

[19] George A. Olah et al. Recycling of carbon dioxide into methylalcohol and related oxygenaters for hydrocarbons, 1999.

[20] George A. Olah, Alain Goeppert, and G. K.Surya Prakash. Beyond Oil and Gas: The Methanol Economy: Second Edition. *Beyond Oil and Gas: The Methanol Economy: Second Edition*, pages 1–334, 2009. ISSN 14337851. doi: 10.1002/9783527627806.

[21] J. Albo, M. Alvarez-Guerra, P. Castaño, and A. Irabien. Towards the electrochemical conversion of carbon dioxide into methanol. *Green Chem.*, 17(4):2304–2324, 2015. ISSN 1463-9262. doi: 10.1039/C4GC02453B. URL http://xlink.rsc.org/?DOI=C4GC02453B.

[22] Maxim Lyubovsky Friday. Shifting the paradigm: Synthetic liquid fuels offer vehicle for monetizing wind and solar energy. *Journal of Energy Security*, 2017.

[23] Engineering, BSE, 2017. URL http://www.bse-leipzig.de/en/methanol.html.

[24] Thomas J Schmidt and Jochen Baurmeister. Properties of high-temperature PEFC Celtec®-P 1000 MEAs in start/stop operation mode. *Journal of Power Sources*, 176(2):428–434, 2008. doi: http://dx.doi.org/10.1016/j.jpowsour.2007.08.055. URL http://www.sciencedirect.com/science/article/pii/S0378775307016047.

[25] Thomas J. Schmidt and Jochen Baurmeister. Durability and Reliability in High-Temperature Reformed Hydrogen PEFCs. *ECS Transactions*, 3 (1):861–869, oct 2006. ISSN 1938-5862. doi: 10.1149/1.2356204. URL http://ecst.ecsdl.org/content/3/1/861.abstract.

[26] Q. Li, R. He, J.O. Jensen, and N.J. Bjerrum. PBI-Based Polymer Membranes for High Temperature Fuel Cells– Preparation, Characterization and Fuel Cell Demonstration. *Fuel Cells*, 4(3):147–159, aug 2004. ISSN 1615-6846. doi: 10.1002/fuce.200400020. URL http://doi.wiley.com/10.1002/fuce.200400020.

[27] Samuel Simon Araya, Fan Zhou, Vincenzo Liso, Simon Lennart Sahlin, Jakob Rabjerg Vang, Sobi Thomas, Xin Gao, Christian Jeppesen, and Søren Knudsen Kær. A comprehensive review of PBI-based high temperature PEM fuel cells, 2016. ISSN 03603199.

[28] Juan Antonio Asensio, Eduardo M. Sánchez, and Pedro Gómez-Romero. Proton-conducting membranes based on benzimidazole polymers for high-temperature PEM fuel cells. A chemical quest. *Chemical Society Reviews*, 39(8):3210, aug 2010. ISSN 0306-0012. doi: 10.1039/b922650h. URL http://xlink.rsc.org/?DOI=b922650h.

[29] Qingfeng Li, Ronghuan He, Ji-An Gao, Jens Oluf Jensen, and Niels. J Bjerrum. The CO Poisoning Effect in PEMFCs Operational at Temperatures up to 200°C. *Journal of the Electrochemical Society*, 150(12):A1599–A1605, 2003. doi: 10.1149/1.1619984. URL http://jes.ecsdl.org/content/150/12/A1599.abstract.

[30] Yannick Garsany, Benjamin D. Gould, Olga a. Baturina, and Karen E. Swider-Lyons. Comparison of the Sulfur Poisoning of PBI and Nafion PEMFC Cathodes. *Electrochemical and Solid-State Letters*, 12:B138, 2009. ISSN 10990062. doi: 10.1149/1.3168516.

[31] Chaojie Song and Jiujun Zhang. PEM Fuel cell electrocatalyst and catalyst layers, fundamentals and applications. In *PEM Fuel cell electrocatalyst and catalyst layers, fundamentals and applications*, pages 861–888. Springer London, 2008. ISBN 978-1-84800-935-6.

[32] Julia Song and Taraneh Foster. First fuel cell CHP system designed for residential and small-scale commercial use. *Fuel Cells Bulletin*, 2011(7): 12–14, 2011. ISSN 14642859. doi: 10.1016/S1464-2859(11)70229-2. URL http://dx.doi.org/10.1016/S1464-2859(11)70229-2.

[33] Intelec Orlando. Trenergi completes HTPEM residential CHP proof-of-concept. *Fuel Cells Bulletin*, 2010(7):6, 2010. ISSN 14642859. doi: 10.1016/S1464-2859(10)70216-9. URL http://linkinghub.elsevier.com/retrieve/pii/S1464285910702169.

[34] Surya Subianto. Recent advances in polybenzimidazole/phosphoric acid membranes for high-temperature fuel cells. *Polymer International*, 63(7):1134–1144, 2014. ISSN 10970126. doi: 10.1002/pi.4708.

[35] Vicki P. McConnell. High-temperature PEM fuel cells: Hotter, simpler, cheaper. *Fuel Cells Bulletin*, 2009(12):12–16, 2009. ISSN 14642859. doi: 10.1016/S1464-2859(09)70411-0. URL http://dx.doi.org/10.1016/S1464-2859(09)70411-0.

[36] Amrit Chandan, Mariska Hattenberger, Ahmad El-kharouf, Shangfeng Du, Aman Dhir, Valerie Self, Bruno G. Pollet, Andrew Ingram, and Waldemar Bujalski. High temperature (HT) polymer electrolyte membrane fuel cells (PEMFC) – A review. *Journal of Power Sources*, 231: 264–278, jun 2013. ISSN 03787753. doi: 10.1016/j.jpowsour.2012.11.126. URL http://www.sciencedirect.com/science/article/pii/S0378775312018113http://linkinghub.elsevier.com/retrieve/pii/S0378775312018113.

[37] Johan Agrell, Henrik Birgersson, and Magali Boutonnet. Steam reforming of methanol over a Cu/ZnO/Al2O3 catalyst: A kinetic analysis and

strategies for suppression of CO formation. *Journal of Power Sources*, 106(1-2):249–257, 2002. ISSN 03787753. doi: 10.1016/S0378-7753(01)01027-8.

[38] A. Iulianelli, P. Ribeirinha, A. Mendes, and A. Basile. Methanol steam reforming for hydrogen generation via conventional and membrane reactors: A review. *Renewable and Sustainable Energy Reviews*, 29, 2014. ISSN 13640321. doi: 10.1016/j.rser.2013.08.032.

[39] Kristian Kjær. *Reformed Methanol Fuel Cell Systems - and their use in Electric Hybrid Systems*. Aalborg Universitetsforlag. (Ph.d.-serien for Det Teknisk-Naturvidenskabelige Fakultet, Aalborg Universitet), 2015. ISBN 9788792846723.

[40] The Danish Partnership for Hydrogen and Fuel Cells. Balancing the Future Danish Energy System Hydrogen and Fuel Cells – Technologies for the Future. Technical report, The Danish Partnership for Hydrogen and Fuel Cells facilitates, 2012. URL http://www.hydrogennet.dk/129/.

[41] Dimitrios Papageorgopoulos. FY 2016 Annual Progress Report - Fuel Cells Program Overview INTRODUCTION. Technical report, DOE Hydrogen and Fuel Cells Program, 2016.

[42] Marge Ryan. Methanol – Clean Fuel for the Future? *Fuel Cell Today*, 2013(April), 2013. URL http://www.fuelcelltoday.com/analysis/analyst-views/2013/13-05-08-methanol-\T1\textendash-clean-fuel-for-the-future.

[43] Energy Efficiency and Renewable Energy. Comparison of Fuel Cell Technologies. Technical Report February, Department of Energy, US, 2011. URL http://www1.eere.energy.gov/hydrogenandfuelcells/fuelcells/fc{_}types.html.

[44] C. Siegel, editor. *High temperature polymer electrolyte membrane fuel cells. Modeling, simulation, and segmented measurements*. Logos Verlag Berlin – Academic Publications in Science and Journal of Medical Humanities, 2015.

[45] Susanta K Das, Antonio Reis, and K J Berry. Experimental evaluation of CO poisoning on the performance of a high temperature proton exchange membrane fuel cell. *Journal of Power Sources*, 193 (2):691–698, 2009. doi: http://dx.doi.org/10.1016/j.jpowsour.2009.04.021. URL http://www.sciencedirect.com/science/article/pii/S037877530900706X.

[46] Ying Zhu, Wenhua H. Zhu, and Bruce J. Tatarchuk. Performance comparison between high temperature and traditional proton exchange membrane fuel cell stacks using electrochemical impedance spectroscopy. *Journal of Power Sources*, 256:250–257, jun 2014. ISSN 03787753. doi: 10.1016/j.jpowsour.2014.01.049. URL http://www.sciencedirect.com/science/article/pii/S037877531400072X.

[47] Caizhi Zhang, Lan Zhang, Weijiang Zhou, Youyi Wang, and Siew Hwa Chan. Investigation of water transport and its effect on performance of high-temperature PEM fuel cells. *Electrochimica Acta*, 149:271–277, dec 2014. ISSN 00134686. doi: 10.1016/j.electacta.2014.10.059. URL http://www.sciencedirect.com/science/article/pii/S0013468614020660.

[48] Niels J. Bjerrum Ronghuan He, Qingfeng Li, Gang Xiao. Proton conductivity of phosphoric acid doped polybenzimidazole and its composites with inorganic proton conductors. *Journal of Membrane Science*, 226(1-2):169–184, dec 2003. ISSN 03767388. doi: 10.1016/j.memsci.2003.09.002. URL http://www.sciencedirect.com/science/article/pii/S0376738803004216.

[49] Anders Risum Korsgaard, Mads Pagh Nielsen, Mads Bang, and Søren Knudsen Kær. Modeling of CO Influence in PBI Electrolyte PEM Fuel Cells. In *Proceedings of the 4th International ASME Conference on Fuel Cell Science, Engineering and Technology*, volume 2006, pages 911–915. ASME Press, 2006. ISBN 0-7918-4247-9. doi: 10.1115/FUELCELL2006-97214. URL http://proceedings.asmedigitalcollection.asme.org/proceeding.aspx?articleid=1592989.

[50] E. Romero-Pascual and J. Soler. Modelling of an HTPEM-based micro-combined heat and power fuel cell system with methanol. *International Journal of Hydrogen Energy*, 39(8):4053–4059, mar 2014. ISSN 0360-3199. doi: http://dx.doi.org/10.1016/j.ijhydene.2013.07.015. URL http://linkinghub.elsevier.com/retrieve/pii/S0360319913017151http://www.sciencedirect.com/science/article/pii/S0360319913017151.

[51] Søren Juhl Andreasen, Søren Knudsen Kær, and Simon Sahlin. Control and experimental characterization of a methanol reformer for a 350 W high temperature polymer electrolyte membrane fuel cell system. *International Journal of Hydrogen Energy*, 38(3):1676–1684, feb 2013. ISSN 03603199. doi: 10.1016/j.ijhydene.2012.09.032. URL http://www.sciencedirect.com/science/article/pii/S0360319912020678.

[52] F. Javier Pinar, Maren Rastedt, Nadine Pilinski, Peter Wagner, and Alexander Dyck. Demonstrating feasibility of a high temperature

polymer electrolyte membrane fuel cell operation with natural gas reformate composition. *International Journal of Hydrogen Energy*, 2017. ISSN 03603199. doi: 10.1016/j.ijhydene.2017.03.161. URL http://www.sciencedirect.com/science/article/pii/S0360319917311667.

[53] Sobi Thomas, Jakob Rabjerg Vang, Samuel Simon Araya, and Søren Knudsen Kær. Experimental study to distinguish the effects of methanol slip and water vapour on a high temperature PEM fuel cell at different operating conditions. *Applied Energy*, 192:422–436, apr 2016. ISSN 0306-2619. doi: http://dx.doi.org/10.1016/j.apenergy.2016.11.063. URL http://linkinghub.elsevier.com/retrieve/pii/S0306261916316488http://www.sciencedirect.com/science/article/pii/S0306261916316488.

[54] Fan Zhou, Søren Juhl Andreasen, Søren Knudsen Kær, and Jung O. Park. Experimental investigation of carbon monoxide poisoning effect on a PBI/H3PO4 high temperature polymer electrolyte membrane fuel cell: Influence of anode humidification and carbon dioxide. *International Journal of Hydrogen Energy*, 2015. ISSN 03603199. doi: 10.1016/j.ijhydene.2015.09.056. URL http://www.sciencedirect.com/science/article/pii/S0360319915023460.

[55] A.D. D Modestov, M.R. R Tarasevich, V.Ya. Filimonov, and E.S. S Davydova. CO tolerance and CO oxidation at Pt and Pt–Ru anode catalysts in fuel cell with polybenzimidazole–H3PO4 membrane. *Electrochimica Acta*, 55(20):6073–6080, aug 2010. ISSN 00134686. doi: 10.1016/j.electacta.2010.05.068. URL http://www.sciencedirect.com/science/article/pii/S001346861000770Xhttp://linkinghub.elsevier.com/retrieve/pii/S001346861000770X.

[56] Kui Jiao, Yibo Zhou, Qing Du, Yan Yin, Shuhai Yu, and Xianguo Li. Numerical simulations of carbon monoxide poisoning in high temperature proton exchange membrane fuel cells with various flow channel designs. *Applied Energy*, 104:21–41, apr 2013. ISSN 03062619. doi: 10.1016/j.apenergy.2012.10.059. URL http://linkinghub.elsevier.com/retrieve/pii/S0306261912007787.

[57] T. Engl, J. Kase, L. Gubler, and T. J. Schmidt. On the Positive Effect of CO during Start/Stop in High-Temperature Polymer Electrolyte Fuel Cells. *ECS Electrochemistry Letters*, 3(7):F47—-F49, may 2014. ISSN 2162-8726. doi: 10.1149/2.0011407eel. URL http://eel.ecsdl.org/cgi/doi/10.1149/2.0011407eel.

[58] T. Engl, L. Gubler, and T. J. Schmidt. Think different! Carbon corrosion mitigation strategy in high temperature PEFC: A rapid aging study.

Journal of the Electrochemical Society, 162(3):F291–F297, jan 2015. ISSN 0013-4651. doi: 10.1149/2.0681503jes. URL http://jes.ecsdl.org/cgi/doi/10.1149/2.0681503jeshttp://www.scopus.com/inward/record.url?eid=2-s2.0-84923324787{&}partnerID=40{&}md5=b1941d38d83cd6f345355ff568d7a323.

[59] Chen-Yu Chen and Wei-Hsiang Lai. Effects of temperature and humidity on the cell performance and resistance of a phosphoric acid doped polybenzimidazole fuel cell. *Journal of Power Sources*, 195(21): 7152–7159, nov 2010. ISSN 03787753. doi: 10.1016/j.jpowsour.2010.05.057. URL http://www.sciencedirect.com/science/article/pii/S0378775310009250.

[60] Purushothama Chippar, Kyungmun Kang, Young-Don Lim, Whan-Gi Kim, and Hyunchul Ju. Effects of inlet relative humidity (RH) on the performance of a high temperature-proton exchange membrane fuel cell (HT-PEMFC). *International Journal of Hydrogen Energy*, 39(6): 2767–2775, feb 2014. ISSN 03603199. doi: 10.1016/j.ijhydene.2013.05.115. URL http://www.sciencedirect.com/science/article/pii/S0360319913013475.

[61] Li Qingfeng, H.A. Hjuler, and N.J. Bjerrum. Phosphoric acid doped polybenzimidazole membranes: Physiochemical characterization and fuel cell applications. *Journal of Applied Electrochemistry*, 31(7):773–779, 2001. ISSN 1572-8838. doi: 10.1023/A:1017558523354. URL http://link.springer.com/article/10.1023/A{%}7B{%}25{%}7D3A1017558523354http://link.springer.com/article/10.1023/A{%}3A1017558523354.

[62] Caizhi Zhang, Weijiang Zhou, Lan Zhang, Siew Hwa Chan, and Youyi Wang. An experimental study on anode water management in high temperature PEM fuel cell. *International Journal of Hydrogen Energy*, 40 (13):4666–4672, apr 2015. ISSN 03603199. doi: 10.1016/j.ijhydene.2015.02.037. URL http://www.sciencedirect.com/science/article/pii/S0360319915003663.

[63] Dario Bezmalinović, Stephan Strahl, Vicente Roda, and Attila Husar. Water transport study in a high temperature proton exchange membrane fuel cell stack. *International Journal of Hydrogen Energy*, 39(20): 10627–10640, jul 2014. ISSN 03603199. doi: 10.1016/j.ijhydene.2014.04.186. URL http://www.sciencedirect.com/science/article/pii/S0360319914012762.

[64] Samuel Simon Araya, Søren Juhl Andreasen, Heidi Venstrup Kær Nielsen, and Søren Knudsen. Investigating the effects of methanol-water vapor mixture on a PBI-based high temperature PEM fuel

cell. *International Journal of ...*, pages 1–26, 2012. URL http://www.sciencedirect.com/science/article/pii/S0360319912020125.

[65] Samuel Simon Araya, Ionela Florentina Grigoras, Fan Zhou, Søren Juhl Andreasen, and Søren Knudsen Kær. Performance and endurance of a high temperature PEM fuel cell operated on methanol reformate. *International Journal of Hydrogen Energy*, 39(32):18343–18350, oct 2014. ISSN 03603199. doi: 10.1016/j.ijhydene.2014.09.007. URL http://linkinghub.elsevier.com/retrieve/pii/S0360319914025269http://www.sciencedirect.com/science/article/pii/S0360319914025269.

[66] Fan Zhou, Samuel Simon Araya, Ionela Florentina Grigoras, Søren Juhl Andreasen, and Søren Knudsen Kær. Performance Degradation Tests of Phosphoric Acid Doped PBI Membrane Based High Temperature PEM Fuel Cells. *... on Fuel Cell ...*, 2014. URL http://proceedings.asmedigitalcollection.asme.org/data/Conferences/ASMEP/81457/V001T06A004-FuelCell2014-6358.pdf.

[67] N Pilinski, M. Rastedt, and P. Wagner. Investigation of Phosphoric Acid Distribution in PBI based HT-PEM Fuel Cells. *Electrochemical Society Proceedings*, 69(17):323–335, 2015.

[68] Uwe Reimer, Birgit Schumacher, and Werner Lehnert. Accelerated Degradation of High-Temperature Polymer Electrolyte Fuel Cells: Discussion and Empirical Modeling. *Journal of the Electrochemical Society*, 162(1):F153—-F164, dec 2014. ISSN 0013-4651. doi: 10.1149/2.0961501jes. URL http://jes.ecsdl.org/cgi/doi/10.1149/2.0961501jeshttp://jes.ecsdl.org/content/162/1/F153.abstracthttp://jes.ecsdl.org/content/162/1/F153.full.

[69] J. S. Wainright. Acid-Doped Polybenzimidazoles: A New Polymer Electrolyte. *Journal of The Electrochemical Society*, 142(7):L121, jul 1995. ISSN 00134651. doi: 10.1149/1.2044337. URL http://jes.ecsdl.org/content/142/7/L121.abstract.

[70] Y.-L. Ma, J. S. Wainright, M. H. Litt, and R. F. Savinell. Conductivity of PBI Membranes for High-Temperature Polymer Electrolyte Fuel Cells. *Journal of the Electrochemical Society*, 151(1):A8–A16, jan 2004. ISSN 00134651. doi: 10.1149/1.1630037. URL http://jes.ecsdl.org/content/151/1/A8.abstracthttp://jes.ecsdl.org/content/151/1/A8.full.

[71] Lixiang Xiao, Haifeng Zhang, Eugene Scanlon, L. S. Ramanathan, Eui-Won Choe, Diana Rogers, Tom Apple, and Brian C. Benicewicz. High-Temperature Polybenzimidazole Fuel Cell Membranes via a Sol - Gel

Process. *Chem. Mater.*, 17(21):5328–5333, 2005. ISSN 0897-4756. doi: 10.1021/cm050831. URL http://pubs.acs.org/doi/full/10.1021/cm050831+.

[72] Jakob Rabjerg Vang, Søren Juhl Andreasen, Samuel Simon Araya, and Søren Knudsen Kær. Comparative study of the break in process of post doped and sol–gel high temperature proton exchange membrane fuel cells. *International Journal of Hydrogen Energy*, 39(27):14959–14968, sep 2014. ISSN 03603199. doi: 10.1016/j.ijhydene.2014.07.017. URL http://www.sciencedirect.com/science/article/pii/S0360319914019727.

[73] Der-Tau Chin and Howard H. Chang. On the conductivity of phosphoric acid electrolyte. *Journal of Applied Electrochemistry*, 19(1):95–99, jan 1989. ISSN 0021-891X. doi: 10.1007/BF01039396. URL http://link.springer.com/10.1007/BF01039396.

[74] Linas Vilciauskas, Stephen J Paddison, and Klaus-Dieter Kreuer. Ab initio modeling of proton transfer in phosphoric acid clusters. *The journal of physical chemistry. A*, 113(32):9193–201, aug 2009. ISSN 1520-5215. doi: 10.1021/jp903005r. URL http://www.ncbi.nlm.nih.gov/pubmed/19569665.

[75] Linas Vilčiauskas, Mark E. Tuckerman, Gabriel Bester, Stephen J. Paddison, and Klaus-Dieter Kreuer. The mechanism of proton conduction in phosphoric acid. *Nature Chemistry*, 4(6):461–466, apr 2012. ISSN 1755-4330. doi: 10.1038/NCHEM.1329. URL http://www.nature.com/doifinder/10.1038/nchem.1329http://dx.doi.org/10.1038/nchem.1329https://www.nature.com/nchem/journal/v4/n6/pdf/nchem.1329.pdf.

[76] Jan-Patrick Melchior, Klaus-Dieter Kreuer, and Joachim Maier. Proton conduction mechanisms in the phosphoric acid–water system (H ₄ P ₂ O ₇ –H ₃ PO ₄ ·2H ₂ O): a ¹ H, ³¹ P and ¹⁷ O PFG-NMR and conductivity study. *Phys. Chem. Chem. Phys.*, 19(1):587–600, 2017. ISSN 1463-9076. doi: 10.1039/C6CP04855B. URL http://xlink.rsc.org/?DOI=C6CP04855B.

[77] Hongting Pu, Wolfgang H. Meyer, and Gerhard Wegner. Proton transport in polybenzimidazole blended with H3PO4 or H2SO4. *Journal of Polymer Science, Part B: Polymer Physics*, 40(7):663–669, 2002. ISSN 08876266. doi: 10.1002/polb.10132.

[78] M. Heres, Y. Wang, P. J. Griffin, C. Gainaru, and A. P. Sokolov. Proton Conductivity in Phosphoric Acid: The Role of Quantum Ef-

fects. *Physical Review Letters*, 117(15):1–5, 2016. ISSN 10797114. doi: 10.1103/PhysRevLett.117.156001.

[79] Yuichi Aihara, Atsuo Sonai, Mineyuki Hattori, and Kikuko Hayamizu. Ion conduction mechanisms and thermal properties of hydrated and anhydrous phosphoric acids studied with 1H, 2H, and 31P NMR. *The journal of physical chemistry. B*, 110(49):24999–5006, dec 2006. ISSN 1520-6106. doi: 10.1021/jp064452v. URL http://www.ncbi.nlm.nih.gov/pubmed/17149922.

[80] Th Dippel, K. D. Kreuer, J. C. Lassègues, and D. Rodriguez. Proton conductivity in fused phosphoric acid; A 1H/31P PFG-NMR and QNS study. *Solid State Ionics*, 61(1-3):41–46, 1993. ISSN 01672738. doi: 10.1016/0167-2738(93)90332-W.

[81] Kyungjung Kwon, Tae Young Kim, Duck Young Yoo, Suk-Gi Hong, and Jung Ock Park. Maximization of high-temperature proton exchange membrane fuel cell performance with the optimum distribution of phosphoric acid. *Journal of Power Sources*, 188(2):463–467, 2009. doi: http://dx.doi.org/10.1016/j.jpowsour.2008.11.104. URL http://www.sciencedirect.com/science/article/pii/S0378775308022878.

[82] Christoph Wannek, Irene Konradi, Jürgen Mergel, and Werner Lehnert. Redistribution of phosphoric acid in membrane electrode assemblies for high-temperature polymer electrolyte fuel cells. *International Journal of Hydrogen Energy*, 34(23):9479–9485, 2009. doi: http://dx.doi.org/10.1016/j.ijhydene.2009.09.076. URL http://www.sciencedirect.com/science/article/pii/S036031990901516X.

[83] P. Boillat, J. Biesdorf, P. Oberholzer, A. Kaestner, and T. J. Schmidt. Evaluation of Neutron Imaging for Measuring Phosphoric Acid Distribution in High Temperature PEFCs. *Journal of the Electrochemical Society*, 161(3):F192—-F198, dec 2013. ISSN 0013-4651. doi: 10.1149/2.023403jes. URL http://jes.ecsdl.org/content/161/3/F192.fullhttp://jes.ecsdl.org/cgi/doi/10.1149/2.023403jes.

[84] Yeon Hun Jeong, Kyeongmin Oh, Sungha Ahn, Na Young Kim, Ayeong Byeon, Hee Young Park, So Young Lee, Hyun S. Park, Sung Jong Yoo, Jong Hyun Jang, Hyoung Juhn Kim, Hyunchul Ju, and Jin Young Kim. Investigation of electrolyte leaching in the performance degradation of phosphoric acid-doped polybenzimidazole membrane-based high temperature fuel cells. *Journal of Power Sources*, 363:365–374, 2017. ISSN 03787753. doi: 10.1016/j.jpowsour.2017.07.109. URL http://dx.doi.org/10.1016/j.jpowsour.2017.07.109.

[85] Sebastian Lang, Timur J. Kazdal, Frank Kühl, and Manfred J. Hampe. Experimental investigation and numerical simulation of the electrolyte loss in a HT-PEM fuel cell. *International Journal of Hydrogen Energy*, 40 (2):1163–1172, jan 2015. ISSN 03603199. doi: 10.1016/j.ijhydene.2014.11.041. URL http://www.sciencedirect.com/science/article/pii/S036031991403119X.

[86] Samuele Galbiati, Andrea Baricci, Andrea Casalegno, and Renzo Marchesi. Experimental study of water transport in a polybenzimidazole-based high temperature PEMFC. *International Journal of Hydrogen Energy*, 37(3):2462–2469, feb 2012. ISSN 03603199. doi: 10.1016/j.ijhydene.2011.09.159. URL http://linkinghub.elsevier.com/retrieve/pii/S0360319911024463http://www.sciencedirect.com/science/article/pii/S0360319911024463.

[87] Maria K. Daletou, Joannis K. Kallitsis, George Voyiatzis, and Stylianos G. Neophytides. The interaction of water vapors with H3PO4 imbibed electrolyte based on PBI/polysulfone copolymer blends. *Journal of Membrane Science*, 326(1):76–83, jan 2009. ISSN 03767388. doi: 10.1016/j.memsci.2008.09.040. URL http://www.sciencedirect.com/science/article/pii/S0376738808008466.

[88] Ronghuan He, Qingfeng Li, Anders Bach, Jens Oluf Jensen, and Niels J. Bjerrum. Physicochemical properties of phosphoric acid doped polybenzimidazole membranes for fuel cells. *Journal of Membrane Science*, 277(1-2):38–45, 2006. ISSN 03767388. doi: 10.1016/j.memsci.2005.10.005.

[89] Yuka Oono, Atsuo Sounai, and Michio Hori. Influence of the phosphoric acid-doping level in a polybenzimidazole membrane on the cell performance of high-temperature proton exchange membrane fuel cells. *Journal of Power Sources*, 189(2):943–949, 2009. ISSN 03787753. doi: 10.1016/j.jpowsour.2008.12.115.

[90] K. Wippermann, C. Wannek, H.-F. Oetjen, J. Mergel, and W. Lehnert. Cell resistances of poly(2,5-benzimidazole)-based high temperature polymer membrane fuel cell membrane electrode assemblies: Time dependence and influence of operating parameters. *Journal of Power Sources*, 195(9):2806–2809, may 2010. ISSN 03787753. doi: 10.1016/j.jpowsour.2009.10.100. URL http://www.sciencedirect.com/science/article/pii/S0378775309019776.

[91] Uwe Reimer, Jannik Ehlert, Holger Janßen, and Werner Lehnert. Water distribution in high temperature polymer electrolyte fuel cells. *International Journal of Hydrogen Energy*, 41(3):1837–1845, dec 2015. ISSN 03603199. doi: 10.1016/j.ijhydene.2015.11.106. URL http://www.sciencedirect.com/science/article/pii/S0360319915305632.

[92] Florian Mack, Stefan Heissler, Ruben Laukenmann, and Roswitha Zeis. Phosphoric acid distribution and its impact on the performance of polybenzimidazole membranes. *Journal of Power Sources*, 270(0):627–633, 2014. doi: http://dx.doi.org/10.1016/j.jpowsour.2014.06.171. URL http://www.sciencedirect.com/science/article/pii/S0378775314012142.

[93] S. Chevalier, M. Fazeli, F. Mack, S. Galbiati, Ingo Manke, A. Bazylak, and R. Zeis. Role of the microporous layer in the redistribution of phosphoric acid in high temperature PEM fuel cell gas diffusion electrodes. *Electrochimica Acta*, 212:187–194, 2016. ISSN 00134686. doi: 10.1016/j.electacta.2016.06.121.

[94] Wiebke Maier, Tobias Arlt, Christoph Wannek, Ingo Manke, Heinrich Riesemeier, Philipp Krüger, Joachim Scholta, Werner Lehnert, John Banhart, and Detlef Stolten. In-situ synchrotron X-ray radiography on high temperature polymer electrolyte fuel cells. *Electrochemistry Communications*, 12(10):1436–1438, oct 2010. ISSN 13882481. doi: 10.1016/j.elecom.2010.08.002. URL http://www.sciencedirect.com/science/article/pii/S1388248110003474.

[95] R. Kuhn, J. Scholta, Ph. Krüger, Ch. Hartnig, W. Lehnert, T. Arlt, and I. Manke. Measuring device for synchrotron X-ray imaging and first results of high temperature polymer electrolyte membrane fuel cells. *Journal of Power Sources*, 196(12):5231–5239, jun 2011. ISSN 03787753. doi: 10.1016/j.jpowsour.2010.11.025. URL http://www.sciencedirect.com/science/article/pii/S0378775310019312http://linkinghub.elsevier.com/retrieve/pii/S0378775310019312.

[96] Tobias Arlt, Wiebke Maier, Christian Tötzke, Christoph Wannek, Henning Markötter, Frank Wieder, John Banhart, Werner Lehnert, and Ingo Manke. Synchrotron X-ray radioscopic in situ study of high-temperature polymer electrolyte fuel cells - Effect of operation conditions on structure of membrane. *Journal of Power Sources*, 246:290–298, jan 2014. ISSN 03787753. doi: 10.1016/j.jpowsour.2013.07.094. URL http://www.sciencedirect.com/science/article/pii/S0378775313013037.

[97] S. H. Eberhardt, T. Lochner, F. N. Büchi, and T. J. Schmidt. Correlating Electrolyte Inventory and Lifetime of HT-PEFC by Accelerated Stress Testing. *Journal of The Electrochemical Society*, 162(12):F1367–F1372, sep 2015. ISSN 0013-4651. doi: 10.1149/2.0591512jes. URL http://jes.ecsdl.org/lookup/doi/10.1149/2.0591512jes.

[98] S. H. Eberhardt, M. Toulec, F. Marone, M. Stampanoni, F N Büchi, and T. J. Schmidt. Dynamic Operation of HT-PEFC: In-Operando Imaging of Phosphoric Acid Profiles and (Re)distribution. *Journal of The Electrochemical Society*, 162(3): F310–F316, jan 2015. ISSN 0013-4651. doi: 10.1149/2.0751503jes. URL http://jes.ecsdl.org/content/162/3/F310.abstracthttp://jes.ecsdl.org/cgi/doi/10.1149/2.0751503jes.

[99] S. H. Eberhardt, F. Marone, M. Stampanoni, F. N. Büchi, and T. J. Schmidt. Operando X-ray Tomographic Microscopy Imaging of HT-PEFC: A Comparative Study of Phosphoric Acid Electrolyte Migration. *Journal of The Electrochemical Society*, 163(8):F842–F847, jun 2016. ISSN 0013-4651. doi: 10.1149/2.0801608jes. URL http://jes.ecsdl.org/lookup/doi/10.1149/2.0801608jes.

[100] Hans Becker, Lars Nilausen Cleemann, David Aili, Jens Oluf Jensen, and Qingfeng Li. Probing phosphoric acid redistribution and anion migration in polybenzimidazole membranes. *Electrochemistry Communications*, 82(July):21–24, 2017. ISSN 13882481. doi: 10.1016/j.elecom.2017.07.005. URL http://dx.doi.org/10.1016/j.elecom.2017.07.005.

[101] Qingfeng Li, Xiao Gang, H.A. Hjuler, R.W. Berg, N.J Bjerrum. Limiting Current of Oxygen Reduction on Gas-Diffusion Electrodes for Phosphoric Acid Fuel Cells. *Journal of The Electrochemical Society*, 141 (11):3114, 1994. ISSN 00134651. doi: 10.1149/1.2059286. URL http://jes.ecsdl.org/cgi/doi/10.1149/1.2059286.

[102] Daniel R Baker, David A Caulk, Kenneth C Neyerlin, and Michael W Murphy. Measurement of oxygen transport resistance in pem fuel cells by limiting current methods. *Journal of Electrochemical Society*, 2009. doi: 10.1149/1.3152226.

[103] Franz B. Spingler, Adam Phillips, Tobias Schuler, Michael C. Tucker, and Adam Z. Weber. Investigating fuel-cell transport limitations using hydrogen limiting current. *International Journal of Hydrogen Energy*, 42 (19):13960–13969, 2017. ISSN 03603199. doi: 10.1016/j.ijhydene.2017.01.036. URL http://dx.doi.org/10.1016/j.ijhydene.2017.01.036.

[104] Paul Monk. *Fundamentals of electroanalytical chemistry. Analytical techniques in the sciences*. John Wiley & Sons, Ltd, 2007.

[105] Xiaozi Yuan, Haijiang Wang, Jian Colin Sun, and Jiujun Zhang. AC impedance technique in PEM fuel cell diagnosis—A review. *International Journal of Hydrogen Energy*, 32(17):4365–4380, dec 2007. ISSN 0360-3199. doi: http://dx.doi.org/10.1016/j.ijhydene.2007.05.

036. URL http://www.sciencedirect.com/science/article/pii/S036031990700328X.

[106] T. Romero-Castañón, L. G. Arriaga, and U. Cano-Castillo. Impedance spectroscopy as a tool in the evaluation of MEA's. *Journal of Power Sources*, 118(1-2):179–182, 2003. ISSN 03787753. doi: 10.1016/S0378-7753(03)00085-5.

[107] N. Wagner. Characterization of membrane electrode assemblies in polymer electrolyte fuel cells using a.c. impedance spectroscopy. *Journal of Applied Electrochemistry*, 32(8):859–863, 2002. ISSN 0021891X. doi: 10.1023/A:1020551609230.

[108] M Eikerling and A.A Kornyshev. Electrochemical impedance of the cathode catalyst layer in polymer electrolyte fuel cells. *Journal of Electroanalytical Chemistry*, 475(2):107–123, 1999. ISSN 15726657. doi: 10.1016/S0022-0728(99)00335-6.

[109] M.C. Lefebvre, R.B. Martin, and P.G. Pickup. Characterization of ionic conductivity profiles within proton exchange membrane fuel cell gas diffusion electrodes by impedance spectroscopy. *Electrochemical and Solid-State Letters*, 2(6):259–261, 1999. ISSN 10990062. doi: 10.1149/1.1390804.

[110] Jinfeng Wu, Xiao Zi YUAN, Haijiang Wang, Mauricio Blanco, Jonathan J Martin, and Jiujun ZHANG. Diagnostic tools in PEM fuel cell research: Part I Electrochemical techniques. *International Journal of Hydrogen Energy*, 33(6):1735–1746, mar 2008. ISSN 0360-3199. doi: http://dx.doi.org/10.1016/j.ijhydene.2008.01.013. URL http://www.sciencedirect.com/science/article/pii/S0360319908000700.

[111] Christian Jeppesen, Samuel Simon Araya, Simon Lennart Sahlin, Sobi Thomas, Søren Juhl Andreasen, and Søren Knudsen Kær. Fault detection and isolation of high temperature proton exchange membrane fuel cell stack under the influence of degradation. *Journal of Power Sources*, 359:37–47, 2017. ISSN 03787753. doi: 10.1016/j.jpowsour.2017.05.021. URL http://dx.doi.org/10.1016/j.jpowsour.2017.05.021.

[112] Søren Juhl Andreasen, Jakob Rabjerg Vang, and Søren Knudsen Kær. High temperature PEM fuel cell performance characterisation with CO and CO2 using electrochemical impedance spectroscopy. *International Journal of Hydrogen Energy*, 36(16):9815–9830, aug 2011. ISSN 03603199. doi: http://dx.doi.org/10.1016/j.ijhydene.2011.04.076. URL http://www.sciencedirect.com/science/article/pii/S0360319911009414.

[113] Mikhail S. Kondratenko, Marat O. Gallyamov, and Alexei R. Khokhlov. Performance of high temperature fuel cells with different types of PBI membranes as analysed by impedance spectroscopy. *International Journal of Hydrogen Energy*, 37(3):2596–2602, feb 2012. ISSN 03603199. doi: 10.1016/j.ijhydene.2011.10.087. URL http://linkinghub.elsevier.com/retrieve/pii/S036031991102461Xhttp://www.sciencedirect.com/science/article/pii/S036031991102461X.

[114] S J Andreasen, J L Jespersen, E Schaltz, and S K Kær. Characterisation and Modelling of a High Temperature PEM Fuel Cell Stack using Electrochemical Impedance Spectroscopy. *Fuel Cells*, 9(4):463–473, 2009. doi: 10.1002/fuce.200800137. URL http://dx.doi.org/10.1002/fuce.200800137.

[115] D Bergmann, A ; Kurz, T ; Gerteisen, D ; Hebling, C ; Grube, T ; Stolten. Spatially Resolved Impedance Spectroscopy in PEM Fuel Cells up to 200 °C, 2010. URL file:///C:/Users/sot/Downloads/00b7d537b1ff3f3edd000000.pdf.

[116] N. Zamel, A. Bhattarai, and D. Gerteisen. Measurement of Spatially Resolved Impedance Spectroscopy with Local Perturbation. *Fuel Cells*, pages n/a—-n/a, jun 2013. ISSN 16156846. doi: 10.1002/fuce.201200223. URL http://doi.wiley.com/10.1002/fuce.201200223.

[117] Bernard Orazem, Mark E. and Tribollet. Experimental Design. In *Electrochemical Impedance Spectroscopy*, pages 165–189. John Wiley & Sons, Inc., 2017. ISBN 9781119363682. doi: 10.1002/9781119363682.ch8. URL http://dx.doi.org/10.1002/9781119363682.ch8.

[118] Vitor V. Lopes, Carmen M. Rangel, and Augusto Q. Novais. *23rd European Symposium on Computer Aided Process Engineering*, volume 32 of *Computer Aided Chemical Engineering*. Elsevier, 2013. ISBN 9780444632340. doi: 10.1016/B978-0-444-63234-0.50048-8. URL http://www.sciencedirect.com/science/article/pii/B9780444632340500488.

[119] Jingwei Hu, Huamin Zhang, Yunfeng Zhai, Gang Liu, and Baolian Yi. 500h continuous aging life test on pbi/h3po4 high-temperature pemfc. *International Journal of Hydrogen Energy*, 31(13):1855 – 1862, 2006. ISSN 0360-3199. doi: https://doi.org/10.1016/j.ijhydene.2006.05.001. URL http://www.sciencedirect.com/science/article/pii/S0360319906001662. Fuel Cells.

[120] Marta Boaventura and Adelio Magalhaes et al. Mendes. Activation procedures characterization of MEA based on phosphoric acid doped

PBI membranes. *International Journal of Hydrogen Energy*, 35(20):11649–11660, oct 2010. ISSN 03603199. doi: 10.1016/j.ijhydene.2010.03.137. URL http://www.sciencedirect.com/science/article/pii/S0360319910006555http://linkinghub.elsevier.com/retrieve/pii/S0360319910006555.

[121] T E Springer, T A Zawodzinski, M S Wilson, and S Gottesfeld. Characterization of Polymer Electrolyte Fuel Cells Using AC Impedance Spectroscopy. *Journal of The Electrochemical Society*, 143(2):587–599, 1996. doi: 10.1149/1.1836485. URL http://link.aip.org/link/?JES/143/587/1.

[122] Ryan P. O'Hayre, Fritz B. Prinz Ryan O'Hayre, Suk-Won Cha, Whitney Colella, Suk-Won Cha, Whitney G Colella, and Fritz B Prinz. *Fuel Cell Fundamentals*. John Wiley & Sons, Inc., 2nd edition, 2008. ISBN 978-0-470-25843-9. URL http://www.amazon.com/Fuel-Cell-Fundamentals-Ryan-OHayre/dp/0470258438http://books.google.dk/books/about/Fuel{_}cell{_}fundamentals.html?id=CrOQAQAAMAAJ{&}pgis=1.

[123] J. Lobato, P. Cañizares, M. A. Rodrigo, J. J. Linares, and G. Manjavacas. Synthesis and characterisation of poly[2,2-(m-phenylene)-5,5-bibenzimidazole] as polymer electrolyte membrane for high temperature PEMFCs. *Journal of Membrane Science*, 280(1-2):351–362, 2006. ISSN 03767388. doi: 10.1016/j.memsci.2006.01.049.

[124] Gaël Maranzana, Julia Mainka, Olivier Lottin, Jerome Dillet, Adrien Lamibrac, Anthony Thomas, and Sophie Didierjean. A proton exchange membrane fuel cell impedance model taking into account convection along the air channel: On the bias between the low frequency limit of the impedance and the slope of the polarization curve. *Electrochimica Acta*, 83:13–27, 2012. URL http://www.sciencedirect.com/science/article/pii/S0013468612011954.

[125] I A Schneider, D Kramer, A Wokaun, and G G Scherer. Oscillations in gas channels II. Unraveling the characteristics of the low frequency loop in air-fed PEFC impedance spectra. *Journal of The Electrochemical Society*, 154(8):B770, 2007. ISSN 00134651. doi: 10.1149/1.2742291. URL http://jes.ecsdl.org/cgi/doi/10.1149/1.2742291http://jes.ecsdl.org/content/154/8/B770.short.

[126] I A Schneider, S A Freunberger, D Kramer, A Wokaun, and G G Scherer. Oscillations in gas channels Part I. The forgotten player in impedance spectroscopy in PEFCs. *Journal of the Electrochemical Society*, 154(4):B383—-B388, 2007. ISSN 00134651. doi: 10.1149/1.2435706. URL http://jes.ecsdl.org/cgi/doi/10.1149/1.2435706.

[127] Dellis Jean-Luc. Zfit. Software; 2010., 2010. URL https://se.mathworks.com/matlabcentral/fileexchange/19460-zfit.

[128] Suthida Authayanun, Dang Saebea, Yaneeporn Patcharavorachot, and Amornchai Arpornwichanop. Effect of different fuel options on performance of high-temperature PEMFC (proton exchange membrane fuel cell) systems. *Energy*, 68(0):989–997, 2014. ISSN 0360-5442. doi: http://dx.doi.org/10.1016/j.energy.2014.02.099. URL http://www.sciencedirect.com/science/article/pii/S0360544214002461.

[129] Chris de Beer, Paul Barendse, Pragasen Pillay, Brian Bullecks, and Raghunathan Rengaswamy. Electrical circuit analysis of CO poisoning in high temperature PEM fuel cells for rapid fault diagnostics. In *2013 IEEE Energy Conversion Congress and Exposition*, pages 4623–4630. IEEE, sep 2013. ISBN 978-1-4799-0336-8. doi: 10.1109/ECCE.2013.6647320. URL http://ieeexplore.ieee.org/articleDetails.jsp?arnumber=6647320.

[130] a. Bergmann, D Gerteisen, and T Kurz. Modelling of CO Poisoning and its Dynamics in HTPEM Fuel Cells. *Fuel Cells*, 10(2):278–287, apr 2010. ISSN 16156846. doi: 10.1002/fuce.200900128. URL http://doi.wiley.com/10.1002/fuce.200900128.

[131] S. Thomas, S.S. Aarya, S.K. Kær, and J.R. Vang. Investigating the effect of water vapor and residual methanol on the anode of high temperature pem fuel cell. In *Proceedings of the 6th European Fuel Cell - Piero Lunghi Conference, EFC 2015*, 2015. ISBN 9788882863241.

[132] David Aili, Anton Vassiliev, Jens Oluf Jensen, Thomas J. Schmidt, and Qingfeng Li. Methyl phosphate formation as a major degradation mode of direct methanol fuel cells with phosphoric acid based electrolytes. *Journal of Power Sources*, 279:517–521, apr 2015. ISSN 03787753. doi: 10.1016/j.jpowsour.2015.01.010. URL http://www.sciencedirect.com/science/article/pii/S0378775315000117.

[133] Qingfeng Li, Jens Oluf Jensen, Robert F. Savinell, and Niels J. Bjerrum. High temperature proton exchange membranes based on polybenzimidazoles for fuel cells. *Progress in Polymer Science*, 34(5):449–477, may 2009. ISSN 00796700. doi: 10.1016/j.progpolymsci.2008.12.003. URL http://www.sciencedirect.com/science/article/pii/S0079670009000100http://linkinghub.elsevier.com/retrieve/pii/S0079670009000100.

[134] Sobi Thomas, Christian Jeppesen, Thomas Steenberg, Samuel Simon Araya, Jakob Rabjerg Vang, and Søren Knudsen Kær. New load cycling strategy for enhanced durability of high temperature proton exchange

membrane fuel cell. *International Journal of Hydrogen Energy*, 42(44): 27230–27240, 2017. ISSN 03603199. doi: 10.1016/j.ijhydene.2017.09.018.

[135] R. Taccani, T. Chinese, and M. Boaro. Effect of accelerated ageing tests on PBI HTPEM fuel cells performance degradation. *International Journal of Hydrogen Energy*, 42(3):1875–1883, 2017. ISSN 03603199. doi: 10.1016/j.ijhydene.2016.09.164. URL http://www.sciencedirect.com/science/article/pii/S0360319916316421.

[136] Samuele Galbiati, Andrea Baricci, Andrea Casalegno, and Renzo Marchesi. Degradation in phosphoric acid doped polymer fuel cells: A 6000 h parametric investigation. *International Journal of Hydrogen Energy*, 38(15):6469–6480, 2013. doi: http://dx.doi.org/10.1016/j.ijhydene.2013.03.012. URL http://www.sciencedirect.com/science/article/pii/S0360319913005867.

Papers

Paper A

Experimental study to distinguish the effects of methanol slip and water vapour on a high temperature PEM fuel cell at different operating conditions

Sobi Thomas, Jakob Rabjerg Vang, Samuel Simon Araya, Søren Knudsen Kær

The paper has been published in the
Applied Energy Vol. 192(2017), pp. 422–436, 2017.

The layout has been revised.

Experimental study to distinguish the effects of methanol slip and water vapour on a high temperature PEM fuel cell at different operating conditions

Sobi Thomas[a,*], Jakob Rabjerg Vang[a], Samuel Simon Araya[a], Søren Knudsen Kær[a,*]

[a]*Department of Energy Technology, Pontoppidanstraede, Aalborg University, Aalborg East -9220, Denmark*

Abstract

The objective of this paper is to separate out the effects of methanol and water vapour on a high temperature polymer electrolyte membrane fuel cell under different temperatures (160 °C and 180 °C) and current densities (0.2 A cm^{-2}, 0.4 A cm^{-2} and 0.6 A cm^{-2}). The degradation rates at the different current densities and temperatures are analysed and discussed. The results are supported by IV curves and impedance spectroscopy. The individual resistance variations are extracted by equivalent circuit model fitting of the impedance spectra. The presence of water in the anode feed enhances the performance while the presence of 5 % methanol tends to degrade the cell performance. However, the presence of H_2O mitigates some of the adverse effects of methanol. The effect of varying fuel compositions was found to be more prominent at lower current densities. The voltage improves significantly when adding water vapour to the anode after pure hydrogen operation at 180 °C. A decrease in the total resistance corresponding to the voltage improvement is observed from the impedance spectra. There is minimal variation in performance with the introduction of 3 % and 5 % methanol along with water vapour in the anode feed at all current densities and operating temperatures. The overall degradation over a period of 1915 h is -44 µV h^{-1}. The test time includes 595 h of test with pure H_2 and 300 h test each with 15 % H_2O, 3 % CH_3OH + 15 % H_2O and 5 % CH_3OH+15 % H_2O at varying current densities and temperatures.

Keywords: Reformed methanol, Impedance, HT-PEMFC, Equivalent circuit model

*Corresponding author
Email addresses: sot@et.aau.dk (Sobi Thomas), skk@et.aau.dk (Søren Knudsen Kær)

1. Introduction

In the last few decades, the polymer electrolyte membrane (PEM) fuel cell has matured and is now being considered as an alternative power source with high energy density and low environmental impact. Among the various kinds of PEM fuel cells, high temperature phosphoric acid (PA)-doped, PBI-based fuel cells have advantages in terms of higher CO tolerance, simpler water management and lower operational complexities [1, 2, 3, 4]. To harness the aforementioned advantages more work is needed to overcome the various constraints (i.e., durability, cost, fuel storage and distribution etc.)

The use of H_2 as a fuel is both difficult and costly due to lack of distribution infrastructure and efficient storage systems. The ability of an HT-PEMFC to withstand higher contents of impurities like carbon monoxide (CO) and carbon dioxide (CO_2), has led the research to different fuel options for HT-PEMFCs [5, 6, 7]. Jiao et al. [8] investigated the relationship between different flow channel designs and CO poisoning in an HT-PEMFC. They concluded at high CO percentage in the fuel, parallel flow channels have minimum poisoning effects from CO. At lower CO % the effect was insignificant. Najafi et al. [9] developed an operational strategy for HT-PEMFC based combined heat and power (CHP) system. The fuel was natural gas and the focus was to increase the efficiency of the overall system by controlling the fuel flow to adjust the thermal and electrical output from the unit. As an alternative, reformed methanol is also being explored as a fuel in HT-PEMFCs. Methanol as a fuel has advantages in terms of reduced handling complexities and the possibility of low cost on-site H_2 production. Methanol has the lowest reforming temperature (250-300 °C) compared to other fuels. As a liquid fuel, methanol also has higher volumetric energy density compared to hydrogen [10, 11].

In an HT-PEMFC, proton conductivity is induced by PA present in the membrane electrode assembly (MEA). Thus, the parameters which affect the conductivity of PA are of great importance in this kind of fuel cell. The conductivity of PA is influenced by a number of parameters, such as temperature, viscosity of PA, PA doping level of the membrane, the distribution of PA within the cell and presence of water vapour in the cell [12].

The temperature has both positive and negative effects on the performance of an HT-PEMFC. All other things being equal, higher temperature increases the ionic conductivity and enhances the reaction kinetics. However, higher temperature at a constant water vapour pressure dehydrates the acid, which leads to lower proton conductivity [13, 14]. On the other hand, an excess

quantity of water vapour in the cell can also lead to adverse effect on cell performance. The mass transport issues become more prominent as a result of two phenomena. Firstly, an increase in the acid volume due to increased water absorption pushes acid to the catalyst layer and blocks the pores. Secondly, the presence of water vapour in the reacting gases reduces the mole fraction of the reactants [15, 16, 17].

The relationship between temperature, weight fraction of H_3PO_4, water vapour pressure, and ionic conductivity of PA is shown in Fig. 1. Part (a) of the figure shows how the conductivity varies with acid concentration at different temperatures. The conductivity decreases with increasing concentration. The decrease is faster when the H_3PO_4 weight fraction approaches 1 at temperatures above 100 °C. [18, 19]. Part (b) shows the relation between concentration and water vapour pressure above the acid. At a constant vapour pressure, the acid concentration increases with increase in temperature. The effect becomes more prominent at higher water vapour pressures. On the other hand, at a constant temperature, a small change in vapour pressure can produce a large change in concentration at acid concentrations above 100 % H_3PO_4 [18]. Thus, increasing the temperature will produce two opposite effects on the conductivity. The increase with temperature will generally be dominant, but dehydration may become important at very dry conditions.

He et al. [20] carried out studies to understand the proton conduction mechanism and the factors affecting conductivity of phosphoric acid-doped PBI membranes. Their studies showed strong influence of relative humidity on the proton conductivity at higher temperatures, while below 100 °C the effect of water on the conductivity was concluded to be negligible. The addition of water vapour increases the dissociation of acid and decreases the viscosity of the solution. Both these factors have a positive influence on the proton conductivity. The study also demonstrated that conductivity increases with temperature under higher acid doping levels [20]. Ma et al. [21] also studied the mechanism of proton conductivity in a PBI-H_3PO_4 fuel cell. The results show a positive effect of relative humidity on the proton conduction mechanism at temperatures above 130 °C. Higher relative humidity (RH) is suggested to reduce the formation of pyrophosphoric acid ($H_4P_2O_7$) and the presence of a higher concentration of $H_4P_2O_7$ reduces proton conductivity [21]. A study to understand the interaction of water and PA based membranes revealed the importance of water vapour to enhance HT-PEMFC performance. A higher performance with water vapour was attributed to two reasons; the increased charge carrier concentration and formation

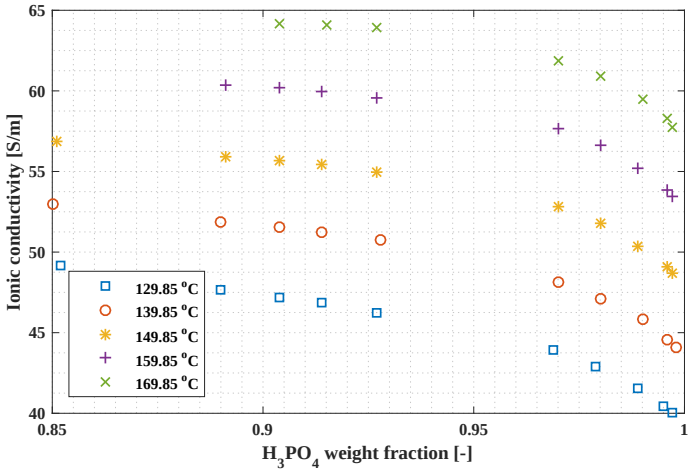

(a)

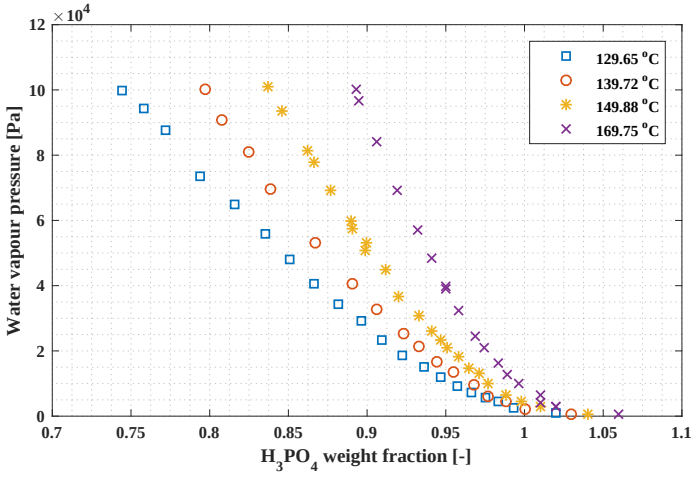

(b)

Figure 1: **The effect of temperature and weight fraction of H_3PO_4 on the ionic conductivity (a) and the H_2O vapour pressure (b) [18].**

of PA as a result of reaction between pyrophosphoric acid and water [22]. The chemical reaction governing the phenomenon is shown by Eqn 1,

$$H_4P_2O_7 + H_2O \rightleftharpoons {}_2H_3PO_4 \tag{1}$$

Chen and Lai [16] analysed the effect of temperature and humidity on the fuel cell performance using impedance spectroscopy. Their study concluded minimal effect of humidity on the performance, while the membrane resistance changed with humidity. Performance and resistance comparison under different current densities and humidity levels was carried out. The charge transfer resistance decreased with increase in humidity at low current density, while it showed the opposite trend under higher current density [16]. The water transport phenomenon and its effect on HT-PEMFC performance was investigated by Zhang et al. [23]. Two operational modes, namely open-through mode and dead-end mode, were investigated to understand the movement of generated water from the cathode to anode. When operated under dead-end mode, the excess water on the anode reduced the performance, which was regained on changing to open mode. They concluded that the high affinity of phosphoric acid towards water enhances the phosphoric acid conductivity, which decreases membrane resistance, but the excess water on the anode under dead-end operation dilutes the fuel which results in deteriorated performance [23].

Chippar et al. [24] developed a new water transport model for PBI membranes and investigated the effect of varying RH on the cathode. A decrease in performance was observed when increasing RH in spite of an improvement on the proton conductivity. This was attributed to the dilution of the oxidant supply being more significant than the increase of membrane conductivity [24]. In another study, the water transport phenomenon was studied experimentally by regulating the relative humidity under varying current densities (0.1 $A\,cm^{-2}$ to 0.7 $A\,cm^{-2}$), cathode stoichiometry (1.5 to 3) and cell temperature (160 °C and 140 °C)[25]. The authors concluded that water transport to the anode side is proportional to current density and inversely proportional to the cathode stoichiometry.

Humidification not only improves the conductivity, but also helps in mitigating some reformate gas effects on an HT-PEMFC [26, 27, 28]. It was reported that the CO poisoning of the catalyst is mitigated when humid gas was supplied to the anode [27]. The electrochemical oxidation of CO at HT-PEM operating temperature of 160 °C to 180 °C is slow. Thus, it becomes

important that the CO gets oxidized through the water gas shift reaction. When dry gases are used, the water for the reaction comes from the product water, which may not be sufficient at higher CO concentrations. Therefore, when humid gas is used on the anode, it creates favourable conditions for CO poisoning mitigation [27, 28].

The oxygen reduction reaction (ORR) activity in a PBI-H_3PO_4 fuel cell was studied by Liu et al. [29]. A strong dependency of oxygen diffusion on the volume fraction of amorphous PA was reported. The presence of water reduces the viscosity of amorphous H_3PO_4, which in turn improves the oxygen solubility, but the partial pressure of oxygen decreases due to dilution as a result of more water vapour in the system. A minimal effect of humidity on the ORR activity in HT-PEMFC was reported by Liu et al. [29].

Phosphoric acid has the tendency to reacts with methanol to form esters [30]. Aili et al. [31] reported the formation of methyl phosphate with higher concentration of methanol. When PA forms esters with methanol, the proton conductivity decreases due to reduced PA content in the membrane. At higher water content, the decreased proton conductivity due to acid loss through ester formation is compensated in the short term by the high water activity improving the conductivity as discussed in previous paragraphs. In the presence of water vapour, internal reforming of methanol may also occur as shown in Eqn. (2). Methanol self-dissociates into CO, which has a tendency to poison the platinum catalyst. The presence of water reduces this poisoning effect by converting the CO into CO_2, which is inert. However, the long term degradation effects of methanol on the performance are yet to be reported.

$$CH_3OH \longrightarrow CO + 4\,H^+ + 4\,e^- \tag{2}$$

$$H_2O \longrightarrow H^+ + OH^- \tag{3}$$

$$CO + OH^- \longrightarrow CO_2 + H^+ + e^- \tag{4}$$

Araya et al. [32] investigated the methanol effect by introducing different concentrations of methanol and water vapour mixture on the anode feed. The degradation under high methanol concentration (8% by volume) was reported to be severe (around -3.4 mV h^{-1} with increasing trend). When switching to 3%, the degradation was reversed and the cell voltage recovered.

The reported recovery was 0.03 V over a period of 157 h. The investigation also concluded that some degradation effects due to methanol were reversible when switching to pure hydrogen. In another work [11], the effect of temperature and methanol slip on an HT-PEMFC was studied using simulated reformate with 100 % to 90 % conversion. A degradation rate of -55 μV h^{-1} was recorded with 90% converted reformate gas over a period of 100 h at an operating temperature of 160 °C and current density 0.33 A cm^{-2} .

The present study focuses on understanding the operational constraints with wet reformate fuel feed on HT-PEMFCs. The effect of the unreacted fraction of methanol and water vapour in the reformate gas which slips into the fuel cell and affects its performance is studied. The study is important in order to understand how the methanol slip in the reformate affects the performance and durability of the fuel cell. It is also of importance in order to understand how the presence of water mitigates some of the methanol effects like the formation of esters with PA [31], which reduces the lifetime of HT-PEMFCs. In literature, tests have been carried out by feeding methanol and water vapour as a mixture. In this work, we feed water vapour alone and in mixture with methanol, thereby isolating the effects of methanol slip. The tests help in understanding the separate effects of methanol and water vapour on an HT-PEMFC. The study also focuses on understanding the influence of temperature and current density on these effects. The previous studies focussed on mixture of methanol and water vapour or water vapour at one current density and/or temperature.

In the present work, the effects of water and methanol under three different current densities, 0.2 A cm^{-2} , 0.4 A cm^{-2} and 0.6 A cm^{-2} have been investigated. The three operating points were selected to understand the degradation mechanisms over the entire feasible operating range. Polarization and impedance data was recorded to understand the phenomena. The experiment was carried out at two different temperatures, namely 160 °C and 180 °C to understand the influence of temperature.

2. Experimental

This section presents the experimental setup and the test procedure. The tests were carried out to evaluate the short term effects of adding different amounts of water and methanol to the fuel.

2.1. Test setup

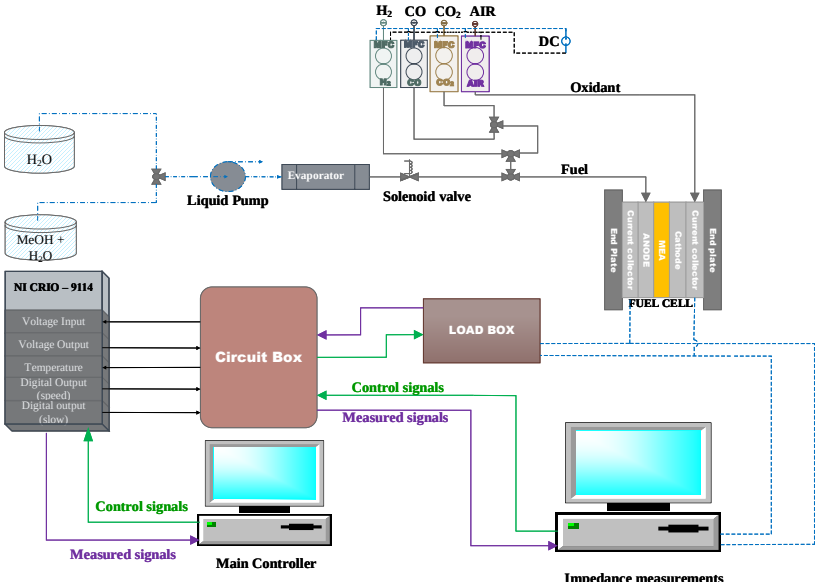

Figure 2: **In-house single cell test bench**

The test setup used for the experiments is shown in Fig. 2. The setup features an integrated control system for carrying out load cycling and electrochemical impedance spectroscopy (EIS) measurements. The setup is able to introduce CO and CO_2 to the anode feed. It also incorporates a methanol pump to feed either water or a mixture of water and methanol to the cell. The pump is connected to three feed containers. One containing a solution of CH_3OH and H_2O mixed in the mole fraction of 3:15, the second containing solution of CH_3OH and H_2O mixed in the mole fraction of 5:15 while the third one contains pure H_2O. The feed can be changed using a solenoid valve. The pump feeds the liquid to the evaporator which converts it to vapour state before feeding it to the fuel cell along with H_2. The flow range for the pump is 0.0008-0.8 ml min^{-1}. The mass flow controllers (MFCs) for H_2 and air have an uncertainty of less than 0.3 %. The MEA is a DPS-G77 from Danish Power Systems with an active area of 45 cm^2 and platinum loading of 1.5 mg cm^{-2} on both anode and cathode. Hard PTFE gaskets are used for sealing the cell. The gaskets are 150 µm on both sides. The cell is heated using four 100W cartridge heaters

placed in the stainless steel end plates. The temperature is measured using K-type thermocouples placed on the anode and cathode flow plates. The difference between the measured temperatures of cathode and anode was less than 0.5 °C. The voltage measurements were carried out using NI-9205 modules, which have an uncertainty of less than 6mV, while the NI-PCIe 6259 card used for EIS measurement has an uncertainty of less than 2 mV.

2.2. Test procedure

In Table 2, the anode gas composition variations and the temperature variations during the tests are listed. The stoichiometric ratios of hydrogen and air were kept constant at 1.2 and 4, respectively. The 15 % H_2O, 3 % CH_3OH and 5 % CH_3OH are added on top of the H_2 stoichiometric ratio. The percentages are based on the dry hydrogen flow required for the particular current density. The flow rates are dynamically calculated by the software based on the set point current at the given stoichiometric ratio. The table lists percentages with respect to the total flow as well as to the H_2 flow. Whenever percentages of water and methanol are mentioned in the text, it is with respect to the flow of dry hydrogen.

Exp. No.	x_{H_2}/x_{total}	x_{H_2O}/x_{H_2}	x_{H_2O}/x_{total}	x_{CH_3OH}/x_{H_2}	x_{CH_3OH}/x_{total}	Temp. [°C]
1	100.0	00.0	00.0	0.0	0.0	160
2	87.0	15.0	13.0	0.0	0.0	160
3	84.8	15.0	12.7	3.0	2.5	160
4	83.4	15.0	12.5	5.0	4.2	160
5	100.0	00.0	00.0	0.0	0.0	180
6	87.0	15.0	13.0	0.0	0.0	180
7	84.8	15.0	12.7	3.0	2.5	180
8	83.3	15.0	12.5	5.0	4.2	180

Table 2: **The various fuel compositions on the anode during each test sequence. The values are % with respect to the H_2 flow and the total flow respectively.**

The sequences 1-4 and 5-8 in Table 2 are repeated for each of the current densities, 0.2, 0.6 and 0.4 A cm^{-2} . Step 1-4 are performed at each current density before changing the temperature

to perform steps 5-8. The test sequence includes test with pure H2 followed by water and then 3 % and 5 % for each current density. To maintain these low flow rates of pure methanol for a single cell is not possible due to the minimum flow constraints of the pump. A water mole fraction of 15 % meets the minimum flow requirement of the pump. So the test was performed with pure H_2, H_2 + H_2O and H_2 + H_2O + CH_3OH. To understand the methanol effect, the H_2 + H_2O case was used as reference. This is deemed feasible since, in a real system, methanol will only be present in combination with water as a result incomplete reforming. The two temperatures were chosen to understand the temperature effects and to compare the methanol effect at different temperatures. The results show that the positive effect of water is more significant than the methanol degradation effect at higher temperatures.

A break-in at 0.2 A cm^{-2} was carried out for 100 h using pure hydrogen and air before starting the test sequence. IV curves were recorded at an interval of 50 h, while impedance spectra were recorded at an interval of 25 h. The test with H_2 continued for another 135 h before switching to H_2O test and CH_3OH tests.

EIS scans were carried out between a frequency of 10 kHz and 0.1 Hz. The IV curves were recorded at a scan rate of 0.11 A cm^{-2} min^{-1} to a maximum of 1.11 A cm^{-2} .

The pump was set at maximum flow rate for three minutes every time the fuel composition was changed. This time period was required for the liquid to travel from the start of solenoid valve to the evaporator. This was done to make sure that the anode fuel composition matches the specified composition for a particular set point.

The test was stopped three times due to gas leakages. The instants of stop can be seen in Fig. 3, where the data points are missing (time $\triangleq$ 1000, 1600, 1650 h). On restarting the cell after a stop, a slight improvement in the performance was observed as seen in Fig. 3. The possible reason for improvement could be attributed to two reasons. Firstly, due to the phosphoric acid absorbing more water at lower temperatures, leading to higher conductivity for a short time, until the water was evaporated. Secondly, Eberhardt et al. [33] suggested that back diffusion of PA from the anode to membrane occurs at low current density, which improves the membrane conductivity.

2.3. Equivalent circuit modeling

In order to aid the analysis, the EIS data is fitted to an equivalent circuit model as shown in Fig. 4. The fitting is performed using the Matlab function Zfit [34]. The circuit consists of

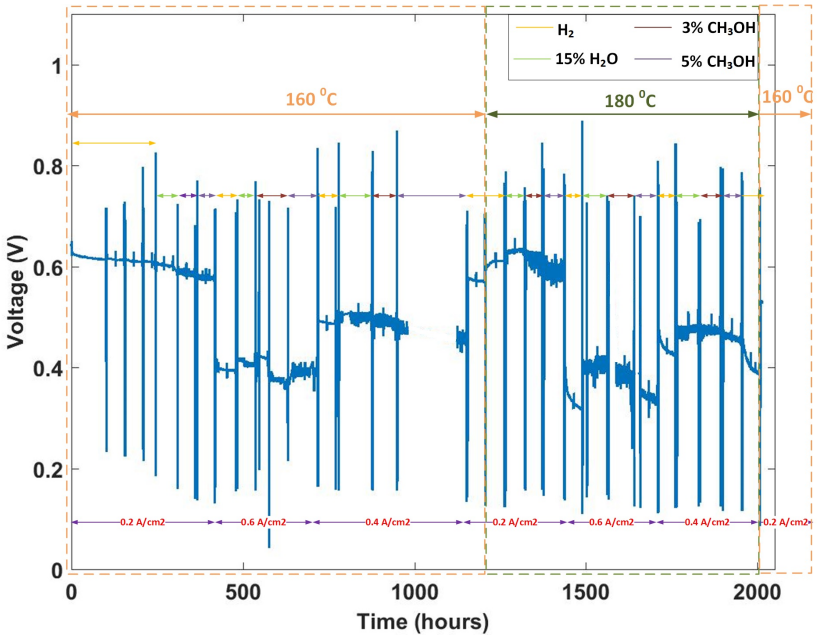

Figure 3: **Voltage profile under different anode gas composition and current densities**

a resistance (R_L) and inductor (L) in parallel accounting for the high frequency inductance part of the impedance which becomes significant above 400 Hz. It is followed by a pure resistance (R_{ohm}), which corresponds to the point of intersection of impedance loop with the real axis in the Nyquist plot.

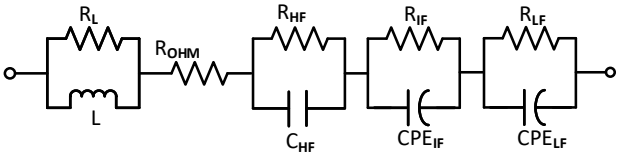

Figure 4: **Equivalent circuit model used for fitting impedance data**

The circuit includes a series combination of three parallel resistance and capacitor branches.

Each of these branches correspond to the high, intermediate and low frequency loops in the Nyquist plot, respectively. The intermediate and low frequency branches consist of a constant phase element (CPE) instead of a pure capacitor. The impedance of a CPE is calculated as in Eqn. 5:

$$Z_{CPE} = \frac{1}{Q(j\omega)^c} \tag{5}$$

Initially, the CPE exponent c was fixed at 0.85 as suggested by some researchers [35], but the fits were deviating in the intermediate and low frequency ranges. Therefore, the value of c included in the optimisation to achieve a proper fit. An example of the agreement between the measured data and simulation is shown in Fig. 5.

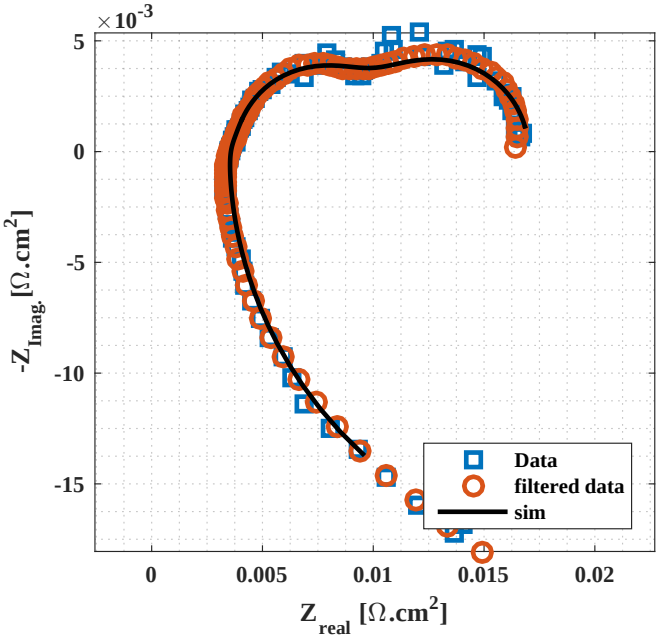

Figure 5: **Equivalent circuit model fitted data**

The equivalent circuit used in this work has been made as simple as possible, while at the same time reasonably able to capture the prominent features observed in the impedance spectra. The use of simple R-C or R-CPE loops to capture the loops in the fuel cell impedance spectrum is a well established practice in literature [16, 36, 37, 38, 39, 40]. Other sources use some form of the Randles circuit to represent the intermediate and low frequency loops [41, 42, 43, 44]. In the event that the same number and types of circuit elements are used, the two approaches can provide exactly the same fit to an impedance spectrum, given the right choice of parameters. The presently adopted approach is convenient as it allows easy separation of the impedance loops.

While the equivalent circuit model itself includes no direct physical meaning, the loops in the recorded impedance spectra stem from various physical processes in the fuel cell. Interpretations of each loop are given below:

In the high frequency range, the inductive effects become prominent and are visible in all the impedance plots. This is attributed to wires in the setup rather than any physical significance with the fuel cell operating conditions [45, 46].

The R_{ohm} accounts for the ohmic losses in the cell. This derives primarily from the resistance of the membrane, but contact resistances and electrical resistance of the GDL and cell components also play a role.

The high frequency loop is interpreted in various ways in the literature. Some sources see it as a 45 ° slope, which is related to potential gradients within the catalyst layer [47, 48]. Others interpret it as a semicircle related to anode activation losses [49, 50, 16].

The intermediate frequency loop primarily accounts for the cathode process. Depending on how the other loops are interpreted, it also may include diffusion losses and/or anode polarisation.

The low frequency loop also lends itself to interpretation. Rezaei Niya et al. [51] modelled LT-PEMFC impedance and they interpreted the loop as stemming from transport of water in the membrane. The importance of water in the conductivity of PA could make this interpretation plausible in HT-PEMFC as well. Other studies attribute the effect to oscillations in gas composition within the flow-fields [52, 53, 54].

A study using a combined polarisation and EIS model developed by Vang et al. [55] supports the hypotheses that the high frequency loop stems from resistance in the catalyst layer, that the intermediate frequency loop is a combination of activation and diffusion losses and that the low frequency loop results from flow channel dynamics.

3. Results

In this section, the results of the experimental investigation are presented. First, the development of the cell voltage over time is discussed. Then the changes happening in the impedance spectra and the IV curves during the course of the experiment are presented. Significant history effects are observed, when recording polarisation curves.

3.1. Voltage development

The voltage variations during the test are shown in Fig. 3. The voltage decreased during the initial 100 h break-in, but gradually stabilised. After recording initial EIS and polarisation curve, the test was continued with H_2 for another 135 h before injecting 15% water vapour. The various trends observed with water vapour and methanol under different temperature and current density are explained below. To further demonstrate the voltage variations during different test sequences, detail views of parts of Fig 3 are provided in Fig. 6 for 160 °C and Fig. 10 for 180 °C.

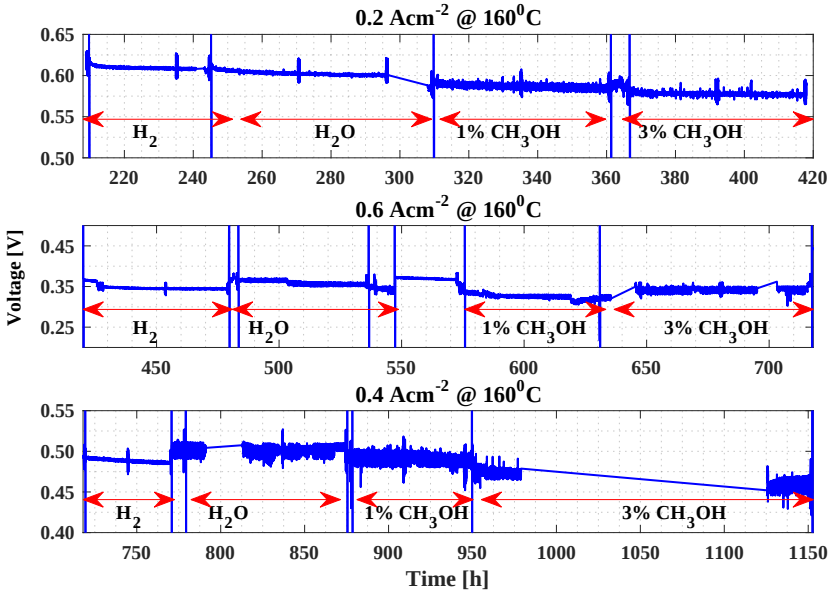

Figure 6: **Voltage profile under different anode gas composition and current density at 160** °C

The voltage profile shows fluctuations when a liquid (H_2O or H_2O + CH_3OH) is fed to the system. A possible reason could be some liquid droplets entering the system from the evaporator [27] or possibly due to transient variations in the evaporation rate inside the evaporator. The variation in voltage is maximum 20 mV, when operated with water vapour or methanol vapour in the fuel. The average degradation rate during the test at 160 °C is recorded as -39 $\mu V\,h^{-1}$ over a period of 1106 h. The initial voltage used for calculating degradation is after initial break-in test of 100 h in the case of 160 °C operation. The average degradation at 180 °C is recorded to be -37 $\mu V\,h^{-1}$ over a period of 800 h, while the overall average degradation rate is -44 $\mu V\,h^{-1}$ over a period of 1915 h. The total time used includes the unexpected shut-downs mentioned earlier.

The degradation rates are higher than generally reported in the literature. For pure H_2 operation at a constant current density of 0.2 $A\,cm^{-2}$ and temperature 160 °C, a degradation rate of -6 $\mu V\,h^{-1}$ after 6000 h operation was reported by Schmidt [56]. A degradation rate of -20 $\mu V\,h^{-1}$ was reported when operated with 60% H_2, 21% H_2O, 17% CO_2, 5 ppm H_2S and 2% CO at 180 °C [57]. In another study, a degradation rate of -40 $\mu V\,h^{-1}$ was reported when operated under load or thermal cycling [58]. A degradation rate of -55 $\mu V\,h^{-1}$ was reported with 3% methanol and -900 $\mu V\,h^{-1}$ with 5% methanol [11, 32]. However, a direct comparison is not possible since the H_2 and water mole fractions differ from the present study. The degradation rates are also influenced by the current density and temperature which are different from the current test sequence. The degradation also depends on the doping level of the MEA. The MEA in the present studies use post-doped membranes with doping level around 10 H_3PO_4 per repeat unit (PRU). The MEAs whose degradation rates were reported by Schmidt et al. [56, 57] and Araya et al. [59], Simon Araya et al. [32] used sol-gel based membranes with doping level up to 70 PRU [56]. The membranes with higher doping level would be able to withstand significantly larger acid losses before the impact on performance would be tangible.

3.2. Experimental results at 160 °C

The test results in terms of voltage profile, IV curves and impedance spectra recorded before and after a change in test sequence are presented and analysed below. At 160 °C, the sequence was repeated for three current densities. The variations between current densities are discussed below. The impedance spectra recorded are analysed based on the parameters extracted from the equivalent circuit fitting.

The voltage profile shown in Fig. 6 indicates the voltage variations with different current density and different fuel compositions over time at 160 °C. The voltage fluctuates with liquid in the feed and the fluctuation increases over time. This is a clear indication that there is some water droplet or uneven boiling rate in the membrane in the presence of PA. In the case of 0.2 A cm^{-2} there is minimal variation in the voltage slope over time in all the four cases of different fuel composition. These variations are larger at higher current density. The presence of water in the fuel results in increased performance, while the degradation rate with 3% and 5% methanol is seen to be similar at 0.6 A cm^{-2}. At 0.4 A cm^{-2} its hard to understand the voltage profile with 5% methanol because of unintended breaks, while with 3% there is some decrease in voltage compared to the voltage profile with H_2O alone.

3.2.1. Performance analysis at 0.2 A cm^{-2}

As seen from Fig. 7(a), The IV curves during different stages of operation at 0.2 A cm^{-2} show a maximum voltage difference of 0.105 V at 0.8 A cm^{-2} (linear operating region in the curve), when operated under different anode stream compositions. A variation in the voltage at higher current density can be seen in Fig. 7 (a).

The performance is best with pure H_2. When adding water to the anode, it becomes worse. The probable reasons governing the different phenomena are summarised in Table 3. When adding methanol to the anode feed, the IV curve is translated vertically, corresponding to a decrease in the exchange current density due to poisoning of the anode catalyst. A similar, though less pronounced effect is seen when increasing the methanol content from 3% to 5%. The voltage seems stable in Fig. 3.

The corresponding impedance spectra in Fig. 7 (b) show a maximum difference of 8.4 mω/c^2m in the ohmic resistances while a small change in the low frequency resistance is recorded. At higher current density the generated water also adds to the dilution effect. The decrease in performance observed in the polarisation curve after a test of 50 h with 3% CH_3OH can be explained by some phosphoric acid having been removed along with water [24].

3.2.2. Performance analysis at 0.6 A cm^{-2}

The IV curves recorded under various stages of 0.6 A cm^{-2} operation are shown in Fig. 8 (a). The performance decreases with addition of 5% CH_3OH, while it increases with addition of water vapour. This is attributed to increased charge carrier concentration, which enhances the

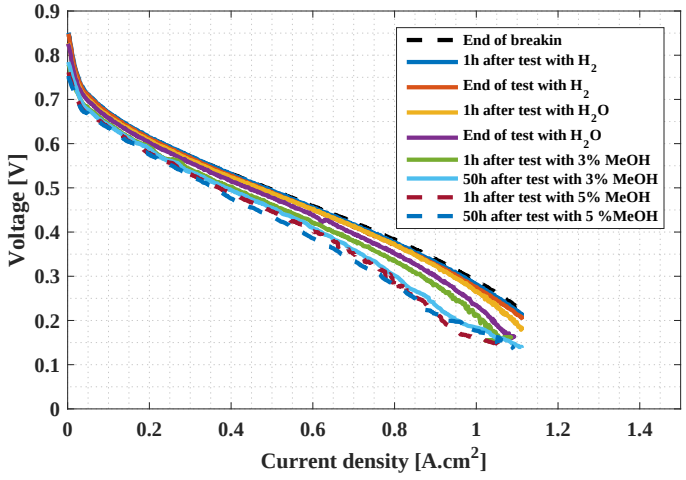

(a)

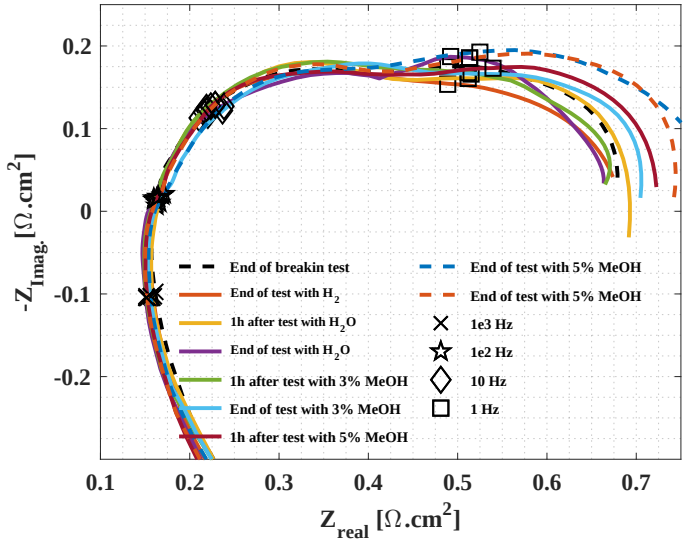

(b)

Figure 7: **Polarisation curve and impedance spectra comparison @ 0.2** A cm^{-2} **and 160** °C

proton conductivity. The variation of the IV curves under 0.6 A cm^{-2} is lower compared with 0.2 A cm^{-2} operation. The voltage variation is 0.052 V at 0.8 A cm^{-2}, which is half of what is observed at 0.2 A cm^{-2} operation. This is probably due to the increased water content in the cell enhancing CO conversion to CO_2 as shown in Eqn. 4, thereby increasing the catalyst active surface area.

The impedance is shown in Fig. 8 (b) has similar trend as seen at 0.2 A cm^{-2}. The polarisation performance is worse with pure H_2 but better with CH_3OH compared to 0.2 A cm^{-2}. An increase in the intermediate frequency resistance is probably due to dilution as similar trends were reported by Niya et al. [51].

3.2.3. Performance analysis at 0.4 A cm^{-2}

The performance has a similar trend as for 0.2 A cm^{-2} and 0.6 A cm^{-2}. The relation between polarisation performance and fuel composition is shown in Fig. 9(a). The presence of water improves the performance compared with pure H_2, while the performance is reduced on mixing methanol. Similar to other tests, the performance improves after 50 h operation with water vapour.

The impedance data shown in Fig. 9 (b) suggest a negative effect of 5% methanol on the overall performance. The ohmic resistance is significantly higher for 5% methanol operation compared to other fuel compositions. This could be due to the combination of catalyst poisoning and some degradation resulting from the unexpected abrupt shutdowns.

The voltage after 1200 h of operation at 160 °C with different fuel composition on the anode and varying current density shows a drop of 45 mV which is equivalent to a degradation rate of -37.5 $\mu V\,h^{-1}$. The degradation rate is higher than reported in literature with H_2 as discussed earlier but are found to be better than those reported with methanol in the feed. The results indicate that 15% water vapour has a positive influence on the fuel cell impedance at 160 °C, while the presence of methanol increases the impedance. The performance decreases at all current densities with the addition of methanol. This decrease in performance is presumed to be resulting from dilution.

3.3. Experimental results at 180 °C

This section discusses the results at 180 °C. The test sequence is is identical to that at 160 °C operation. The voltage profile for 180 °C operation is shown in Fig. 10. The effects of water

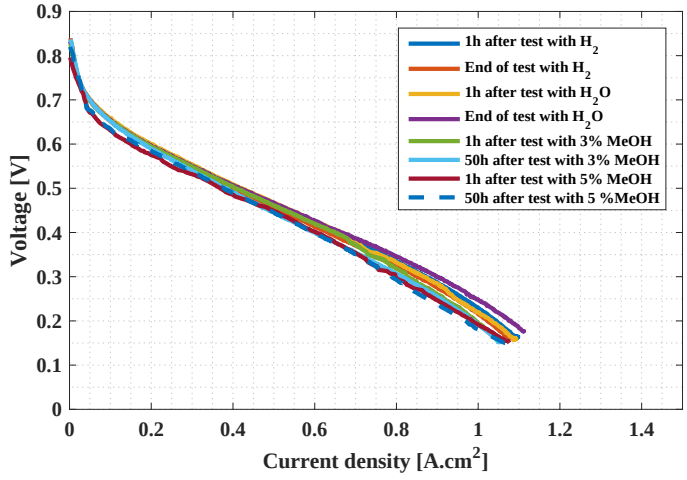

(a)

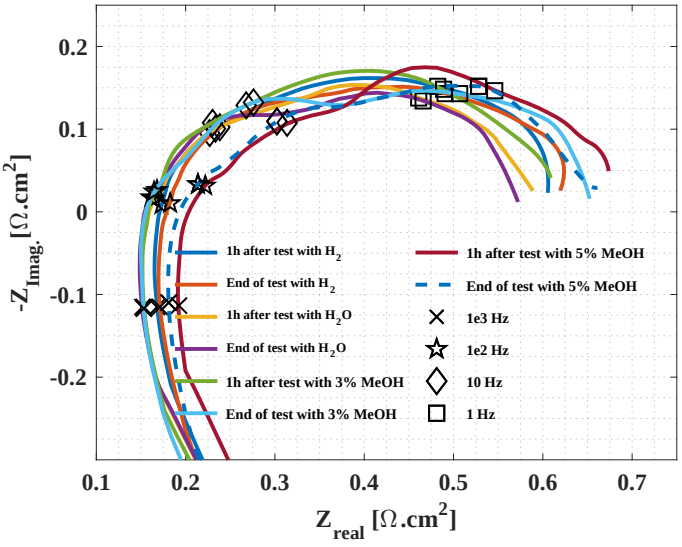

(b)

Figure 8: **Polarisation curve and impedance spectra comparison @ 0.6** A cm^{-2} **and 160** °C

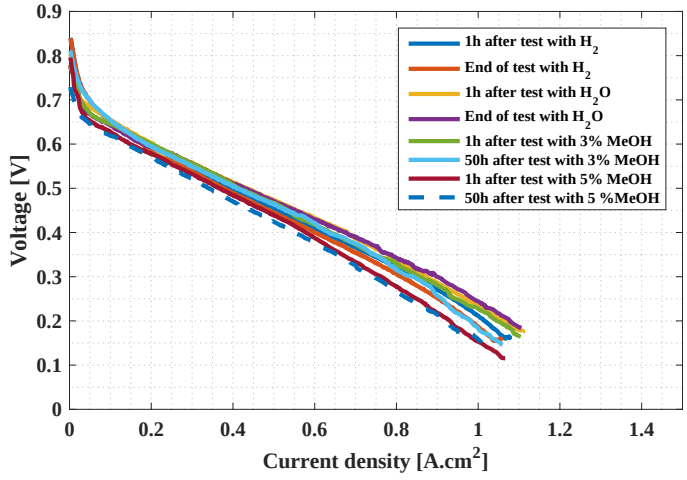

(a)

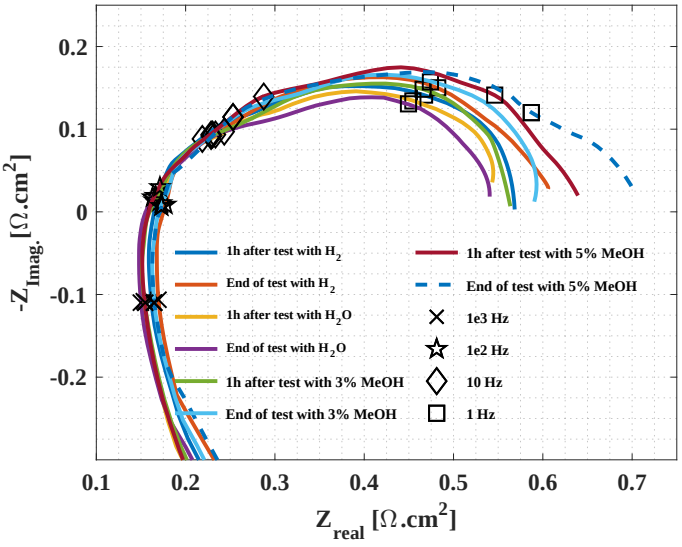

(b)

Figure 9: **Polarisation curve and impedance spectra comparison @ 0.4** A cm^{-2} **and 160** °C

are significant in all of the test sequences at 180 °C. At 0.2 A cm^{-2} operation, the performance with pure H_2 increases due to the temperature increase and on adding water it further increases. In the presence of 3% and 5% methanol in the anode feed, the voltage remains above that at 160 °C. When increasing the current density to 0.6 A cm^{-2} the voltage with pure hydrogen drops considerably, while with the addition of H_2O it regains the performance. This implies that the loss in voltage was due to dehydration and was temporary. At this current density, a reasonable performance is achieved with 3% methanol in the feed, while 5% methanol causes a significant decrease in performance. This could be due to a combined effect of methanol and the unintended shutdown of the system at 1650 h, which also plays a role in the voltage decrease. At 0.4 A cm^{-2}, the voltage follows a similar trend as at 0.6 A cm^{-2} operation. The voltage at 0.4 A cm^{-2} with pure H_2 is the lowest, which indicates the importance of the effect of dehydration in an HT-PEMFC. The performance with CH_3OH is better than with pure H_2. The voltage profiles with H_2O and 3% CH_3OH follow similar trends and no loss in voltage is observed. The voltage decreases with 5% CH_3OH but is still higher than with pure H_2 operation.

3.3.1. Performance analysis @ 0.2 A cm^{-2}

The IV curves recorded at different anode fuel compositions at 180 °C and 0.2 A cm^{-2} is shown in Fig. 11 (a). The voltage shows an improvement compared to the operation at 160 °C as seen in Fig. 3. The initial improvement in voltage is attributed to improved reaction kinetics and conductivity of PA at higher temperature.

The performance decreases rapidly thereafter as a result of dehydration of the membrane which increases the resistance to proton conduction. The impedance data supports this claim, as a high ohmic resistance is recorded for pure H_2 operation. A decrease of 23% in the ohmic resistance is recorded on changing from pure hydrogen to water. This clearly highlights the importance of keeping the membrane hydrated at 180 °C.

3.3.2. Performance analysis at 0.6 A cm^{-2}

The IV curves are shown in Fig. 12. Here high performance is recorded with H_2 and 15% H_2O after 50 h of operation. The improvement after 1 h is lower than what is recorded after 50 h of H_2 and 15% H_2O operation, which suggests gradual improvement as the membrane is hydrated. The performance decreases when adding 3% and 5% methanol at 0.2 A cm^{-2}, while at 0.6 A cm^{-2} the performance is better compared to 1 h after water injection. The reason for the

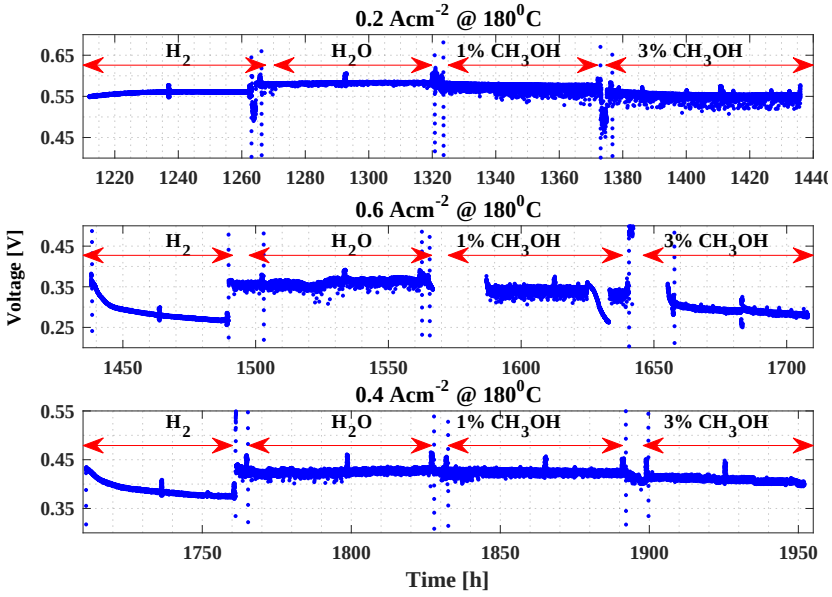

Figure 10: **Voltage profile under different anode gas composition and current densities at 180** °C

above may be twofold. Firstly, the water vapour in the feed hydrates the membrane, which increases the PA mobility and hence the proton conductivity. The time dependence is mostly related to the time it takes for PA to reach an equilibrium with water vapour in the system. Secondly, the addition of methanol on top of H_2O dilutes the fuel, which results in lower performance.

Compared with 0.2 A cm^{-2} operation there is a minimal decrease in performance after 1 h of test with H_2. This is attributed to a larger amount of product water being generated at 0.6 A cm_2, which keeps the membrane hydrated for longer time. Also, the test at 0.2 A cm^{-2} was operated immediately after operation at 160 °C and 0.4 A cm^{-2}, which again adds to the time taken for stable temperature distribution and equilibrium state of PA and water due to change in temperature. The open circuit voltage with pure H_2 is higher compared with other fuel compositions with water vapour and methanol. The open circuit voltage depends on the fuel composition and is reduced on diluting the fuel [50].

The impedance spectra are shown in Fig. 12 (b). The performance is higher after 50 h of

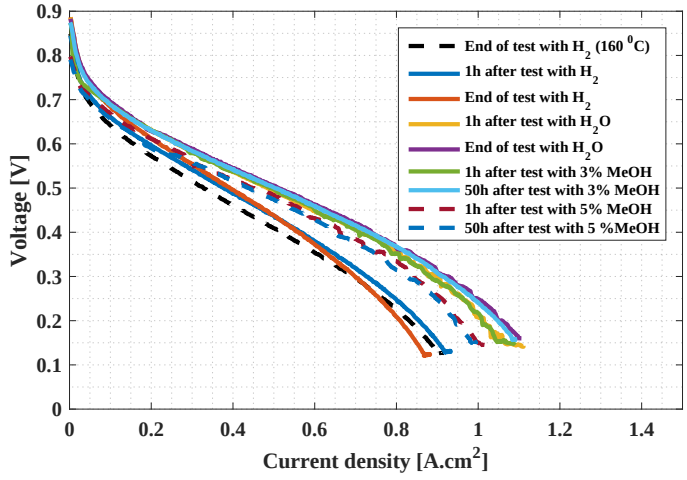

(a)

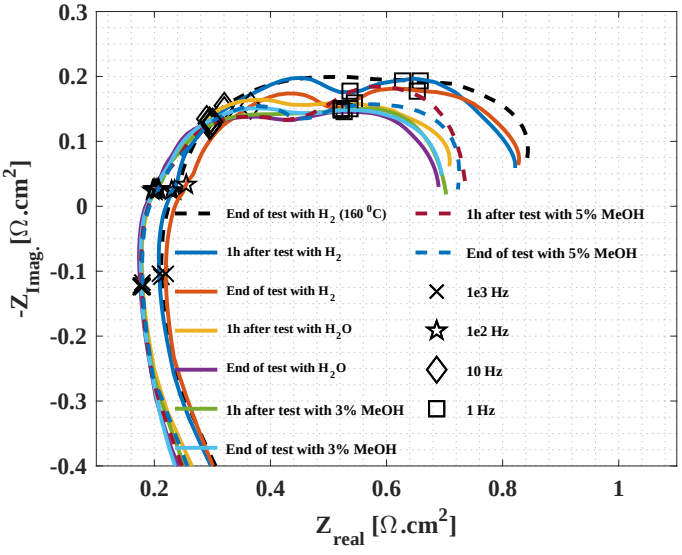

(b)

Figure 11: **Polarisation curve and impedance spectra comparison @ 0.2** A cm^{-2} **and 180** °C

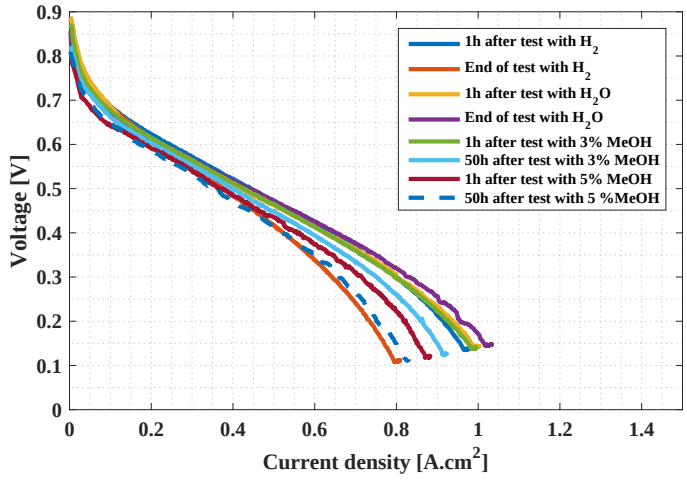

(a)

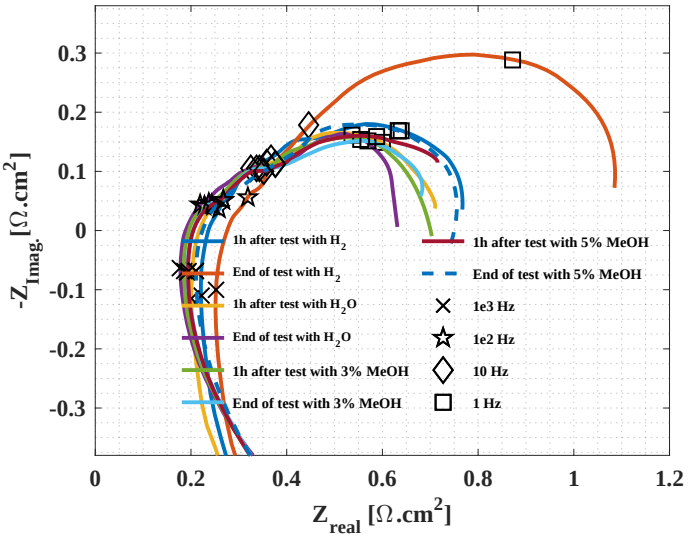

(b)

Figure 12: **Polarisation curve and impedance spectra comparison @ 0.6** A cm^{-2} **and 180** °C

operation with H_2O which suggests that it requires a few hours of operation before an equilibrium of water and PA is achieved, resulting on higher proton conductivity. There is a notable difference in the impedance at low and intermediate frequency with pure H_2 operation over a period of 50 h. The low and intermediate frequency loops expand significantly compared to the spectra recorded with water vapour in the anode feed.

3.3.3. Performance analysis at 0.4 $\mathrm{A\,cm^{-2}}$

The performance at 0.4 $\mathrm{A\,cm^{-2}}$ is shown in Fig. 13 (a). A notable point is the minimal differences in the voltages compared with 0.2 $\mathrm{A\,cm^{-2}}$ setpoint and higher compared to 0.6 $\mathrm{A\,cm^{-2}}$ setpoint. At lower current densities the voltage difference at 0.6 $\mathrm{A\,cm^{-2}}$ current density is highest when operating at 0.4 $\mathrm{A\,cm^{-2}}$ setpoint. This suggests that at intermediate current density and temperature of 180 °C, the performance variation is attributed to prolonged operation with methanol, rather than current density variation seen in the case of 160 °C operation.

The decrease in performance compared to 0.2 and 0.6 $\mathrm{A\,cm^{-2}}$ operation could be mainly attributed to degradation due to long time operation. The performance at 0.2 $\mathrm{A\,cm^{-2}}$ is higher than at 0.6 $\mathrm{A\,cm^{-2}}$, which is again higher than at 0.4 $\mathrm{A\,cm^{-2}}$ operation. The degradation is likely to be associated mainly to the poisoning of catalyst during operation with methanol. During long term operation some catalyst may be dissolving or agglomerating. Catalyst agglomeration is a common phenomenon in HT-PEMFC [56].

As seen in Fig. 13 (b), a trend in the impedance variation similar to that at 0.6 $\mathrm{A\,cm^{-2}}$ can be observed. The ohmic resistance is high with pure hydrogen. On adding water, it decreases and subsequently increases on adding methanol. On the other hand, the high frequency resistance trend is different, showing a lower resistance with methanol than with pure H_2. A similar trend was observed at 0.2 $\mathrm{A\,cm^{-2}}$ as well.

4. Discussion

In this section, the different phenomena influencing the voltage profile, IV curve and impedance spectra are discussed. The different phenomena are attributed to one or more probable causes. A summary of all the observed phenomena and the probable reasons are highlighted in table 3

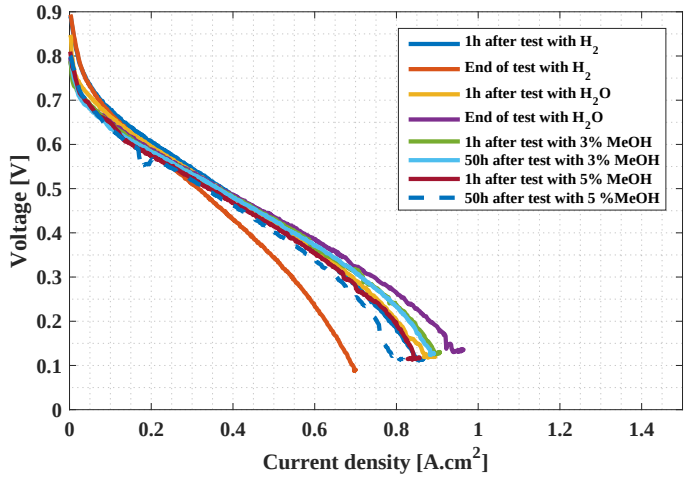

(a)

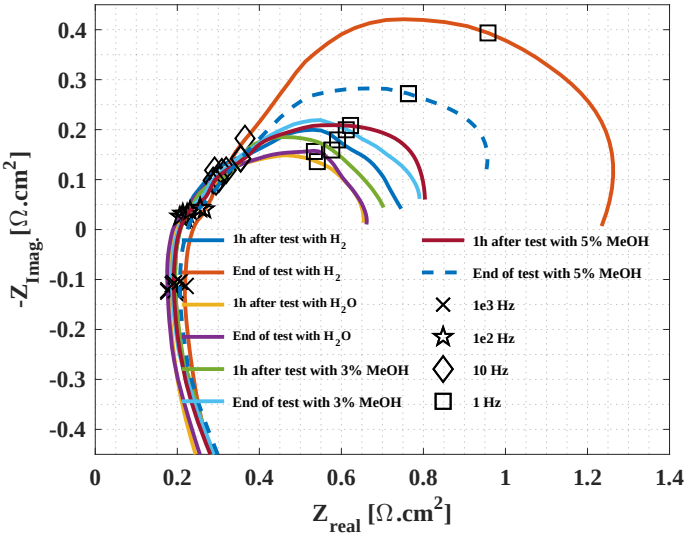

(b)

Figure 13: **Polarisation curve and impedance spectra comparison @ 0.4** A cm^{-2} **and 180** °C

4.1. Effect of water vapour under different temperatures (160 °C and 180 °C)

The presence of water vapour in the anode feed generally improves the performance. The most significant improvement is observed at 180 °C. When operated under higher temperature, membrane drying takes place and proton conductivity decreases due to lower conductivity of PA. As PA has a high affinity towards water, the PA is diluted and dissociates more easily when the system is fed with 15 % water vapour. This leads to a higher proton conductivity and the performance improves as seen in Fig. 7–13. The voltage profiles seen in Fig. 6 and Fig. 10 support the claim. An exception is at 0.2 A cm^{-2} and 160 °C. The variation in trend at 0.2 A cm^{-2} and 160 °C operation is probably due to low current density, where the amount of water generated along with the supplied water may not be enough to make a difference in the proton conductivity of the membrane. However, at low current density and 180 °C, the membrane is at a more dehydrated state compared to 160 °C. That is why the increase in performance with the addition of water is more visible at higher current densities and higher temperature operation. The addition of methanol causes some poisoning of the catalyst by the formation of CO as illustrated by Eqn. (5). The presence of water could also mitigate some of the negative effects of methanol seen in Fig. 8. The performance varies less compared with 0.2 A cm^{-2} and 160 °C operation. This is possibly due to better conversion of CO to CO_2 at higher temperature. Reduced CO concentration increases the active surface area of the catalyst for reaction.

The advantage of humidification is more prominently visible under 180 °C operation. The performance is regained immediately upon addition of water to the system. The differences are visible on the IV curves as shown in Fig. 11–13. The change in impedance is more pronounced at 0.6 A cm^{-2} operation compared to 0.2 A cm^{-2} operation. This phenomenon suggests that the generated water along with higher current density results in movement of PA from the membrane to the anode CL and GDL as observed by Eberhardt et al. [33]. Thus the increased conductivity due to added water is not sufficient to make up for the movement of PA.

4.2. Effect of methanol under different temperatures (160 °C and 180 °C)

At 160 °C, the poisoning effect of methanol at current densities of 0.2 A cm^{-2} and 0.4 A cm^{-2} is more significant compared with 0.6 A cm^{-2} as seen in Figs. 7, 8, and 9. The trend reverses when the temperature is changed from 160 °C to 180 °C. The voltage variation at 0.2 A cm^{-2} setpoint has the maximum variations in terms of voltage in the IV curves. This suggests the

detrimental effects of methanol are mitigated at higher current density when the cell is operated at 160 °C. The possible reason could be the reaction of water and pyrophosphoric acid to form PA as shown in Eqn. (1). At 0.6 A cm^{-2}, more water is generated in the cell, increasing the overall water mole fraction, and thus, assisting the CO oxidation into CO_2. At 0.2 A cm^{-2}, pyrophosphoric acid is formed due to drier conditions and this results in reduced performance due to reduced proton conductivity. Also, some CO poisoning is induced over a period of 50 h operation with CH_3OH which becomes pronounced with time. The poisoning covers some portion of the catalyst, which results in protons travelling longer distance to reach the active reaction sites. The combination of these two effects leads to a more severe reduction in the performance at 0.4 A cm^{-2} operation with 5 % methanol.

The effect is quite different at 180 °C operating temperature. At higher temperature, the dehydration of the membrane more dominant compared to the effect of methanol. The performance is lowest with pure H_2. This is attributed to dehydration of the membrane, which reduces the proton conductivity. When water is added the performance improves immediately. The performance with CH_3OH and H_2O is higher compared with dry H_2. The possible reason for better performance with CH_3OH and H_2O is attributed to faster reaction kinetics and presence of H_2O leading to more pyrophosphoric acid being converted to PA.

At 160 °C and 0.6 A cm^{-2} operation, a maximum difference of 8.4 mω/c^2m in the ohmic resistances and a small change in the low frequency resistance is observed. At higher current density the generated water also adds to the dilution effect. The decrease in performance after a test of 50 h with 3 % CH_3OH can be explained by some phosphoric acid removal by water [24]. At 160 °C and 0.6 A cm^{-2}, the ohmic resistance change is less than 5 % for the entire test sequence, while a drift in the impedance at low and intermediate frequency is seen. This change is around 12 % of the low frequency resistance and 25 % of the intermediate frequency resistance during the test sequence. The variations are attributed to mainly three reasons: Firstly, the addition of water vapour improves ion conductivity. Secondly, dilution effects increase mass transport losses and thirdly the presence of methanol poisons the catalyst thereby reducing catalyst activity. The results indicate that the second and third reasons are more dominant at higher current density. The increase in the intermediate frequency resistance is probably due to dilution as similar trends were reported by Rezaei Niya et al. [51].

The different resistances were determined based on the equivalent circuit model fit. The re-

sistances are plotted in Figs. 14–17. The plots represent the trends followed under different current densities and temperatures. In Fig. 14, the ohmic resistance variations are shown. The ohmic resistance, which is strongly dependent on the membrane structural and electrical properties, shows only minimal changes at 160 °C. The ohmic resistance decreases with the addition of water vapour and increases on adding CH_3OH. The possible reason could be poisoning or catalyst deactivation close to the membrane due to the reaction shown in eqn. 5. This results in the anode side reactions happening further away from the membrane. A more significant change is seen when adding 5 % methanol at 0.4 A cm^{-2}. This could be due to a combination of CO poisoning of the catalyst and dilution of the fuel on the anode making the anodic reaction more sluggish.

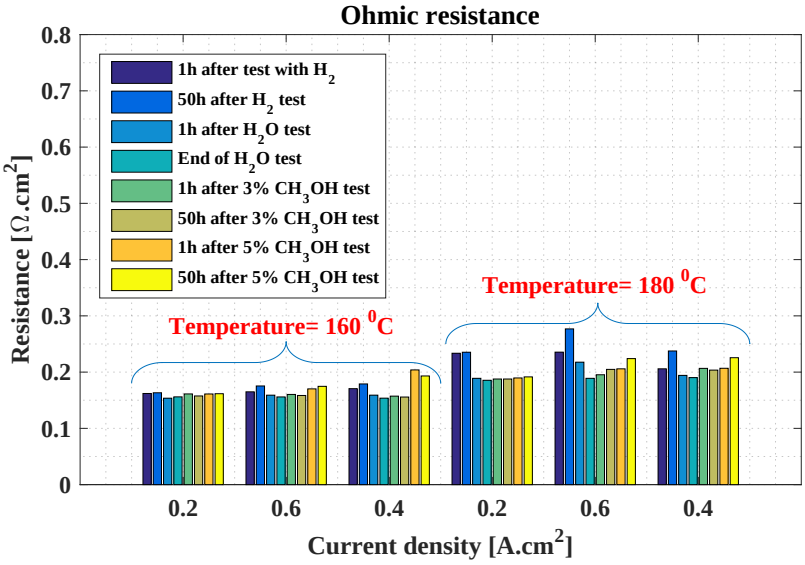

Figure 14: **Ohmic resistances as fitted using the equivalent circuit model.**

The variation of ohmic resistance is more prominent when operated at 180 °C. The resistance is recorded to be highest when operated with pure H_2. High temperature and low humidity dehydrates the membrane and the resulting effect is reduced proton conductivity due to less mobile charge carriers within the PA in the membrane. This is well demonstrated by the decrease

in ohmic resistance on adding water to the anode feed. There is also some variation in ohmic resistance with 5 % methanol at higher current densities (0.6 and 0.4 A cm^{-2}). This is also indicated in the IV curves (Fig. 12 and Fig. 13). There is a direct relationship between limiting current density and methanol concentration at 180 °C. The limiting current decreases with an increase in methanol concentration and the operating current density. The differences in limiting current density are more visible at 180 °C rather than at 160 °C. This effect of temperature on the limiting current densities is seen in Fig. 11–13. The formation of methyl phosphate could be the possible reason. This could be suppressed by the addition of excess water, which reduces the CH_3OH activity [31].

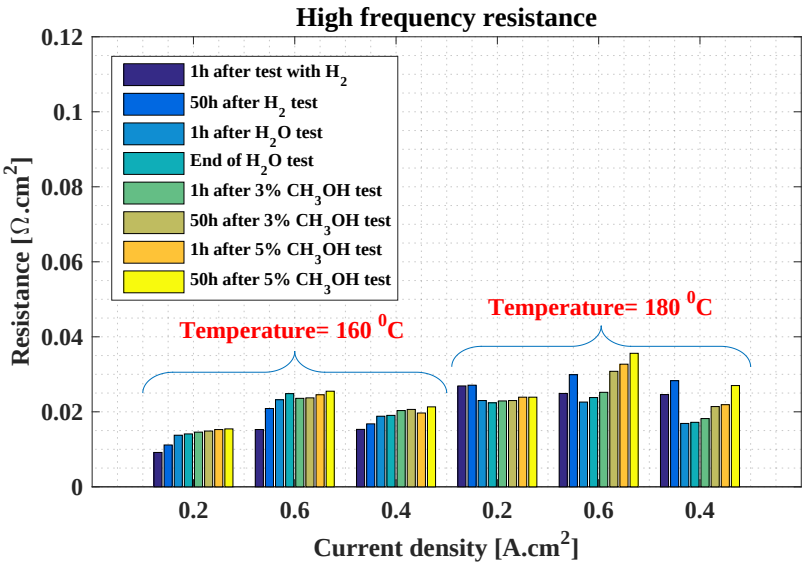

Figure 15: **High frequency resistances as fitted using the equivalent circuit model.**

Fig. 15 shows variations of the high frequency resistance (HFR). The HFR is assumed to be related to potential gradients in the catalyst layer. At 160 °C the variation between the highest and the lowest resistance is up to 50 %. The resistance is lowest for the pure H_2 tests. When the temperature is changed to 180 °C the changes in the high frequency resistance change character. At 0.6 and 0.4 A cm^{-2}, the resistance with 5 % methanol is higher, indicating the negative effects

of methanol in the anode feed. This is different from what is seen for LT-PEMFC, where the HFR is independent of temperature and current density [51]. Here the HFR strongly depends on the current density and increases with temperature as shown in Fig. 15. A possible reason for this behaviour could be fuel dilution, which increases with current density. As a result, the current distribution across the catalyst layer is affected. Changes in conductivity or poisoning of the anode catalyst layer affecting the current distribution within the catalyst layer could have a similar effect. This is aligned with the interpretation of the high frequency loop as resulting from CL potential gradients.

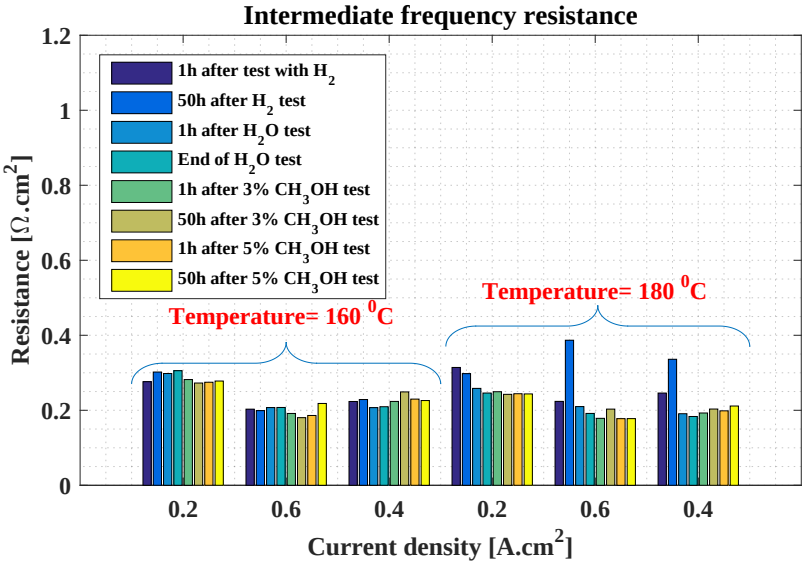

Figure 16: **Intermediate frequency resistances as fitted using the equivalent circuit model.**

In Fig. 16, the intermediate frequency (IF) resistance variations are shown. The IF loop is usually associated with cathode related issues and is often considered to be independent of the anode related issues. However, for the complex processes in an electrochemical cell, time scales overlap. In the present case, the fuel composition has some effect on the IF resistance. The variations probably stem from a combination of drying and fuel dilution on the anode. At 0.2 A cm^{-2}, the resistances are high, while at 0.6 A cm^{-2}, the loops shrink. This is a direct effect

of the slope of polarization curve levelling out at higher current densities. Similar trends are reported found in literature [60, 61].

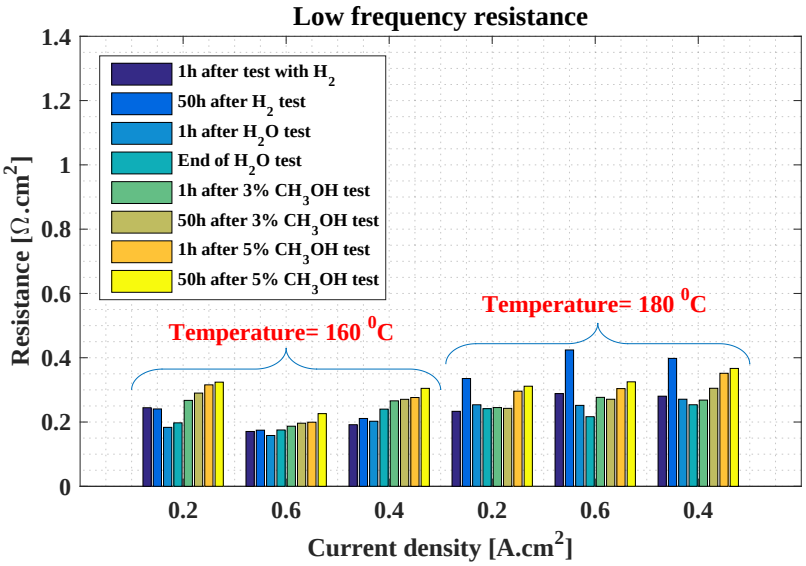

Figure 17: **Low frequency resistances as fitted using the equivalent circuit model.**

The low frequency loop is attributed to flow channel dynamics. There is simply not enough gas in the CL and the GDL for their dynamics to have an effect at frequencies below 1 Hz. The low frequency resistance development is shown in Fig. 17. It shows that temperature, current density and the fuel composition all have an effect on the low frequency resistance. At 160 °C, the resistance decreases with current density in a manner similar to that of the intermediate frequency resistance. At 180 °C this effect absent. On the other hand, at 180 °C the resistance is high after running for 50 h with pure H_2. This is likely a result of dehydration of the acid in the catalyst layer. As dehydration reduces conductivity, the reaction from moves closer to the membrane, resulting in longer diffusion paths and larger local amplitude of reactant activity at low frequencies. When water is added, the resistance is reduced, corresponding to shortening of the diffusion path, which more than makes up for the dilution from adding water.

When the fuel is further diluted by the addition of methanol, the channel composition changes.

Also the catalytic area is reduced due to poisoning. The combined effect is to increase the low frequency resistance.

Fuel composition *[mole fraction in %]*	**Current density** A cm^{-2}	**Temperature** *[°C]*	**Experimental observations**	**Probable reasons**
H_2 - 100	0.2	160	Best performance (Fig. 7). Lower Ohmic, HF and LF resistance (Figs. 14,15 and 17).	- No hysteresis effects of methanol. - Voltage is stabilised after break-in. - Operational degradation is low.
	0.2/0.6/0.4	160/180	Open circuit voltage is highest (Figs. 7–13).	-Fuel dilution reduces Gibbs free energy available for work.
	0.2/0.6/0.4	180	Performance is lowest (Figs. 11–13). High Ohmic, HF and LF resistances (Figs. 14,16,and 17).	- Degradation due to long term operation. - Catalyst agglomeration and dissolution. - Enhanced formation of $H_4P_2O_7$ due to dehydration of membrane at 180 ^{0}C (Eqn.1). - Hysteresis effect of CO poisoning (CH_3OH operation, Eqn. 2).
H_2-87 + H_2O-13	0.2	160	Performance decreasing (Fig. 7). Higher ohmic and IF resistance (Figs. 14 and16).	- Dilution of reactants. - Diluted acid flooding the catalyst layer.

	0.6/0.4	160	Performance better than other fuel compositions (Figs. 8–9). The ohmic and LF resistances are low (Figs. 14 and 17).	- Increase in number of charge carriers i.e., H_3PO_4 (Eqn. 1) [23]. - Enhanced conversion of CO to CO_2 (Eqn. 4).
	0.2/0.6/0.4	180	Performance is better than other fuel compositions (Fig. 11–13). The ohmic and HF resistances are low (Fig. 14 and 15).	- Hydration of the membrane improves proton conductivity. - Increase in number of charge carriers i.e., H_3PO_4 (Eqn. 1). - Higher temperature also improves reaction kinetics which is aided by high proton conductivity.
H_2-84.8+ H_2O-12.7 + CH_3OH-2.5	0.2/0.6/0.4	160	Performance better than at higher methanol concentration (5 %). All resistances are low except IF resistance at 0.4 A cm^{-2} set point (Figs. 14–17).	- Dilution is dominant compared to poisoning of the catalyst. - The presence of water vapour reduces the CH_3OH activity. - Higher proton conductivity with H_2O compensates the dilution effects.
	0.2/0.6/0.4	180	Better performance than pure H_2 operation, also evident from the ohmic, IF and LF resistances (Figs. 14,16 and 17)	- At higher temperature, the dehydration of the membrane is worse than poisoning and dilution effects.

				- Catalyst poisoning due to CH_3OH.
H_2-83.4+ H_2O-12.5 + CH_3OH-4.2	0.2	160	Performance lowest (Figs. 7–9). Mostly evident from HF and LF resistances (Figs. 15 and 17).	- Combined effects of poisoning and fuel dilution - Operation with 3 % and then 5 % CH_3OH over 50 h each worsen catalyst poisoning
	0.2/0.6/0.4	180	Better performance compared to pure H_2 (Figs. 11–13). Higher ohmic, LF and HF resistances (Figs. 14,16 and 17)	- Dehydration of membrane degrades the proton conductivity. - Presence of H_2O with CH_3OH aids in higher proton conductivity which prevails over poisoning of the catalyst & dilution effects.

Table 3: **This table summarises the observations made from comparing the IV curves, the impedance spectra (Figs. 7–13) and the equivalent circuit model resistances (Figs. 14–17) and lists the probable reasons for the observed behaviour.**

5. Conclusion

Tests with pure hydrogen, 15 % water vapour and methanol (3 % and 5 %) at different current densities (0.2 A cm^{-2}, 0.4 A cm^{-2} and 0.6 A cm^{-2}) and different temperatures (160 °C and 180 °C) were carried out to understand separately the effects of water vapour and methanol in enhancing or degrading a HT-PEM fuel cell. An overall degradation of -44 $\mu V\,h^{-1}$ is recorded over a period of 1915 h test after a break-in of 100 h. The degradation is -39 $\mu V\,h^{-1}$ over a period of 1106 h and -37 $\mu V\,h^{-1}$ over a period of 800 h at 160 °C and 180 °C operation, respectively. This shows that the degradation with reformate in the anode feed is not affected by operating at

higher temperature, which improves the reaction.

At 0.2 $A\,cm^{-2}$ and 160 °C the voltage with pure H_2 is higher than the rest. The probable reason assumed is that at low current density the amount of water generated together with the supplied is not enough to make a difference in the proton conductivity of the membrane. However, at low current density and higher temperature (180 °C) the membrane is at a more dehydrated state compared to when operated at 160 °C. That is why the performance at low current densities and higher temperature operation is higher than pure H_2 operation, as the water effect comes into play. The water in the feed counteracts the negative effect of methanol in the feed. The positive effect of water is more prominently seen at 180 °C compared to 160 °C. The proton conductivity improvement with the water in the feed is evident from the results.

The experimental results suggest that the direct integration of methanol reformer with an HT-PEMFC is rather easy. The reformer outlet, which may contain few percentages (less than 3 %) of CH_3OH will not drastically affect the fuel cell performance as the water present mitigates some of the degrading effects. 15 % water and 3 % CH_3OH are realistic numbers of a methanol reformer output. Thus, reformate mixture, including the unreacted CH_3OH can be directly fed to the HT-PEM fuel cell system without any pre-purification.

Acknowledgement

The authors would like to thank the Innovation Fund Denmark for funding the work through the 4M project. The authors are also thankful to Danish Power Systems for providing the MEA used in the experiment.

[1] J. S. Wainright. Acid-Doped Polybenzimidazoles: A New Polymer Electrolyte. *Journal of The Electrochemical Society*, 142(7):L121, jul 1995. ISSN 00134651. doi: 10.1149/1.2044337. URL http://jes.ecsdl.org/content/142/7/L121.abstract.

[2] Qingfeng Li, Ronghuan He, Jens Oluf Jensen, and Niels J. Bjerrum. Approaches and Recent Development of Polymer Electrolyte Membranes for Fuel Cells Operating above 100 ÂřC. *Chemistry of Materials*, 15(26):4896–4915, dec 2003. ISSN 0897-4756. doi: 10.1021/cm0310519. URL http://www.scopus.com/inward/record.url?eid=2-s2.0-0347418166{&}partnerID=tZ0tx3y1http://www.scopus.com/inward/record.url?eid=2-s2.0-0347418166{%}7B{&}{%}7DpartnerID=tZ0tx3y1.

[3] Jiujun Jianlu Zhang, Zhong Xie, Jiujun Jianlu Zhang, Yanghua Tang, Chaojie Song, Titichai Navessin, Zhiqing Shi, Datong Song, Haijiang Wang, David P Wilkinson, Zhong-Sheng Liu, and Steven Holdcroft. High temperature PEM fuel cells. *Journal of Power Sources*, 160(2):872–891, oct 2006. ISSN 03787753. doi: http://dx.doi.org/10.1016/j.jpowsour.2006.05.034. URL http://www.sciencedirect.com/science/article/pii/S0378775306010299.

[4] Hong Sun, Chen Xie, Hao Chen, and Saif Almheiri. A numerical study on the effects of temperature and mass transfer in high temperature PEM fuel cells with ab-PBI membrane. *Applied Energy*, 160:937–944, mar 2015. ISSN 03062619. doi: 10.1016/j.apenergy.2015.02.053. URL http://www.sciencedirect.com/science/article/pii/S0306261915002305.

[5] Vikas Jaggi and S Jayanti. A conceptual model of a high-efficiency, stand-alone power unit based on a fuel cell stack with an integrated auto-thermal ethanol reformer. *Applied Energy*, 110(0):295–303, 2013. ISSN 0306-2619. doi: http://dx.doi.org/10.1016/j.apenergy.2013.04.001. URL http://www.sciencedirect.com/science/article/pii/S0306261913002833.

[6] Nicola Zuliani and Rodolfo Taccani. Microcogeneration system based on HTPEM fuel cell fueled with natural gas: Performance analysis. *Applied Energy*, 97:802–808, sep 2012. ISSN 03062619. doi: 10.1016/j.apenergy.2011.12.089. URL http://www.sciencedirect.com/science/article/pii/S0306261911008956http://www.scopus.com/inward/record.url?eid=2-s2.0-84862316706{&}partnerID=40{&}md5=dc1dc920b6055a2b12a9f020af702a31.

[7] Remzi Can Samsun, Joachim Pasel, Holger Janßen, Werner Lehnert, Ralf Peters, and Detlef Stolten. Design and test of a 5kWe high-temperature polymer electrolyte fuel cell system operated with diesel and kerosene. *Applied Energy*, 114:238–249, feb 2014. ISSN 03062619. doi: 10.1016/j.apenergy.2013.09.054. URL http://www.sciencedirect.com/science/article/pii/S0306261913008015.

[8] Kui Jiao, Yibo Zhou, Qing Du, Yan Yin, Shuhai Yu, and Xianguo Li. Numerical simulations of carbon monoxide poisoning in high temperature proton exchange membrane fuel cells with various flow channel designs. *Applied Energy*, 104:21–41, apr 2013. ISSN 03062619. doi: 10.1016/j.apenergy.2012.10.059. URL http://linkinghub.elsevier.com/retrieve/pii/S0306261912007787.

[9] Behzad Najafi, Alireza Haghighat Mamaghani, Fabio Rinaldi, and Andrea Casalegno. Long-term performance analysis of an HT-PEM fuel cell based micro-CHP system: Operational strategies. *Applied Energy*, 147:582–592, jun 2015. ISSN 03062619. doi: 10.1016/j.apenergy.2015.03.043. URL http://www.sciencedirect.com/science/article/pii/S030626191500327X.

[10] Joan M Ogden, Margaret M Steinbugler, and Thomas G Kreutz. A comparison of hydrogen, methanol and gasoline as fuels for fuel cell vehicles: implications for vehicle design and infrastructure development. *Journal of Power Sources*, 79(2):143–168, jun 1999. ISSN 03787753. doi: 10.1016/S0378-7753(99)00057-9. URL http://www.sciencedirect.com/science/article/pii/S0378775399000579.

[11] Samuel Simon Araya, Ionela Florentina Grigoras, Fan Zhou, Søren Juhl Andreasen, and Søren Knudsen Kær. Performance and endurance of a high temperature PEM fuel cell operated on methanol reformate. *International Journal of Hydrogen Energy*, 39(32):18343–18350, oct 2014. ISSN 03603199. doi: 10.1016/j.ijhydene.2014.09.007. URL http://linkinghub.elsevier.com/retrieve/pii/S0360319914025269.

[12] Qingfeng Li, David Aili, Hans Aage Hjuler, and Jens Oluf Jensen, editors. *High Temperature Polymer Electrolyte Membrane Fuel Cells: Approaches, Status, and Perspectives*. Springer, 1 edition, 2015. ISBN 3319170821. doi: 10.1007/978-3-319-17082-4. URL https://books.google.com/books?id=corDCgAAQBAJ{&}pgis=1https://books.google.com/books?id=corDCgAAQBAJ{%}7B{&}{%}7Dpgis=1.

[13] Li Qingfeng, H.A. A Hjuler, and N.J. J Bjerrum. Phosphoric acid doped polybenzimidazole membranes: Physiochemical characterization and fuel cell applications. *Journal of Applied Elec-*

trochemistry, 31(7):773–779, 2001. ISSN 1572-8838. doi: 10.1023/A:1017558523354. URL http://link.springer.com/article/10.1023/A{%}7B{%}25{%}7D3A1017558523354http://link.springer.com/article/10.1023/A{%}3A1017558523354.

[14] Justo Lobato, Pablo Cañizares, Manuel A Rodrigo, and José J Linares. PBI-based polymer electrolyte membranes fuel cells: Temperature effects on cell performance and catalyst stability. *Electrochimica acta*, 52(12):3910–3920, mar 2007. URL http://linkinghub.elsevier.com/retrieve/pii/S0013468606011613http://www.sciencedirect.com/science/article/pii/S0013468606011613http://linkinghub.elsevier.com/retrieve/pii/S0013468606011613http://www.sciencedirect.com/science/article/pii/S00134686060116.

[15] Samuele Galbiati, Andrea Baricci, Andrea Casalegno, and Renzo Marchesi. Experimental study of water transport in a polybenzimidazole-based high temperature PEMFC. *International Journal of Hydrogen Energy*, 37(3):2462–2469, feb 2012. ISSN 03603199. doi: 10.1016/j.ijhydene.2011.09.159. URL http://linkinghub.elsevier.com/retrieve/pii/S0360319911024463http://www.sciencedirect.com/science/article/pii/S0360319911024463.

[16] Chen-Yu Chen and Wei-Hsiang Lai. Effects of temperature and humidity on the cell performance and resistance of a phosphoric acid doped polybenzimidazole fuel cell. *Journal of Power Sources*, 195(21):7152–7159, nov 2010. ISSN 03787753. doi: 10.1016/j.jpowsour.2010.05.057. URL http://www.sciencedirect.com/science/article/pii/S0378775310009250.

[17] Yeh-Hung Lai and Gerald W Fly. In-situ diagnostics and degradation mapping of a mixed-mode accelerated stress test for proton exchange membranes. *Journal of Power Sources*, 274(0):1162–1172, 2015. doi: http://dx.doi.org/10.1016/j.jpowsour.2014.10.116. URL http://www.sciencedirect.com/science/article/pii/S037877531401725X.

[18] David I. MacDonald and James R. Boyack. Density, electrical conductivity, and vapor pressure of concentrated phosphoric acid. *Journal of Chemical {&} Engineering Data*, 14(3):380–384, jul 1969. ISSN 0021-9568. doi: 10.1021/je60042a013. URL http://dx.doi.org/10.1021/je60042a013.

[19] Der-Tau Chin and Howard H. Chang. On the conductivity of phosphoric acid electrolyte. *Journal of Applied Electrochemistry*, 19(1):95–99, jan 1989. ISSN 0021-891X. doi: 10.1007/BF01039396. URL http://link.springer.com/10.1007/BF01039396.

[20] Niels J. Bjerrum Ronghuan He, Qingfeng Li, Gang Xiao. Proton conductivity of phosphoric acid doped polybenzimidazole and its composites with inorganic proton conductors. *Journal of Membrane Science*, 226(1-2):169–184, dec 2003. ISSN 03767388. doi: 10.1016/j.memsci.2003.09.002. URL http://www.sciencedirect.com/science/article/pii/S0376738803004216.

[21] Y.-L. Ma, J. S. Wainright, M. H. Litt, and R. F. Savinell. Conductivity of PBI Membranes for High-Temperature Polymer Electrolyte Fuel Cells. *Journal of the Electrochemical Society*, 151(1):A8–A16, jan 2004. ISSN 00134651. doi: 10.1149/1.1630037. URL http://jes.ecsdl.org/content/151/1/A8.abstracthttp://jes.ecsdl.org/content/151/1/A8.full.

[22] Maria K. Daletou, Joannis K. Kallitsis, George Voyiatzis, and Stylianos G. Neophytides. The interaction of water vapors with H3PO4 imbibed electrolyte based on PBI/polysulfone copolymer blends. *Journal of Membrane Science*, 326(1):76–83, jan 2009. ISSN 03767388. doi: 10.1016/j.memsci.2008.09.040. URL http:

//www.sciencedirect.com/science/article/pii/S0376738808008466.

[23] Caizhi Zhang, Lan Zhang, Weijiang Zhou, Youyi Wang, and Siew Hwa Chan. Investigation of water transport and its effect on performance of high-temperature PEM fuel cells. *Electrochimica Acta*, 149:271–277, dec 2014. ISSN 00134686. doi: 10.1016/j.electacta.2014.10.059. URL http://www.sciencedirect.com/science/article/pii/S0013468614020660.

[24] Purushothama Chippar, Kyungmun Kang, Young-Don Lim, Whan-Gi Kim, and Hyunchul Ju. Effects of inlet relative humidity (RH) on the performance of a high temperature-proton exchange membrane fuel cell (HT-PEMFC). *International Journal of Hydrogen Energy*, 39(6):2767–2775, feb 2014. ISSN 03603199. doi: 10.1016/j.ijhydene.2013.05.115. URL http://www.sciencedirect.com/science/article/pii/S0360319913013475.

[25] Dario Bezmalinović, Stephan Strahl, Vicente Roda, and Attila Husar. Water transport study in a high temperature proton exchange membrane fuel cell stack. *International Journal of Hydrogen Energy*, 39(20):10627–10640, jul 2014. ISSN 03603199. doi: 10.1016/j.ijhydene.2014.04.186. URL http://www.sciencedirect.com/science/article/pii/S0360319914012762.

[26] José J. Linares, Cassandra Sanches, Valdecir A. Paganin, and Ernesto R. Gonzalez. Performance of a poly(2,5-benzimidazole)-based polymer electrolyte membrane fuel cell. *International Journal of Hydrogen Energy*, 37(8):7212–7220, apr 2012. ISSN 03603199. doi: 10.1016/j.ijhydene.2011.12.030. URL http://www.sciencedirect.com/science/article/pii/S0360319911026826.

[27] Fan Zhou, Søren Juhl Andreasen, Søren Knudsen Kær, and Jung O. Park. Experimental investigation of carbon monoxide poisoning effect on a PBI/H3PO4 high temperature polymer electrolyte membrane fuel cell: Influence of anode humidification and carbon dioxide. *International Journal of Hydrogen Energy*, 2015. ISSN 03603199. doi: 10.1016/j.ijhydene.2015.09.056. URL http://www.sciencedirect.com/science/article/pii/S0360319915023460.

[28] A.D. D Modestov, M.R. R Tarasevich, V.Ya. Filimonov, and E.S. S Davydova. CO tolerance and CO oxidation at Pt and PtâĂŞRu anode catalysts in fuel cell with polybenzimidazoleâĂŞH3PO4 membrane. *Electrochimica Acta*, 55(20):6073–6080, aug 2010. ISSN 00134686. doi: 10.1016/j.electacta.2010.05.068. URL http://www.sciencedirect.com/science/article/pii/S001346861000770Xhttp://linkinghub.elsevier.com/retrieve/pii/S001346861000770X.

[29] Zhenyu Liu, Jesse S. Wainright, Morton H. Litt, and Robert F. Savinell. Study of the oxygen reduction reaction (ORR) at Pt interfaced with phosphoric acid doped polybenzimidazole at elevated temperature and low relative humidity. *Electrochimica Acta*, 51(19):3914–3923, may 2006. ISSN 00134686. doi: 10.1016/j.electacta.2005.11.019. URL http://www.sciencedirect.com/science/article/pii/S0013468605012922.

[30] Guenter Uphues and Uwe Ploog. Direct esterification of o-phosphoric acid, aug 1989. URL http://www.freepatentsonline.com/4921990.html.

[31] David Aili, Anton Vassiliev, Jens Oluf Jensen, Thomas J. Schmidt, and Qingfeng Li. Methyl phosphate formation as a major degradation mode of direct methanol fuel cells with phosphoric acid based electrolytes. *Journal of Power Sources*, 279:517–521, apr 2015. ISSN 03787753. doi: 10.1016/j.jpowsour.2015.01.010. URL http://www.sciencedirect.com/science/article/pii/S0378775315000117.

[32] Samuel Simon Araya, Søren Juhl Andreasen, Heidi Venstrup Nielsen, and Søren Knudsen Kær. Investigating the effects of methanol-water vapor mixture on a PBI-based high temperature PEM fuel cell. *International Journal*

of Hydrogen Energy, 37(23):18231–18242, 2012. doi: http://dx.doi.org/10.1016/j.ijhydene.2012.09.009. URL http://www.sciencedirect.com/science/article/pii/S0360319912020125.

[33] S. H. Eberhardt, M. Toulec, F. Marone, M. Stampanoni, F N Büchi, and T. J. Schmidt. Dynamic Operation of HT-PEFC: In-Operando Imaging of Phosphoric Acid Profiles and (Re)distribution. *Journal of The Electrochemical Society*, 162(3):F310–F316, jan 2015. ISSN 0013-4651. doi: 10.1149/2.0751503jes. URL http://jes.ecsdl.org/content/162/3/F310.abstracthttp://jes.ecsdl.org/cgi/doi/10.1149/2.0751503jes.

[34] Jean-Luc Dellis. Zfit. Software, 2010. URL http://kr.mathworks.com/matlabcentral/fileexchange/19460-zfit.

[35] Søren Juhl Andreasen, Jakob Rabjerg Vang, and Søren Knudsen Kær. High temperature PEM fuel cell performance characterisation with CO and CO2 using electrochemical impedance spectroscopy. *International Journal of Hydrogen Energy*, 36(16):9815–9830, aug 2011. ISSN 03603199. URL http://www.sciencedirect.com/science/article/pii/S0360319911009414.

[36] Samuele Galbiati, Andrea Baricci, Andrea Casalegno, Giulia Carcassola, and Renzo Marchesi. On the activation of polybenzimidazole-based membrane electrode assemblies doped with phosphoric acid. *International Journal of Hydrogen Energy*, 37(19):14475–14481, 2012. doi: 10.1016/j.ijhydene.2012.07.032. URL http://linkinghub.elsevier.com/retrieve/pii/S0360319912016096.

[37] SS Samuel Simon Araya and SJ Andreasen. Investigating the effects of methanol-water vapor mixture on a PBI-based high temperature PEM fuel cell. *International Journal of ...*, pages 1–26, 2012. URL http://www.sciencedirect.com/science/article/pii/S0360319912020125.

[38] Samuele Galbiati, Andrea Baricci, Andrea Casalegno, and Renzo Marchesi. Degradation in phosphoric acid doped polymer fuel cells: A 6000 h parametric investigation. *International Journal of Hydrogen Energy*, 38(15):6469–6480, 2013. doi: http://dx.doi.org/10.1016/j.ijhydene.2013.03.012. URL http://www.sciencedirect.com/science/article/pii/S0360319913005867.

[39] M. Boaventura, H. Sander, K.A. A Friedrich, and A. Mendes. The influence of CO on the current density distribution of high temperature polymer electrolyte membrane fuel cells. *Electrochimica Acta*, 56(25):9467–9475, oct 2011. ISSN 00134686. doi: 10.1016/j.electacta.2011.08.039. URL http://dx.doi.org/10.1016/j.electacta.2011.08.039http://www.sciencedirect.com/science/article/pii/S0013468611012552.

[40] F. Javier Pinar, Nadine Pilinski, Maren Rastedt, and Peter Wagner. Performance of a high-temperature PEM fuel cell operated with oxygen enriched cathode air and hydrogen from synthetic reformate. *International Journal of Hydrogen Energy*, dec 2014. ISSN 03603199. URL http://www.sciencedirect.com/science/article/pii/S0360319914033503.

[41] M. Mamlouk and K. Scott. Analysis of high temperature polymer electrolyte membrane fuel cell electrodes using electrochemical impedance spectroscopy. *Electrochimica Acta*, 56(16):5493–5512, jun 2011. ISSN 00134686. doi: 10.1016/j.electacta.2011.03.056. URL http://www.sciencedirect.com/science/article/pii/S0013468611004348.

[42] Jesper Lebæk Jespersen, Erik Schaltz, and Søren Knudsen Kær. Electrochemical characterization of a polybenzimidazole-based high temperature proton exchange membrane unit cell. *Journal of Power Sources*, 191(2):289–296, jun 2009. ISSN 03787753. doi: 10.1016/j.jpowsour.2009.02.025. URL http://www.sciencedirect.

com/science/article/pii/S0378775309002742.

[43] M. Chandesris, C. Robin, M. Gerard, and Y. Bultel. Investigation of the difference between the low frequency limit of the impedance spectrum and the slope of the polarization curve. *Electrochimica Acta*, 180(JANUARY):581–590, oct 2015. ISSN 00134686. doi: 10.1016/j.electacta.2015.08.089. URL http://linkinghub.elsevier.com/retrieve/pii/S001346861530339X.

[44] Jakob Rabjerg Vang, Søren Juhl Andreasen, Samuel Simon Araya, and Søren Knudsen Kær. Comparative study of the break in process of post doped and solâĂŞgel high temperature proton exchange membrane fuel cells. *International Journal of Hydrogen Energy*, 39(27):14959–14968, aug 2014. ISSN 03603199. doi: 10.1016/j.ijhydene.2014.07.017. URL http://www.sciencedirect.com/science/article/pii/S0360319914019727.

[45] Jingwei Hu, Huamin Zhang, and Liu Gang. Diffusion-convection/electrochemical model studies on polybenzimidazole (PBI) fuel cell based on AC impedance technique. *Energy Conversion and Management*, 49 (5):1019–1027, 2008. URL http://www.sciencedirect.com/science/article/B6V2P-4R8KST5-3/2/c41ead66427dbac6167c853ec99a5ca3.

[46] J HU, H ZHANG, Y ZHAI, G LIU, and B YI. 500h Continuous aging life test on PBI/H3PO4 high-temperature PEMFC. *International Journal of Hydrogen Energy*, 31(13):1855–1862, oct 2006. ISSN 03603199. doi: 10.1016/j.ijhydene.2006.05.001. URL http://www.sciencedirect.com/science/article/pii/S0360319906001662.

[47] Xiaozi Yuan, Haijiang Wang, Jian Colin Sun, and Jiujun Zhang. AC impedance technique in PEM fuel cell diagnosisâĂŞA review. *International Journal of Hydrogen Energy*, 32(17):4365 – 4380, 2007. ISSN 0360-3199. doi: DOI:10.1016/j.ijhydene.2007.05.036. URL http://www.sciencedirect.com/science/article/B6V3F-4P5YK26-1/2/8d98edc8e2b445980931039f7cb4c716.

[48] T E Springer, T A Zawodzinski, M S Wilson, and S Gottesfeld. Characterization of Polymer Electrolyte Fuel Cells Using AC Impedance Spectroscopy. *Journal of The Electrochemical Society*, 143(2):587–599, 1996. doi: 10.1149/1.1836485. URL http://link.aip.org/link/?JES/143/587/1.

[49] Søren Juhl Andreasen and Soỳren Knudsen Kær. Dynamic Model of the High Temperature Proton Exchange Membrane Fuel Cell Stack Temperature. *Journal of Fuel Cell Science and Technology*, 6(4):41006, 2009. ISSN 1550624X. doi: 10.1115/1.3081461. URL http://fuelcellscience.asmedigitalcollection.asme.org/article.aspx?articleid=1472107http://dx.doi.org/10.1115/1.3081461.

[50] Ryan P. O'Hayre, Fritz B. Prinz Ryan O'Hayre, Suk-Won Cha, Whitney Colella, Suk-Won Cha, Whitney G Colella, and Fritz B Prinz. *Fuel Cell Fundamentals*. John Wiley & Sons, Inc., 2nd edition, 2008. ISBN 978-0-470-25843-9. URL http://www.amazon.com/Fuel-Cell-Fundamentals-Ryan-OHayre/dp/0470258438http://books.google.dk/books/about/Fuel{_}cell{_}fundamentals.html?id=CrOQAQAAMAAJ{&}pgis=1.

[51] Seyed Mohammad Rezaei Niya, Ryan K. Phillips, and Mina Hoorfar. Process modeling of the impedance characteristics of proton exchange membrane fuel cells. *Electrochimica Acta*, 191:594–605, feb 2016. ISSN 00134686. doi: 10.1016/j.electacta.2016.01.128. URL http://www.sciencedirect.com/science/article/pii/S001346861630130X.

[52] I A Schneider, S A Freunberger, D Kramer, A Wokaun, and G G Scherer. Oscillations in gas channels Part I. The forgotten player in impedance spectroscopy in PEFCs. *Journal of the Electrochemical Society*, 154(4):B383—-B388, 2007. ISSN 00134651. doi: 10.1149/1.2435706. URL http://jes.ecsdl.org/cgi/doi/10.1149/1.

2435706.

[53] I A Schneider, D Kramer, A Wokaun, and G G Scherer. Oscillations in gas channels II. Unraveling the characteristics of the low frequency loop in air-fed PEFC impedance spectra. *Journal of The Electrochemical Society*, 154(8): B770, 2007. ISSN 00134651. doi: 10.1149/1.2742291. URL http://jes.ecsdl.org/cgi/doi/10.1149/1.2742291http://jes.ecsdl.org/content/154/8/B770.short.

[54] Gaël Maranzana, Julia Mainka, Olivier Lottin, Jerome Dillet, Adrien Lamibrac, Anthony Thomas, and Sophie Didierjean. A proton exchange membrane fuel cell impedance model taking into account convection along the air channel: On the bias between the low frequency limit of the impedance and the slope of the polarization curve. *Electrochimica Acta*, 83:13–27, 2012. URL http://www.sciencedirect.com/science/article/pii/S0013468612011954.

[55] J. R. Vang, F. Zhou, S. J. Andreasen, S K Kær, and S. K. Kaer. Estimating important electrode parameters of high temperature PEM fuel cells by fitting a model to polarisation curves and impedance spectra. *ECS Transactions*, 68(3):13–34, dec 2015. ISSN 1938-6737. doi: 10.1149/06803.0013ecst. URL http://ecst.ecsdl.org/cgi/doi/10.1149/06803.0013ecsthttp://www.scopus.com/inward/record.url?eid=2-s2.0-84957028504{&}partnerID=40{&}md5=6ab562ab6cf11264bff193c5b51effff.

[56] Thomas J Schmidt. Durability and Degradation in High-Temperature Polymer Electrolyte Fuel Cells. *ECS Transactions*, 1(8):19–31, jun 2006. doi: 10.1149/1.2214541. URL http://ecst.ecsdl.org/content/1/8/19.abstract.

[57] Thomas J. Schmidt and Jochen Baurmeister. Durability and Reliability in High-Temperature Reformed Hydrogen PEFCs. In *ECS Transactions*, volume 3, pages 861–869. ECS, oct 2006. doi: 10.1149/1.2356204. URL http://ecst.ecsdl.org/content/3/1/861.abstract.

[58] Qingfeng Li, Jens Oluf Jensen, Robert F. Savinell, and Niels J. Bjerrum. High temperature proton exchange membranes based on polybenzimidazoles for fuel cells. *Progress in Polymer Science*, 34(5):449–477, may 2009. ISSN 00796700. doi: 10.1016/j.progpolymsci.2008.12.003. URL http://www.sciencedirect.com/science/article/pii/S0079670009000100http://linkinghub.elsevier.com/retrieve/pii/S0079670009000100.

[59] SS Araya, SJ Andreasen, and SK Kær. Experimental characterization of the poisoning effects of methanol-based reformate impurities on a PBI-based high temperature PEM fuel cell. *Energies*, 2012. URL http://www.mdpi.com/1996-1073/5/11/4251/pdf.

[60] N. V. Dale, M. D. Mann, H. Salehfar, A. M. Dhirde, and T. Han. ac Impedance Study of a Proton Exchange Membrane Fuel Cell Stack Under Various Loading Conditions. *Journal of Fuel Cell Science and Technology*, 7(3):31010, jun 2010. ISSN 1550624X. doi: 10.1115/1.3207871. URL http://electrochemical.asmedigitalcollection.asme.org/article.aspx?articleid=1472180.

[61] Michael A. Danzer and Eberhard P. Hofer. Analysis of the electrochemical behaviour of polymer electrolyte fuel cells using simple impedance models. *Journal of Power Sources*, 190(1):25–33, may 2009. ISSN 03787753. doi: 10.1016/j.jpowsour.2008.10.003. URL http://www.sciencedirect.com/science/article/pii/S0378775308019010.

Paper B

Investigating different breakin procedures for reformed methanol high temperature proton exchange fuel cells

Sobi Thomas, Jakob Rabjerg Vang, Samuel Simon Araya, Søren Knudsen Kær

The paper has been submitted in the
International journal of Hydrogen Energy.

The layout has been revised.

Investigating different break-in procedures for reformed methanol high temperature proton exchange fuel cells

Sobi Thomas[a,*], Samuel Simon Araya[a], Jakob Rabjerg Vang[a], Søren Knudsen Kær[a]

[a]*Department of Energy Technology, Pontoppidanstraede, Aalborg University, Aalborg-9220, Denmark*

Abstract

The present work focuses on reducing the complexities involved in the mass production of HT-PEM fuel cell system integrated with a methanol reformer. In this work, different break-in procedures are investigated on a single HT-PEMFC. The work is divided into two parts, the first one focuses on reducing the usual break-in time and, second one focuses on break-in with simulated reformed fuel to understand the impact on degradation over time. The break-in time suggested by the MEA manufacturer is 80 100 h.

In this study, two set of tests namely test 1 and test 2 is carried out with different break-in times. The normal break-in (100 h), intermediate break-in (30 and 50 h) and no break-in (0 h) are used as break-in time sequence. All the cells after respective break-in time is subjected to a load cycling profile between 0.2 and 0.6 A cm^{-2} with 5 min at each current density. The test 3 involves the comparison of cell performance over time when the break-in is carried out with simulated reformed gas with a composition of 64.7 % H_2, 21.3 % CO_2, 12 % H_2O and 2 % CH_3OH. The break-in time for this test was 100 h. The cells are operated at 0.2 A cm^{-2} during break-in and thereafter at 0.6 A cm^{-2} under normal operation. The cell performance and impedance change over time is analysed. The different resistances are deduced using equivalent circuit models and analysed to understand the changes occurring in the MEA during break-in and how they affect the long-time operation of the cell. The degradation rate for the different operating strategy is calculated from the voltage trajectory over time. The comparison of degradation and break-in time suggests that the normal break-in induces an uniformity in the cell ohmic resistance change over time while the fast cycling lead to non-uniform changes in resistances. However, the performance and degradation is not significantly affected over $\approx$ 750 h test. The test with simulated reformed fuel clearly indicates that the break-in with H_2 is important for longer durability. The cell with reformed fuel break-in degrades much faster compared to the cell with

H_2 break-in.

Keywords: HTPEM, EIS, break-in, reformed fuel, load cycling

1. Introduction

Fuel cell is a technology with lower environmental issues and higher efficiency. Among the various classification of fuel cells, polymer electrolyte membrane (PEM) fuel cells is a promising and matured technology. The research in this field has improved the efficiency, cost and durability to some extend. There are different kinds of PEM fuel cells, among them of recent high temperature PEM with phosphoric acid (PA) doped polybenzimidizole membrane (PBI) is being explored as an alternative to internal combustion engines and for stationary power source. In a high temperature PEM fuel cell, the proton conductor is PA unlike water in LTPEM fuel cells. The advantage of operating a fuel cell at higher temperature (150 ^{0}C- 180 ^{0}C) includes higher reaction kinetics, increased tolerance to impurities mainly CO in the fuel [1]. Another advantage of HT-PEMFC is reduced water management complexities as the proton conductivity depends on PA distribution and concentration rather than water as in LT-PEM fuel cells [2]. However, HT-PEM fuel cells are also associated with some hurdles in terms of operation and start-up which makes the technology costly. One such problem associated with the manufacturing is the break-in of MEA before installing the stack to system.

The PA doped MEA when assembled in a cell leads to a non-uniform distribution of acid within the membrane electrode assembly (MEA). The process taking place during the break-in of an HT-PEMFC is not well known. However, it is supposed to improve the performance, as a result of uniform distribution of phosphoric acid, increased catalyst activity by impurity removal and improved membrane conductivity after break-in of 80-100 h at 0.2 A cm^{-2}. Thus, it is suggested to carry out a break-in at 0.2 A cm^{-2} for 100 h before drawing maximum output power [3, 4].

Boaventura and Mendes [5] studied the process taking place in an HTPEM fuel cell during activation. They used different characterization techniques (Polarization, EIS and CV) to understand the various phenomenons taking place within the cell during break-in. It was reported that

*Corresponding author
Email address: sot@et.aau.dk (Sobi Thomas)

the ohmic resistance improves in the presence of water but degrades the cathode by PA removal in the presence of excess water. Galvanostatic break-in was suggested to draw higher performance. A strategy to activate an HT-PEMFC rapidly and to ensure repeatable baseline performance different strategies were investigated by Tingelöf and Ihonen [6]. They reported potential cycling after 100 h of 0.2 A cm^{-2} did not contribute much to reach a stable repeatable performance. They suggested a higher temperature of 200 °C operation under galvanostatic mode for 24 h followed by 48 h operation at 160 °C is the best to achieve reproducible performance of an HT-PEMFC.

Eberhardt et al. [7] investigated the cause of degradation in an HTPEM fuel cell under operation using synchrotron based X-ray tomographic microscopic imaging. The focus was on understanding the dynamic distribution of PA under a load cycling profile. The tests quantified the migration of PA from the cathode to anode under high current density and an opposite trend under low current density (i.e., migration of PA from the anode GDL and flow field to membrane). They attributed the phenomenon to electrochemical pumping, resulting from the non-zero transport number of hydrogen phosphate anions which drags the electrolyte from the cathode to anode [8]. The migration is observed to be fast under high current density while at low current density it is a slow migration process.

In this paper, different strategies are employed to reduce the break-in time and at the same time investigating the long term implications of the break-in procedure on the durability of HT-PEMFC. THe tests are subdivided into three sets namely test 1 and test 2 with different break-in times and test 3 with simulated reformed fuel. The objective was to obtain a stable and reproducible performance with a rapid break-in strategy. As known from literature [3, 5], one major factor influenced during break-in is the acid redistribution which improves the ohmic resistance and also reduces the mass transport resistance as a result of uniform redistribution of phosphoric acid during break-in. Also, acid movement was reported to be a function of current density [7]. Thus, based on these knowledge in this study, the cells were subjected to current cycling procedure to redistribute the acid faster. The reformed fuel break-in was also investigated to do away with the intermediate step of HT-PEMFC stack break-in with H_2 before integrating to a reformer.

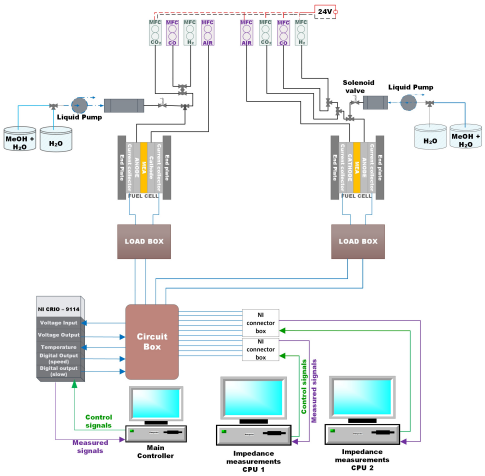

Figure 1: The schematic of the test setup used for the experiments (a) For load cycling test, (b) Reformed fuel based tests.

2. Experimental

2.1. Test setup

The test 1 and test 2 as described in Table1 was carried out using an in-house built test set-up and is shown in Fig. 1 (b). It consists of five single cells in parallel capable of carrying out IV curves and EIS parallel. The MFCs are from burkert (H_2-8711 , Air -8712). The flow rates are 0-1 L min^{-1} for H_2 and 0-2 L min^{-1} for air. Test 3 with simulated reformed fuel was carried out using a two cell in-house set up, shown in Fig. 1 (a). The addition to this set is the evaporator, pump for CH_3OH and H_2O, and CO_2 MFCs.

The MEA is from BASF prototype Celtec P2100. The active area of the MEA is 45 cm^2 and thickness of the MEA was 860 μm. The gaskets were 300 μm on the anode and 350 μm on the cathode. The compression force applied was 7 N m. This was controlled using springs. The anode flow field is two channel serpentine while the cathode is 3 channel serpentine. The cells are heater with cartridge heaters of 160 W on each plate (anode and cathode). The stoichiometry was fixed at 1.2 on the anode and 4.0 on the cathode. The electrochemical impedance spectroscopy (EIS) was recorded between 10 kHz and 0.1 Hz. The applied signal was 5 % of the DC load. The IV curve was recorded at a rate of 5 A min^{-1} upto a maximum of 30 A . The maximum current was restricted to 30 A based on the maximum flow of the flow meters.

2.2. Test procedure

The test was performed on six single cells for load cycling method and two for reformed fuel injected break-in. In the load cycling the break-in time of 0 h, 30 h, and 100 h was selected for the first set of tests. In the second set the break-in times of 0 h, 50 h and 100 h. The reformed fuel break-in is carried out using 64.7 % H_2, 21.3 % CO_2, 12 % H_2O and 2 % CH_3OH on the anode and compressed air on the cathode.

The test 1 and test 2 as described in the Table 1. Test 1 and Test 2 are tests with different break-in times and test 3 is the test with reformed fuel break-in. In test 1 and test 2 the cells were cycled between 0.2 A cm^{-2} and 0.6 A cm^{-2} with a time duration of 5 min at each current density. The cycling was started immediately after the respective break-in times as mentioned in Table 1. The objective was to enhance the speed of acid redistribution within the cell and reach a stable voltage as fast as possible in order to achieve peak performance at the operating condition.

Table 1: Description of different test with the anode fuel composition and the break-in time

Test 1 with 0 h**, 30** h **and 100** h			
Cell name	**Anode fuel**	**Break-in time**	**Operation time**
-	-	[h]	[h]
Cell 1	H_2	0	730
Cell 2	H_2	30	803
Cell 3	H_2	100	791
Test 2 with 0 h**, 50** h **and 100** h **break-in**			
Cell 4	H_2	0	711
Cell 5	H_2	50	710
Cell 6	H_2	100	710
Test 3 with reformed fuel and H_2 break-in			
Cell 1	H_2, CH_3OH, H_2O and CO_2	100	625
Cell 2	H_2	100	436

In test 3, one cell was operated with reformed fuel and the other with pure hydrogen for comparison during initial 100 h of break-in at 0.2 A cm^{-2}. After the break-in both the cells were operated with reformed fuel the composition as mentioned above at 0.6 A cm^{-2}. The objective was to remove the intermediate step of pure hydrogen break-in and directly integrated the HT-PEMFC stack with the reformer.

3. Modelling

3.1. Equivalent circuit model

Equivalent circuit models are probably the most widely used tools for analysing impedance spectroscopy data and attempting to separate individual contributions to the impedance spectrum.

The model used in this study is chosen purely to be able to reproduce the features observed in the impedance spectra. The model consists of three types of behaviour. The parallel resistor (R_L) and inductor (L) is meant to capture the high frequency inductive loop stemming from wires and other cell components. The resistor (R_Ω) captures the resistive losses in (primarily) the electrolyte. Three sets of parallel capacitors and resistors capture the three capacitive loops at

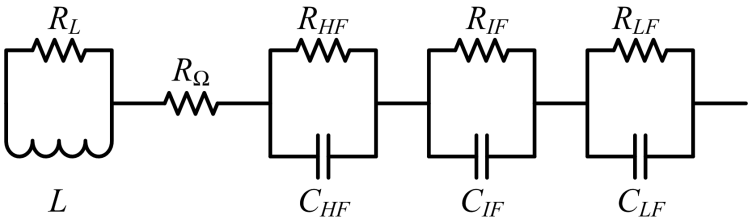

Figure 2: The equivalent circuit model used in the study. L is the wire inductance R_L is the associated resistance. R_Ω is the ohmic resistance. The subscripts HF, IF and LF refer to the high, intermediate and low frequency capacitive loops respectively.

high (HF), intermediate (IF) and low (LF) frequency. The equivalent circuit model is shown in figure 2.

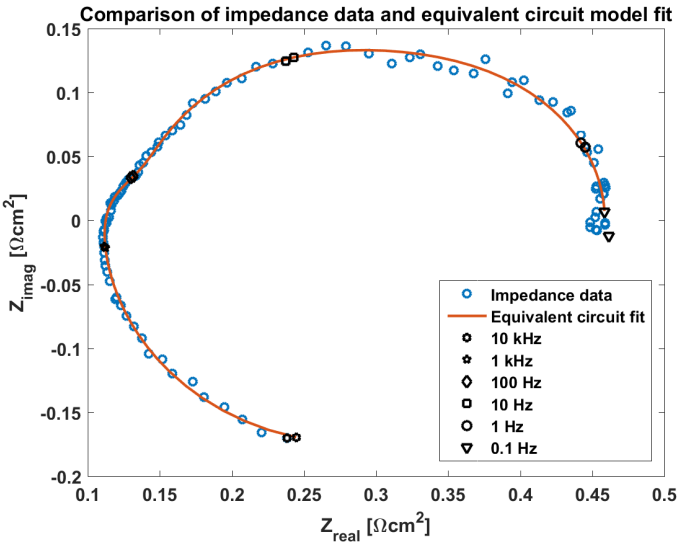

Figure 3: This figure shows an example of the agreement between the impedance data and the equivalent circuit model. The data is from cell 1 at 9A at the beginning of break-in.

The model is fitted to the experimental data using the Zfit algorithm [9] with the Matlab 2015b package. Figure 3 shows an example of the agreement between the data and the model for cell 1 at the beginning of break-in. For this fit, $R^2 = 0.998$. Note that the regression line lies within the random variation of the points and that the decade frequencies agree closely, except at 0.1 Hz. This is due to the lack of a low frequency inductive loop. The low frequency inductive loop has been left out due to the scatter of the data in this frequency range. Adding more model complexity in this region would not provide more information, since the random variations stemming from drifting of the operating temperature become increasingly important at lower frequencies. The R_Ω in the circuit is attributed to the membrane resistance even though some effects of contact resistance and compression also contributed to the same. The HF resistance is mainly associated with the non uniform catalyst distribution and anode activation losses [10], IF resistance is usually contributed by the losses on the cathode and the LF resistance is more related to mass transport issues which could be due to flow channel dynamic [11] or water and acid redistribution [10].

4. Results and discussion

This section is divided into two parts, the first part is on different break-in times and the second part on break-in with reformed fuel. The results deduced based on I-V curves and impedances are analysed.

4.1. Effect of break-in times

The voltage profile for test 1 and test 2 with different break-in time is shown in Fig. 4. The cell are cycled between 0.2 $\mathrm{A\,cm^{-2}}$ and 0.8 $\mathrm{A\,cm^{-2}}$. The voltage shows minimal differences between the different break-in strategies. In test 1, there was an unintended stop at $\approx$ 200 h. The cells behaving in a similar fashion suggests that the break-in for respective times as described in the test procedure, followed by load cycling has minimal effect on the performance over time. This could be due to non-uniformity in the MEA production or could be related to cells having minimal effect on the long term degradation when operated with H_2 under load cycling.

The I-V curves before and after the completion of different break-in time tests are shown in fig. 5. The IV curves show no trend based on the different break-in times which could also be an influence of the differences in the MEA characteristics. Thus, it is difficult to compare the trend

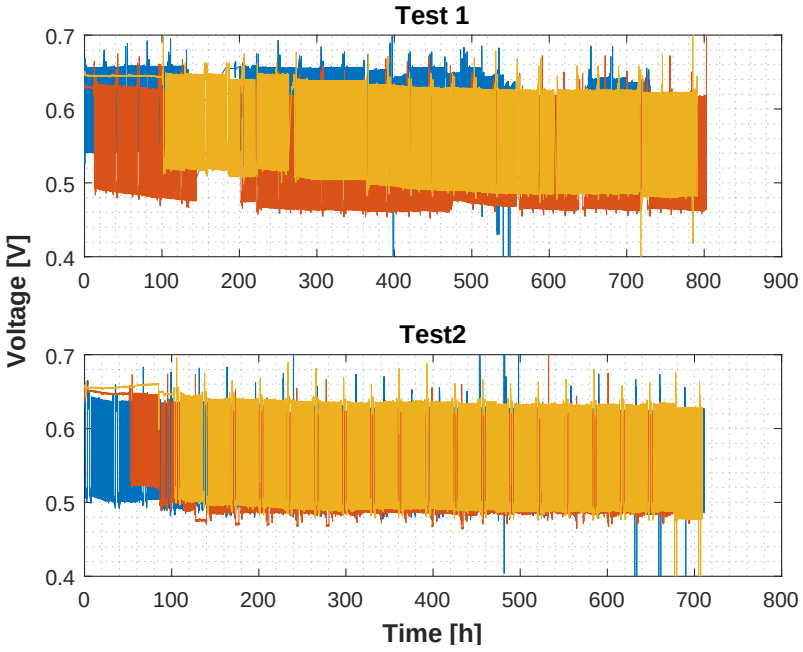

Figure 4: Comparison of voltage for different break-in time

based on the IV curves. However, on comparing the change in voltage at 0.6 A cm^{-2} before and after the test it suggest they behave similar irrespective of the differences in the break-in time. The changes in percentage are shown in Fig. 5 (a) and (b). This is interesting to note that the cells operating with less or no break-in times have similar changes in performance compared to the cells operated with normal break-in. The possibility is that the load cycling after break-in is beneficial in break-in the cell faster. During break-in the performance improves over time but load cycling thereafter leads to a fast loss and then all the cells tends to perform in a similar fashion. All the cells were operated for ¿ 700 h with losses in performance being similar.

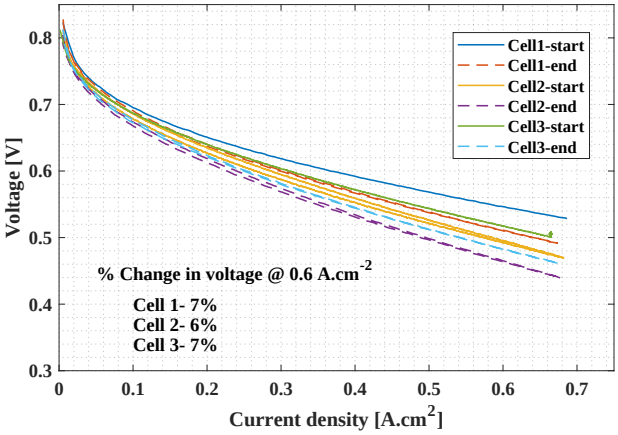

(a) Comparison of performance before and after the test 1

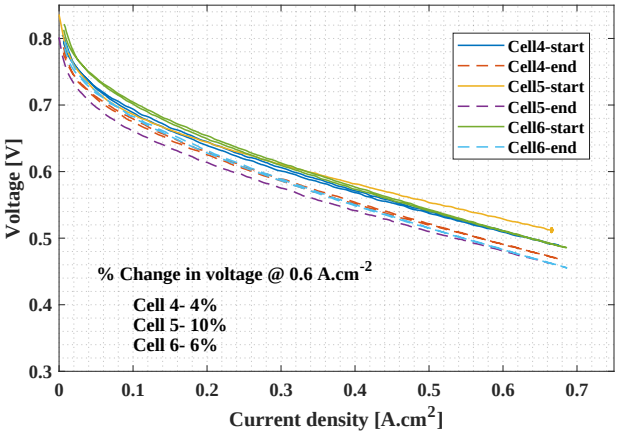

(b) Comparison of performance before and after the test 2

Figure 5: Performance comparison of cells with different break-in time, (a) Test 1, (b) Test 2

4.2. Effect of reformed fuel during break-in

The test with simulated reformed fuel shows no or minimal changes in the voltage during break-in as highlighted in Fig. 6. After break-in at 0.2 A cm^{-2} for 100 h, both the cells were operated with simulated reformed fuel as mentioned in the test procedure at 0.6 A cm^{-2}. The

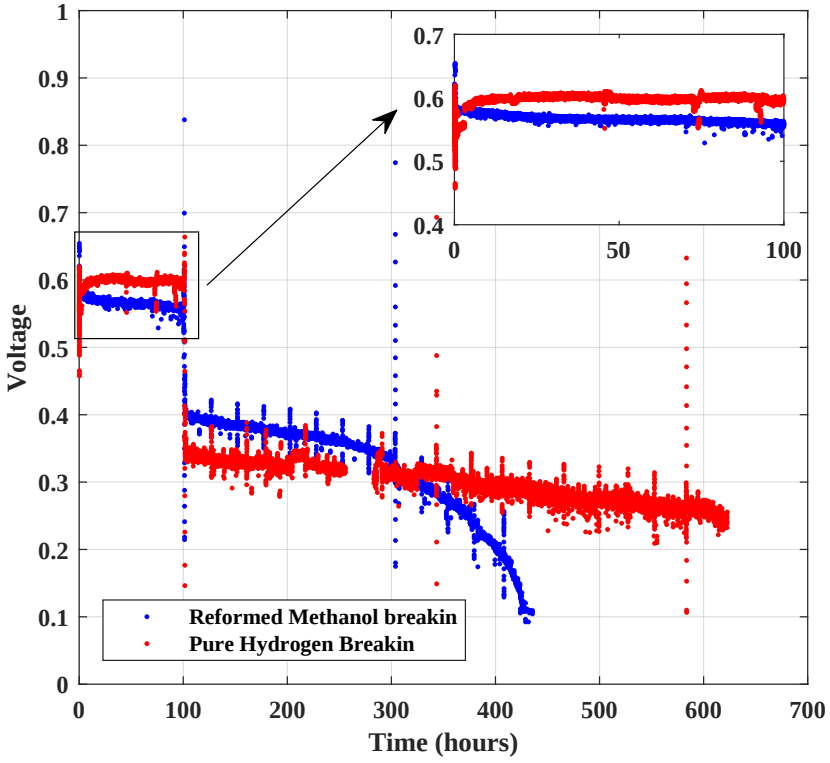

Figure 6: Comparison of breakin with reformed methanol and hydrogen

change of current results in a higher voltage drop for the cell 2 and lower drop in voltage for cell 1, even though the voltage for cell 2 was higher than cell voltage during break-in. This could be due to the change in fuel composition at the anode compartment for cell 2which results

However, the voltage degrades much faster for cell 1 compared to cell 2 and after ≈400 h cell 2 voltage falls to 0.1 V and therefore the test on cell 2 was stopped. This suggest that the break-in with reformed fuel has an implication on the long term durability of HT-PEMFCs.

5. Discussion

The impedance data recorded were fitted with an equivalent circuit and the resistances calculated are compared for different break-in times. The ohmic resistance for different break-in times is shown in Fig. 7.

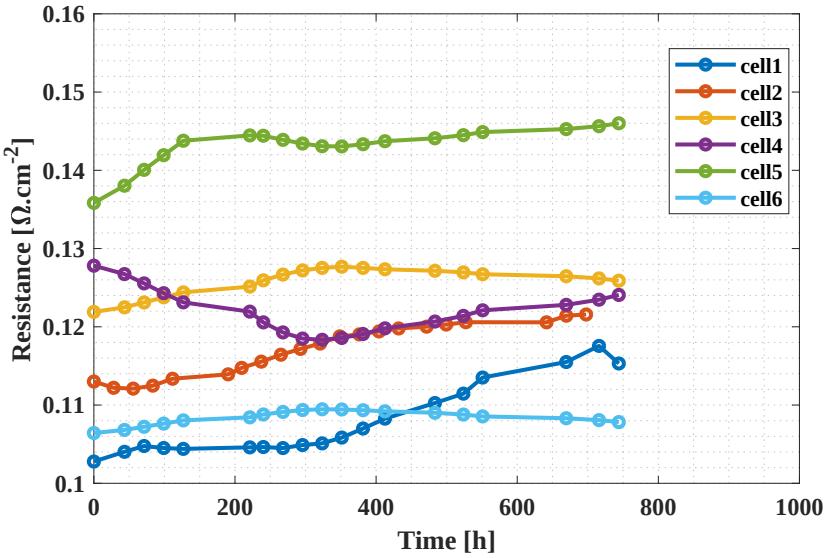

Figure 7: Comparison of fitted ohmic resistance over time for different break-in times.

The ohmic resistance which is attributed mostly to the membrane resistance [12, 13] show a significant difference in the change of resistance over time. The ohmic resistance initially decreases for no break-in cells 1 and cell 4 and thereafter around ≈300 h tends to increase for both the cells. This could be due to redistribution of PA in the cell under load cycling. When operating at high current density the water generated is higher and this could be attracted by the acid near the catalyst and in the initial 300 h the acid hydration is taking place and the conductivity improves by load cycling. Another possibility is removal of acid taking place during the initial period which makes the membrane thinner and makes proton conductivity. The second reason is more probable as the resistance increase after 300 h which could be due to lower acid

content making proton conductivity poorer. In case of normal break-in, the ohmic resistance in cell 1 and cell 6 increases over time and then gets stabilised similar to what was reported by [14]. They attributed the phenomena to hydration and dehydration of MEA.

In Fig. 8, the low frequency resistance which is mainly associated with mass transport resistance [13] is shown. The fitted resistance suggest that the different break-in procedures have minimal effect of the mass transport resistance and they stay fairly constant for all the cells. This suggests that load cycling of cell is not a problem considering the fact that hydration and dehydration of acid under load cycling could lead to acid loss or flooding of GDL. It has been reported that the acid flooding of GDL cause an increase of mass transport resistance[15]. however, the difference in this case was the high current density. In this work the cycling is between 0.2 $A\,cm^{-2}$ and 0.6 $A\,cm^{-2}$. While the flooding was reported for a higher current density of 0.8 $A\,cm^{-2}$ [16].

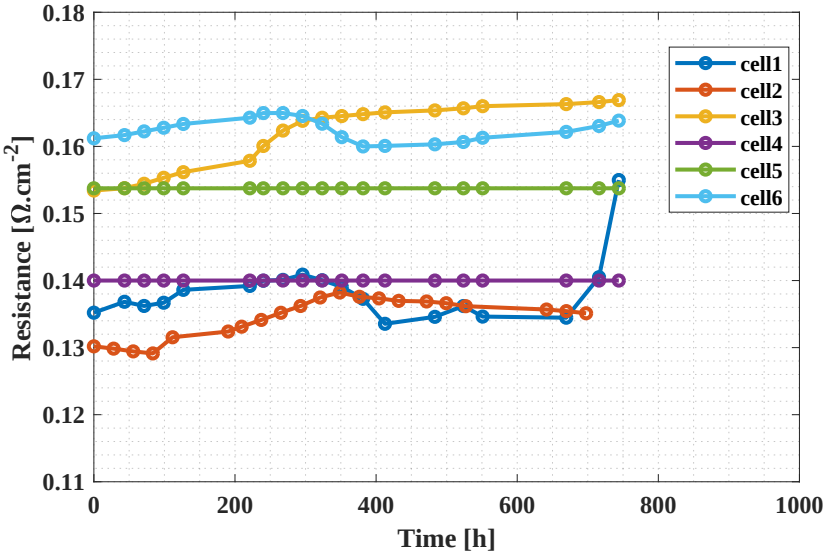

Figure 8: Comparison of fitted low frequency resistance over time for different break-in times.

To analysis better the break-in process with reformed fuel, the impedance recorded before and after the break-in was compared with and without IR corrected resistance and is shown in

Fig. 9. The change in high frequency intercept or ohmic resistance is shown seen in Fig. 9 and is found to be very small. The comparison shows a small decrease in the ohmic resistance for H_2 break-in,Cell 2 in Fig. 8, while a small increase was recorded for reformed fuel case, cell 1 in Fig. 8. A decrease in the series resistance was also reported by Galbiati et al. [3] and the possibility of acid re-distribution leading to the better proton conductivity was suggested. Therefore, the trends observed in the present case is in line with ones in the literature.

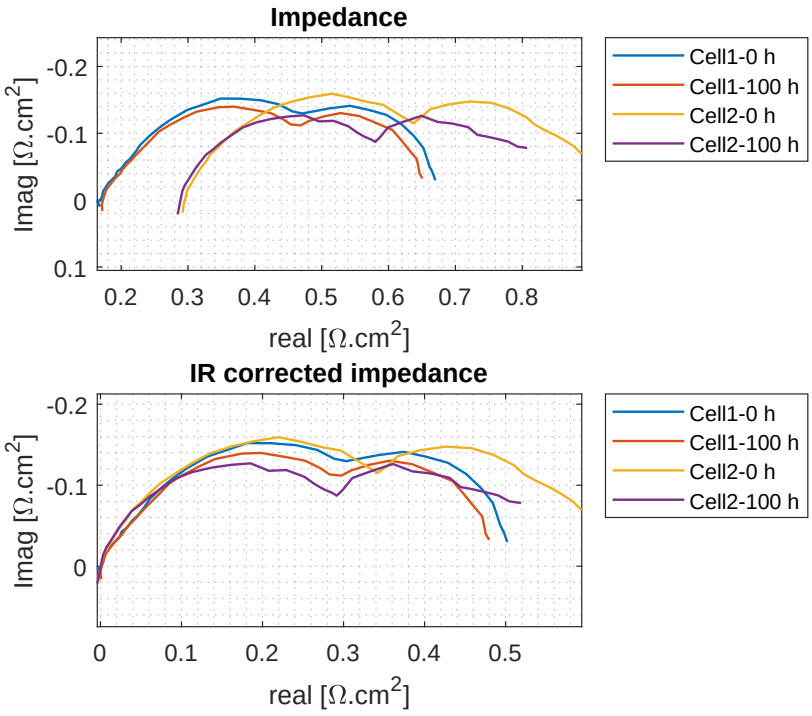

Figure 9: Comparison of impedance before and after break-in @0.2 A cm^{-2} (a) Complete impedance comparison (b) Impedance comparison with IR corrected

In fig. 9 (b), the resistance comparison with the IR corrected is shown and it shows the major difference between cell 1 and cell 2. The IR corrected resistance was plotted to remove

the differences in the ohmic resistance of the two MEAs which was very significant. Both the cells show an improvement in the intermediate and low frequency resistance after the break-in process of 100 h. The improvement is more dominant for H_2 breakin compared to reformed fuel operation. This suggests that the presence of diluted fuel and H_2O in the feed somehow does not help in the improvement of different resistances during break-in. The presence of CH_3OH being low seems not to be affecting the resistances. The minimal effect of less than 3 % CH_3OH on the cell performance and resistances was also reported in [10, 17]. Therefore, the possibility could be acid removal happening during the break-in with the presence of water which was also observed by Boaventura and Mendes [5].

The durability test resulted in a faster degrading voltage profile for the cell with reformed fuel break-in. Thus, to understand the cause of faster degradation, the EIS data record over time at 0.6 A cm^{-2} was fitted with an equivalent circuit model and the different resistances are shown in Fig. 10. In both the cases at R_{OHM} shows similar increase over time which suggests that the proton conductivity losses for both the cells are similar. The low frequency resistance increases drastically for the cell 1 with reformed fuel break-in as seen in Fig. 10 (a), compared to Fig. 10 (b). This clearly is the cause of fast degradation of cell 1. The possible reason for the same is assumed to be some acid blocking the GDL pores and also the possibility of some acid reaching the gas channels and blocking the gases from reaching the reaction site. Another possibility could be acid is flooding the catalyst layer which is influenced by the presence of H_2O and thereby, the reaction sites are blocked. A steep increase in the intermediate and high frequency resistance suggests that the increase of mass transport resistance is influencing the cathode and the anode reaction rates.

The results were analysed to understand the importance of break-in on the durability of HT-PEMFCs. The degradations for the different cells operated under different condition is shown in Table 5 with the respective operating hours. The differences in the MEA was visible in the degradation rates calculated at different operating current densities. However, the comparison of cells in test 1 and test 2 suggest that the degradation and the performance of the cell was not effected by the different break-in procedure for the present tests. The cell with no break-in and intermediate break-in show a lower degradation rate for at both the current densities expect for cell 5 at 0.6 A cm^{-2}. The degradation rates not showing drastic differences with or without break-in suggests that the load cycling results in the same affect on the cell performance as

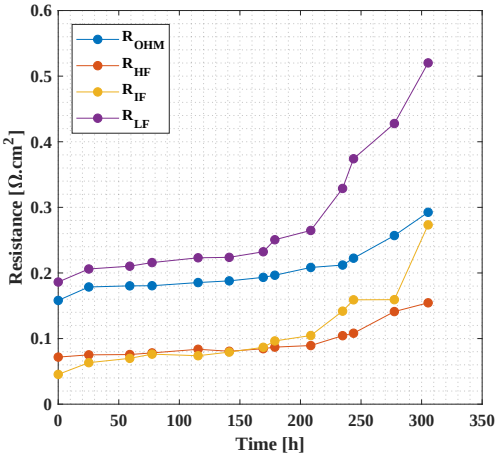

(a) Fitted resistance for the cell operated after break-in with reformed fuel

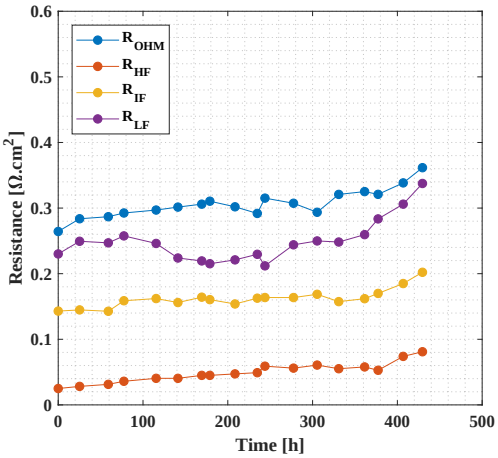

(b) Fitted resistance for the cell operated after break-in with H_2

Figure 10: Comparison of different resistances for cells operated with different fuel during break-in (a) Reformed fuel break-in, (b) Hydrogen break-in

Test 1 degradation rate				
Cell name	**@ 0.2** A cm^{-2}	**@ 0.6** A cm^{-2}	**Operation time @ 0.2** A cm^{-2}	**Operation time @ 0.6** A cm^{-2}
-	[μV h^{-1}]	[μV h^{-1}]	[h]	[h]
Cell 1	-26	-39	365	365
Cell 2	-13	-40	416	386
Cell 3	-31	-52	447	342
Cell 4	-33	-30	355	355
Cell 5	-42	-53	382	327
Cell 6	-44	-42	299	409
Test 2 degradation rate				
Cell 1	-614	-680	100	334
Cell 2	+310	-177	100	521

constant current density operation at 0.2 A cm^{-2} for 100 h. This would be of great importance in the production stage of HT-PEMFC. However, more tests needs to be carried out with minimal difference in the MEAs to obtain a better reproducibility of the results. The degradation rates shown were similar to reported in [18, 19, 20] under load cycling tests.

In case of test 3 involving break-in with reformed fuel show a positive degradation for H_2 break-in at 0.2 A cm^{-2} while the reformed fuel break-in shows a high negative degradation rate for both current density. This could be related to water in the fuel stream attracts some PA from the cell and gets lost with gas. A similar observation of PA loss on the cathode was reported in [5]. The possibility is that the acid which get squeezed out during assemble have a tendency to get lost in the presence of excess H_2O on the anode instead of getting redistributed into the membrane.

The degradation at 0.6 A cm^{-2} shows a higher degradation rate for both the cells. This could be related to the reformed fuel operation which needs to be further investigated. The degradation rate with H_2, CO, CO_2, H_2O and H_2S was reported as -40 μV h^{-1}. Araya et al. [21] reported a degradation of -55 μV h^{-1} with 3 % CH_3OH for a short term test of 100 h. HU et al. [22] also reported a higher degradation rate when operating at 0.64 A cm^{-2} for a test with pure hydrogen for 500 h. Thus, it is difficult to compare the degradation rates because the lower degradation

rates are reported for low current density operation and the higher degradation rate is reported for high current density operation but with pure hydrogen. In the present study, the test involves a combination of high current density operation and also the the presence of reformed fuel on the anode.

6. Conclusion

Three different test were carried out to develop an operating strategy for reformed methanol HT-PEMFC. The objective was to reduce the complexity involved in the break-in process of HT-PEMFC. The first two tests focussed on reducing the break-in time to intermediate times and/or to completely do away with the break-in process. The test 2 was same as test 1 with the only exception being intermediate break-in time was 30 h in test 1 and 50 h in test 2. The third test involved the break-in using simulated reformed fuel on the anode for break-in. The performance, impedance and degradation rates were analysed to suggest the optimal way for break-in an HT-PEMFC to draw maximum power and reproducible voltages. However, the significant variations seen among the different MEAs prevented the one on one comparison between the different cells. Thus, the MEA inventory over time was investigated separately to understand the different break-in procedures.

The tests with different break-in time show a similar voltage profile after an operation of 700 h. This suggests that the break-in does not affect the cell performance under load cycling test. This was further confirmed from the degradation rate calculated for the different cells. The degradation rates were similar irrespective of the break-in with small variations. The comparison of the different resistances show no trend with different break-in times. However, the ohmic resistance show similar trend when normal break-in of 100 h was carried out. The other break-in times showed no similarities. This suggests that break-in could be useful to make sure the cells operate with reproducible performance over time. The results in the present case suggest that a cell operating under load cycling profile could do away with the break-in procedure. A further investigation with minimal variations in the MEA design would be useful to conclude the same.

The test with simulated reformed fuel was investigated and the results suggest that break-in with hydrogen is important to ensure a longer durability of HT-PEMFC when operating with reformed methanol. The degradations are high and is contributed mainly in by the mass transport issues as seen from the fitted resistances recorded over time. The degrading mass transport also

influences the catalyst reaction and anode activity. The mass transport issues are supposed to be influenced by the redistribution of acid in the presence of H_2O in the fuel. During the initial period when the acid is present all over the MEA non-uniformly, the water in the fuel has a tendency to drag the acid away. Thus, it is suggested to have a break-in to make sure the acid reaches the membrane from the GDL and other components before supplying reformed fuel rich in water.

Acknowledgment

The authors would like to thank the Innovation Fund Denmark for funding the work through the 4M project. The authors are also thankful to Serenergy for providing the MEA used in the experiments.

References

[1] R.E. Rosli, A.B. Sulong, W.R.W. Daud, M.A. Zulkifley, T. Husaini, M.I. Rosli, E.H. Majlan, and M.A. Haque. A review of high-temperature proton exchange membrane fuel cell (HT-PEMFC) system. *International Journal of Hydrogen Energy*, pages 1–22, 2016. ISSN 03603199. doi: 10.1016/j.ijhydene.2016.06.211. URL `http://linkinghub.elsevier.com/retrieve/pii/S0360319915313069`.

[2] Thomas J Schmidt and Jochen Baurmeister. Properties of high-temperature PEFC Celtec®-P 1000 MEAs in start/stop operation mode. *Journal of Power Sources*, 176(2):428–434, 2008. doi: http://dx.doi.org/10.1016/j.jpowsour.2007.08.055. URL `http://www.sciencedirect.com/science/article/pii/S0378775307016047`.

[3] Samuele Galbiati, Andrea Baricci, Andrea Casalegno, Giulia Carcassola, and Renzo Marchesi. On the activation of polybenzimidazole-based membrane electrode assemblies doped with phosphoric acid. *International Journal of Hydrogen Energy*, 37(19):14475–14481, 2012. doi: 10.1016/j.ijhydene.2012.07.032. URL `http://linkinghub.elsevier.com/retrieve/pii/S0360319912016096`.

[4] Christoph Wannek, Irene Konradi, Jürgen Mergel, and Werner Lehnert. Redistribution of phosphoric acid in membrane electrode assemblies for high-temperature polymer electrolyte fuel cells. *International Journal of Hydrogen Energy*, 34(23):9479–9485, 2009. doi: http://dx.doi.org/10.1016/j.ijhydene.2009.09.076. URL `http://www.sciencedirect.com/science/article/pii/S036031990901516X`.

[5] Marta Boaventura and Adelio Magalhaes Mendes. Activation procedures characterization of MEA based on phosphoric acid doped PBI membranes. *International Journal of Hydrogen Energy*, 35(20):11649–11660, oct 2010. ISSN 03603199. doi: 10.1016/j.ijhydene.2010.03.137. URL `http://linkinghub.elsevier.com/retrieve/pii/S0360319910006555`.

[6] Thomas Tingelöf and Jari K. Ihonen. A rapid break-in procedure for PBI fuel cells. *International Journal of Hydrogen Energy*, 34(15):6452–6456, aug 2009. ISSN 03603199. doi: 10.1016/j.ijhydene.2009.

05.003. URL http://dx.doi.org/10.1016/j.ijhydene.2009.05.003http://linkinghub.elsevier.com/retrieve/pii/S0360319909006867.

[7] S. H. Eberhardt, M. Toulec, F. Marone, M. Stampanoni, F N Büchi, T. J. Schmidt, F. N. Buchi, and T. J. Schmidt. Dynamic Operation of HT-PEFC: In-Operando Imaging of Phosphoric Acid Profiles and (Re)distribution. *Journal of The Electrochemical Society*, 162(3):F310–F316, jan 2015. ISSN 0013-4651. doi: 10.1149/2.0751503jes. URL http://jes.ecsdl.org/cgi/doi/10.1149/2.0751503jeshttp://jes.ecsdl.org/content/162/3/F310.abstract.

[8] Harold R. Kunz. Lessons Learned from Phosphoric Acid Electrolyte Fuel Cell Development Pertinent to PEMFCs. In *ECS Transactions*, volume 11, pages 1447–1460. ECS, sep 2007. doi: 10.1149/1.2781058. URL http://ecst.ecsdl.org/content/11/1/1447.abstract.

[9] Dellis Jean-Luc. Zfit. Software; 2010., 2010. URL https://se.mathworks.com/matlabcentral/fileexchange/19460-zfit.

[10] Sobi Thomas, Jakob Rabjerg Vang, Samuel Simon Araya, and Søren Knudsen Kær. Experimental study to distinguish the effects of methanol slip and water vapour on a high temperature PEM fuel cell at different operating conditions. *Applied Energy*, 192:422–436, apr 2016. ISSN 0306-2619. doi: http://dx.doi.org/10.1016/j.apenergy.2016.11.063. URL http://linkinghub.elsevier.com/retrieve/pii/S0306261916316488http://www.sciencedirect.com/science/article/pii/S0306261916316488.

[11] J. R. Vang, F. Zhou, S. J. Andreasen, and S. K. Kaer. Estimating Important Electrode Parameters of High Temperature PEM Fuel Cells by Fitting a Model to Polarisation Curves and Impedance Spectra. *ECS Transactions*, 68(3):13–34, dec 2015. ISSN 1938-6737. doi: 10.1149/06803.0013ecst. URL http://ecst.ecsdl.org/cgi/doi/10.1149/06803.0013ecst.

[12] Nikhil H. Jalani, Manikandan Ramani, Kristina Ohlsson, Steve Buelte, Greg Pacifico, Richard Pollard, Rhonda Staudt, and Ravindra Datta. Performance analysis and impedance spectral signatures of high temperature PBIphosphoric acid gel membrane fuel cells. *Journal of Power Sources*, 160(2):1096–1103, oct 2006. ISSN 03787753. doi: 10.1016/j.jpowsour.2006.02.094. URL http://www.sciencedirect.com/science/article/pii/S0378775306004150.

[13] S. M. Rezaei Niya, R. K. Phillips, and M. Hoorfar. Sensitivity Analysis of the Impedance Characteristics of Proton Exchange Membrane Fuel Cells. *Fuel Cells*, 16(5):547–556, jul 2016. ISSN 16156854. doi: 10.1002/fuce.201600060. URL http://doi.wiley.com/10.1002/fuce.201600060.

[14] Jakob Rabjerg Vang, Søren Juhl Andreasen, Samuel Simon Araya, and Søren Knudsen Kær. Comparative study of the break in process of post doped and solgel high temperature proton exchange membrane fuel cells. *International Journal of Hydrogen Energy*, 39(27):14959–14968, sep 2014. ISSN 03603199. doi: 10.1016/j.ijhydene.2014.07.017. URL http://www.sciencedirect.com/science/article/pii/S0360319914019727.

[15] Sebastian H. Eberhardt, Federica Marone, Marco Stampanoni, Felix N Büchi, Thomas J. Schmidt, F. N. Buchi, and Thomas J. Schmidt. Imaging Phosphoric Acid Migration in High Temperature Polymer Electrolyte Fuel Cells by X-Ray Tomographic Microscopy. *ECS Transactions*, 69(17):591–599, oct 2015. ISSN 1938-6737. doi: 10.1149/06917.0591ecst. URL http://ecst.ecsdl.org/cgi/doi/10.1149/06917.0591ecsthttp://www.scopus.com/inward/record.url?eid=2-s2.0-84946021791{&}partnerID=tZOtx3y1.

[16] S. H. Eberhardt, F. Marone, M. Stampanoni, F. N. Büchi, and T. J. Schmidt. Quantifying phosphoric acid

in high-temperature polymer electrolyte fuel cell components by X-ray tomographic microscopy. *Journal of Synchrotron Radiation*, 21(6):1319–1326, nov 2014. ISSN 1600-5775. doi: 10.1107/S1600577514016348. URL http://www.ncbi.nlm.nih.gov/pubmed/25343801http://scripts.iucr.org/cgi-bin/paper?S1600577514016348.

[17] Samuel Simon Araya. Investigating the effects of methanol-water vapor mixture on a PBI-based high temperature PEM fuel cell. *International Journal of Hydrogen Energy*, pages 1–26, 2012. URL http://www.sciencedirect.com/science/article/pii/S0360319912020125.

[18] Qingfeng Li, Jens Oluf Jensen, Robert F. Savinell, and Niels J. Bjerrum. High temperature proton exchange membranes based on polybenzimidazoles for fuel cells. *Progress in Polymer Science*, 34(5):449–477, may 2009. ISSN 00796700. doi: 10.1016/j.progpolymsci.2008.12.003. URL http://www.sciencedirect.com/science/article/pii/S0079670009000100.

[19] Sobi Thomas, Christian Jeppesen, Thomas Steenberg, Samuel Simon Araya, Jakob Rabjerg Vang, and Søren Knudsen Kær. New load cycling strategy for enhanced durability of high temperature proton exchange membrane fuel cell. *International Journal of Hydrogen Energy*, 42(44):27230–27240, 2017. ISSN 03603199. doi: 10.1016/j.ijhydene.2017.09.018.

[20] R. Taccani, T. Chinese, and M. Boaro. Effect of accelerated ageing tests on PBI HTPEM fuel cells performance degradation. *International Journal of Hydrogen Energy*, 42(3):1875–1883, 2017. ISSN 03603199. doi: 10.1016/j.ijhydene.2016.09.164. URL http://linkinghub.elsevier.com/retrieve/pii/S0360319916316421.

[21] SS Araya, SJ Andreasen, and SK Kær. Experimental characterization of the poisoning effects of methanol-based reformate impurities on a PBI-based high temperature PEM fuel cell. *Energies*, 2012. URL http://www.mdpi.com/1996-1073/5/11/4251/pdf.

[22] J HU, H ZHANG, Y ZHAI, G LIU, and B YI. 500h Continuous aging life test on PBI/H3PO4 high-temperature PEMFC. *International Journal of Hydrogen Energy*, 31(13):1855–1862, oct 2006. ISSN 03603199. doi: 10.1016/j.ijhydene.2006.05.001. URL http://www.sciencedirect.com/science/article/pii/S0360319906001662.

Appendix

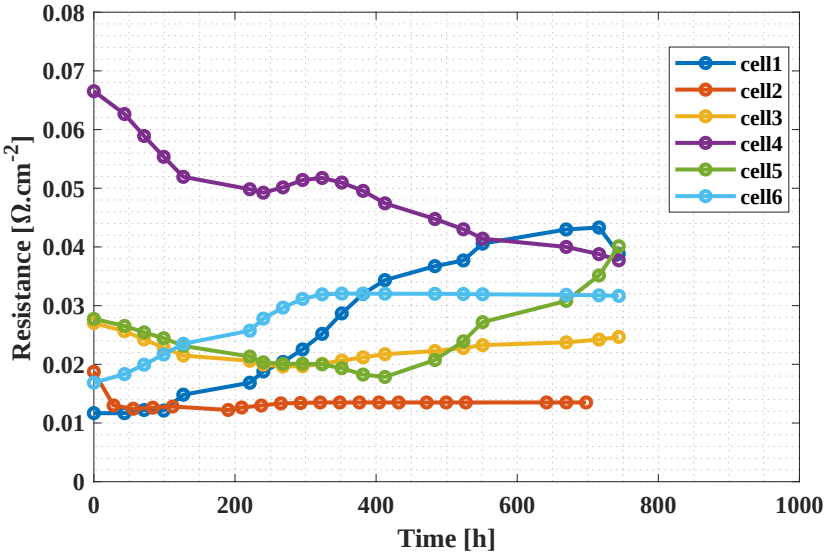

Figure 11: Comparison of fitted high frequency resistance over time for different break-in times.

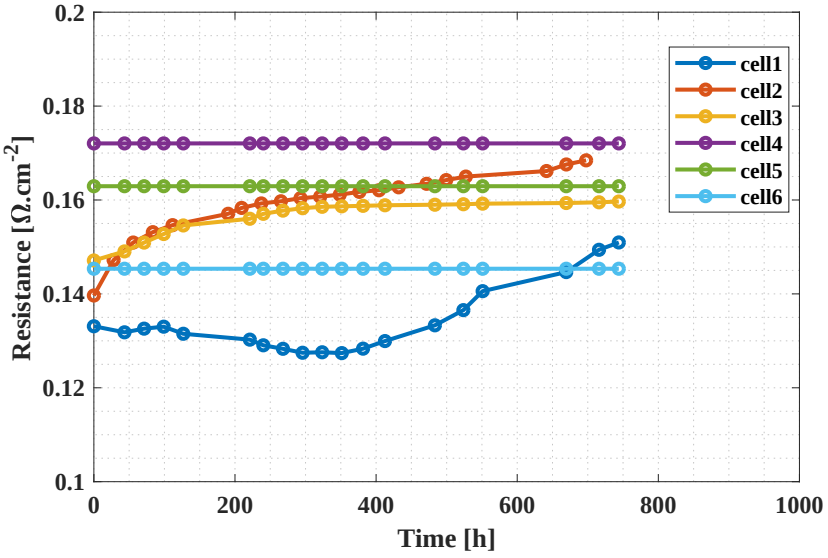

Figure 12: Comparison of fitted intermediate frequency resistance over time for different break-in times.

Paper C

The Influence of Phosphoric Acid Migration on the Performance of High Temperature Polymer Electrolyte Fuel Cells

Jonathan Halter, Sobi Thomas, Søren Knudsen Kær, Thomas Justus Schmidt, Felix Büchi

The paper has been submitted in the
Electrochimica Acta.

The layout has been revised.

The Influence of Phosphoric Acid Migration on the Performance of High Temperature Polymer Electrolyte Fuel Cells

J. Halter,[a,*] S. Thomas,[b,*] S.K. Kær,[b] T.J. Schmidt,[a,c] F.N. Büchi[a,z]

[a] *Electrochemistry Laboratory, Paul Scherrer Institut, 5232 Villigen PSI, Switzerland*

[b] *Department of Energy Technology, Pontoppidanstræde, Aalborg University, Aalborg East - 9220, Denmark*

[c] *Laboratory of Physical Chemistry, ETH Zürich, 8093 Zürich, Switzerland*

Abstract

In high temperature polymer electrolyte fuel cells phosphoric acid migration induces flooding of the anode gas diffusion layer at high current densities. The present study focuses on determining the influence of phosphoric acid flooding of the anode GDL on hydrogen mass transport limitations. Two methods for quantifying the performance losses at high current densities, related to acid migration, are discussed: anodic limiting current density measurements and electrochemical impedance spectroscopy. It is demonstrated that the limiting current, the common method for determining transport resistances is unable to detect the changes induced by acid migration, due to the transient time required when switching to the required low hydrogen concentrations, while EIS is able to capture the changes induced by acid migration because it is faster and less invasive. For diluted hydrogen an increase of the transport resistance is measured, however the effect on the cell performance is negligible. The time constants for anode GDL flooding and de-flooding are determined based on the EIS data and found to be 8.1 ± 0.1 minutes for flooding and about 4.8 ± 0.9 minutes for de-flooding under the applied conditions.

Keywords: HT-PEFC, Mass transport resistance, Limiting current, EIS, Phosphoric acid migration

[Z] E-Mail: felix.buechi@psi.ch

* Equally contributed

1. Introduction

High temperature polymer electrolyte fuel cells (HT-PEFC) operate at temperatures between 160 ^{0}C - 180 ^{0}C. This allows for easier heat recovery, increases the tolerance towards impurities in the fuel. It also has advantages in reduced complexities with the balance of plant like gas humidification or reformer when natural gas is used as the fuel, which are generally associated with low temperature polymer electrolyte fuel cells (LT-PEFC) [1–3].

The unique feature of HT-PEFCs is their membrane chemistry based on polybenzimidazole, which is doped with phosphoric acid as the electrolyte [1, 4]. Unlike in the perfluoro-sulfonic acid polymers of LT-PEFCs, the electrolyte is not chemically bound to the membrane polymer and only a fraction of the electrolyte is interacting with it [5]. As demonstrated by Eberhardt et al. [6, 7] bulk of the electrolyte is mobile and able to migrate within the membrane and can also invade the gas diffusion layer (GDL) or even the flow field channels. This can lead to a loss of electrolyte, which makes phosphoric acid redistribution a major limitation for the lifetime of HT-PEFC [8, 9].

As found by Eberhardt et al. [6, 7], a crucial parameter for phosphoric acid migration in HT-PEFCs is the current density. At high current density, phosphoric acid migrates towards the anode, thereby flooding the anode GDL, and in the worst case even the flow-field channels. The reason for this is that since the electrolyte is not covalently bound to the base polymer, a fraction of the ionic current is carried by migration of hydrogen phosphate anions towards the anode, i.e. the transport number for the proton is less than unity. This effect is also known from phosphoric acid fuel cells (PAFCs) [10], where phosphoric acid is confined in a silicon carbide matrix. The flooding of the anode GDL and flow field channels with phosphoric acid is not only a concern for the durability of HT-PEFCs, but is expected to also affect the hydrogen transport through the GDL and therefore, the performance of HT-PEFCs. This is of special importance when operating the cell with reformate gas as the fuel, where hydrogen is

diluted and the hydrogen partial pressure is lower compared to operation with pure hydrogen. Also, the hydrogen partial pressure further decreases from channel inlets to outlets. The reduced hydrogen partial pressure in the channel leads to a smaller concentration gradient between channel and catalyst layer and therefore, amplifies the increasing transport resistance in the GDL.

This effect is well known from LT-PEFCs, where water can flood the cathode GDL at high current densities and/or high cathode gas humidity and the water saturation in the GDL introduces oxygen transport limitations [11–13].

The goal of the study is to quantify the transport losses induced by phosphoric acid migration into the anode GDL. Two methods were adapted: the first one utilizes anodic limiting current measurements while the second method is based on electrochemical impedance spectroscopy (EIS). The advantages and disadvantages of each method are discussed and the influence of phosphoric acid migration on the fuel cell performance is analyzed. To the best of the authors' knowledge, this is the first time that these methods were used in the context of phosphoric acid migration in HT-PEFC.

2. Experimental setup and procedures

a. Test setup

All experiments were performed with a so-called differential cell setup, minimizing all gradients in the direction of the gas flows. The MEA used was assembled in-house using BASF Celtec® membranes with an acid loading of 34-36 $mg_{H3PO4}cm^{-2}$ and a ratio of phosphoric acid (PA) to PBI units of n_{PA}/n_{PBI} = 33±2 [14]. The membrane area was 10*10 cm^2. The catalyst layer consisted of Pt/Vulcan XC-72 supported platinum catalyst, with $1mg_{Pt}cm^{-2}$, coated onto the microporous layer of an SGL-38 carbon paper and an area of 7*7 cm^2 for both anode and cathode. To achieve a differential cell operation, the cell area was

reduced to 2 cm^2 by a kapton sheet of 25 µm thickness with a window (near the cathode outlet) of 1.1 x 1.8 cm^2 placed between the cathode GDL and the membrane. The resulting MEA was placed between two 45 cm^2 flow fields made from pyrolitically surface treated and sealed graphite (proprietary surface treatment by POCO Graphite, USA). The anode plate had a two-channel serpentine flow geometry while the cathode consisted of three channel serpentine flow geometry. The channels had 1.2 mm width and 2 mm depth. A hard-stop perfluoroalkoxy alkane (PFA) gasket of thickness 320 µm was used on both sides; resulting in a MEA compression of about 30%. The compressed total MEA thickness was 830 µm**.**

The control and data acquisition of the test parameters was carried out using LabVIEW software. There were two thermocouples to sense and control the anode and the cathode temperatures. A Biologic SP-300 potentiostat was used for controlling the electric parameters.

The break-in of the cell was carried out for 80-100 h at 160 °C with a fixed flow of 833 $mLmin^{-1}$ of hydrogen and air. All j/E curves were measured from open circuit voltage (OCV) down to 0.1 V with a ramp rate of 10 mV/s. All gases were humidified at room temperature and fed with constant flows on both anode (H_2 or H_2 diluted in N_2, 1667 $mLmin^{-1}$) and the cathode (oxygen, 833 mL min^{-1}). This corresponds to a stoichiometry of about 598 for the anode (with pure hydrogen) and the cathode at a current density of 0.2 Acm^{-2} respectively. The cell temperature was 160 °C for all experiments.

b. Anodic limiting current measurement

For determination of the anodic limiting current, two current density sequences were used as shown in Figure 1 a, where the time duration 'T_1' was 1440 minutes (24 h) for slow cycling and 30 minutes for fast cycling. The limiting current experiments were carried out with hydrogen concentrations between 0.05 and 1.0 mol%, with the balance being nitrogen in all cases.

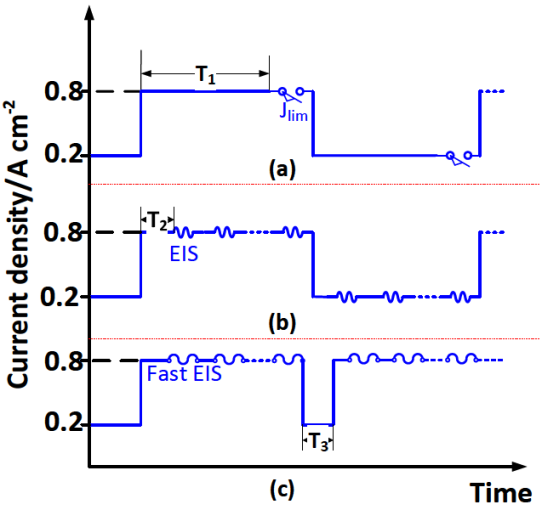

Figure 1: Test sequences with change between low (0.2 Acm^{-2}) and high current density (0.8 Acm^{-2}) for a) for anodic limiting current method, (b) for EIS method to measure flooding and de-flooding kinetics and (c) for fast EIS to investigate the first 2 minutes of flooding and de-flooding kinetics.

The limiting current measurement sequence at the end of the high and low current density periods was as follows:

Operation was changed from constant current to constant voltage at 0.75 V before changing the gas mixture from pure hydrogen to 1 %. This was to avoid a surge in the current density when going to limiting current conditions. Then a constant voltage of 0.2 V was maintained for the different hydrogen dilutions, with the 1st dilution at 1 % for 15 min and other dilutions for 2 min each. The long step in the beginning was necessary to reach constant conditions due to the time taken by the gases to reach a uniform concentration in the humidifier and cell.

c. Electrochemical impedance spectroscopy

For the EIS analysis and its interpretation the concept of the differential cell is particularly useful as disturbance of along-the channel artifacts are avoided [15]. The test protocol (cf.

Figure 1 b) was used to trigger phosphoric acid flooding and de-flooding with a holding time of 4 h at each current density. EIS spectra were recorded by scanning the frequency from 100 KHz to 100 mHz with 5 points per decade; resulting in a measurement time of ca. 50 s per spectrum. The AC signal applied was 5 % of the DC load.

Unless otherwise stated, impedance spectra were measured every 2 minutes for 60 minutes after a current step. Impedance spectra were measured at standard conditions at 160 °C with standard flows of 1666 $mLmin^{-1}$ for the anode (10 % H_2 in N_2) and 833 $mLmin^{-1}$ for the cathode (pure O_2).

In order to investigate the dynamics of the first 2 minutes after a current step, the test protocol according to figure 1 c was adapted. The holding time of 4 h for 0.8 Acm^{-2} was kept, but the holding time at 0.2 Acm^{-2}, T_3 was reduced to 2 minutes. Impedance was measured only at 0.8 Acm^{-2} and only the 1 Hz point was measured every 10 seconds (s. Figure 1 c). This allowed measuring the dynamics of the first 2 minutes with a better time resolution and also enabled a higher accuracy, as all measurements were done at the high current density, where the sensitivity towards PA migration was improved compared to the low current density.

3. Theoretical background

The transport resistance of hydrogen in the GDL (R_T) is related to the limiting current (j_{lim}) by the following relationship [16]:

$$R_T = 4F\frac{\Delta c}{j_{lim}} \qquad (1)$$

where j_{lim} is the limiting current density, F the Faraday constant and Δc is the concentration difference between the channel and the catalyst layer, which is calculated as shown below.

By definition, a limiting current is obtained when the concentration on the catalyst surface is zero. Thus, under limiting current condition, $\Delta c = c_1$, which is given by

$$c_1 = \frac{p - p_{H_2O}}{RT}\chi_{H_2}^{dry-in} \qquad (2)$$

Where $x_{H_2}^{dry-in}$ is the dry hydrogen inlet mole fraction, p is the total gas pressure (101.3 kPa), p_{H_2O} is the water vapor pressure (3.2 kPa at 25 °C), R the universal gas constant and T the cell temperature. Thus, the transport resistance R_T can be calculated as:

$$R_T = \frac{4F\chi_{H_2}^{dry-in}}{j_{lim}} \frac{p-p_{H_2O}}{RT} \quad (3)$$

4. Results

a. Determination of anodic limitation

When operating HT-PEFCs with pure hydrogen and oxygen, mass transport phenomena rather occur at the cathode side than at the anode side [17]. The reason for this is the lower diffusion coefficient of oxygen as compared to hydrogen [18]. If air is used instead of oxygen, cathodic mass transport is even more dominant due to the reduced oxygen partial pressure. Therefore, conditions to guarantee limitation of the current by anodic mass transport had to be investigated. To do so, polarization curves with different hydrogen dilutions in nitrogen at the anode and pure oxygen at the cathode were recorded (cf. Figure 2).

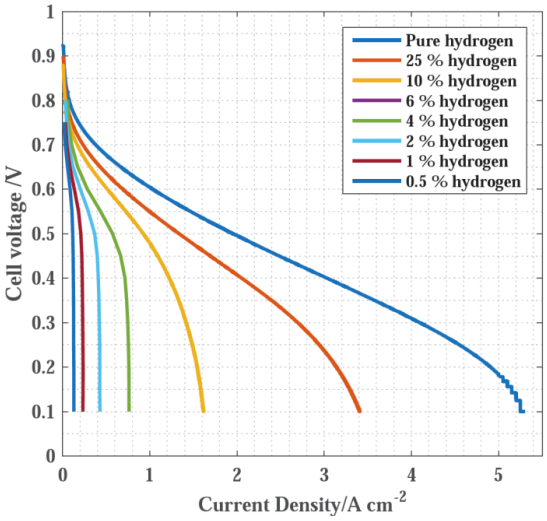

Figure 2: Polarization curves at 160 °C with constant gas flows at both anode (H_2 or H_2 diluted in N_2, 1667 mLmin^{-1}) and cathode (oxygen, 833 mLmin^{-1}).

Mass transport limitation by gas diffusion is associated with a sharp drop of the corresponding j/E curve. Even when further lowering the potential, no higher current can be drawn; i.e. the current is limited by gas transport.

For high hydrogen concentrations, the limitation by gas diffusion is less dominant and therefore at concentrations of 25 % hydrogen in nitrogen or above, no significant mass transport losses can be observed. Real mass transport limitations were found for hydrogen concentrations of 4 % and less. As the cathode was fed with pure oxygen, the mass transport losses at low hydrogen concentrations can only be interpreted as anodic mass transport limitations. Based on the findings presented in figure 2, a constant cell voltage of 0.2 V was chosen for determining the limiting current density for all hydrogen dilutions.

b. Limiting current measurements

Limiting current measurements are the common method to determine transport resistances in the gas diffusion layer. The transport resistance (R_T) of hydrogen in the anodic gas diffusion layer is assumed to be influenced by the acid migration towards the anode at high current densities (0.8 Acm^{-2}). Limiting current measurements were therefore carried out to determine the transport resistance of hydrogen in the anode GDL. As deduced from Figure 2, at true current limiting behavior, current densities significantly below 1 Acm^{-2} are observed. The definition and calculation of the transport resistance is described in detail in the theoretical background section.

A current cycling protocol (see Figure 1 a) with a cycle time between low (0.2 Acm^{-2}) and high current density (0.8 Acm^{-2}) of 24 hours was used to provoke acid migration. Even though the anode GDL flooding cannot be directly observed in these experiments, in analogy to the

characterization of the same MEA materials with X-ray imaging [6] the measurement after the high current density was considered to reflect the properties of the anode GDL containing migrated phosphoric acid, and is hence called the “flooded” state, while after measurements at low current density the GDL was assumed to be acid-free and therefore called the “de-flooded” state. At the end of each current density level the limiting current was measured with diluted hydrogen.

Figure 3 shows the mean value of three limiting current measurement for the operation after high (blue symbols) and low (red symbols) current density for hydrogen concentrations between 0.05 and 1 mol%. A clear linear relation between hydrogen concentration and the measured current density is observed as shown in Figure 3 a. The quality of the linear fit and the fact, that it intersects the ordinate very close to the origin is confirming that the measured limiting current is only dependent on the hydrogen concentration. A similar verification has been shown by Baker et al. [16] for oxygen concentration limiting currents in low temperature PEFCs.

The slope of the linear regression can be used to calculate the transport resistance. For the flooded state a value of 0.424 $s \cdot cm^{-1}$ was calculated; for the unflooded state a value of 0.428 $s \cdot cm^{-1}$. This difference between the transport resistances being less than 1 %, lies within the experimental error, so no difference for the transport resistance between the “flooded” and “unflooded” state was found.

The determination of the limiting current was also performed for the current cycling protocol with 30 min hold time to restrict the complete de-flooding of acid in the GDL and possibly evoke a higher acid saturation in the anode GDL over cycling and therefore increase the difference between the transport resistance measured at high and at low current density. The limiting current was measured after a period of 24 h (12 cycles between high and low current density).

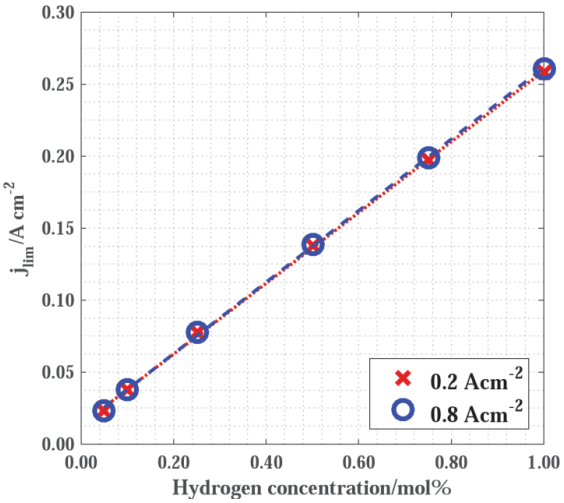

Figure 3: Limiting current vs hydrogen concentration at 160 °C after operation at low current density (red) and high current density (blue).

However, for the fast cycling case, a transport resistance of 0.422 s·cm^{-1} for the flooded state and of 0.424 s·cm^{-1} for the unflooded state, just like for the slow cycling experiments, was calculated. The difference between the transport resistances lies again within the experimental error.

The calculated hydrogen transport resistances are only slightly lower to what Baker et al. [16] reported for oxygen transport resistance, which was about 0.5 s·cm^{-1} for dry GDLs. One might expect a larger difference, due to the large difference for the self-diffusion coefficient of hydrogen (1.604 cm^{2}s^{-1} at 273 K) and oxygen (0.192 cm^{2}s^{-1} at 273 K) [19], however, when strongly diluting hydrogen or oxygen in nitrogen, binary diffusion coefficients are more representative. In this case, the difference between the hydrogen (0.876 cm^{2}s^{-1} at 324 K) and oxygen (0.258 cm^{2}s^{-1} at 324 K) is smaller [20]. Also, a thicker and more compressed GDL from a different supplier was used for this work compared to the work of Baker et al., which also explains the rather small difference between the transport resistances for hydrogen in the present case and oxygen in the work of Baker et al..

The summary of all calculated transport resistances are shown in Table 1:

Cycle time	R_T unflooded state [s cm^{-1}]	R_T flooded state [s cm^{-1}]
T_1 =24 h	0.428±0.002	0.424±0.002
T_1 =30 min	0.424±0.001	0.422±0.001

Table 1: Calculated hydrogen transport resistances for the flooded and unflooded states for both slow and fast current cycling at 160 °C.

On first view, it is surprising, that no difference in the transport resistance between the two states was found, as gas diffusion in phosphoric acid is orders of magnitudes slower [18, 21, 22] than in air and therefore, the transport resistance in the flooded GDL should be higher than in an unflooded GDL.

The limiting current method, however, requires switching of the anode gas to low concentrations with equilibration times to allow for constant gas composition of 15 minutes (cf. experimental section); it is therefore comparably slow and an invasive method. It does also not allow to measure dynamics of the "flooding" or "de-flooding" processes. To be able to assess the dynamics, a method based on electrochemical impedance spectroscopy has been developed.

c. Electrochemical impedance spectroscopy

Electrochemical impedance spectroscopy (EIS) was chosen because it can be configured to be fast and it is non-invasive, allowing for a better temporal measurement resolution and much less disturbance of the cell, as compared to the limiting current method. EIS can be performed without changing the current density or the gas dilution, therefore also eliminating the need for equilibration times.

All experiments were performed with pure O_2 at the cathode and 10 % hydrogen in nitrogen at gas stoichiometries > 10. The dilution of 10 % H_2 in N_2 was chosen as with pure hydrogen

little anodic limitations are expected. With hydrogen dilutions of 4 % or less, the current density of 0.8 Acm^{-2} cannot be reached. Also a hydrogen dilution of 4 % does not directly reflect a real world operating condition, even when reformate gas is used. The dilution of 10 % hydrogen is still representative for reformate operation (e.g., when reformate from autothermal reformers are used); especially when factoring in the decreasing hydrogen partial pressure from inlet to outlet when operating the fuel cell stoichiometrically.

In Figure 4, the EIS spectra for positive current step (0.2 to 0.8 Acm^{-2}; "flooding") and the negative current step ("de-flooding") are shown. The case for the flooding of the GDL shows a prominent change in the low frequency resistance over time. The changes in the low frequency range are assumed to be associated with mass transport issues arising due to acid migrating towards the anode at the high current density (Figure 4a, 0.8 Acm^{-2}). For the de-flooding case, measured at 0.2 Acm^{-2} on the other hand, the trend is inverted and the changes observed are less pronounced (Figure 4b).

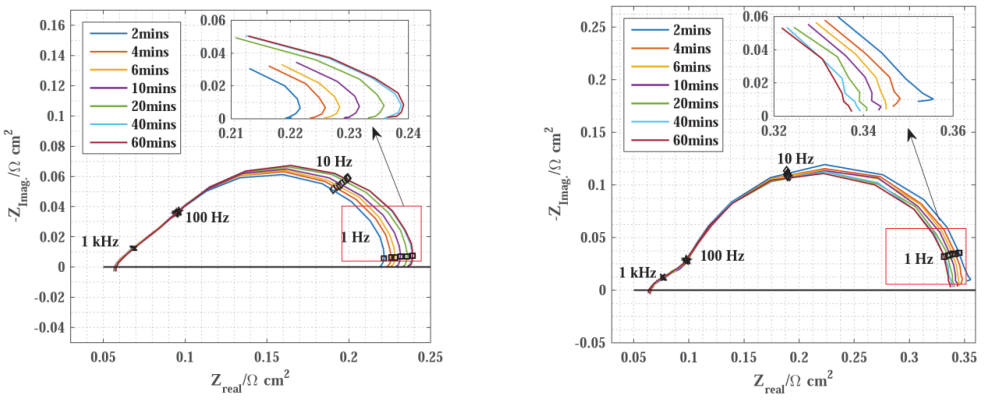

Figure 4: Impedance spectra comparison carried out in 2 minutes intervals, a) during flooding (0.8 Acm^{-2}) and, b) during de-flooding (0.2 Acm^{-2}).

The low frequency intercept in EIS is equivalent to the slope of the j/E-curve in the evaluated current density point. An increase in the low frequency intercept and thus a steeper j/E-curve can be interpreted as an increased transport resistance. Also literature suggests that (hydrogen) mass transport is reflected in EIS at low frequencies [23–25].

With recording full EIS spectra, the first 2 minutes cannot be resolved. In order to do so, the procedure described in Figure 1 c was carried out to determine the change in the first two minutes. After complete de-flooding (24 h at 0.2 Acm^{-2}), the 1 Hz signal was measured for a positive current step and the respective change for complete flooding was recorded as baseline (see Figure 5). In order to probe the first 2 minutes of de-flooding, the current was lowered for two minutes only after which the 1 Hz impedance was measured again at 0.8 Acm^{-2}.

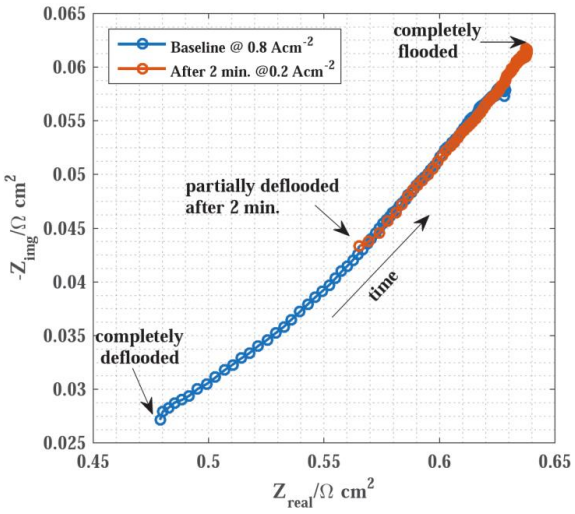

Figure 5: Comparison of 1 Hz impedance, at a step to 0.8 Acm^{-2} after 24 h at 0.2 Acm^{-2} (called baseline) and 2 min time at 0.2 Acm^{-2} to determine the de-flooding effect in the first two minutes.

This procedure allowed a faster recording speed and to calculate a time constant for the acid flooding and de-flooding processes. Data for the positive and negative current steps (i.e. flooding and de-flooding) are shown in Figure 6.

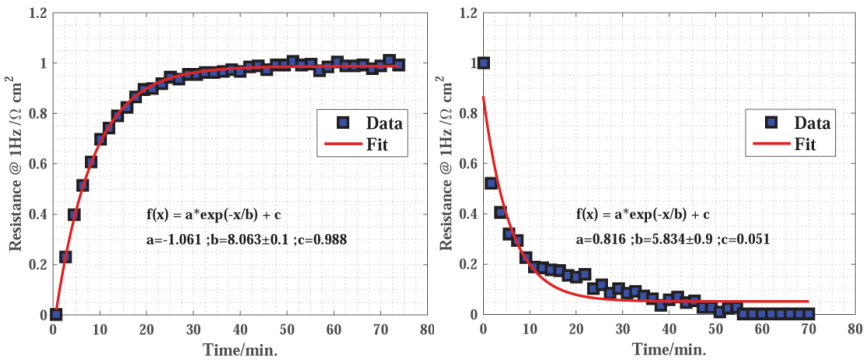

Figure 6: Flooding (a) and de-flooding (b) kinetics deduced from 1 Hz resistances.

In Figure 6, the real part of the impedance at 1 Hz is shown. The real part is normalized for the interval between completely de-flooded (=0) and flooded (=1) after 1 hour at 0.8 Acm^{-2}. Figure 6 a shows the time dependence for the flooding step and Figure 6 b vice versa for the de-flooding signal.

In order to determine the time constant of the flooding and de-flooding kinetics, data points were fitted with equation (4):

$$f(x) = a * \exp\left(\frac{-x}{b}\right) + c \qquad (4)$$

Where the parameter b represents the time constant; the other fitting parameters are not relevant for this study.

The time constant for flooding was determined to be 8.1 ± 0.1 minutes. When closely examining the data of Eberhardt et al. [6], who determined the kinetics of liquid saturation of phosphoric acid in the anode GDL with *operando* X-ray tomographic microscopy with a lower time resolution, one can observe a similar flooding kinetic after stepping to high current

density (0.8 Acm^{-2}). The flooding of the anode GDL reaches a steady state after about 30 minutes, which is in line with the results of this study. This shows that the increase of the low frequency impedance at high current density is closely correlated with the phosphoric acid saturation in the anode GDL.

As shown in Figure 5, the impedance change after 2 minutes of de-flooding corresponds to 52 % of the total signal or about half of the de-flooding process had occurred during the first 2 minutes. To account for this, the 2 minutes de-flooding signal was set to 52 % for determining the overall de-flooding kinetics.

The de-flooding kinetics, shown in Figure 6 b, are faster than the flooding one with a time constant of about 4.8 ± 0.9 minutes. The reason for the higher standard deviation for the de-flooding case is the reduced sensitivity for the 1 Hz signal at the current density of 0.2 Acm^{-2}.

The fast de-flooding kinetics explains why the limiting current method was unable to detect a change in mass transport resistance as the time required time for equilibration after the hydrogen concentration reduction is too long (~15 minutes) at current densities, where de-flooding is triggered.

Despite the fact, that after switching to 0.8 Acm^{-2} an increasing resistance at 1 Hz can be measured, the cell voltage did not significantly change with time (± 2 mV only). This is likely due to the fact, that the increase in transport resistance is compensated by improvement in the kinetics. It cannot be distinguished, whether this is due to better wetting of the anode or (more likely) a slight improvement in the cathode induced by acid migration. It is expected, that at lower hydrogen concentrations, the losses due to H_2 diffusion would become more dominant and would also be reflected in the cell voltage. However, as reasoned above, on the one hand a hydrogen partial pressure of 10 % was chosen to reflect operation with reformate gas in the

downstream section of the cell and on the other hand at significantly lower hydrogen concentration 0.8 Acm^{-2} cannot be reached and the extent of acid migration would differ.

Also for the de-flooding case, no clear trend in cell voltage was observed. Thus, under conditions reflecting operation with reformate gas, the impact of phosphoric acid migration on the performance of HT-PEFCs can possibly be neglected. However, phosphoric acid migration still remains an important issue for the durability of HT-PEFCs due to the possibly increased loss of the electrolyte over time [26, 27].

5. Conclusion

In HT-PEFC, phosphoric acid migrates at high current densities towards the anode. As observed in previous work, flooding of the anode GDL is trigged by high current density (i.e. 0.8 Acm^{-2}) operation, while de-flooding occurs at low current density (i.e. 0.2 Acm^{-2}). In order to understand the impact of phosphoric acid migration on the performance of HT-PEFCs; two different characterization methods were used.

Anodic limiting current measurements need to be made at very low hydrogen concentrations (0.05 – 1 mol%) and at low current densities. The transition time of 15 minutes, when switching from pure hydrogen to the very diluted hydrogen operation and the stabilization time at the different low hydrogen concentrations were sufficient to trigger de-flooding in the anode GDL and therefore, the limiting current measurements represent the unflooded state. On the other hand, the method using electrochemical impedance spectroscopy (EIS) was able to capture these differences, as impedance spectroscopy is fast, less invasive and gas dilution and equilibration times are not needed.

With EIS phosphoric acid flooding kinetics of the anode GDL with a time constant of 8.1 minutes and de-flooding kinetics with a time constant of 4.8 minutes were determined. However, the influence of phosphoric acid migration on the performance of a HT-PEFC was

found to be insignificant, even for an anode gas composition with only 10 % hydrogen in nitrogen. Hydrogen concentrations of 4 % or less are needed to observe true anodic limitations. For pure hydrogen and at gas compositions reflecting reformate operation, the impact of acid migration on performance is therefore negligible.

Acknowledgement

S. Thomas thanks PSI for hosting him to contribute to the experimental work for 5 month. S. Thomas also acknowledges the financial support from Aalborg University and Innovation Fund Denmark through the 4M project. The authors like to thank T. Gloor for support with the test bench and programming. All MEA materials were provided by BASF SE, which is gratefully acknowledged.

References

[1] T.J. Schmidt, J. Baurmeister, Properties of high-temperature PEFC Celtec®-P 1000 MEAs in start/stop operation mode, J. Power Sources. 176 (2008) 428–434. doi:10.1016/j.jpowsour.2007.08.055.

[2] J.R. Vang, S.J. Andreasen, S.S. Araya, S.K. Kær, Comparative study of the break in process of post doped and sol–gel high temperature proton exchange membrane fuel cells, Int. J. Hydrogen Energy. 39 (2014) 14959–14968. doi:10.1016/j.ijhydene.2014.07.017.

[3] T.J. Schmidt, Durability and Degradation in High-Temperature Polymer Electrolyte Fuel Cells, ECS Trans. 1 (2006) 19–31. doi:10.1149/1.2214541.

[4] Q. Li, J.O. Jensen, R.F. Savinell, N.J. Bjerrum, High temperature proton exchange membranes based on polybenzimidazoles for fuel cells, Prog. Polym. Sci. 34 (2009) 449–477. doi:10.1016/j.progpolymsci.2008.12.003.

[5] R. Zeis, Materials and characterization techniques for high-temperature polymer electrolyte membrane fuel cells, Beilstein J. Nanotechnol. 6 (2015) 68-83.

[6] S.H. Eberhardt, M. Toulec, F. Marone, M. Stampanoni, F.N. Büchi, T.J. Schmidt, Dynamic Operation of HT-PEFC: In-Operando Imaging of Phosphoric Acid Profiles and (Re)distribution, J. Electrochem. Soc. 162 (2015) F310–F316. doi:10.1149/2.0751503jes.

[7] S.H. Eberhardt, F. Marone, M. Stampanoni, F.N. Büchi, T.J. Schmidt, Operando X-ray Tomographic Microscopy Imaging of HT-PEFC: A Comparative Study of Phosphoric Acid Electrolyte Migration, J. Electrochem. Soc. 163 (2016) F842–F847. doi:10.1149/2.0801608jes.

[8] S. Chevalier, M. Fazeli, F. Mack, S. Galbiati, I. Manke, A. Bazylak, R. Zeis, Role of the microporous layer in the redistribution of phosphoric acid in high temperature PEM fuel cell gas diffusion electrodes, Electrochim. Acta. 212 (2016) 187–194. doi:10.1016/j.electacta.2016.06.121.

[9] S. Lang, T.J. Kazdal, F. Kühl, M.J. Hampe, Experimental investigation and numerical simulation of the electrolyte loss in a HT-PEM fuel cell, Int. J. Hydrogen Energy. 40 (2015) 1163–1172. doi:10.1016/j.ijhydene.2014.11.041.

[10] H.R. Kunz, Electrolyte Migration in Fuel Cell Modeling, J. Electrochem. Soc. Proc. 99–14 (1999) 191–207.

[11] J. Eller, F. Marone, M. Stampanoni, F.N. Büchi, Operando Properties of Gas Diffusion Layers : Saturation and, 164 (2017). doi:10.1149/2.0881702jes.

[12] T. Rosen, J. Eller, J. Kang, N.I. Prasianakis, J. Mantzaras, F.N. Büchi, Saturation Dependent Effective Transport Properties of PEFC Gas Diffusion Layers, J. Electrochem. Soc. 159 (2012) F536–F544. doi:10.1149/2.005209jes.

[13] J.P. Owejan, T.A. Trabold, M.M. Mench, Oxygen transport resistance correlated to liquid water saturation in the gas diffusion layer of PEM fuel cells, Int. J. Heat Mass Transf. 71 (2014) 585–592. doi:10.1016/j.ijheatmasstransfer.2013.12.059.

[14] T.J. Schmidt, J. Baurmeister, Durability and Reliability in High-Temperature Reformed Hydrogen PEFCs, ECS Trans. 3 (2006) 861–869. doi:10.1149/1.2356204.

[15] I.A. Schneider, S.A. Freunberger, D. Kramer, A. Wokaun, G.G. Scherer, Oscillations in Gas Channels, J. Electrochem. Soc. 154 (2007) B383-B388. doi:10.1149/1.2435706.

[16] D.R. Baker, D.A. Caulk, K.C. Neyerlin, M.W. Murphy, Measurement of Oxygen Transport Resistance in PEM Fuel Cells by Limiting Current Methods, J. Electrochem. Soc. 156 (2009) B991-B1003. doi:10.1149/1.3152226.

[17] C. Wannek, I. Konradi, J. Mergel, W. Lehnert, Redistribution of phosphoric acid in membrane electrode assemblies for high-temperature polymer electrolyte fuel cells, Int. J. Hydrogen Energy. 34 (2009) 9479–9485. doi:10.1016/j.ijhydene.2009.09.076.

[18] C.J. Bapat, S.T. Thynell, Effect of anisotropic thermal conductivity of the GDL and current collector rib width on two-phase transport in a PEM fuel cell, J. Power Sources. 179 (2008) 240–251. doi:10.1016/j.jpowsour.2007.12.033.

[19] Mostinsky IL, Diffusion coefficient. http://www.thermopedia.com/content/696/., n.d. doi:10.1615/AtoZ.d.diffusion_coefficient.

[20] G. Karaiskakis, D. Gavril, Determination of diffusion coefficients by gas chromatography, J. Chromatogr. A. 1037 (2004) 147–189. doi:10.1016/j.chroma.2004.01.015.

[21] E. Razaq, M. Razaq, A. Yeager, Perfluorosulfonimide as an Additive in Phosphoric

Acid Fuel Cell, J. Electrochem. Soc. 136 (1989) 385-390. doi:10.1149/1.2096641.

[22] X. Gang, H.A. Hjuler, C.A. Olsen, R.W. Berg, N. Bjerrum, Electrolyte Additives for Phosphoric Acid Fuel Cells, J. Electrochem. Soc. 140 (1993) 896–902. doi:10.1149/1.2056224.

[23] S.S. Araya, F. Zhou, V. Liso, S.L. Sahlin, J.R. Vang, S. Thomas, X. Gao, C. Jeppesen, S.K. Kær, A comprehensive review of PBI-based high temperature PEM fuel cells, Int. J. Hydrogen Energy. 41 (2016) 21310–21344. doi:10.1016/j.ijhydene.2016.09.024.

[24] Q. Li, D. Aili, H.A. Hjuler, J.O. Jensen, eds., High Temperature Polymer Electrolyte Membrane Fuel Cells: Approaches, Status, and Perspectives, 1st ed., Springer, 2015. doi:10.1007/978-3-319-17082-4.

[25] S. Thomas, S.C. Lee, A.K. Sahu, S. Park, Online health monitoring of a fuel cell using total harmonic distortion analysis, Int. J. Hydrogen Energy. 39 (2014) 4558–4565. doi:10.1016/j.ijhydene.2013.12.180.

[26] S. Yu, L. Xiao, B.C. Benicewicz, Durability studies of PBI-based high temperature PEMFCs, Fuel Cells. 8 (2008) 165–174. doi:10.1002/fuce.200800024.

[27] S.H. Eberhardt, T. Lochner, F.N. Büchi, T.J. Schmidt, Correlating Electrolyte Inventory and Lifetime of HT-PEFC by Accelerated Stress Testing, J. Electrochem. Soc. 162 (2015) F1367–F1372. doi:10.1149/2.0591512jes.

Paper D

Mapping phosphoric acid migration with differently doped PBI membrane in an HT-PEM fuel cell

Sobi Thomas, Samuel Simon Araya, Thomas Steenberg, Steffen Henrik Frensch, Søren Knudsen Kær

The paper has been submitted in the
Journal of Power Sources.

The layout has been revised.

Quantifying hydrogen mass transport changes in an HTPEM fuel as a function of current density and acid doping

Sobi Thomas[a,*], Samuel Simon Araya[a], Steffen Henrik Frensch[a], Thomas Steenberg[b], Søren Knudsen Kær[a,*]

[a]*Department of Energy Technology, Pontoppidanstræde, Aalborg University, Aalborg East -9220, Denmark*
[b]*Danish Power Systems, Egeskowej 6c, DK-3490 Kvistgaard, Denmark*

Abstract

High temperature polymer electrolyte membrane fuel cells (HTPEM) have phosphoric acid doped membrane for the proton conductivity. Thus, it reduces the need for complex humidification system. However, PA present in the membrane is mobile and has a tendency to move out of the cell depending on the acid doping level. The migration of acid towards the anode at high current density > 0.4 A cm^{-2} causes GDL flooding which thereby results higher resistance to hydrogen transport and a performance degradation is seen. Thus, it becomes of great interest to understand the acid doping level which is optimal for an HTPEM fuel cell.In this study, mapping of doping level with current density and acid migration was investigated. Three different doping levels 11, 8.3 and 7 mgH3PO4cm^2 were investigated. Electrochemical impedance spectroscopy is used to characterize the different MEAs. The EIS measurement was restricted to low frequency spectra to calculate the time constant for resistance change at low and high current density switching. The time constants were 2.8±0.3, 5.7±0.5, 9.5±0.8 min at low current density and 3.1±0.2, 3.3±0.5 and 5.6±0.5 min for high current density. The resistance decreases at high current density and increases at low current density for all the doping levels, only the time constants vary. This is attributed to low doping level having lower capillary pressure to push the acid from reaching the membrane and/or catalyst layer into the GDL pores on the anode. However, the improve in mass transport resistance was assumed to be result of more three phase boundary created due to the drag of acid into the catalyst layer.

Keywords: Load cycling, Impedance, Fuel cell, high temperature PEM, Phosphoric acid

1. Introduction

High temperature PEM fuel cells (HT-PEMFC) have several advantages in terms of higher CO tolerance and minimal humidification complexities [1, 2]. The most commonly used membrane is phosphoric acid doped polybenzimidizole (PBI) membranes. The advantage is the possibility of elevated fuel cell operation which enhances the reaction kinetics and reduces engineering problems associated with system design. HT-PEM fuel cells are operated at a temperature of around 160-180 °C. The proton conductor in these fuel cells are PA which makes the fuel cell operation at elevated temperature possible without humidification. The presence of acid required for the proton conduction is also associated with some problems. The PBI matrix which is doped with PA takes up two acid molecules per PBI repetitive unit. However, the acid doping required is high to achieve reasonable performance. The doping level also depends on the membrane preparation method. Two most commonly used MEAs in HT-PEM fuel cells are sol-gel type and post-doped MEAs. In case of sol-gel MEA's the acid doping level (70 per repetitive unit) is much higher compared to post-doped MEAs (10-12).

Nevertheless, in both the cases, a large amount of acid is free within the cell which could move to other parts in the cell like the GDL, catalyst layer and also the flow-field from where the chances of it getting removed with the gases are high. The loss of phosphoric acid is a highly debatable topic considering the fact that differently doped MEAs as mentioned above are available commercially. Some reported that there is loss of acid by evaporation which leads to the degradation of HT-PEMFC in the long term when the doping is high [3, 4]. The other argument reported is that the acid loss is not an issue to the durability under certain operating conditions [5, 6].

Yu et al. [6], investigated the cause of degradation in an HT-PEMFC using continuous 550 h. The test results show a degradation rate of 0.18 $\mathrm{mV\,h^{-1}}$ after an activation for 90 h. The analysis based on different characterization methods suggest that the degradation was a result of catalyst agglomeration and thereby leading to acid leaching from the catalyst and getting lost. The investigation of acid redistribution on an operating HT-PEM fuel was carried out as a function of current density. When a load (140 $\mathrm{mA\,cm^{-2}}$) was applied on a cell operating at open circuit voltage (OCV), the membrane was seen to swell by $\approx$20%. This increase was attributed to increment

*Corresponding author
Email addresses: sot@et.aau.dk (Sobi Thomas), skk@et.aau.dk (Søren Knudsen Kær)

in the water generated which gets attracted by the PA. Further increment of current density to 550 mA cm^{-2} did not further increase the membrane thickness [7]. The lifetime investigation of HT-PEM fuel cell under accelerated stress test was investigated by [4]. The parameters considered which could influence the acid loss were temperature and reactant flow rates. They reported 40% loss in acid from a beginning doping level of ≈36 mg$H_3PO_4$$cm^{-1}$ resulted minimal loss in the performance. They also reported same rate of acid loss over a period of 2830 h up to a PA loss of 90 %, suggesting no effect on the MEA doping level [4].

Maier et al. [7] reported 20 % of generated water on the cathode migrates to the anode under the influence difference in acid concentration and PA affinity for water. In different studies using NMR [8, 9] it is reported that the proton conductivity in PA-doped PBI membrane is dominated by H_3O^+ and H_2O species at low PA doping levels and by $H_4PO_4{}^+$ and H_3PO_4 molecules when the PA doping is higher.

The cause of degradation as function of cell resistivity, PA loss and catalyst agglomeration was investigated by Wannek et al. [5] under different operating conditions. They reported that the loss of acid in PA-doped AB-PBI membrane was not the main reason for the cell degradation, even when operated at temperatures below 100 °C. The investigation of platinum particle size indicate that the degradation was more dominated by the catalyst. The degradation of start/stop with purging was reported lower compared to cell cycling at 160 over the entire test period [5]. The loss of acid affects the proton conductivity and that leads to cell degradation [10, 6]. **?**], investigated the effect of PA loading on the anode catalyst when operating with reformate feed. The study suggests PA loading needs to be low on the anode catalyst and the presence of PA assists in faster transfer of protons.

The present study aims to map the acid migration towards anode as a function of current density and acid concentration. The acid concentration effect on acid migration will be interesting to understand how the performance gets affected and also the optimal acid concentration requirement to avoid acid migration.

2. Experimental setup and procedure

The MEAs used in the present study are from Dapazol® with platinum loading of 1.30 mg cm^{-2} on both sides. The doping level of the membrane are varied and three different concentrations are used 65 %, 75 % and 85 % for the doping process. The corresponding doping levels were

7 mgH_3PO_4/cm^2 8.3 mgH_3PO_4/cm^2 and 11 mgH_3PO_4/cm^2 respectively. The active area of the membrane is 45 cm^2 and the electrode size is reduced to 2 cm^2(1.8*1.1). This was to achieve uniform flow distribution across the area. To avoid mass transport issues which may arise due to non-uniform flow of gases in the channel. The anode flow field was two channel and cathode three channel serpentine. The gaskets used were of Teflon with a thickness of 150 μm on both sides. The end plates were of aluminium and the torque applied was 700 kg using 8 tie-rods and spring assembly.

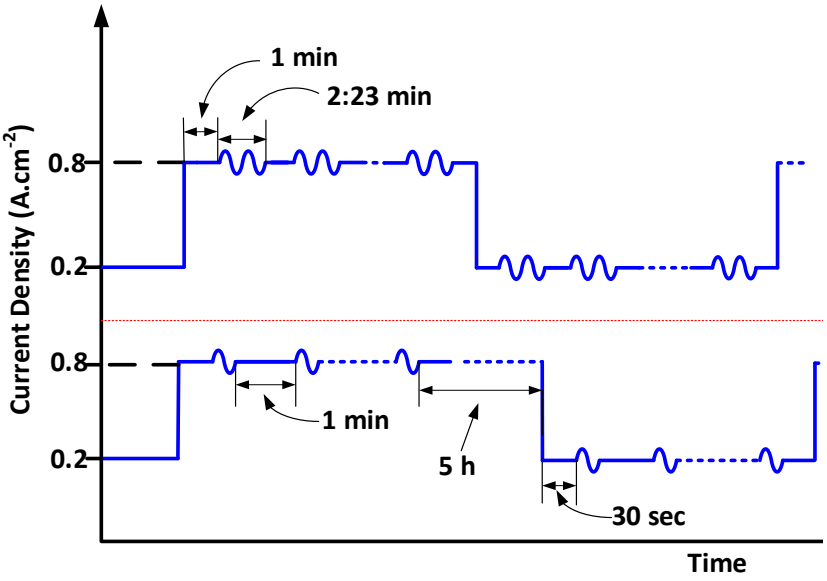

Figure 1: The test sequence of load cycling between 0.2 A cm^{-2} and 0.8 A cm^{-2}, (a) Normal EIS, (b) EIS measurement at one frequency

The tests are carried out with the Greenlight Innovation fuel cell test stand. The electrochemical impedance spectroscopy was carried using Gamry Reference 3000. A break-in process was carried for 100 h at 0.2 A cm^{-2}. The break-in was carried out with hydrogen on the anode and oxygen on the cathode. The flow rates were fixed at 0.2 L min^{-1}. The gases were humidified at room temperature (30 °C) on both sides. The humidification of gases was to avoid the drying of membrane at high flow rates.

The flow rates were fixed at 1 $L\,min^{-1}$ on both sides for the IV curves and as well as the EIS measurements. The test sequence for the experiments are shown in Fig. 1. All the EIS was carried out under galvanostatic mode with the amplitude fixed at 5 % of the load and points per decade (ppd) was fixed at 5. The points per decade was low to reduce the time duration of the measurements. The frequency was scanned from 10 kHz to 1 Hz. The single frequency measurements were carried out under potenstiostatic mode with the amplitude fixed at 10 mV. All IV curves were measured by scanning the current at a ramp rate of 0.50 $A\,min^{-1}$ and the lower voltage limit was set to 0.1 V.

3. Results and discussion

The anode side mass transport is comparatively faster compared to cathode side where the solubility of O_2 in PA is slower [**?** 11]. Thus, to determine the mass transport limitations on the anode, the IV curve was recorded under different H_2 concentration on the anode and pure oxygen on the cathode as shown in Fig. 2. To make the gas flow constant for all the IV curves, N_2 was mixed with anode fuel to make it 100 %. The mass transport issues are more dominantly visible for H_2 concentrations below 10 %. A decrease in the limiting current with lower H_2 concentration as seen in Fig. 2 confirms the assumption that mass transport issues are from the anode and not dominated by cathode where oxygen is supplied. The IV curve was to determine the concentration suitable for cycling the cell between 0.2 and 0.8 $A\,cm^{-2}$. Based on the results to capture the anode mass transport issues on the anode due to acid filling the GDL pore a concentration of 5 % was chosen. The concentration was chosen such that the voltage was always above 0.4 $A\,cm^{-2}$. A lower concentration of anode fuel was to make the mass transport issue on the anode more dominant. The low concentration also simulates the scenario, where some areas on the catalyst have a very low H_2 concentration when operating with reformed fuel.

The first experiment was carried out with commercially available DPS MEAs (85 % concentrated PA used for doping to reach 11 mgH_3PO_4/cm^2). The EIS recorded with an interval of 1 min is shown in Fig. 3. The EIS was recorded after changing the current to 0.8 $A\,cm^{-2}$ and 1 min rest time after an operation of $\approx$5 h at 0.2 $A\,cm^{-2}$. The anode fuel concentration was fixed at 5 % H_2 and 95 % N_2 during the tests. The measurement time for each EIS spetra was 2 min and 23 s. The results indicate no significant difference in the EIS spectra when changing from high to low current density. The analysis of EIS data shows no or minimal differences in the

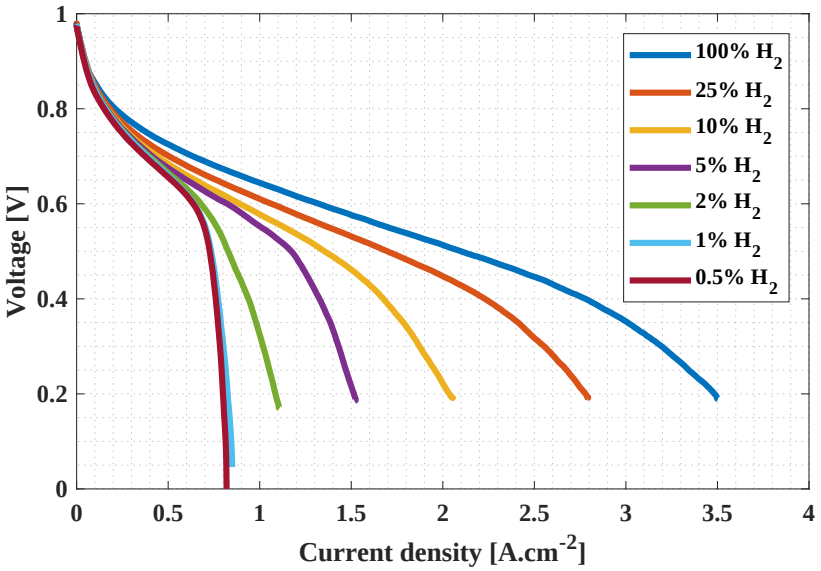

Figure 2: IV curve at different H_2 concentrations.

spectra over time. This suggests that acid migration from the membrane to the anode GDL (if any), which is assumed to affect the mass transport issue is not captured by the full spectra EIS measurement. However, based on previous experience and results from [12], it is known that acid migration and redistribution is a fast process and the time taken to record the EIS could be long for detecting the acid kinetics related phenomena.

The EIS interpretations in the literature [13, 14] suggests that the mass transport issues are dominant in the low frequency region <10 Hz of the EIS spectra. Thus, to reduce the measurement time and be able to detect the fast acid kinetics related mass transport issues on the anode, the range of frequency scan was reduced. A frequency range from 10 Hz to 0.5 Hz with 5 points per decade was selected. The EIS recorded is shown in Fig. 4. The impedance at frequencies below 1.6 Hz shows an increase over time at 0.2 A cm^{-2}. While at high current density (0.8 A cm^{-2}), the points overlap. This suggests that change of current density has an effect on the low frequency resistance which is mainly contributed by the mass transport issues [14, 13]. However, when similar measurement is carried out at high current density the mass transport

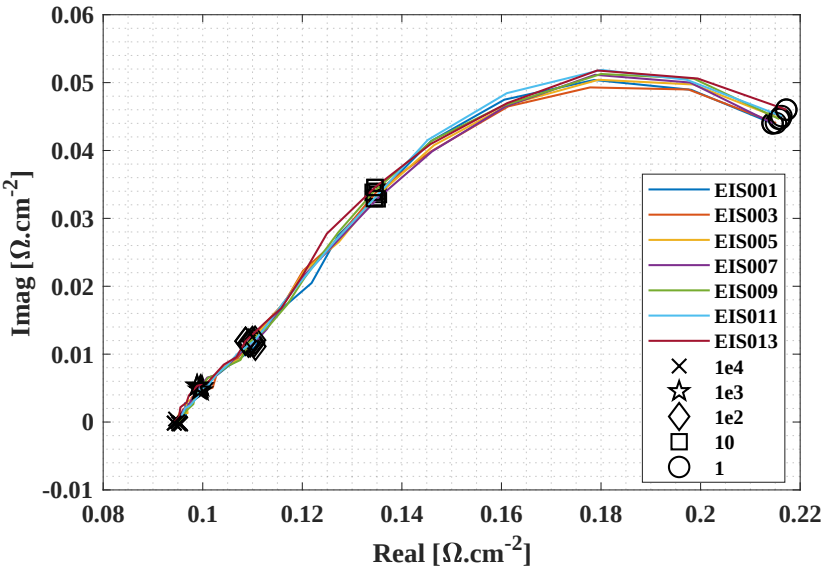

Figure 3: EIS over time at 0.2 A cm^{-2} with 5 points per decade

issues are not visible dominant or not captured by the fast frequency scan. This could be either due to fast acid kinetics at high current density or the noise in the measurement at high current density (low voltage) is shadowing the small resistance change at low frequency.

Thus, the next step was to carry out impedance measurement at a single frequency. The cell was operated at one current density for 5 h before changing the current density and starting the measurements. This was to make sure that the acid-water balance within the system has reached a uniform distribution within the cell. The measurements were repeated for three cycles and the mean value was plotted. This was to eliminate the experimental error and to have a statistical validation of the data.

In Fig. 4 (a), the resistance at 1 Hz measured for 1 h at 0.8 A cm^{-2} is shown. A decrease in resistance at the beginning is measured and then it stabilizes. The resistance for three different doping levels also show a difference in the low frequency resistance. A lower doping level has a higher resistance and the difference is quite significant. Similarly, the resistance over time measured at 0.8 A cm^{-2} is shown in Fig. 4 (b). The resistance decreases over time for high

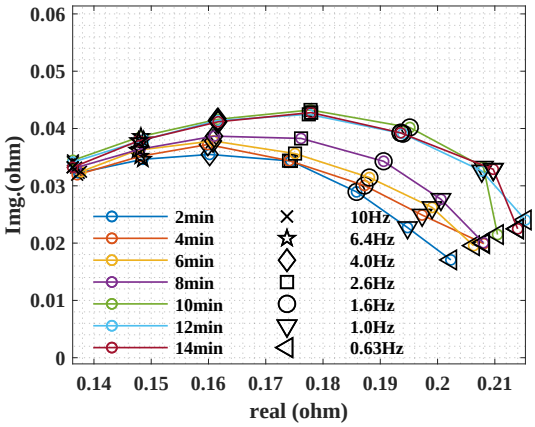

(a) Low frequency (10 to 0.5 Hz) EIS recorded over time at 0.2 A cm^{-2}

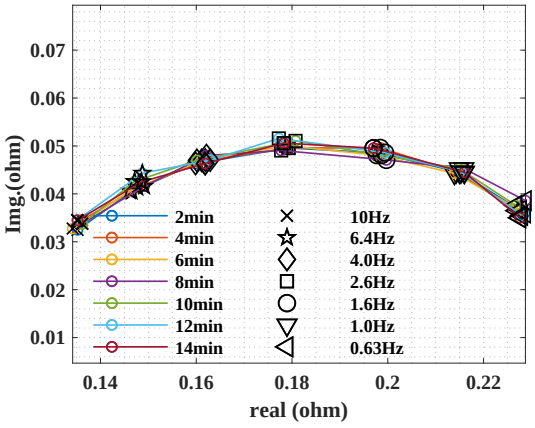

(b) Low frequency (10 to 0.5 Hz) EIS recorded over time at 0.8 A cm^{-2}

Figure 4: Low frequency (10 to 0.5 Hz) EIS recorded over time at 0.2 A cm^{-2} and 0.8 A cm^{-2}

current density operation at the beginning and then the resistance stabilizes. The 1 Hz frequency resistance over time shows an increase at low current density (0.2 A cm^{-2}) and decrease at high current density (0.8 A cm^{-2}).

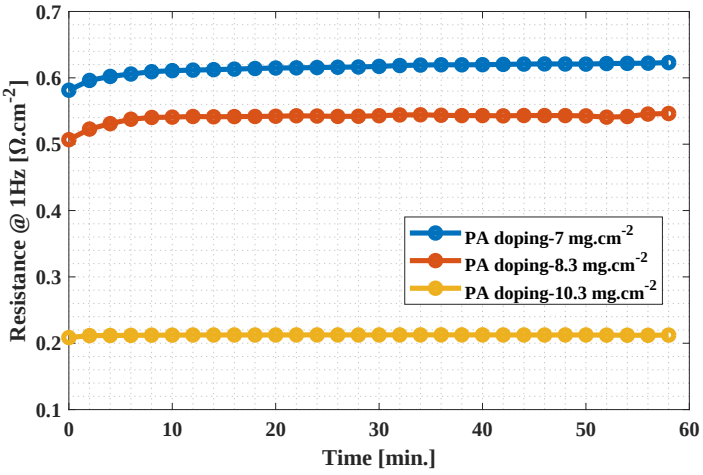

(a) Resistance change over time at 0.2 A cm^{-2}

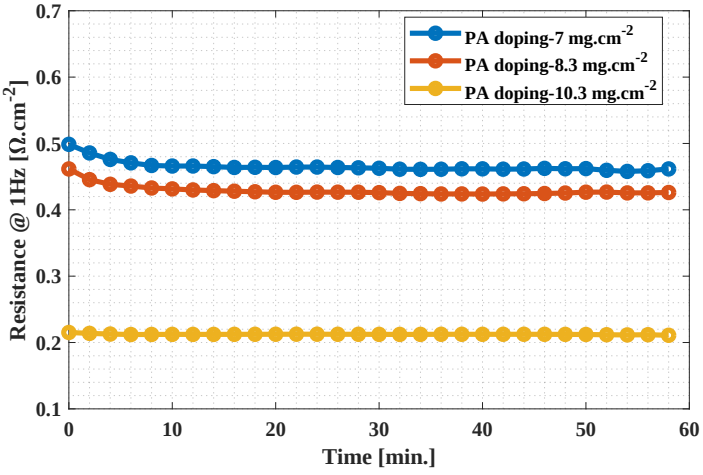

(b) Resistance change over time at 0.8 A cm^{-2}

Figure 5: Low frequency resistance change over time at @ 0.2 A cm^{-2} and 0.8 A cm^{-2}

The comparison of plots in Fig. 4 (a) and (b) for each doping level shows a variation in the difference between the two current density. The shrinking of impedance as the current increase is

because of the change of slope on the IV curve which is equivalent to the low frequency intercept of the impedance spectra with the real axis [15]. Thus, at higher current the low frequency resistance should be lower compared to at higher current density. However, in this case the doping level based slope change is seen. The difference in percentage was calculated to be 3.5 %, 9.8 % and 17 % for a doping level of 10.3, 8.3 and 7 mgH_3PO_4 /cm^2 respectively. This suggests that the voltage change with current density are different for the the differently doped MEAs. This is of interest to predict the performance with different doping levels.

4. Discussion

To have a direct comparison of three different MEAs, the resistances were normalised to 1. This was done by finding the maxima and minima from the data and plotting then in a scale of 0 to 1. The comparison graph is shown in Fig. 6. The fitting is shown only for the MEA with doping level of 10.3 mgH_3PO_4 /cm^2, while the other two doping levels are included as appendix in this Paper.

To map the doping level, hydrogen mass transport and current density, the normalized change in resistance is fitted with a function as defined by Eqn. 1 The time constants are similar for the high and low current density in this case and is around 3 min. However, the time constants for lower doping levels are higher and shows an increasing trend with decrease in doping level for both high and low current density measurements.

$$f(x) = a \times \exp(\frac{-x}{b}) + c \tag{1}$$

where a and c are constants and b is the time constant of function 'f'. In literature [16, 17, 18] it is reported that at high current densities the acid/water migrates from the cathode to the anode and back-diffuses at low current densities. The acid/water migrating to anode builds up a capillary force due to change in the concentration of PA which pushes the acid into the GDL and thereby hinders the pathway for the H_2. The opposite happens at higher current densities.

However, in the present case the acid doping level is 3 times lower compared to the reported one[16] and hence seems to behave in a different way. In the present case, the assumption that at low current density operation, the H_2 mass transport resistance decreases due to back diffusion of acid under the influence of concentration difference and at high current density (0.8 A cm^{-2})

the resistance increases due to migration into the GDL by the capillary force developed is not valid for low doped MEAs as shown in Fig. 5 and Fig. 6.

Becker et al. [17] used MEAs with doping level similar to the present study. They reported the acid is migrating from the cathode to the anode at high current density and back-diffusion happens at low current density using ohmic resistance measurement of the membrane. They reported a balancing of back diffusion and migration could be achieved with proper doping levels and width of the membrane. The relationship of back diffusion at steady-state is calculated using Fick's law as shown in Eqn. 2. A higher doping level increases back-diffusion and thinner membrane facilitates faster back-diffusion.

$$J_m = D \times \Delta[H_3PO_4]/w \tag{2}$$

A lower acid concentration also results in a thinner membrane compared to higher doped MEAs which swells with the acid uptake. Thus, the back-diffusion could be faster depending on which parameter of the two mentioned above is more dominant.

The possibility is that the migration of acid is taking place from the membrane to the anode catalyst under high current density operation and the capillary force generated which facilitates the drag of acid to the GDl is lower. The acid doping being low the concentration distribution of acid in the catalyst layer is possibly lower. Therefore, the migration of acid/water towards anode facilitates in the formation of more active three phase boundary closer to the catalyst active sites and hence H_2 access to the three phase boundary becomes easier and the transport of generated proton also becomes easier provided the acid has a connectivity to the membrane. This assumption is valid as many have reported the strong interaction of acid and PBI [19, 20] Another possibility is the influence of higher water generation leads to better proton conductivity which could be influencing the mass transport resistance.

The calculated time constant are shown in Table 1 In the present case, the flow rates are 1 L min^{-1} on both sides which corresponds to a stoichiometric ratio of above 80 on both sides with pure H_2 and O_2. Thus, the change in resistance arising due to cathode flow variation seems unlikely. The three doping levels have different time constant of rise and fall at low and high current densities. The highest time constants are for the MEAs with least doping. These time constants are calculated by fitting the mean of three measurements of each current density. This is a clear indication that the acid movement dynamics are influenced by the doping level.

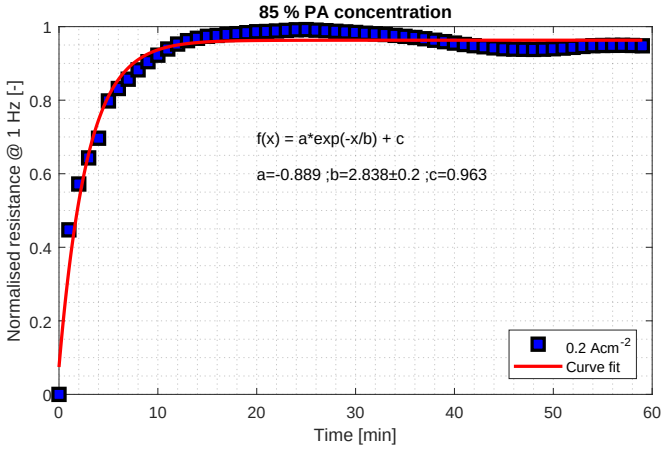

(a) Normalised resistance kinetics at 0.2 A cm^{-2}

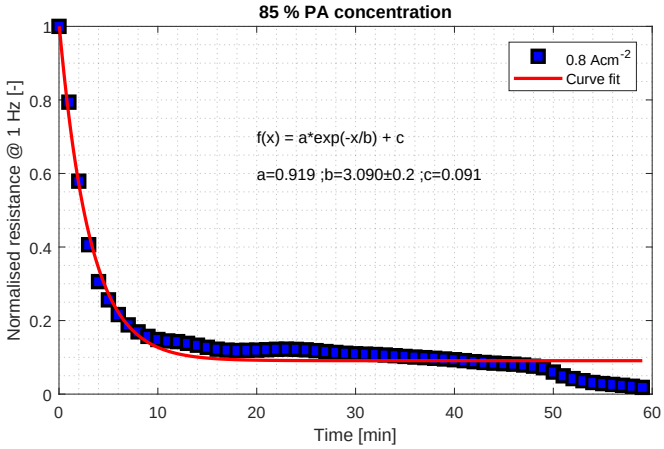

(b) Normalised resistance kinetics at 0.8 A cm^{-2}

Figure 6: Fitted resistances showing the time constants at @ 0.2 A cm^{-2} and @ 0.8 A cm^{-2}

To understand the phenomena better the resistance at 1 kHz was recorded over time. The Ohmic resistance also follows the same trend as the low frequency resistance as shown in Fig. 7. A similar result was reported in [18]. They saw a increase in high frequency intercept when the

Table 1: Time constant taken for the resistance to become stable at 0.2 A cm^{-2} and 0.8 A cm^{-2}

Cellname	Acid doping	Time constant (@0.2 A cm^{-2})	Time constant (@0.8 A cm^{-2})
	mgH_3PO_4 /cm^2	[min]	[min]
MEA 1	11	2.8±0.2	3.1±0.2
MEA2	8.3	5.7±0.5	3.3±0.5
MEA3	7	9.5±0.8	5.6±0.5

current was switched off and then an decrease in HFR when current was applied. They explained the phenomena based on hydration/dehydration of PA in the membrane.

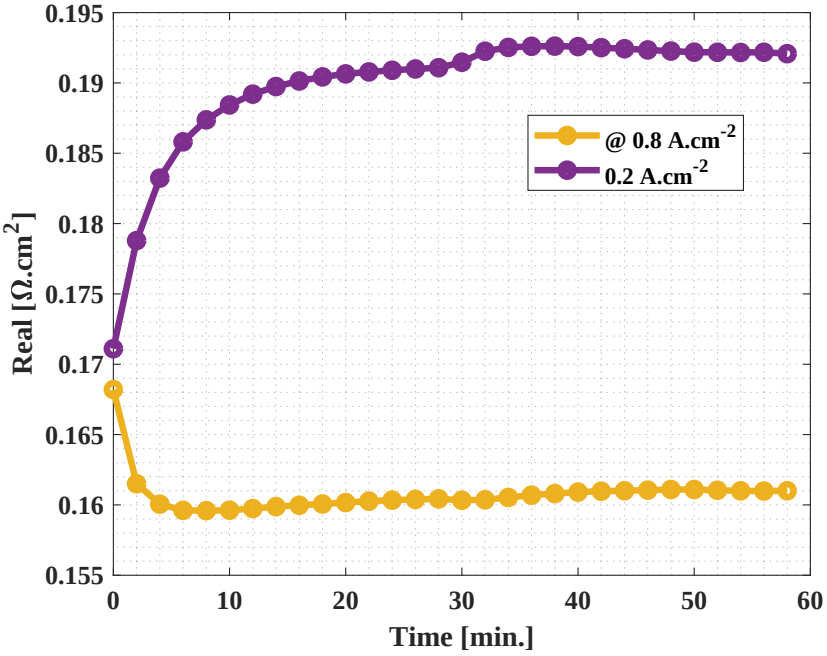

Figure 7: Ohmic resistance over time at 0.2 A cm^{-2}

5. Conclusion

Three MEAs with doping levels of 10.3, 8.3 and 7 mgH_3PO_4/cm^2 was investigated with EIS and modified EIS methods. The objective was to map the doping level, current density and H_2 mass transport resistance. A low current density of 0.2 A cm^{-2} and a high current density of 0.8 A cm^{-2} was selected. The tests were carried out to quantify issues related to acid/water migrating towards the cathode at high current density and back-diffusion when operating at low current density. The fast EIS of two different frequency region were used to quantify the process occurring at the anode. To ensure that the anode limitations are recorded the cathode was supplied with pure oxygen at a high stoichiometry and the anode supply was 5 % H_2 and 95 % N_2 mixture. The assumption here was the low H_2 concentration would enhance the anode effect and at the same time simulate the concentration at some portions of a fuel cell operating with reformed fuel.

At low current density the resistance at 1 Hz frequency and at 10 kHz increased immediately for a short time before getting stabilised. While on the other hand at high current density the resistance at both high and low frequency decreased before stabilizing. The low frequency region which is associated with mass transport (in this case H_2 mass transport) improved when the current was high for a short time before stabilizing and it degraded when the current was low.

The time constants for these changes in resistance were calculated as 2.8±0.2, 5.7±0.5 and 9.5±0.8 min and 3.1±0.2, 3.3±0.5 and 5.6±0.5 min for for 10.3, 8.3 and 7 mgH_3PO_4/cm^2 at 0.2 A cm^{-2} and 0.8 A cm^{-2} respectively.

The high frequency resistance measurement suggest that the changes seen in the low frequency is dominantly influenced by the changes in the proton conductivity of the membrane and the mass transport is not influenced by the current density when the doping levels are lower that $\approx$11 mgH_3PO_4/cm^2. This is an interesting finding as it suggest that when the doping level is low the GDL and MPL flooding and thereby loss of acid by evaporation is not a major issue in the durability of HT-PEMFC operating under load cycles. Another interesting aspect which could be deduced is the optimal acid doping level for HT-PEMFC to operate with minimal acid loss could be somewhere between 33 and 11 mgH_3PO_4/cm^2 as the first one has been investigated by others [4] suggesting flooding of GDL.

Acknowledgement

The authors would like to thank the Innovation Fund Denmark for funding the work through the 4M project. The authors are also thankful to Danish Power Systems for providing the MEA used in the experiment.

References

[1] Thomas J Schmidt. Durability and Degradation in High-Temperature Polymer Electrolyte Fuel Cells. *ECS Transactions*, 1(8):19–31, jun 2006. doi: 10.1149/1.2214541. URL http://ecst.ecsdl.org/content/1/8/19.abstract.

[2] Samuel Simon Araya, Fan Zhou, Vincenzo Liso, Simon Lennart Sahlin, Jakob Rabjerg Vang, Sobi Thomas, Xin Gao, Christian Jeppesen, and Søren Knudsen Kær. A comprehensive review of PBI-based high temperature PEM fuel cells. *International Journal of Hydrogen Energy*, 41(46):21310–21344, 2016. ISSN 03603199. doi: 10.1016/j.ijhydene.2016.09.024.

[3] Yuka Oono, Atsuo Sounai, and Michio Hori. Long-term cell degradation mechanism in high-temperature proton exchange membrane fuel cells. *Journal of Power Sources*, 210:366–373, jul 2012. ISSN 03787753. doi: 10.1016/j.jpowsour.2012.02.098. URL http://www.sciencedirect.com/science/article/pii/S0378775312005204.

[4] S. H. Eberhardt, T. Lochner, F. N. Büchi, and T. J. Schmidt. Correlating Electrolyte Inventory and Lifetime of HT-PEFC by Accelerated Stress Testing. *Journal of The Electrochemical Society*, 162(12):F1367–F1372, sep 2015. ISSN 0013-4651. doi: 10.1149/2.0591512jes. URL http://jes.ecsdl.org/lookup/doi/10.1149/2.0591512jes.

[5] C. Wannek, B. Kohnen, H. F. Oetjen, H. Lippert, and J. Mergel. Durability of ABPBI-based MEAs for high temperature PEMFCs at different operating conditions. *Fuel Cells*, 8(2):87–95, 2008. ISSN 16156846. doi: 10.1002/fuce.200700059.

[6] S Yu, L. Xiao, and B. C. Benicewicz. Durability Studies of PBIbased High Temperature PEMFCs. *Fuel Cells*, 8(34):165–174, jul 2008. ISSN 16156846. doi: 10.1002/fuce.200800024. URL http://doi.wiley.com/10.1002/fuce.200800024.

[7] Wiebke Maier, Tobias Arlt, Christoph Wannek, Ingo Manke, Heinrich Riesemeier, Philipp Krüger, Joachim Scholta, Werner Lehnert, John Banhart, and Detlef Stolten. In-situ synchrotron X-ray radiography on high temperature polymer electrolyte fuel cells. *Electrochemistry Communications*, 12(10):1436–1438, oct 2010. ISSN 13882481. doi: 10.1016/j.elecom.2010.08.002. URL http://www.sciencedirect.com/science/article/pii/S1388248110003474.

[8] Yuichi Aihara, Atsuo Sonai, Mineyuki Hattori, and Kikuko Hayamizu. Ion conduction mechanisms and thermal properties of hydrated and anhydrous phosphoric acids studied with 1H, 2H, and 31P NMR. *The journal of physical chemistry. B*, 110(49):24999–5006, dec 2006. ISSN 1520-6106. doi: 10.1021/jp064452v. URL http://www.ncbi.nlm.nih.gov/pubmed/17149922.

[9] Th Dippel, K. D. Kreuer, J. C. Lassègues, and D. Rodriguez. Proton conductivity in fused phosphoric acid; A 1H/31P PFG-NMR and QNS study. *Solid State Ionics*, 61(1-3):41–46, 1993. ISSN 01672738. doi: 10.1016/0167-2738(93)90332-W.

[10] Yunfeng Zhai, Huamin Zhang, Gang Liu, Jingwei Hu, and Baolian Yi. Degradation Study on MEA in H[sub 3]PO[sub 4]PBI High-Temperature PEMFC Life Test. *Journal of The Electrochemical Society*, 154(1):B72, jan 2007. ISSN 00134651. doi: 10.1149/1.2372687. URL http://jes.ecsdl.org/cgi/doi/10.1149/1.2372687.

[11] Zhenyu Liu, Jesse S. Wainright, Morton H. Litt, and Robert F. Savinell. Study of the oxygen reduction reaction (ORR) at Pt interfaced with phosphoric acid doped polybenzimidazole at elevated temperature and low relative humidity. *Electrochimica Acta*, 51(19):3914–3923, may 2006. ISSN 00134686. doi: 10.1016/j.electacta.2005.11.019. URL http://www.sciencedirect.com/science/article/pii/S0013468605012922.

[12] S. H. Eberhardt, F. Marone, M. Stampanoni, F. N. Büchi, and T. J. Schmidt. Quantifying phosphoric acid in high-temperature polymer electrolyte fuel cell components by X-ray tomographic microscopy. *Journal of Synchrotron Radiation*, 21(6):1319–1326, nov 2014. ISSN 1600-5775. doi: 10.1107/S1600577514016348. URL http://www.ncbi.nlm.nih.gov/pubmed/25343801http://scripts.iucr.org/cgi-bin/paper?S1600577514016348.

[13] Sobi Thomas, Jakob Rabjerg Vang, Samuel Simon Araya, and Søren Knudsen Kær. Experimental study to distinguish the effects of methanol slip and water vapour on a high temperature PEM fuel cell at different operating conditions. *Applied Energy*, 192:422–436, apr 2016. ISSN 0306-2619. doi: http://dx.doi.org/10.1016/j.apenergy.2016.11.063. URL http://linkinghub.elsevier.com/retrieve/pii/S0306261916316488http://www.sciencedirect.com/science/article/pii/S0306261916316488.

[14] S. M. Rezaei Niya, R. K. Phillips, and M. Hoorfar. Sensitivity Analysis of the Impedance Characteristics of Proton Exchange Membrane Fuel Cells. *Fuel Cells*, 16(5):547–556, jul 2016. ISSN 16156854. doi: 10.1002/fuce.201600060. URL http://doi.wiley.com/10.1002/fuce.201600060.

[15] M Chandesris, C Robin, M Gerard, and Y Bultel. Investigation of the difference between the low frequency limit of the impedance spectrum and the slope of the polarization curve. *Electrochimica Acta*, 180(JANUARY):581–590, 2015. ISSN 00134686. doi: 10.1016/j.electacta.2015.08.089. URL http://linkinghub.elsevier.com/retrieve/pii/S001346861530339X.

[16] S. H. Eberhardt, M. Toulec, F. Marone, M. Stampanoni, F N Büchi, T. J. Schmidt, F. N. Buchi, and T. J. Schmidt. Dynamic Operation of HT-PEFC: In-Operando Imaging of Phosphoric Acid Profiles and (Re)distribution. *Journal of The Electrochemical Society*, 162(3):F310–F316, jan 2015. ISSN 0013-4651. doi: 10.1149/2.0751503jes. URL http://jes.ecsdl.org/content/162/3/F310.abstracthttp://jes.ecsdl.org/cgi/doi/10.1149/2.0751503jes.

[17] Hans Becker, Lars Nilausen Cleemann, David Aili, Jens Oluf Jensen, and Qingfeng Li. Probing phosphoric acid redistribution and anion migration in polybenzimidazole membranes. *Electrochemistry Communications*, 82(July):21–24, 2017. ISSN 13882481. doi: 10.1016/j.elecom.2017.07.005. URL http://dx.doi.org/10.1016/j.elecom.2017.07.005.

[18] K. Wippermann, C. Wannek, H.-F. Oetjen, J. Mergel, and W. Lehnert. Cell resistances of poly(2,5-benzimidazole)-based high temperature polymer membrane fuel cell membrane electrode assemblies: Time dependence and in-

fluence of operating parameters. *Journal of Power Sources*, 195(9):2806–2809, may 2010. ISSN 03787753. doi: 10.1016/j.jpowsour.2009.10.100. URL http://www.sciencedirect.com/science/article/pii/S0378775309019776.

[19] R Zeis. Materials and characterization techniques for high-temperature polymer electrolyte membrane fuel cells. *Beilstein Journal of Nanotechnology*, 2015. URL http://www.beilstein-journals.org/bjnano/content/html/2190-4286-6-8.html.

[20] Proton Motor fuel cell powers hybrid mid-size commercial truck. *Fuel Cells Bulletin*, 2013(10):2–3, 2013. doi: http://dx.doi.org/10.1016/S1464-2859(13)70339-0. URL http://www.sciencedirect.com/science/article/pii/S1464285913703390.

Appendix

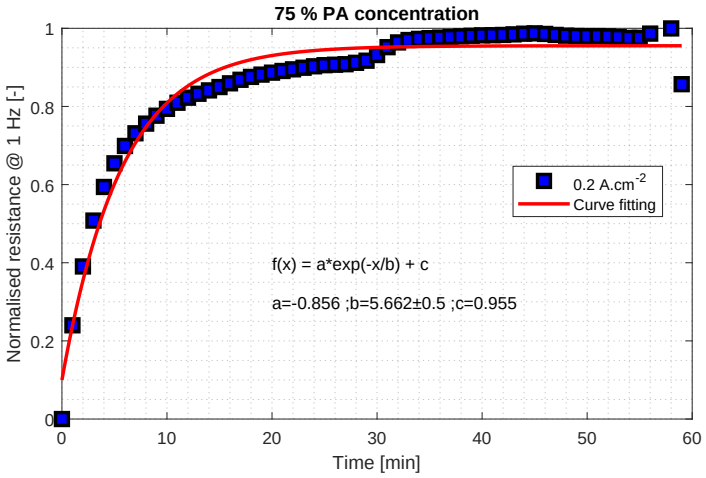

(a) Real part of the resistance @ 0.8 A cm^{-2}

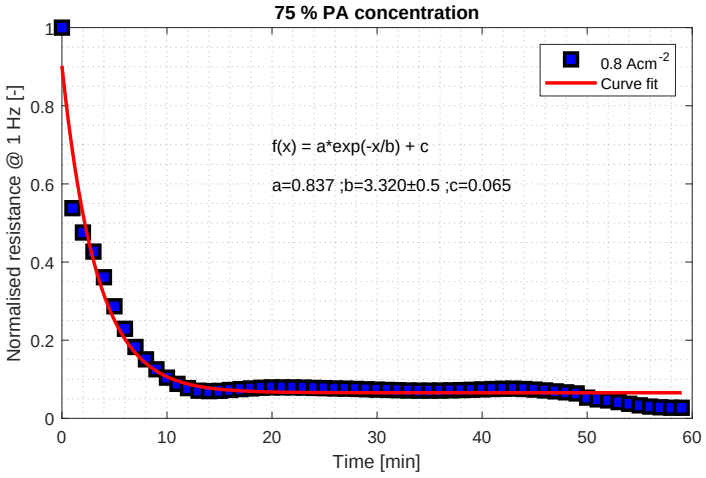

(b) Normalised resistance kinetics at 0.8 A cm^{-2}

Figure 8: Fitted resistances showing the time constants at @ 0.2 A cm^{-2} and @ 0.8 A cm^{-2}

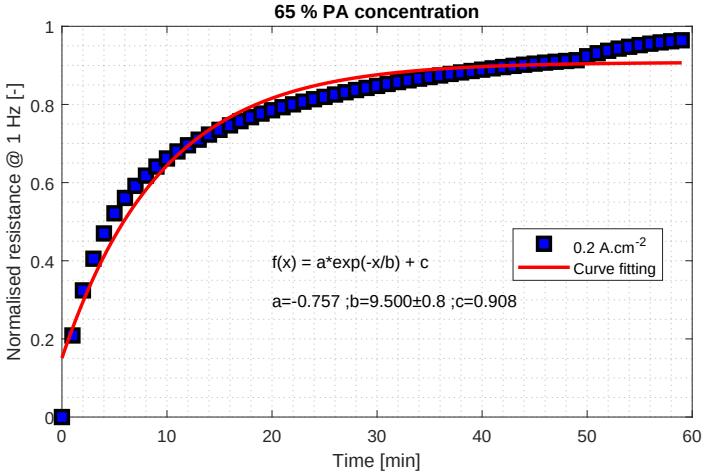

(a) Real part of the resistance @ 0.8 A cm^{-2}

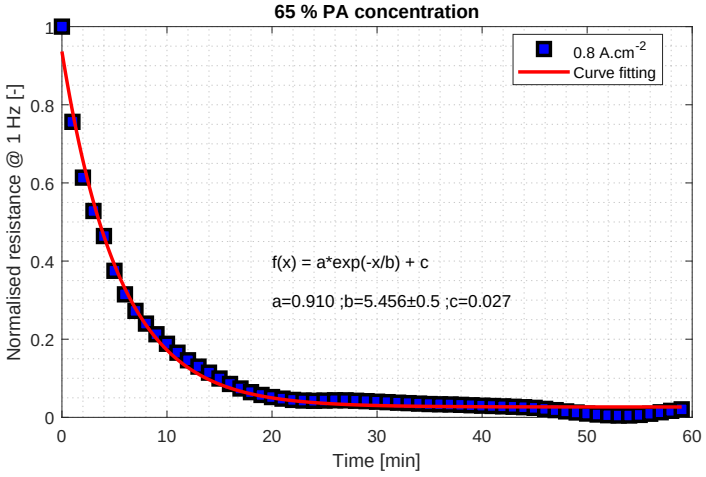

(b) Normalised resistance kinetics at 0.8 A cm^{-2}

Figure 9: Fitted resistances showing the time constants at @ 0.2 A cm^{-2} and @ 0.8 A cm^{-2}

Paper E

New Load Cycling Strategy for Enhanced Durability of High Temperature Protom Exchange Membrane Fuel Cell

Sobi Thomas, Christian Jeppesen, Thomas Steenberg, Samuel Simon Araya, Jakob Rabjerg Vang, Søren Knudsen Kær

The paper has been published online in the
International Journal of Hydrogen Energy.

The layout has been revised.

New Load Cycling Strategy for Enhanced Durability of High Temperature Proton Exchange Membrane Fuel Cell

Sobi Thomas[a,*], Christian Jeppesen[a], Thomas Steenberg[b], Samuel Simon Araya[a,*], Jakob Rabjerg Vang[a], Søren Knudsen Kær[a]

[a]*Department of Energy Technology, Pontoppidanstræde, Aalborg University, Aalborg East -9220, Denmark*
[b]*Danish Power Systems, Egeskowej 6c, DK-3490 Kvistgaard, Denmark*

Abstract

The objective of this paper is to develop a new operational strategy to increase the lifetime of a high temperature proton exchange membrane (HT-PEMFCs) fuel cell system by using load cycling patterns to reduce the phosphoric acid loss from the fuel cell. Four single cells were operated under different current cycling profile, while one cell was operated at constant current density for comparison. Polarization curves and electrochemical impedance spectroscopy measurements were recorded during the course of the tests and analysed. Two different current densities, 0.2 $\mathrm{A\,cm^{-2}}$ for the lower end and 0.8 $\mathrm{A\,cm^{-2}}$ for the higher end, were selected for the load cycling operation. The relaxation time, which is the period of time spent at low current density operation, is varied to understand how the performance over prolonged period behaves. The duration of the high current density operation is selected based on the relaxation time in order to have the same average current density of (0.55 $\mathrm{A\,cm^{-2}}$) for all the cells. Cell 5, with a relaxation time of 2 min performs best and shows lower degradation rate of 36 $\mu\mathrm{V\,h^{-1}}$ compared to other load cycling cells with smaller relaxation times. The cell operated at constant current density shows a degradation rate of 57 $\mu\mathrm{V\,h^{-1}}$, which is 1.5 times higher than the degradation rate of cell 5.

Keywords: Load cycling, Impedance, Fuel cell, high temperature PEM, Phosphoric acid

*Corresponding author
Email addresses: sot@et.aau.dk (Sobi Thomas), ssa@et.aau.dk (Samuel Simon Araya)

1. Introduction

High temperature polymer electrolyte membrane fuel cells (HT-PEMFCs) are promising combined heat and power (CHP) sources with a higher combined efficiency compared to conventional low temperature PEM fuel cells. The advantages of HT-PEMFCs are various in terms of higher tolerance to poisonous gases like CO and H2S due to decreased adsorption and faster reaction kinetics [1], no or less complex humidification system required as the proton conductor in these type of fuel cells are phosphoric acid (PA) and not water. They also generate useful heat, which can be utilized and the combined CHP efficiency is quite high (>75% upto 85% as reported in these literatures) [2, 3]. However, there are also some hurdles, with durability and reliability being the major ones, due to different degradation mechanisms, including loss of electrolyte. The phosphoric acid (PA) in HT-PEMFCs, which acts as an electrolyte is quite mobile. This leads to acid loss during different operating conditions, and therefore, the proton conductivity of the membrane is affected negatively.

Lang et al. [4], carried out long and short-term degradation tests to quantify the effect of acid loss on the performance of an HT-PEMFC. The degradation was higher for short water stress test, which involved higher humidification on the anode and cathode. The test results in terms of impedance and polarization measurements confirmed that the cell degradation was dominated by the acid leaching from the membrane. Rastedt et al. [5] carried out different operational strategies to understand the effects on PA loss. The different operational modes included start/stop, different fuel compositions and long time durability tests. The results indicate minimal effect on PA loss with varying operational strategies. Wannek et al. [6] carried out experiments to understand the influence of acid injecting methodology. The analysis showed no or minimal differences in performance with pre-doped or post-doped MEAs. It was reported that the acid redistribution to reach an equilibrium took several hours. However, the acid distributed on the membrane within a few hours is enough to draw reasonable performance.

Chevalier et al. [7] developed a pore network model to understand the role of micro porous layer (MPL) in the redistribution of PA in the gas diffusion electrode (GDE). The model predicts that the presence of MPL mitigates partially the acid leaching from the catalyst layer (CL) to the flow-field. Galbiati et al. [8] investigated the activation period with different procedure to understand the break-in. An MEA exposed to atmosphere before activation procedure showed a loss but the voltage development during activation was recorded same.

Eberhardt et al. [9] investigated the redistribution of PA in an HT-PEMFC using X-ray tomographic microscopy imaging. The most influencing factor for acid movement from the cathode to the anode was acid doping level and the current density. At higher doping levels and high current density (> 0.4 $A\,cm^{-2}$) , the migration rate increased significantly. In another work by the same group [10], the effect of different operating parameters on the PA loss by evaporation was evaluated by condensation at outlet and accelerated stress test. The parameters considered were current density, gas flow rate and cell temperature. Based on the experiments, a lifetime prediction was calculated as a function of current density and temperature [10]. The influence of current density, different materials and varying PA content was examined to determine the effect of PA migration. The increase in current density above 0.4 $A\,cm^{-2}$ showed an increase in the migration of acid from the anode to the cathode under the influence of higher capillary pressure from the GDE pores. Also, a higher PA loading leads to higher acid migration, with similar behaviour for the different materials [11].

Eberhardt et al. [12] investigated synchrotron-based X-ray tomographic to determine the local distribution of PA in HTPEMFC. The method was developed at room temperature, which they proposed could be further applied in-operando cells with slight modifications to understand the PA migration and redistribution. The same authors [13] investigated the dynamic operation PA redistribution under two different load profiles. The acid migration from the cathode to anode under the influence of current was shown using imaging. The acid migration towards anode GDE and flow-field was reported to be faster than the back diffusion of PA under low current density (0.2 $A\,cm^{-2}$). The process of acid migration is shown to be not completely reversible, some of the acid gets stuck to the flow field and is removed by the gas.

The focus to date has been on understanding the PA migration and redistribution. Only limited number of mitigation strategies has been proposed in the literature. The proposed strategies mostly focus on modified GDE/MPL structures [14, 15, 16].

In this paper, we propose a new operation based strategy to deal with the acid movement towards the anode and thereby decreasing the degradation due to acid loss. The efficiency calculated from the operation is improved marginally. Current cycling tests between a high current density of 0.8$A\,cm^{-2}$ and a low current density of 0.2 $A\,cm^{-2}$ were performed in order to understand how the electrolyte loss could be avoided. The rest time, also described as relaxation time in this work is defined as the period of time the cell is operated at a low current density of

0.2 A cm^{-2} in order to relieve the cell of the high current density stresses.

The focus was to determine the time constants for the flooding and de-flooding of the anode GDE by the migration of acid from the cathode to the anode. The current load strategy is modified to prevent the acid moving towards anode from getting detached and thereby keeping the acid as much as possible within the cell for a longer lifetime. An increase in lifetime is predicted based on the impedance and the voltage inventories.

2. Experimental setup and procedure

This section presents the experimental setup and the procedure followed for the tests. To verify the effect of load cycling on HT-PEM fuel cells, the method is tested on five membrane electrode assemblies (MEAs), where only the duty cycle of the load cycling has been changed. The tests are carried out to evaluate different operational methods to improve the efficiency and lifetime of an HTPEM fuel cell system. The focus is to retain PA in the membrane for a longer period by reducing the PA losses, while also running at higher current density. During the experiments, the average current density is kept constant for all 5 MEAs. The MEAs tested in this work are phosphoric acid-doped PBI-based with platinum as catalyst manufactured by Danish Power Systems

2.1. Test setup

The MEAs are tested in an in-house built five single cell test stand, shown in Fig. 1. The test stand has the ability to record impedance spectroscopy, I-V curves and perform load cycling with varying duty cycles. The assemblies are heated to 160 °C by electric heaters, which are controlled by the fuel cell control system. Two different computer systems handle the data acquisition: an NI-9024 cRIO which controls the fuel cell sequence, temperature, gas mass flow etc. and an NI real time system with a PCIe-6259 installed, controls the electrochemical impedance spectroscopy (EIS) measurements. The NI real time system takes over the control of the electronic loads during EIS measurements. The data logging is carried out at 0.04 Hz during normal operation and load cycling.

For controlling the gas flow, two Bürkert mass flow controllers (MFC) are installed for each of the assemblies. The air MFCs have a range of 0-5 NL min^{-1} , while the hydrogen MFCs have a range of 0-1 NL min^{-1}. The anode gas is supplied from compressed hydrogen bottles and

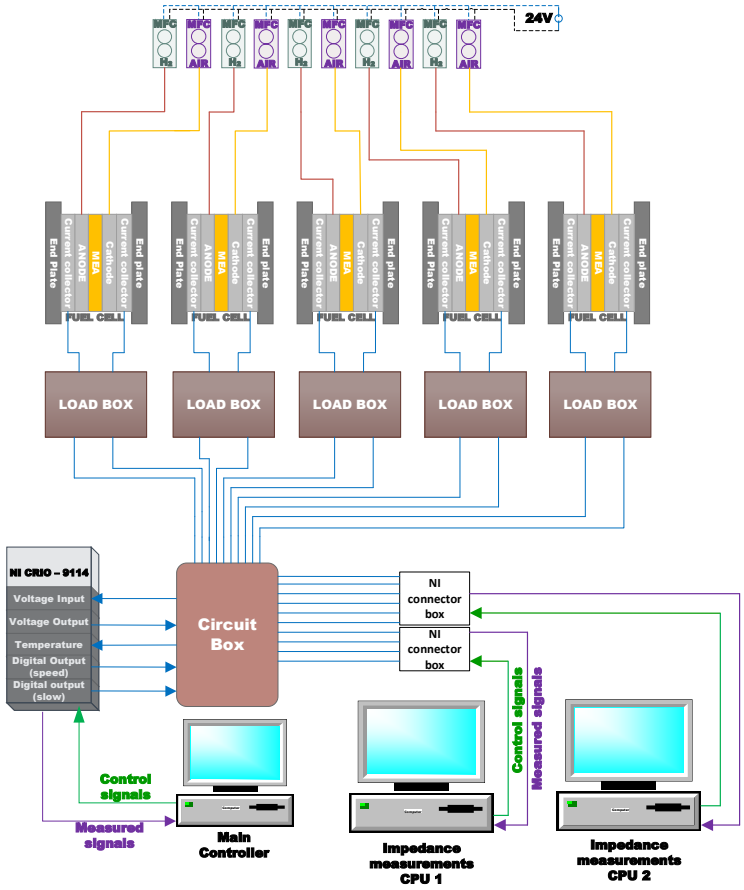

Figure 1: **Schematic of in-house build five single cell test bench.**

the cathode air is supplied from an oil free compressor with a pre-particle filter. The anode and cathode gases are not pre-humidified or preheated. Five TDI RBL-488 electronic loads with a 20 kHz bandwidth controls the fuel cell load current with a current range of 0-150 A.

The EIS measurements are conducted in galvanostatic mode by imposing a small sinusoidal signal (5% of the DC signal) on top of the DC signal, and by measuring the resulting voltage amplitude and phase shift, the impedance can be estimated at any frequency. The frequency

sweep is from a start frequency of 10 kHz to an end frequency of 0.1 Hz, with 10 points per decade. The sinusoidal current signal amplitudes are automatically adjusted in order to maintain a desired RMS amplitude of the responding voltage signal.

2.2. Test procedure

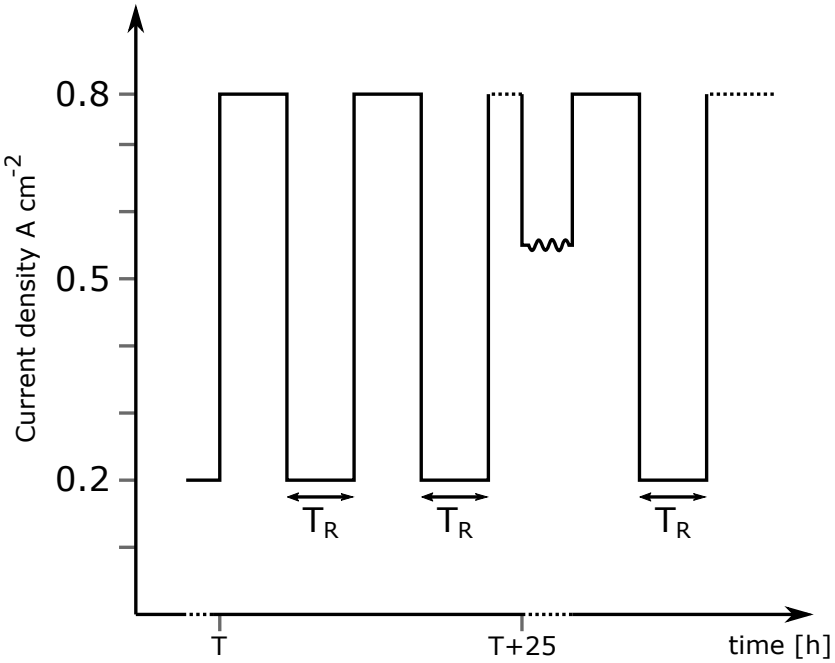

Figure 2: **Experimental procedure for MEA 2 - 5 after the break-in. The load cycling is conducted with a rest time (T_R) and interrupt every 25** hr **for a EIS measurement at 0.55** A cm^{-2}**. The dashed lines indicate a jump in time.**

Before the experiment, all 5 MEAs were operated at 0.2 A cm^{-1} for 100 h for a proper break-in, during which a temperature of 160 C and stoichiometric ratios of λ_{air}=2 and λ_{H_2}=1.5 were maintained. After the break-in procedure, an EIS measurement was conducted, followed by a polarization curve.

After the break-in procedure, MEA 2 - 5 were operated under current load cycling mode, with 0.2 A cm^{-1} at the low current load and 0.8 A cm^{-1} for the high current load. During load

cycling the rest time ((T_R) at the low current load is changed for the MEAs 2 - 5, and the duration at the high current load is adjusted for achieving an average current density 0.55 A cm^{-1}. The rest time ((T_R) for each cell and the time of operation @ 0.8 A cm^{-1} is shown in Table 1. The time in the last column of Table 1 refers to the total operation time.

Table 1: **Rest time, experimental duration and flow mode for the 5 MEAs of experimental subject in this work.**

MEA (No.)	**Time @ 0.2**A cm^{-1} (s)	**Time @ 0.8**A cm^{-1} (s)	**Time** (h)
1	-	-	2000
2	15	21	775
3	30	42	1600
4	60	84	2000
5	120	168	2000

As illustrated in Fig. 2, the load cycling is interrupted every 25 h for an EIS measurement, which is conducted at 0.55 A cm^{-1}. Every 500 h after the break-in procedure a polarization curve was recorded. For the load cycles the anode and cathode flow rates were kept constant at a flow rate corresponding to the high current load.

3. Equivalent circuit modelling

To better understand the EIS data, an equivalent circuit model was fitted to the impedance plot and different resistances were calculated. The model used in the present study is shown in fig. 3.

The fitting of this model to the EIS data was performed using MATLAB function Zfit [17]. The circuit consists of a parallel resistor (RL) and inductor (L), accounting for inductance in the high frequencies, followed by a series resistor which was attributed to the high frequency real axis intercept and two resistor(R)-capacitor(C) loops accounting for the intermediate and low frequency arcs of the spectrum. These electrical components (R, C, & L) represented in the model, relate to different physical meaning in the cells [18]. The R & L loop is related to the setup wiring inductance which is prominent in the high frequency part of the EIS. The series resistance

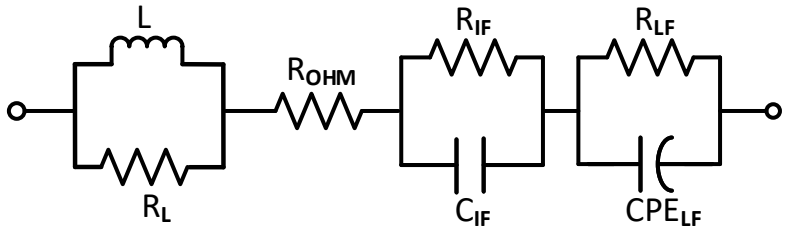

Figure 3: **Equivalent circuit model used for fitting impedance data**

is dominated by the membrane ohmic resistance. While the R & C loops are a combination of cathodic, anodic and the channel dynamics [19, 20].

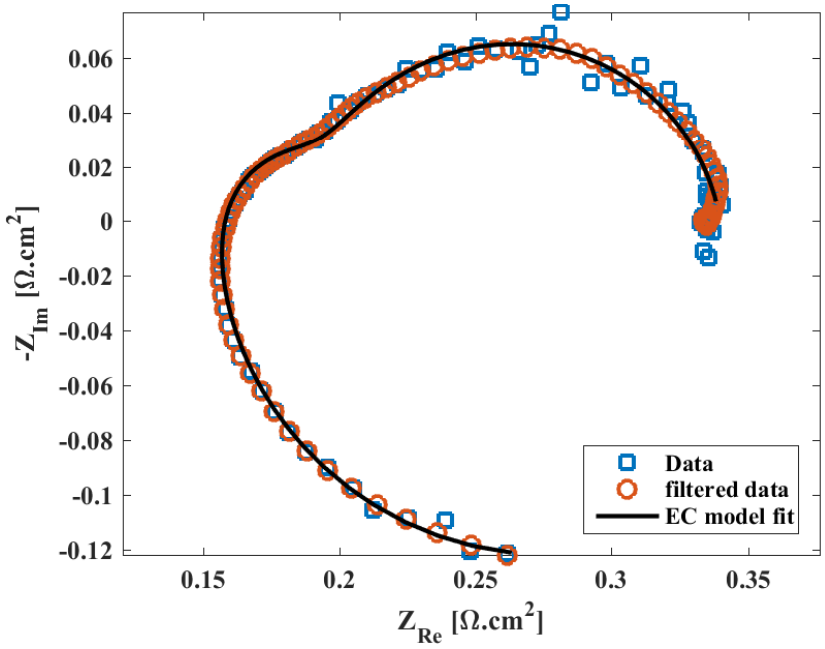

Figure 4: **An example of the fitted model**

The low frequency loop consists of a constant phase element (CPE) instead of a pure ca-

pacitor to account for the depressed shape of the spectra. The impedance of a CPE is given in Equation (1);

$$Z_{\mathrm{CPE}} = \frac{1}{Q(j\omega)^c} \tag{1}$$

The exponent of CPE element 'c' was fixed at 0.9 and the fit quality obtained was good which can be seen from Fig. 4. The value of 'c' was kept constant to obtain a better fit as well as to be closer to realistic capacitor element as suggested in the literature [19].

The quality of the circuit fitting is shown in Fig. 4. The data has some noises in the low frequency region, which was filtered out using 'rloess' function in Matlab. The function is a modified version of locally weighted polynomial regression (LOESS). The function 'LOESS' carries out a local regression using weighted linear least square and a second order polynomial model. The function 'RLOESS' in addition to the regression model assigns lower weights to outliers and assigns zero weight to data outside six mean absolute deviations [21].

4. Results and discussion

In this section, the results are presented in terms of voltage inventory and I–V curves recorded during the experiment. The different cell voltages are not directly comparable because of the differences among the MEAs and the single cell set-up resistances. Thus, the results are analysed based on the trend followed by each cell, rather than using the absolute performance values to compare the cells to each other.

4.1. Experimental results

The experiments were designed for five different cells over a period of 2000 h or a minimum cell voltage of 0.3 V. Three cells (1, 4 and 5) managed to run for a period of 2000 h, while the voltage of cell 2 went below 0.3 V after 775 h and cell 3 failed after 1600 h.

4.1.1. Voltage development

The comparison of voltage trajectories over time, shown in fig. 5, reveals the different degradation rates with varying operational strategies. Cell 2 and Cell 3 degraded much faster compared to the other cells with a higher relaxation time. Cell 1 (constant current density operation) has a degradation slope comparable to cell 4 and cell 5. Cell 5 performs best compared to all the other

cells. However, this cannot be taken as a comparison parameter as the voltages after break-in for cell 5 is higher than the rest. Thus, to have a better comparison between the different cells the degradation rate of each cell at the end of the test was calculated in $\mu V\,h^{-1}$.

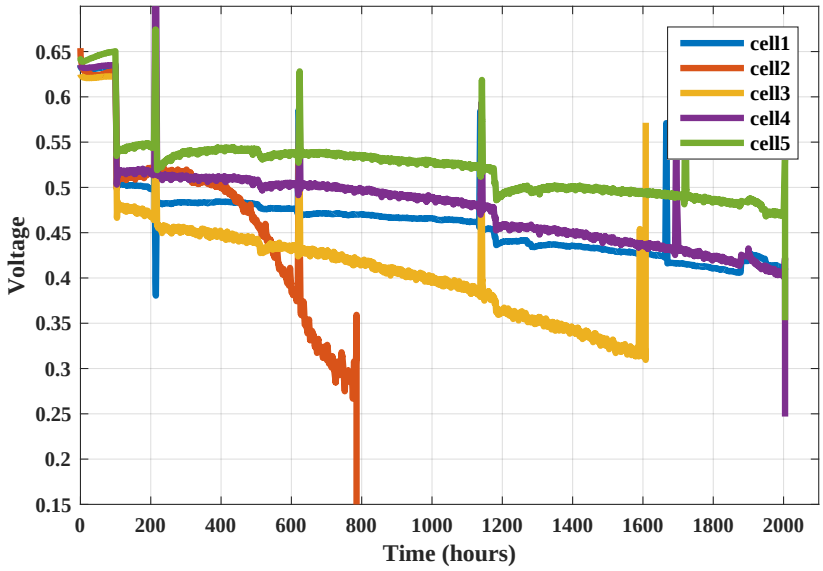

Figure 5: **Cell voltage inventory for five different cells**

The degradations are shown in Table 2 . The degradations were calculated for the high, low and the average current density. The degradation rate is higher at 0.8 $A\,cm^{-2}$ compared to 0.2 $A\,cm^{-2}$ for all cells as expected at higher current density. The degradation at higher current density was assumed to be a direct co-relation to acid migration. The platinum agglomeration at higher current density is lower as reported by Zhai et al. [22]. Thus, the higher degradation rate at higher current density could be attributed to membrane degradation. The degradation for cell 5 is the lowest and is comparable to the ones reported in various literature. However, it is difficult to have a direct comparison, as the MEA manufacturing process and the operating conditions may vary significantly. Taccani et al. [23] reported a degradation of 44 $\mu V\,h^{-1}$ when operated under load cycling between open circuit voltage (OCV) and 0.5 $A\,cm^{-2}$. They attributed the degradation to acid loss and catalyst activity loss as a consequence of OCV operation. Schmidt and

Baurmeister [24]. reported a degradation of 11 $\mu V\,h^{-1}$ when operating under star-stop cycling, with a time period of 12 h of constant current at 0.2 $A\,cm^{-2}$ and 12 h of complete shutdown. They concluded that the main degradation mechanism during the start/stop cycling was the electrolyte flooding of the cathode due to corrosion of the cathode catalyst support.

Table 2: **Degradation calculated at low, high and average current density.**

MEA (No.)	**Rest time (T_R)** (min)	**Duration** (h)	**Degradation** ($\mu V\,h^{-1}$)
1	-	2000	57
2	15	775	460
3	30	1600	109
4	60	2000	52
5	120	2000	36

Schonvogel et al. [25] carried out accelerated stress test by load cycling between 1 $A\,cm^{-2}$ and 0.6 $A\,cm^{-2}$ to understand the degradation due to acid loss and the reported values for a test of 230 h was 116 $\mu V\,h^{-1}$ at 0.6 $A\,cm^{-2}$ and 126 $\mu V\,h^{-1}$ at 1 $A\,cm^{-2}$. However, a direct comparison is not possible as the MEAs used in their experiments had very high acid doping compared to the ones reported in this manuscript. In another test, two different MEAs were tested under load cycling between 0.2 $A\,cm^{-2}$ and 0.6 $A\,cm^{-2}$ with each load at 30 min and a step at OCV for 2 min. The degradation rate reported was 27.9 and 41.3 at low and high current density [26].

The degradation is the lowest for cell 5, while cell 2 has the highest degradation. This stresses the fact that the degradation rate can be varied by cycling the load between 0.2 $A\,cm^{-2}$ and 0.8 $A\,cm^{-2}$. The lower degradation with higher relaxation time is assumed to be due to reduced acid loss from the cell. The claim will be further elaborated in the subsequent sections using the different resistances obtained from the EIS measurements.

The reason for higher degradation with faster load cycling has been linked to combined effect of higher loss in electrochemical surface area as reported by other researchers [27, 28] and also acid accumulation and loss over time. However, in the present test the loads are never going to open circuit voltage which enhances platinum agglomeration as seen by Javier Pinar et al. [27]. Thus, membrane degradation becomes a more pronounced reason for performance loss.

4.1.2. I-V curve comparisons

The I–V curves before and after the tests are shown in Fig. 6. They were recorded at a current ramp rate of 0.11 A cm^{-2} min^{-1} from OCV up-to a maximum current density of 1.11 A cm^{-2}. The performance at the beginning (after break-in) indicates small differences among the different MEAs. Hence, it becomes difficult to compare them among each other, and therefore, the absolute values are not considered.

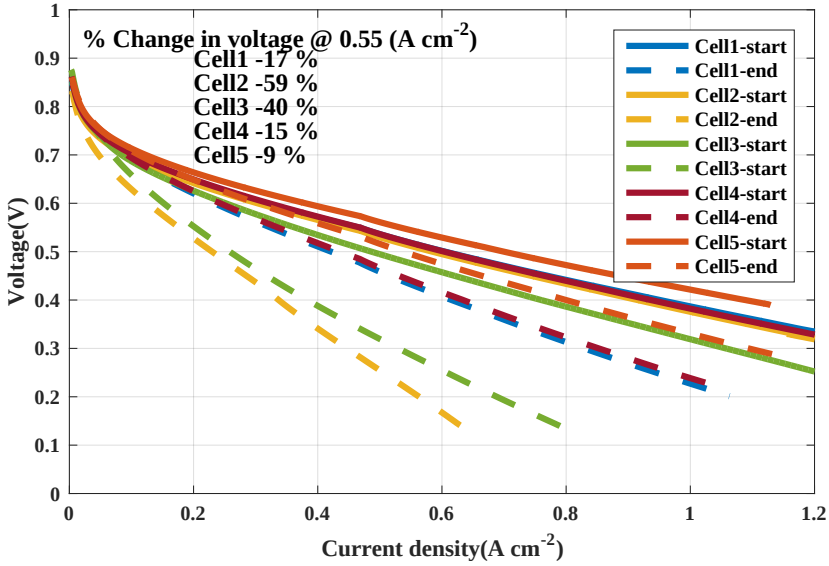

Figure 6: **I-V curve of the five cells recorded after the break-in**

The solid lines in Fig. 6 are recorded immediately after the break-in. The difference in the performance among different cells is minimum after break-in. The differences become more dominant after the load cycling with different relaxation times. The percentage change in voltage for each cell at 0.55 A cm^{-2} between the start and the end of test was calculated from the I–V curve and is shown in Fig. 6. The voltage changes are in the following order, cell 5 < cell 4 < cell 1 < cell 3 < cell 2.

The differences in the IV curves shows that cell 2 and cell 3 degrades much faster compared to the other cells. The voltage difference at 0.55 A cm^{-2} after the break-in is calculated as 12% and

the variation becomes 57% after the completion of the test which suggests that the degradation rates are different for all the different operations presented. These percentage changes account for the variations among different MEAs. To highlight the better performance of cell 5 compared to cell 1, the voltage variation before and after the test was calculated. The voltage at 0.55 A cm^{-2} varied 5% at the beginning and 13% after the test. This is a clear indication that load cycling between 0.8 A cm^{-2} and 0.2 A cm^{-2} with a rest time of 2 min assists in reducing the performance loss over time.

4.1.3. Equivalent circuit model fitting and resistances

The evolution over time of the fitted resistances, namely series resistance, intermediate and low frequency resistances are shown in Figs. 7– 9. The jump in series resistance at time ~200 and ~1100 h are related to unexpected stops due to unexpected software/hardware issues. The interesting fact is that for all cells, the series resistance increases after the stop. However, for cell 5 and cell 1 the resistances decreases over time, while the other cells do not show a significant decrease. The decrease in ohmic resistance over time after the stop is more dominant for cell 5 compared to cell 1. This is an interesting fact because when the fuel cell is stopped a change in the water-acid equilibration takes place and the acid moves to catalyst and GDL. When the cells were restarted, the resistance is high as expected due to the dehydration of the membrane. Then, the cycling between 0.2 A cm^{-2} and 0.8 A cm^{-2} probably results reversible degradation. The decreasing trend over time is assumed to be an effect of the load-cycling which is attributed to reversible degradation being initiated due to load cycling. The most dominant factor assumed is the acid displaced to the catalyst and the gas diffusion layer moving back to the membrane leading to better ion conductivity and also higher active site present for reaction to take place. This suggests that load-cycling could probably be also helpful when unexpected stops occur during operation.

The slope of the increase in the ohmic resistance is lowest for cell 5 as can be seen from Fig.7. The differences in series resistance, which is usually attributed to the membrane resistance (also contributed by contact and electrical resistance of GDE and other components), suggest a lower degradation of the membrane [29, 30]. The membrane resistance is inversely proportional to the acid loss from the membrane. This is a clear indication that cycling the current between 0.2 A cm^{-2} and 0.8 A cm^{-2} with a relaxation time of 2 min helps in reducing the acid loss from the cell.

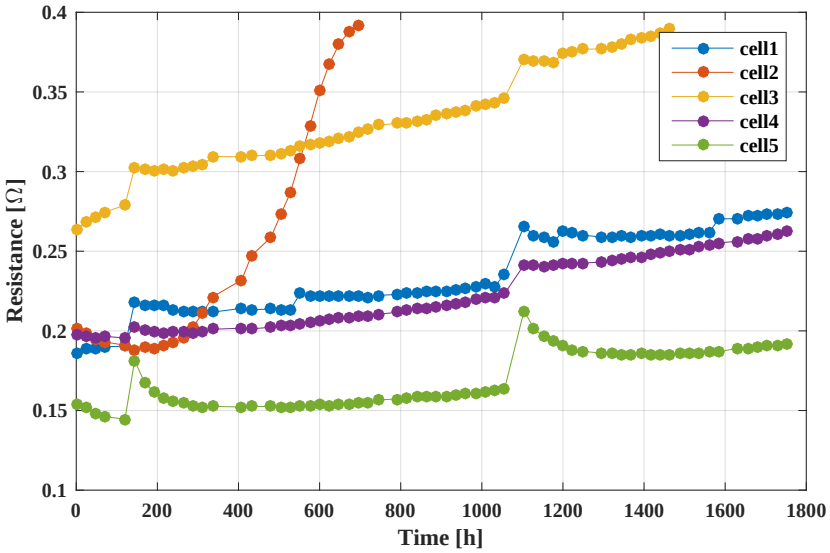

Figure 7: **Ohmic resistances as fitted using the equivalent circuit model.**

The intermediate frequency resistance shown in Fig. 8 starts with similar resistance after the break-in for all the cells and then increases with a similar slope for cell 1, cell 4 and cell 5, while cell 3 shows a steeper increase and the resistance of cell 2 increases even more dramatically. The intermediate frequency loop primarily accounts the cathode processes. However, based on the circuit chosen it is sometimes interpreted as diffusion losses and/or anode polarization [19]. Thus, a higher acid loss or flooding of GDE and/or catalyst may induce an increase in this resistance. The steep increase in cell 2 resistance could be attributed to accumulation of acid on the anode GDE and catalyst, which hinders the diffusion process and also contributed by a acid flooding of catalyst layer on the cathode. The high current density operation generates higher water content on the cathode which has a tendency to attract the acid and thereby flooding the catalyst and oxygen reduction reaction slows down. This is apparent from the lower effects seen in the intermediate frequency for the cells operating with higher rest time. A higher rest time facilitates the sweeping away of excess water produced during the high current density operation, thus, mitigating the cathode related degradation due to acid flooding the catalyst.

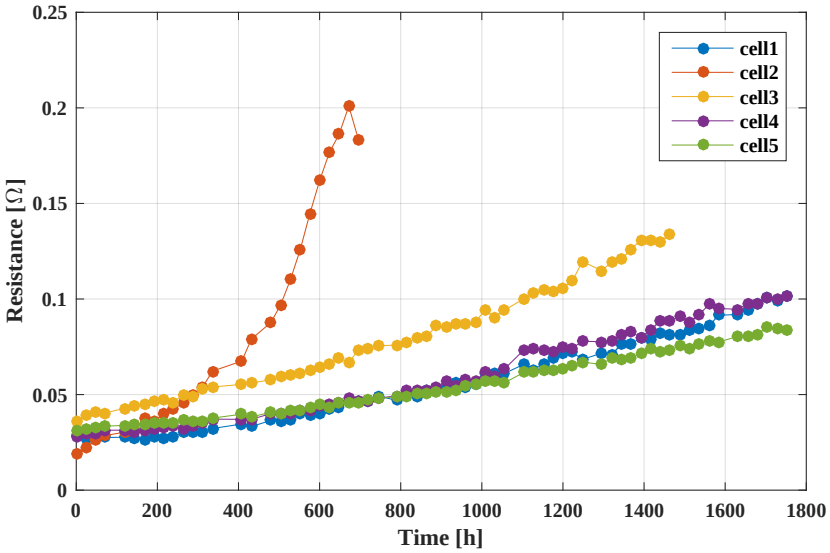

Figure 8: **Intermediate frequency resistances as fitted using the equivalent circuit model.**

The low frequency resistance is shown in Fig. 9. In the literature, this is attributed to mass transport issues, channel dynamics [31]. The low frequency resistance for all the cells except cell 2 stays low and minimal changes are seen. The increase in cell 2 resistance is linked with the acid accumulation on the flow channels, GDE and catalyst. This accumulation restricts the gas flow to the three phase boundary, which in turn increases the mass transport resistance. The fact that the different cells start with similar resistances after the break-in confirms that the effects seen are due to the cycling strategies.

4.2. Effect of load cycling with different time period of relaxation)

The effect of different operating strategies are compared in terms of different resistance changes, power and efficiency.

4.2.1. Resistance development

The resistances shown in Figs. 7 – 9 were further analysed to understand the phenomena taking place when the operating conditions were changed. In Table 3, the initial and final resis-

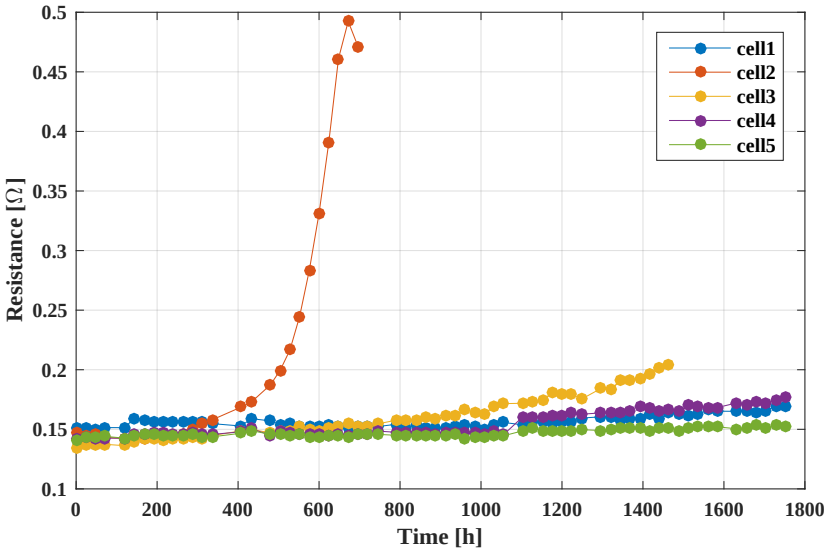

Figure 9: **Low frequency resistances as fitted using the equivalent circuit model.**

tances, the change in resistance and the test duration are shown. The initial and final resistances correspond to the EIS measurements recorded immediately after the break-in and at the end of tests, respectively.

In Table 3, it can be see that cell 5 has the smallest change in ohmic resistance of 0.13 $\Omega\,\mathrm{cm}^2\,\mathrm{min}^{-1}$, followed by cell 4 and cell 1. This confirms the claim that the membrane degradation is minimal with load cycling operation at a relaxation time of 2 min.

In HT-PEMFC, the availability of PA in the membrane for proton conduction determines the membrane conductivity. Thus, a lower change in resistance over time suggests minimal acid loss and a higher resistance change indicates considerable amount of acid loss from the membrane, consequently lower cell performance. This is also evident from the fact that the performance of cell 2 decreases rapidly, which is influenced by the acid loss as seen from the change in ohmic resistance in Table 3.

The changes in intermediate frequency are shown in Table 4. The differences in the percentage of change comparing cell 1, cell 4 and cell 5 are minimal, with cell 5 displaying the least changes. Cell 2 shows bigger changes compared to the other cells. This could be attributed to

Table 3: **Changes in series resistances after the completion of tests.**

MEA no.	Initial ($\Omega\,cm^2$)	Final ($\Omega\,cm^2$)	Change %	Time (h)	Change ($\Omega\,cm^2\,min^{-1}$)
1	0.186	0.275	8.9	1752	0.30
2	0.201	0.392	19.1	696	1.65
3	0.264	0.389	12.5	1464	0.51
4	0.198	0.262	6.4	1752	0.22
5	0.154	0.191	3.7	1752	0.13

Table 4: **Changes in intermediate frequency resistances after the completion of tests.**

MEA No.	Initial ($\Omega\,cm^2$)	Final ($\Omega\,cm^2$)	Change %	Time (h)	Change ($\Omega\,cm^2\,min^{-1}$)
1	0.028	0.101	7.3	1752	0.25
2	0.019	0.201	18.2	696	1.57
3	0.036	0.134	9.8	1464	0.40
4	0.028	0.098	7.0	1752	0.24
5	0.031	0.084	5.3	1752	0.18

degradation on the cathode or anode catalyst. Based on the selected EC model, the intermediate frequency is also influenced by the anode polarization and/or diffusion process as discussed earlier. The small changes in the intermediate frequency loop is more contributed by the hydrogen mass transport issues arising from acid accumulation in the GDE. The smallest change with cell 5 is a confirmation of minimal or no acid accumulation over time. This is attributed to most of the acid flowing back to the membrane at low current density, increasing the lifetime of cell by low membrane degradation rate.

The low frequency resistance calculations show a small change after the test. The changes are shown in Table 5. The low frequency resistance is usually referred to the combination of mass transport issues related to the cathode as well as anode. They become dominant mainly in two cases, when the stoichiometry is reduced, which is not the case in this work, as the flows are constant, or when the acid gets displaced to the catalyst and GDL hindering the mass transport.

Table 5: **Changes in Low frequency resistance after the completion of tests.**

MEA	Initial ($\Omega\,cm^2$)	Final ($\Omega\,cm^2$)	Change %	Time (h)	Change ($\Omega\,cm^2\,min^{-1}$)
1	0.151	0.170	1.9	1752	0.07
2	0.147	0.492	34.5	696	2.97
3	0.135	0.204	6.9	1464	0.28
4	0.142	0.178	3.6	1752	0.12
5	0.141	0.152	1.1	1752	0.04

The latter results in a longer pathway for the hydrogen molecules to reach the reaction sites. A similar phenomenon was explained by Andreasen et al. [19] using CO and CO_2, which covered the platinum site. In the current work, the effect is attributed to PA coverage of the active reaction sites.

4.2.2. Power and efficiency comparison

The power generated and the chemical energy to electrical energy conversion efficiency of each cell operated over the time period as mentioned in Table 2 was calculated and shown in Fig. 10 and Fig. 11, respectively. The comparison shown in Fig. 10 is average electrical power generated by each cell calculated as;

$$P_1 = V_1 \times I_1 \tag{2}$$

The power generated by cell 1, operating at constant current density and cell 5, operating under load cycling profile with a relaxation time of 2 min are comparable, while the power generated by Cell 3, cell 4 and cell 2 are much lower. However, since the performance of cells 2, 3, and 4 were lower immediately after break-in, possibly due to imperfect MEA production process or the human factor during fuel cell assembly, the efficiency and performance comparisons are subject to uncertainties. The efficiency plot in Fig. 11 shows the conversion efficiency from chemical energy to electrical energy.

It is calculated based on the energy input, which in this case is the chemical energy stored in the hydrogen gas, to the energy output, which is a combination of both electrical energy and heat

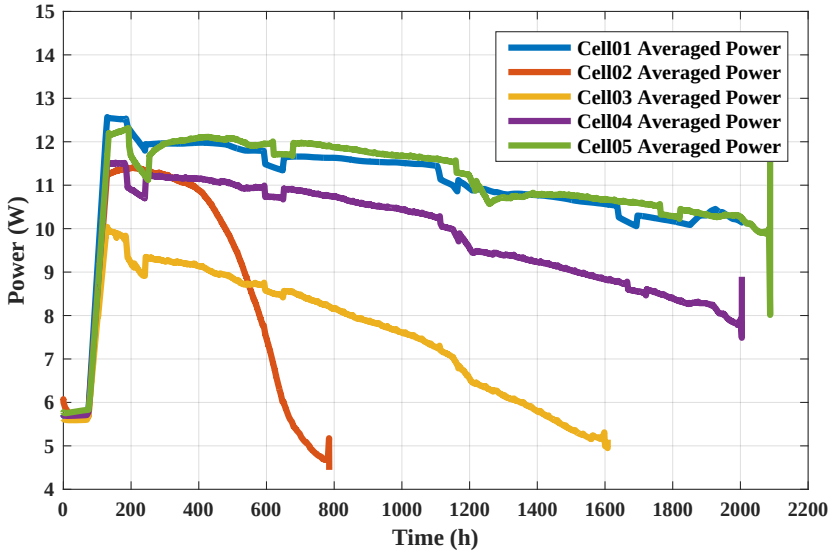

Figure 10: **The power generated by each cell during the course of the experiment**

energy. However in the present study, the useful energy output is assumed to be electrical energy, while the heat energy is neglected for efficiency calculations. The power input by a constant flow of gas is calculated as shown in Equation (3)

$$P_{\mathrm{H_2O}} = \dot{V}_{\mathrm{H_2}} \times \rho_{\mathrm{H_2}} \times LHV_{\mathrm{H_2}} \tag{3}$$

where $\dot{V}_{\mathrm{H_2}}$ is the flow rate of hydrogen in $\mathrm{L\,min^{-1}}$ and $LHV_{\mathrm{H_2}}$ is the lower heating value of hydrogen. The density of hydrogen is denoted by ρ_{H_2}.

$$Efficiency = \frac{Output\ power\ (P_1)}{Input\ power\ (P_{\mathrm{H_2O}}) \times 100}\% \tag{4}$$

The efficiency comparison is more ideal compared to the power comparison in the present study as it determines the direct relationship between the input and output power. The heat generated and/or loss is neglected in the efficiency calculation. The unreacted hydrogen at the anode outlet is neglected in the present calculation. However, as the flow was fixed for all the cells, the concentration of hydrogen at the anode outlet is assumed to be same. Since, an HT-

PEMFC is usually associated with combined heat and power (CHP) systems, taking into account the useful heat generated during the process will see a drastic increase in the efficiency. However, it is difficult to do such a calculation on a single cell level. Cell 5, whose efficiency value is similar to that of cell 1, shows a lower overall degradation rate, confirming the benefit of the load cycling operating strategy adopted for cell 5. Durability is an important issue in HT-PEMFC, and such a strategy seems to increase it without compromising on efficiency.

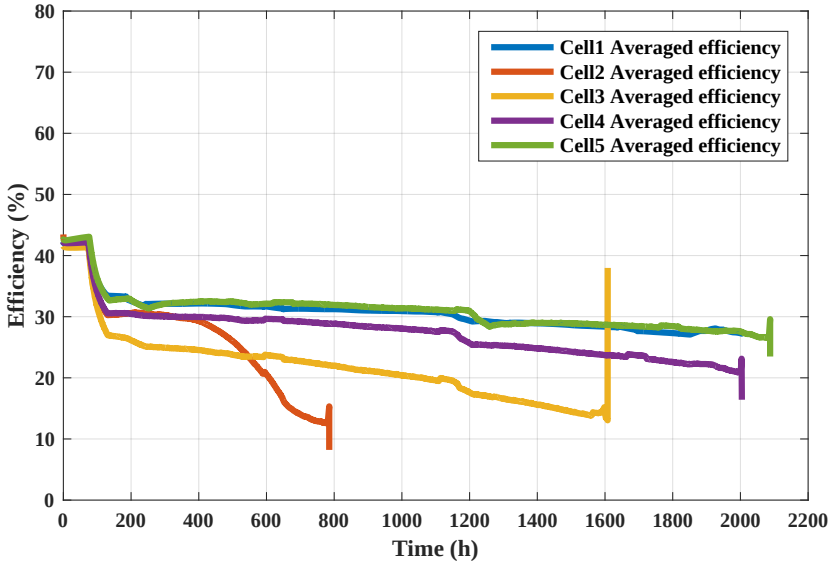

Figure 11: **The averaged efficiency of each cell during the course of the experiment.**

5. Conclusion

The results of five single cells tested under different operating conditions are presented and the results in terms of EIS and I–V curves were analysed. The focus was on improving the lifetime of PA-doped polybenzimidazole HT-PEMFC by reducing the acid loss which is one of the major concerns in the long term operation of these fuel cells. The acid is mobile in HT-PEM fuel cells and the redistribution of this mobile acid is strongly influenced by temperature, doping level and current density.

In this work, the current density function is used to minimize the acid loss. The current cycling between 0.2 $A\,cm^{-2}$ and 0.8 $A\,cm^{-2}$ with a relaxation time of 2 min. results in a lower degradation compared to constant load operation at current density of 0.55 $A\,cm^{-2}$. When operating with lower relaxation time (< min) the degradation was higher than the constant current density operation. This indicates the positive influence of load cycling with a relaxation time of above 2 min.

The analysis of the EIS data using equivalent circuit model helps in understanding the reasons for the different degradation rates of the different cells. The acid loss is one of the factors affecting, the degradation over time. The series resistances show the highest changes, which is mostly associated with variations in the acid loss with the operational strategies.

The power generated and the chemical to electrical energy efficiency were also analysed, and it was shown that cell 1 (operating at constant current density) and cell 5 (operating under load cycling with relaxation time of 2 min) have similar trends. Thus, no loss in efficiency and/or power is induced by the load cycling when relaxation time is 2 min. However, the lower degradation rate of cell 5 suggests a better lifetime with no compromise on performance. Therefore, the lifetime may be improved by operating with the load cycling strategy suggested in this paper.

Acknowledgement

The authors would like to thank the Innovation Fund Denmark for funding the work through the 4M project. The authors are also thankful to Danish Power Systems for providing the MEA used in the experiment.

References

[1] Thomas J. Schmidt and Jochen Baurmeister. Durability and Reliability in High-Temperature Reformed Hydrogen PEFCs. In *ECS Transactions*, volume 3, pages 861–869. ECS, oct 2006. doi: 10.1149/1.2356204. URL `http://ecst.ecsdl.org/content/3/1/861.abstract`.

[2] Nicola Zuliani and Rodolfo Taccani. Microcogeneration system based on HTPEM fuel cell fueled with natural gas: Performance analysis. *Applied Energy*, 97:802–808, sep 2012. ISSN 03062619. doi: 10.1016/j.apenergy.2011.12.089. URL `http://www.sciencedirect.com/science/article/pii/S0306261911008956http://www.scopus.com/inward/record.url?eid=2-s2.0-84862316706{&}partnerID=40{&}md5=dc1dc920b6055a2b12a9f020af702a31`.

[3] A. Arsalis, Mads P. Nielsen, and Søren K. Kær. Modeling and parametric study of a 1 kWe HT-PEMFC-based residential micro-CHP system. *International Journal of Hydrogen Energy*, 36(8):5010–5020, 2011. ISSN

03603199. doi: 10.1016/j.ijhydene.2011.01.121. URL http://www.sciencedirect.com/science/article/pii/S0360319911002114.

[4] Sebastian Lang, Timur J. Kazdal, Frank Kühl, and Manfred J. Hampe. Experimental investigation and numerical simulation of the electrolyte loss in a HT-PEM fuel cell. *International Journal of Hydrogen Energy*, 40(2):1163–1172, jan 2015. ISSN 03603199. doi: 10.1016/j.ijhydene.2014.11.041. URL http://www.sciencedirect.com/science/article/pii/S036031991403119X.

[5] M. Rastedt, F. J. Pinar, N. Pilinski, A. Dyck, and P. Wagner. Effect of Operation Strategies on Phosphoric Acid Loss in HT-PEM Fuel Cells. *ECS Transactions*, 75(14):455–469, sep 2016. ISSN 1938-6737. doi: 10.1149/07514.0455ecst. URL http://ecst.ecsdl.org/cgi/doi/10.1149/07514.0455ecst.

[6] Christoph Wannek, Irene Konradi, Jürgen Mergel, and Werner Lehnert. Redistribution of phosphoric acid in membrane electrode assemblies for high-temperature polymer electrolyte fuel cells. *International Journal of Hydrogen Energy*, 34(23):9479–9485, 2009. doi: http://dx.doi.org/10.1016/j.ijhydene.2009.09.076. URL http://www.sciencedirect.com/science/article/pii/S036031990901516X.

[7] S. Chevalier, M. Fazeli, F. Mack, S. Galbiati, Ingo Manke, A. Bazylak, and R. Zeis. Role of the microporous layer in the redistribution of phosphoric acid in high temperature PEM fuel cell gas diffusion electrodes. *Electrochimica Acta*, 212:187–194, 2016. ISSN 00134686. doi: 10.1016/j.electacta.2016.06.121.

[8] Samuele Galbiati, Andrea Baricci, Andrea Casalegno, Giulia Carcassola, and Renzo Marchesi. On the activation of polybenzimidazole-based membrane electrode assemblies doped with phosphoric acid. *International Journal of Hydrogen Energy*, 37(19):14475–14481, 2012. doi: 10.1016/j.ijhydene.2012.07.032. URL http://linkinghub.elsevier.com/retrieve/pii/S0360319912016096.

[9] S. H. Eberhardt, F. Marone, M. Stampanoni, F. N. Büchi, and T. J. Schmidt. Operando X-ray Tomographic Microscopy Imaging of HT-PEFC: A Comparative Study of Phosphoric Acid Electrolyte Migration. *Journal of The Electrochemical Society*, 163(8):F842–F847, jun 2016. ISSN 0013-4651. doi: 10.1149/2.0801608jes. URL http://jes.ecsdl.org/lookup/doi/10.1149/2.0801608jes.

[10] S. H. Eberhardt, T. Lochner, F. N. Büchi, and T. J. Schmidt. Correlating Electrolyte Inventory and Lifetime of HT-PEFC by Accelerated Stress Testing. *Journal of The Electrochemical Society*, 162(12):F1367–F1372, sep 2015. ISSN 0013-4651. doi: 10.1149/2.0591512jes. URL http://jes.ecsdl.org/lookup/doi/10.1149/2.0591512jes.

[11] Sebastian H. Eberhardt, Federica Marone, Marco Stampanoni, Felix N Büchi, Thomas J. Schmidt, F. N. Buchi, and Thomas J. Schmidt. Imaging Phosphoric Acid Migration in High Temperature Polymer Electrolyte Fuel Cells by X-Ray Tomographic Microscopy. *ECS Transactions*, 69(17):591–599, oct 2015. ISSN 1938-6737. doi: 10.1149/06917.0591ecst. URL http://ecst.ecsdl.org/cgi/doi/10.1149/06917.0591ecsthttp://www.scopus.com/inward/record.url?eid=2-s2.0-84946021791{&}partnerID=tZOtx3y1.

[12] S. H. Eberhardt, F. Marone, M. Stampanoni, F. N. Büchi, and T. J. Schmidt. Quantifying phosphoric acid in high-temperature polymer electrolyte fuel cell components by X-ray tomographic microscopy. *Journal of Synchrotron Radiation*, 21(6):1319–1326, nov 2014. ISSN 1600-5775. doi: 10.1107/S1600577514016348. URL http://www.ncbi.nlm.nih.gov/pubmed/25343801http://scripts.iucr.org/cgi-bin/paper?S1600577514016348.

[13] S. H. Eberhardt, M. Toulec, F. Marone, M. Stampanoni, F N Büchi, and T. J. Schmidt. Dynamic Operation of

HT-PEFC: In-Operando Imaging of Phosphoric Acid Profiles and (Re)distribution. *Journal of The Electrochemical Society*, 162(3):F310–F316, jan 2015. ISSN 0013-4651. doi: 10.1149/2.0751503jes. URL http://jes.ecsdl.org/content/162/3/F310.abstracthttp://jes.ecsdl.org/cgi/doi/10.1149/2.0751503jes.

[14] Huaneng Su, Ting-Chu Jao, Sivakumar Pasupathi, Bernard Jan Bladergroen, Vladimir Linkov, and Bruno G Pollet. A novel dual catalyst layer structured gas diffusion electrode for enhanced performance of high temperature proton exchange membrane fuel cell. *Journal of Power Sources*, 246(0):63–67, 2014. doi: http://dx.doi.org/10.1016/j.jpowsour.2013.07.062. URL http://www.sciencedirect.com/science/article/pii/S0378775313012524.

[15] Christoph Wannek, Werner Lehnert, and Jürgen Mergel. Membrane electrode assemblies for high-temperature polymer electrolyte fuel cells based on poly(2,5-benzimidazole) membranes with phosphoric acid impregnation via the catalyst layers. *Journal of Power Sources*, 192(2):258–266, 2009. ISSN 03787753. doi: 10.1016/j.jpowsour.2009.03.051. URL http://linkinghub.elsevier.com/retrieve/pii/S0378775309005576http://www.sciencedirect.com/science/article/pii/S0378775309005576http://www.sciencedirect.com/science/article/pii/S0378775309005576.

[16] P. Mazúr, J. Soukup, M. Paidar, and K. Bouzek. Gas diffusion electrodes for high temperature PEM-type fuel cells: role of a polymer binder and method of the catalyst layer deposition. *Journal of Applied Electrochemistry*, 41(9):1013–1019, jun 2011. ISSN 0021-891X. doi: 10.1007/s10800-011-0325-9. URL http://link.springer.com/10.1007/s10800-011-0325-9http://link.springer.com/10.1007/s10800-011-0325-9http://search.ebscohost.com/login.aspx?direct=true{%}5C{&}db=aph{%}5C{&}AN=65042073{%}5C{&}site=ehost-live.

[17] Dellis Jean-Luc. Zfit. Software; 2010., 2010. URL https://se.mathworks.com/matlabcentral/fileexchange/19460-zfit.

[18] Qingfeng Li, David Aili, Hans Aage Hjuler, and Jens Oluf Jensen, editors. *High Temperature Polymer Electrolyte Membrane Fuel Cells: Approaches, Status, and Perspectives*. Springer, 1 edition, 2015. ISBN 3319170821. doi: 10.1007/978-3-319-17082-4. URL https://books.google.com/books?id=corDCgAAQBAJ{&}pgis=1https://books.google.com/books?id=corDCgAAQBAJ{%}7B{&}{%}7Dpgis=1.

[19] Søren Juhl Andreasen, Jakob Rabjerg Vang, and Søren Knudsen Kær. High temperature PEM fuel cell performance characterisation with CO and CO2 using electrochemical impedance spectroscopy. *International Journal of Hydrogen Energy*, 36(16):9815–9830, aug 2011. ISSN 03603199. URL http://www.sciencedirect.com/science/article/pii/S0360319911009414.

[20] Samuel Simon Araya, Fan Zhou, Vincenzo Liso, Simon Lennart Sahlin, Jakob Rabjerg Vang, Sobi Thomas, Xin Gao, Christian Jeppesen, and Søren Knudsen Kær. A comprehensive review of PBI-based high temperature PEM fuel cells, 2016. ISSN 03603199.

[21] Matlab. Matlab_smooth function. URL https://se.mathworks.com/help/releases/R2017a/curvefit/smooth.html?searchHighlight=smooth{&}s{_}tid=doc{_}srchtitle.

[22] Yunfeng Zhai, Huamin Zhang, Gang Liu, Jingwei Hu, and Baolian Yi. Degradation Study on MEA in H[sub 3]PO[sub 4]âĹŢPBI High-Temperature PEMFC Life Test. *Journal of The Electrochemical Society*, 154(1):B72, jan 2007. ISSN 00134651. doi: 10.1149/1.2372687. URL http://jes.ecsdl.org/cgi/doi/10.1149/1.2372687.

[23] R. Taccani, T. Chinese, and M. Boaro. Effect of accelerated ageing tests on PBI HTPEM fuel cells performance degradation. *International Journal of Hydrogen Energy*, 42(3):1875–1883, 2017. ISSN 03603199. doi: 10.1016/j.ijhydene.2016.09.164. URL http://www.sciencedirect.com/science/article/pii/S0360319916316421.

[24] Thomas J Schmidt and Jochen Baurmeister. Properties of high-temperature PEFC Celtec®-P 1000 MEAs in start/stop operation mode. *Journal of Power Sources*, 176(2):428–434, 2008. doi: http://dx.doi.org/10.1016/j.jpowsour.2007.08.055. URL http://www.sciencedirect.com/science/article/pii/S0378775307016047.

[25] D. Schonvogel, M. Rastedt, P. Wagner, M. Wark, and A. Dyck. Impact of Accelerated Stress Tests on High Temperature PEMFC Degradation. *Fuel Cells*, 16(4):480–489, aug 2016. ISSN 16156846. doi: 10.1002/fuce.201500160. URL http://doi.wiley.com/10.1002/fuce.201500160.

[26] S. Yu, L. Xiao, and B. C. Benicewicz. Durability Studies of PBIâĂŘbased High Temperature PEMFCs. *Fuel Cells*, 8(3âĂŠ4):165–174, jul 2008. ISSN 16156846. doi: 10.1002/fuce.200800024. URL http://doi.wiley.com/10.1002/fuce.200800024.

[27] F. Javier Pinar, Maren Rastedt, Nadine Pilinski, and Peter Wagner. Effect of idling temperature on high temperature polymer electrolyte membrane fuel cell degradation under simulated start/stop cycling conditions. *International Journal of Hydrogen Energy*, 41(42):19463–19474, 2016. ISSN 03603199. doi: 10.1016/j.ijhydene.2016.05.091. URL http://www.sciencedirect.com/science/article/pii/S0360319916303950.

[28] Yukwon Jeon, So me Juon, Hojung Hwang, Jeongho Park, and Yong-gun Shul. Accelerated Life-time Tests including Different Load Cycling Protocols for High Temperature Polymer Electrolyte Membrane Fuel Cells. *Electrochimica Acta*, 148:15–25, 2014. ISSN 00134686. doi: 10.1016/j.electacta.2014.10.025. URL http://www.sciencedirect.com/science/article/pii/S0013468614020283.

[29] Min Chen, Søren Juhl Andreasen, Lasse Rosendahl, Søren Knudsen Kær, and Thomas Condra. System Modeling and Validation of a Thermoelectric Fluidic Power Source: Proton Exchange Membrane Fuel Cell and Thermoelectric Generator (PEMFC-TEG). *Journal of Electronic Materials*, 39(9):1593–1600, jun 2010. ISSN 0361-5235. doi: 10.1007/s11664-010-1270-9. URL http://link.springer.com/10.1007/s11664-010-1270-9.

[30] Søren Juhl Andreasen and Soİyren Knudsen Kær. Dynamic Model of the High Temperature Proton Exchange Membrane Fuel Cell Stack Temperature. *Journal of Fuel Cell Science and Technology*, 6(4):41006, 2009. ISSN 1550624X. doi: 10.1115/1.3081461. URL http://fuelcellscience.asmedigitalcollection.asme.org/article.aspx?articleid=1472107http://dx.doi.org/10.1115/1.3081461.

[31] J. R. Vang, F. Zhou, S. J. Andreasen, S K Kær, and S. K. Kaer. Estimating important electrode parameters of high temperature PEM fuel cells by fitting a model to polarisation curves and impedance spectra. *ECS Transactions*, 68(3):13–34, dec 2015. ISSN 1938-6737. doi: 10.1149/06803.0013ecst. URL http://ecst.ecsdl.org/cgi/doi/10.1149/06803.0013ecsthttp://www.scopus.com/inward/record.url?eid=2-s2.0-84957028504{&}partnerID=40{&}md5=6ab562ab6cf11264bff193c5b51effff.

Appendix

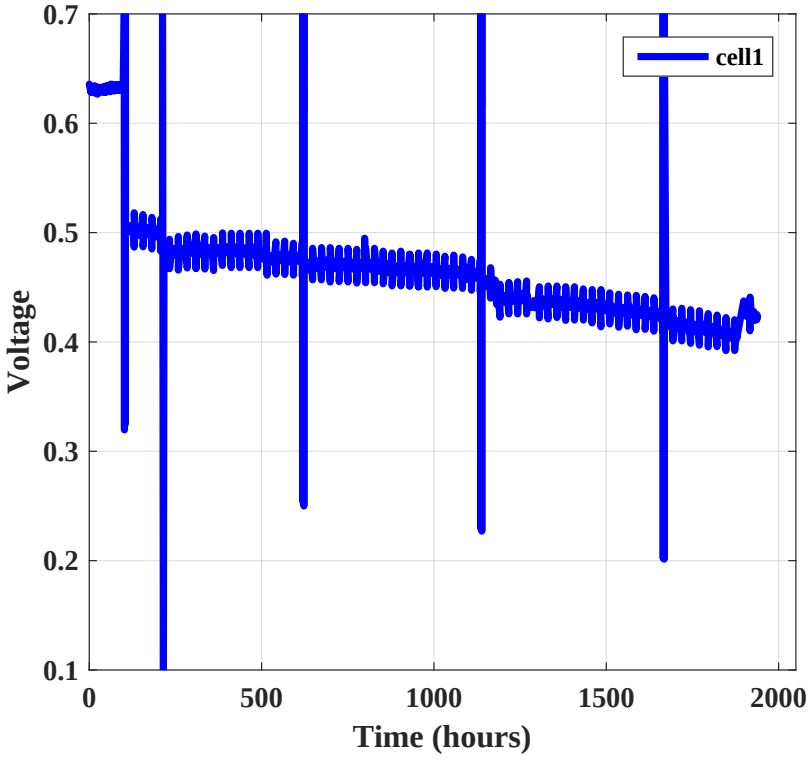

Figure 12: **Voltage profile for cell1**

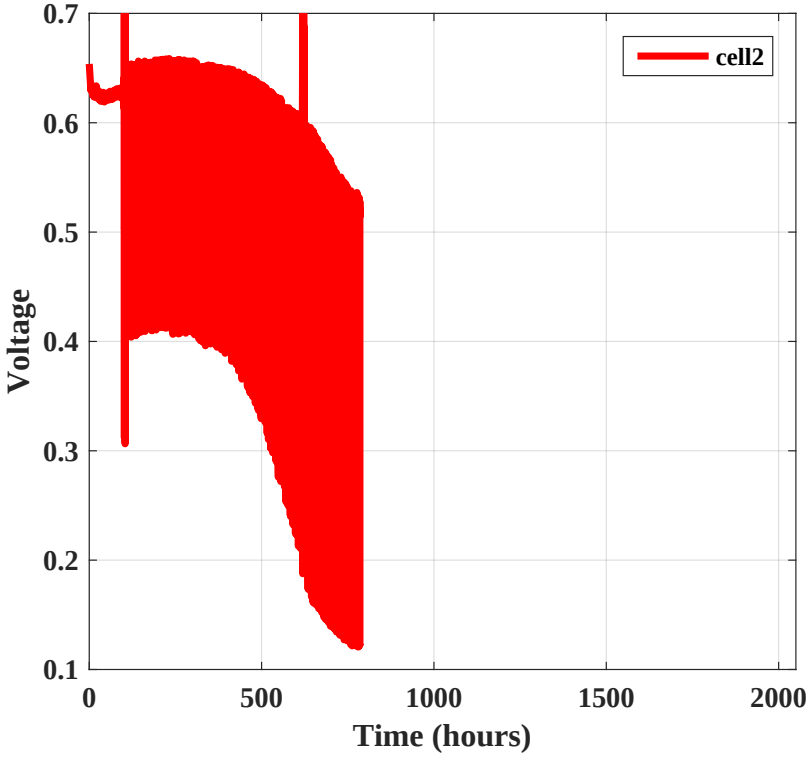

Figure 13: **Voltage profile for cell2**

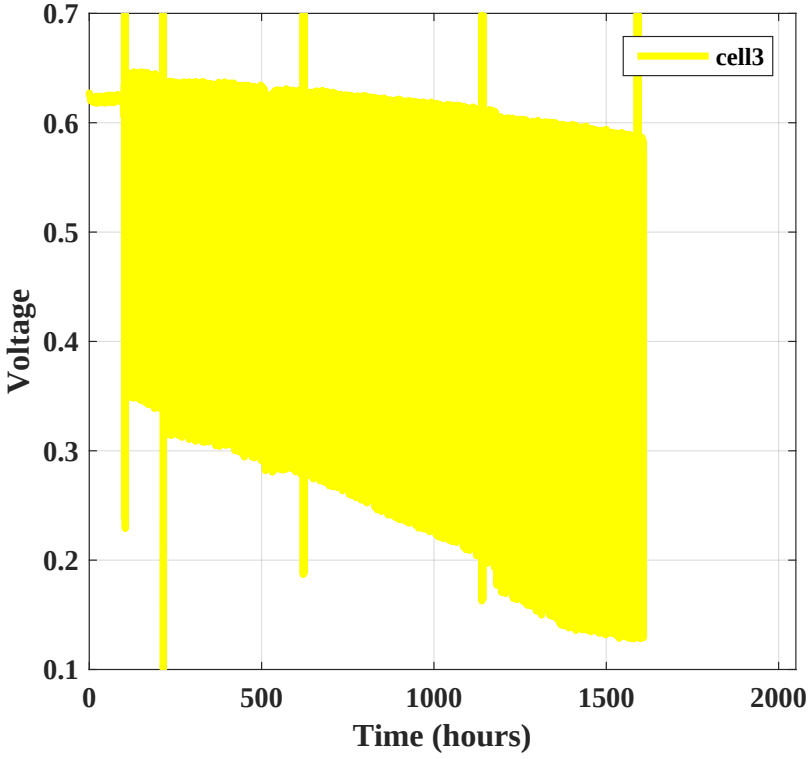

Figure 14: **Voltage profile for cell3**

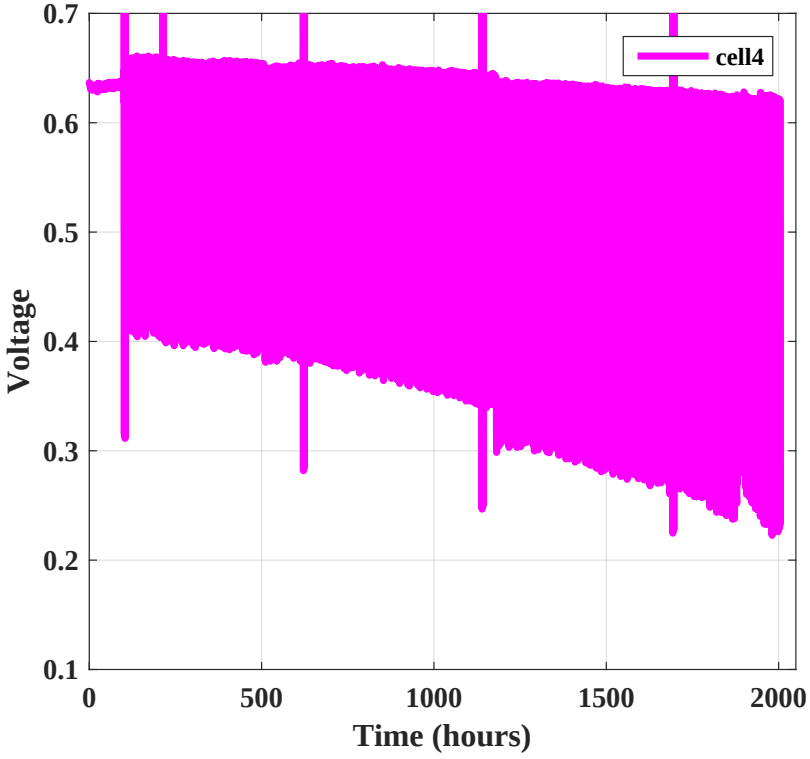

Figure 15: **Voltage profile for cell4**

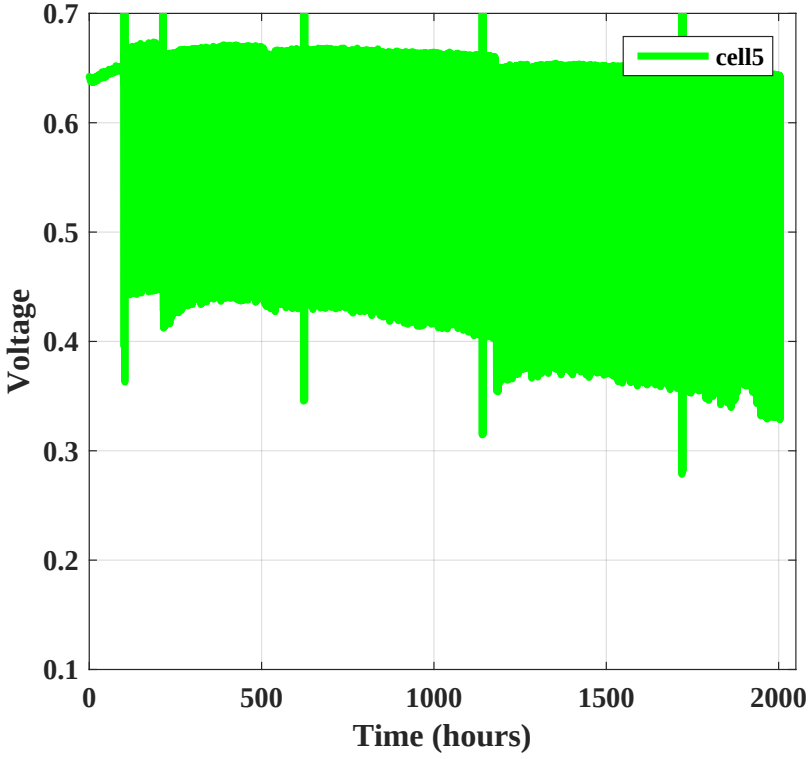

Figure 16: **Voltage profile for cell5**

ISSN (online): 2446-1636
ISBN (online): 978-87-7210-119-4

AALBORG UNIVERSITY PRESS